Bohomolets' Institute of Physiology
National Academy of Sciences, Kyïv, Ukraine
Ukrainian Scientific Research Institute of Medicine of Transport
Ministry of Health of Ukraine, Odesa
Kozyavkin International Rehabilitation Clinic, Truskavets', Ukraine
Yuriy Fed'kovych National University
Ministry of Science and Education, Chernivtsi, Ukraine

Editors

Valeriy Y. Babelyuk
Igor L. Popovych

GAS DISCHARGE VISUALIZATION (ELECTROPHOTONIC IMAGING, KIRLIANOGRAPHY). THEORETICAL AND APPLIED ASPECTS

ODESA
FENIKS
2023

Authors

Valeriy Y. Babelyuk, MD, PhD; Clinical sanatorium "Moldova", Truskavets'; UkrSR Institute of Medicine of Transport valeriybabelyk64@gmail.com

Igor L. Popovych, MD, PhD, senior res. fel.; Bohomolets' Institute of Physiology; Kozyavkin International Rehabilitation Clinic; UkrSR Institute of Medicine of Transport i.l.popovych@gmail.com

Anatoliy I. Gozhenko, MD, DS, Prof.; UkrSR Institute of Medicine of Transport prof.gozhenko@gmail.com

Galyna I. Dubkova, MD, PhD; Clinical sanatorium "Moldova", Truskavets' dubkovahalyna@gmail.com

Olga V. Kozyavkina, MD, PhD; Kozyavkin International Rehabilitation Clinic clinic@kozyavkin.com

Tetyana A. Korolyshyn, MD; UkrSR Institute of Medicine of Transport; Bohomolets' Institute of Physiology Korolushun777@gmail.com

Nazariy V. Babelyuk, MD; Clinical sanatorium "Moldova", Truskavets'

Marta M. Kovbasnyuk, PhD, senior res. fel.; Bohomolets' Institute of Physiology mmkovbasnyuk@gmail.com

Oksana A. Fihura, MD; UkrSR Institute of Medicine of Transport; Ivan Franko State Pedagogical University, Drohobych, Ukraine oksanafigura08@gmail.com

Yuriy G. Dobrovolskyi, DS, Prof. ass.; Yuriy Fed'kovych National University y.dobrovolsky@chnu.edu.ua

Walery Zukow, MD, DS, Prof. ass.; Nicolaus Copernicus University, Torun, Poland w.zukow@wp.pl

Roman I. Yanchij, DS, Prof.; Bohomolets' Institute of Physiology janchij2014@gmail.com

We dedicate the monograph to the 115th anniversary of the birth
of the Luminary of Neurophysiology
Academician Philip Nikolayevich Serkov (1908-2011)
with gratitude for the support of the Truskavetsian Scientific School

The monograph highlights the results of priority clinical-physiological studies of the relationships between gas discharge visualization (electrophotonic imaging, kirlianography) parameters, on the one hand, and electroencephalograms, heart rate variability, immunograms, phagocytosis, the content of the main adaptation hormones (cortisol, aldosterone, testosterone, triiodothyronine, calcitonin) in the blood as well as acupuncture points - on the other hand. It is shown that the GDV/EPI method reliably reflects the state of the body's neuro-endocrine-immune complex as well as others parameters and has the right to take its place in the arsenal of physiological/biophysical methods.

For biophysicists, physiologists, psychophysiologists, endocrinologists, immunologists, medical rehabilitation specialists.

INTRODUCTION

Advances in biophysics, biology, functional genomics, neuroscience, psychology, psychoneuroimmunology, and other fields suggest the existence of a subtle system of "biofield" interactions that organize biological processes from the subatomic, atomic, molecular, cellular, and organismic to the interpersonal and cosmic levels. Biofield interactions may bring about regulation of biochemical, cellular, and neurological processes through means related to electromagnetism, quantum fields, and perhaps other means of modulating biological activity and information flow. The biofield paradigm, in contrast to a reductionist, chemistry-centered viewpoint, emphasizes the informational content of biological processes; biofield interactions are thought to operate in part via low-energy or "subtle" processes such as weak, nonthermal electromagnetic fields (EMFs) or processes potentially related to consciousness and nonlocality. Biofield interactions may also operate through or be reflected in more well-understood informational processes found in EEG and ECG data. Recent advances have led to the development of a wide variety of therapeutic and diagnostic biofield devices, defined as physical instruments best understood from the viewpoint of a biofield paradigm [Muehsam D et al, 2015].

Biofield devices comprise physical instruments that may be most clearly understood from the viewpoint of a biofield paradigm, and a large and diverse number of devices have been developed to measure or manipulate biofield interactions. These include both diagnostic devices (to measure biofield properties) and therapeutic devices (to manipulate biofield interactions). The study of biofield devices is at a nascent stage of development, and much further research is needed to determine clinical efficacy and elucidate the underlying mechanisms of action for many of the devices mentioned here. The biofield devices operate through a variety of modalities rather than a single mechanism. Some biofield devices function through well-understood mechanisms and are already widely used in clinical settings: for example, electroencephalography (EEG)- and electrocardiography (ECG)-based heart rate variability (HRV). Other devices appear to operate through mechanisms that are novel or incompletely understood. However, all of these devices share a common property: rather than functioning primarily in a reductionist, chemistry-centered manner, biofield devices function via the informational content of biological processes and can interact via low-energy or "subtle" processes, including those potentially related to consciousness and nonlocality [Muehsam D et al, 2015].

Here Muehsam D et al [2015] provide a brief overview of the broad categories of biofield devices, with the goal being to stimulate further discussion and research. Authors describe those devices for which thay deemed that sufficient evidence exists to warrant mention. They chose to focus upon devices for which peer-reviewed scientific reports suggesting efficacy are available rather than conference proceedings or manufacturers' white papers. However, in the few cases that specific devices with sufficient promise and relevance lacked a peer-reviewed basis, authors have presented whatever evidence was available. Here, devices are organized according to mode of operation and these modalities include electromagnetic field (EMF)-light, EMF-heat, EMF-nonthermal, electrical current, vibration and sound, physical and mechanical, intentionality and nonlocality, *gas and plasma*, and other (mode of operation not well understood).

Muehsam D et al [2015] deemed that *gas discharge visualization (GDV) is an important example of the use of plasma in biofield science*.

Back in 1880 Nikola Tesla demonstrated that when placing the man in the high-frequency field around the body there is a bright glow [cit. by Korotkov KG, 2001]. In 1892 Nardkevych-Yodko YO recorded glow human hands on photographic plate [cit. by Ciesielska I, 2009]. However, a well-known method of "high-frequency photography" was due to spouses Kirlian SD&VH who in 1939 independently discovered this phenomenon [Kirlian SD

& Kirlian VKh, 1961], later called "Kirlian's effect". This technique has been called corona discharge photography [Boyers DG & Tiller WA, 1973], electrophotography [Earle L, 1975], electrography [Konikiewicz LW, 1979], GDV [Bankovskii NG et al, 1986].

In 1996 Korotkov KG created a new scientific approach, based on the digital videotechnics, modern electronics and computer processing quantitative data, called as method gas discharge visualization (GDV bioelectrography). Parallel uses the terms Kirlianography and Electrophotonic imaging (EPI) [Korotkov KG, 2001; 2007; 2014; Korotkov KG et al, 2002; Wisneski LA & Anderson L, 2009; Jakovleva E & Korotkov K, 2013].

Method of GDV, essence of which consists in registration of photoelectronic emission of skin, induced by high-frequency electromagnetic impulses, allows to estimate integrated psycho-somatic state of organism. The first base parameter of GDV is Area of Gas Discharge Image (GDI) in Right, Frontal and Left projections registered both with and without polyethylene filter. The second base parameter is a coefficient of form/shape (ratio of square of length of external contour of GDI toward his area), which characterizes the measure of serration/fractality of external contour. The third base parameter of GDI is Entropy, id est measure of chaos. It is considered that GDI, taken off without filter, characterizes the functional changes of organism, and with a filter characterizes organic changes. Program estimates also Energy and Asymmetry of virtual Chakras [Korotkov KG, 2001; 2007; 2014].

Nearly 1000 papers have been published (mostly in Russian) on GDV research and a few hundred more in the West. These intriguing data suggest that informatics based upon biofield measurement devices such as the GDV may be useful for gaining deeper understanding of disease states and guiding practitioners and their patients towards states of greater wellness [Muehsam D et al, 2015].

Without regard to the wideuse enough of method in medicine, psychology, valeology and others like that, he yields to the just criticizing for an insufficient physiology ground. There fore we put before itself sweep to analyse relationships between the parameters of GDV - from one side, and by the row of neurodynamics, endocrine, immune. psychophysiological, and other parameters - on the other hand.

Chapter 1

REVIEWS

Biofield science and healing

As noted in your excellent review Rubik B et al [2015], medicine is in transition. Conventional biomedicine is giving way to an expanded, integrative medical model that emphasizes healthcare as well as illness care, treats people not just diseases, and incorporates multiple therapeutic approaches, old and new, to offer patients greater choice [Maizes V et al, 2009]. This emerging model questions the dominant biomedical paradigm of molecular reductionism that focuses on genes, proteins encoded by genes, and molecules synthesized by proteins and that is based on an inherent belief that complex systems can be understood by identifying their components. By contrast, an integrative model of health and medicine appreciates the complexity of our biology, which can give rise to emergent phenomena that are not, in general, predictive from isolated parts. Such a model also views health-care from several perspectives beyond the molecular approach, including what has been called energy medicine [Cassidy CM, 2004]. Advances in biophysics, biology, psychology, and the developing fields of mind-body research such as psychoneuroimmunology and psychosocial genomics have helped substantially to form a foundation for this expanded integrative medical model.

In addition to biochemical signals, the idea that living systems generate and respond to energy fields as integral aspects of physiological regulation reflects a convergence of several disparate paths. Numerous spiritual traditions describe modes and pathways of energy within and surrounding the physical body [Jain S. et al, 2015]. Many complementary and alternative medicine (CAM) therapies utilize variants of "laying-on-of-hands" and other minimally invasive procedures to improve endogenous energy flows. Moreover, Western biomedicine routinely examines electrical fields from the heart (via ECG) and brain (via EEG) as indices of clinical pathology. Furthermore, contemporary cell biology and biophysics provide evidence that endogenous electromagnetic and other types of fields play active roles in development, tissue repair, and an array of homeodynamic processes [Funk RH et al, 2009; Movaffaghi Z & Farsi M, 2009; Bischof M & Del Guidice E, 2013].

The term *biofield* fills the need for a unifying concept to bridge traditional and contemporary explanatory models of energy medicine and provides a common language for aspects of both clinical practice and scientific research that focus on energy fields of the body. Rubik B et al [2015] summarized the recent origins of the biofield concept and described the levels of scale for which the term has been applied, from biophotons and cell membranes to whole organisms to Gaia and the *Tao*. Working definitions of *biofield* and related terms are offered with the proviso that such descriptions are and should be based in the cultural and scientific vantage points of the observers and may not always be completely comparable. In this light, in their descriptions of "the biofield," a Tibetan Buddhist, a neurologist, a Reiki practitioner, a cell biologist, and a physicist (classical or quantum) enrich us all and bring us closer to a complete understanding of this emerging concept.

The term *biofield* was proposed in 1992 by an ad hoc committee of CAM practitioners and researchers convened by the newly established Office of Alternative Medicine (OAM) at the US National Institutes of Health (NIH). The committee was one of several meeting as part of an NIH/OAM-hosted conference in Chantilly, Virginia, to inform the OAM as it established its program priorities and initiatives. The committee had a dual focus on "manual medicine" - consisting of structural and manipulative approaches such as chiropractic, classical osteopathy, and massage - and "energetic therapies" such as Reiki, Therapeutic Touch, and external *qigong*. Most of the latter group of healing modalities were founded on a concept of a vital

force, although each has its own explanatory model and terminology that reflect a particular cultural context. The committee sought to bring unity to the diversity of energetic practices by creating a term that would be amenable to the scientific and broader healthcare communities. Such a term was also needed to describe a central organizing biological field that healers were detecting and interacting with in their practice. The term *biofield* was coined for these purposes with the hope that it would be generic and malleable enough to fit differing explanatory models of therapy.

The committee defined biofield as "a massless field, not necessarily electromagnetic, that surrounds and permeates living bodies and affects the body" [Rubik B et al, 1995]. Subsequently, one committee member succeeded in getting the term *biofield* accepted as a Medical Subject Heading (MeSH term) at the National Library of Medicine so that it became an official search term for scholars to locate peer-reviewed literature. Further, the committee sought to consolidate the diverse modes of energetic healing under the single term *biofield therapies*, which was also accepted by the NIH. An additional realization was that both diagnostics and therapeutics may be involved in these biofield modalities. Subsequently, a round of frontier medicine research grants in biofield science was funded by the National Center for Complementary and Alternative Medicine, the successor to the OAM.

Simultaneously, another of the 1992 ad hoc committees advising the OAM categorized "distant healing" or "distant healing intention" - remote healing over a distance performed through intention and/or intercessory prayer - as a mind-body modality. Thus, energy healing that was performed locally by healers directly on patients, which had been termed biofield therapy, was separated from distant healing due to this initial categorization. A rationale for this separation between local and distant healing was that they may operate by different modes of action. Whereas local or proximal energy healing might involve electromagnetic fields (EMFs) that diminish over distance by an inverse square law, the same fields are unlikely to be involved in healing across large distances. However, local and distant healing are commonly performed by the same practitioner, such as in Reiki, which poses a conundrum. Since antiquity, there have been 2 opposing views on the nature of life. Democritus, who coined the word *atom*, maintained that everything, including organisms, is reducible to its constituents, while Aristotle held that life processes are autonomous and organisms are integral wholes. These 2 viewpoints remain today, with the biochemical view of life represented by molecular reductionism and a holistic view that embraces a field concept of life [Rubik B et al, 2015].

In science, the notion of a vital force or *élan vital* dates back to the 1600s. In vitalism, living matter was believed to involve a life force: a metaphysical entity intrinsic to life that renders it alive. This force was initially considered immeasurable and outside the scope of science. Yet discoveries of bioelectricity challenged the notion that this force was immeasurable. By 1850, experimental electrophysiology had replaced the notion of vital force with electricity, effectively banishing vitalism from biological science [Bischof M, 1995].

Nevertheless, many contemporary CAM practitioners continue to use terms from non-Western explanatory models and medical systems to evoke a vital force or vital energy. For example, there is *Qi* (Chi) in Chinese medicine, *Ki* in Japanese medicine, *Prana* in Ayurveda, and similar terms in other traditions of indigenous medicine. These descriptions of life energy originated from metaphysical considerations of the nature of consciousness and its interaction with mental, emotional, and physical systems [Jain S et al, 2015] and were based on first-person observations by adept spiritual practitioners. In the modern age, the notion of a universal life energy is nearly ubiquitously employed by energy healing practitioners, who often describe energy coming from their hands and other parts of the body. These same practitioners report utilizing energy awareness not only to sense imbalances in patients' energy fields but to regulate energy flow and release energy blockages perceived to be

impeding the healing process. Most traditional healing practices maintain that disease starts with an energetic imbalance such as a blockage or other irregularity in the energy flow through the body. Modern CAM systems such as chiropractic [Senzon SA, 2008], homeopathy [Hahnemann S, 1883], and classical osteopathy [Northrup GW, 1966] are also founded on principles of a vital force. Therapeutics in these practices involves restoring or rebalancing the vital force to promote healing.

The scientific concept of force, however, is very much in the physical realm, whereas the vital force at the basis of many CAM therapies is considered by mainstream science to be a metaphysical concept. Force, as well as field and energy, are fundamentals of physical theory. Force refers to any interaction that tends to change the motion of an object. The concept of a field from physics refers to a spatially distributed nonmaterial element that is able to impart a force upon an object within it. Therefore, a field cannot be detected directly but only through its action upon a suitable probe—for example, a charge in an electric field. Contemporary physics holds that there are only 4 types of force operating throughout nature: gravity, electromagnetism, and the strong and weak nuclear forces, the latter 2 having a range limited to the atomic nucleus. A particular form of energy (defined in physics as the ability to do work: ie, to move a particle through a distance) is associated with each force: for example, electric, magnetic, and electromagnetic energies are associated with the electromagnetic force, which is most important in living systems. The concept of the biofield as proposed herein is firmly grounded in science, although other putative fields, as yet unknown to science, may also be involved [Rubik B et al, 2015].

The concept of a biological field first arose in embryology as an underlying informational template to explain the developmental process. The Ukranian histologist Gurwitsch AG, coined the term *morphogenetic field* to describe the highly coherent and dynamic process that appeared to be guiding development of the unfolding embryo as well as biological regeneration. Gurwitsch AG also discovered mitogenetic radiation, ultraviolet light emission during cell division in onion roots [cyt by Beloussov LV et al, 1997]. From 1900 to 1950, other prominent developmental biologists including Hans Driesch, Paul Weiss, and others worked from this same perspective. Weiss, who discovered that the morphogenetic field was unchanged if he removed portions of embryonic tissue, proposed that the biological field was a holistic property of the entire organism [cyt by Jerman I et al, 2009]. These early embryologists formed the concept of a morphogenetic field guiding development but did not determine its physical basis.

The biofield concept soon gained traction and was extended from an entity "that surrounds and permeates living bodies" to include a more extensive variety of endogenous phenomena generated by living bodies. It has also been "scaled-up" to test its fit to macrolevel concepts including Gaia, a model of our planet as a complex, self-regulatory system. Thus, at this point in time, the concept of "biofield" may be better considered in its plural form of "biofields." From this perspective, the term may continue to be usefully applied across a broad range of disciplines, in manners both evidence-based and speculative, including biophysics, cell biology, therapeutics, and ecology [Rubik B et al, 2015].

One line of research on endogenous biofields followed from the early discovery by Gurwitsch AG, as mentioned above, of ultraviolet light emission during cell division. Recent studies have reported evidence for a variety of biophoton-mediated regulatory processes, including cell-cell communication, cell-cell orientation sensing, secretion of regulatory neurotransmitters, modulation of respiratory activity in white blood cells, and accelerated seed germination [Van Wijk R, 2001]. These findings, as well as results of research correlating biophoton emission with human physiology, suggest the existence of coherent biophoton fields that play fundamental roles in intercellular signaling [Van Wijk R, 2001; Popp FA & Chang JJ, 1998] and human health [Ives J et al, 2014].

More generally, a wide variety of bioelectromagnetic activities has been identified, often associated with interaction energies substantially below that of thermal noise, which produce clinically significant effects, including enhancement of growth, wound repair, regeneration, and the reduction of pain and inflammation [Funk RH & Monsees TK, 2006; Funk RH et al, 2009]. In addition, field-like phenomena appear to contribute to the underlying principles of biological organization, including embryonic development and the coordinated maintenance of biological structure and function. For example, regenerative healing of whole limbs in animals such as salamanders has been shown to involve EMFs [Becker RO, 1961], and limb regeneration in higher animals has also been stimulated by means of externally applied EMFs [Becker RO, 1972]. More recently, the patterning of arrays of cell membrane resting potentials has been shown to play key roles in directing stem cell behavior during embryogenesis and in complex organ regeneration [Levin M, 2014; Adams DS et al, 2013].

The biofield, or information associated with it stemming from multicellular electrical activity, is also the basis of a decades-old clinical tool most commonly in the form of the ECG (the detector of electrical wave forms generated by synchronous activity of heart muscle cells) and EEG (the detector of wave forms reflecting summative spontaneous or evoked electrical activity of neuronal arrays). While the ECG and EEG are readily detected from the body surface, the heart's magnetic field, generated by moving electric charges associated with electrical activity, can be recorded up to several feet from the body surface via a magnetocardiogram [Steinhoff U et al, 2004]. Magnetic fields produced by the heart appear to carry information that may be detectable by other persons or animals [McCraty R et al, 2009]. An example of the informational potential (bioeffectiveness) of these heart fields is cardiac-induced entrainment (or frequency locking) detected when the R-waves of one subject's ECG become precisely synchronized with the onset of EEG alpha waves of another subject at a distance up to 5 feet [McCraty R, 2005].

At the interpersonal level, the biofield concept encompasses a large body of research on the effects of biofield therapies, as practiced both locally with the practitioner in the same room as the patient [Jain S et al, 2015], animals, or cell cultures [Gronowicz G et al, 2015], and nonlocally, which includes distant mental interaction with living systems, as well as intercessory prayer and distant healing [Radin D et al, 2015]. Studies with biofield therapies in clinical settings reflect the propensity of certain practitioners and schools of healing to perform therapy with hands on and/or hands off the body [Jain S & Mills PJP, 2010], therapeutic touch, and healing touch which raise questions about the physical effects of touch itself on biofield interactions and outcomes. However, recent reviews examining nontouch biofield therapies also report significant changes in outcome measures, suggesting that effects of biofield therapies on outcomes may not be ascribed only to effects of physical touch [Hammerschlag R et al, 2014; Roe CA et al, 2015], and an explanation in terms of quantum entanglement or other nonlocal causes may be needed [Thaheld FH, 2005].

Biofield interactions also extend from molecular to planetary levels. At the molecular level, the term biofield may even be invoked to explain fundamental properties of individual molecules by considering them as "ordered electromagnetic structures" [Bischof M & Del Giudice E, 2013].
The argument can be made that molecular interactions, such as between hormone and receptor, are those usually described at close range - eg, ionic, hydrophobic, and aromatic pi-electron interactions. Such properties, however, do not explain how molecular partners attain proximity to each other; the necessary preludes to docking are unlikely to occur via simple diffusion and Brownian motion [Cosic I et al, 2006]. Rather, one proposal is a "resonant recognition model" in which molecules are attracted to their targets by a form of electromagnetic resonance [Cosic I et al, 2006], which clearly falls within the biofield rubric. At the planetary level, there is increasing evidence that the biofield concept can include

effects of geocosmic fields on human health and behavior: for example, solar storms that significantly perturb the geomagnetic field correlate with increased rates and mortality from myocardial infarction [Halberg F et al, 2000; Stoupel E, 2002].

Early biofield studies were motivated in part by the many CAM modalities that appear to involve energy and/or informational fields and are broadly known as "energy medicine." These include energy healing, homeopathy, acupuncture, magnet therapy, bioelectromagnetic therapies, electrodermal therapy, and applied kinesiology, among others. Some of these modalities involve novel ways of obtaining useful information from the body's energy field as well as applying energy fields therapeutically [Rubik B et al, 2015].

"Laying on of hands" is one of the oldest, most ubiquitous forms of healing known to humankind, apparently having emerged independently among ancient cultures worldwide. The father of modern Western medicine, Hippocrates, referred to it as "the force which flows from many people's hands" [Schiegl H, 1983]. There are a growing number of studies on this and other related biofield healing modalities demonstrating a spectrum of beneficial results from the psychological and behavioral levels down to clinically relevant bio-markers [Jain S & Mills PJP, 2010; Lutgendorf SK et al, 2010; Friedman RS et al, 2010; Jain S et al, 2012]. Another area is bioelectromagnetic medicine, where it has now been demonstrated that nonthermal EMFs, often with interaction energies substantially below that of thermal noise, produce a wide variety of clinically significant effects, including enhancement of growth, wound repair, regeneration, and the reduction of pain and inflammation [Rubik B et al, 1995; Shupak N, 2003; Funk RH & Monsees TK, 2006; Funk RH et al, 2009; Muehsam D & Ventura C, 2014].

In addition, the underlying principles of biological organization, including embryonic development and the coordinated maintenance of biological structure and function, are beginning to be better understood, with evidence suggesting that field-like phenomena underlie many of these processes as described earlier [Rubik B et al, 2015].

Field effects have also been invoked as explanations of a large body of research on human intention effects and nonlocality [Radin D & Nelson R, 2003]. Recent reports with relevance to CAM practices include effects on cultured cells [Radin D & Yount G, 2004], seed germination [Creath K et al, 2004], and distant healing of surgical wounds [Schlitz M et al, 2012]. Further, several studies have reported EEG correlations between isolated human subjects [Wackermann J et al, 2003; Standish LJ et al, 2003; 2004; Radin DI, 2004; Richards TL et al, 2005] with in vitro corroboration using neurons adhering to printed circuit boards [Pizzi R et al, 2004]. Experiments performed with shielding suggest that some of these results are not mediated by EMFs [Wackermann J et al, 2003; Pizzi R et al, 2004], perhaps suggesting a role for quantum entanglement or another nonlocal process [Thaheld FH, 2005]. Such phenomena, which clearly call for scientific explanations at levels of organization beyond the molecular realm, may be explained by a common model of biofield effects [Rubik B et al, 2015].

Concepts of sentience, mind, and consciousness have also evolved from the mechanistic approach of biochemical neuroscience to a field-oriented approach. The application of quantum theory to these concepts has led to several proposals of the body-mind as a macroscopic quantum system [Popp FA, 1989; Hameroff SR, 1994; Ho MV et al, 1994; Stapp HP, 2009]. While the predictive power of these models is as yet unclear, there is increasing experimental evidence showing quantum signaling, communication, and conductivity in the cytoskeletal network of microtubules [Hameroff SR et al, 2002; Havelka D et al, 2011], and the electric fields generated by synchronized oscillations of microtubules have been demonstrated to play key roles in the regulation of cell division and chromosome folding and transcription [Zhao Y & Zhan Q, 2012; 2012a]. Similarly, it has been proposed that the acupuncture system and the patterning of cell resting potentials described above [Becker RO,

1961; Levin M, 2014] act through the continuum of liquid crystalline collagen fibers that make up the bulk of the connective tissues [Ho MP & Knight DP, 1998]. In this model, supported by evidence from biochemistry, cell biology, biophysics, and neurophysiology, the collagen matrix provides pathways for rapid intercommunication throughout the body, enabling the organism's mind-body to function as a coherent whole [Ho MP & Knight DP, 1998; Langevin HM, 2006]. Together, these results describe the mind-body as an interconnected system in which electromagnetic and quantum interactions act through field-coherent oscillatory activity to regulate biological processes and mediate interactions correlated with sentience and mental activity [Ho MP & Knight DP, 1998; Plankar M et al, 2013; Ho MV, 2014].

As a regulator and mediator of biological interactions, the biofield appears intimately connected with information delivery within the organism. The biofield thus holds and conveys information that is vital for biocommunication and bioregulation. Here it must be said that the concept of information in biology is nothing new; it is already used successfully to explain numerous molecular mechanisms in molecular biology, such as information encoded in DNA, hormone-receptor interactions, enzyme-substrate interactions, and many other forms of molecular recognition, as well as in ECG and EEG data. Further, many of these well-understood mechanisms may also be thought of as biofield interactions because information itself is often an emergent property of dynamical interactions that cannot be meaningfully understood from a reductionist viewpoint. At the cellular and subcellular levels, oscillatory behaviors emerge from negative feedback loops and coupled positive and negative feedback loops [Ferrell JE et al, 2011] and result from stochastic, nonlinear biological mechanisms interacting with the fluctuating environment [Glass L, 2001]. For example, the emergence of phase-synchrony across large numbers of cells in circadian cooperative systems is the result of nonlinear coupling of oscillators across the cellular and multicellular levels [Bordyugov G et al, 2013; Lara-Aparicio M et al, 2014]. Similarly, electrically phase-coupled systems in neuronal networks give rise to cooperative behaviors across large numbers of neurons [Dodla R & Wilson CJ, 2013].

The concept of biofield regulation offers a shift from a mechanical, chemistry-based view of biology to an information-based view. Unlike machines, living organisms have an immense network of internal and external interconnections across which information flows to modulate life functions. The continuous exchange of information in living systems to maintain their integrity is astounding. Furthermore, new relationships along with new information exchanges emerge at higher levels of organization in life, forming new wholes. The biofield may be considered one such multilevel organizational concept in which information flows within and between the various levels of the organism. A wealth of information exchange, much like a "conversation" between the elements of these various levels of order - the "whispering" between cells and other units of life - is critical to sustaining life and promoting healing. The biofield may be considered to be the language of life [Rubik B et al, 2015].

Biofield information can manifest beyond mechanistic concepts; bioelectromagnetic medicine presents another example of the informational aspect of biofield interactions. The concept of "electromagnetic bioinformation" was advanced by Popp FA [Popp FA et al, 1979; Popp FA, 1989] to describe findings that biophotons and other extremely low-level energy transactions in bioelectromagnetics below the thermal noise limit could induce biological effects. In addition to the above-mentioned weak EMF effects, a large body of literature has demonstrated the existence of nonthermal EMF resonance interactions [Zhadin MN, 2001; Binhi Vn & Rubin AB, 2007; Muehsam DJ & Pilla AA, 2009]. Bioeffects often occur only for particular frequencies, amplitudes, or waveforms, and the precise location of resonances is in general determined by the characteristics of the EMF/biological target system, which can vary with changes in state of health, disease, or injury [Muehsam DJ & Pilla AA, 1999].

Entrainment of physiological functions such as EEG and ECG with external fields [McCraty R, 2005] may be also seen as induced synchronization, which constitutes a flow of information from an external field to the body. Furthermore, other elements of the biofield may carry information important for medical diagnostics, beyond the EEG and ECG, that provide useful medical information and suggest new modes of treatment via informational medicine. Indeed, information offers a unifying concept in the *modus operandi* of CAM and integrative medical modalities [Rubik B, 1995; 1997].

While information is exchanged across multiple levels of order in living systems, perhaps the most definitive information flow in humans is from the "top down" from intention to the material body, to affect health and promote healing with conscious intention, purpose, context, and meaning. Information may thus be seen to mediate or serve as a bridge between mind and body: for example, in mind-body modalities, intent to heal, etc [Rubik et al, 2015].

Typically, information is thought to be carried by either energy or matter. However, Bell's Theorem (quantum nonlocality) supports observations of instantaneous interaction between entangled states [Einstein A et al, 1935; Bell JS, 1964; Aspect A et al, 1982]. The quantum potential function conveys active information everywhere [Aharonov Y & Bohm D, 1959; Bohm D, 1980; Noguchi A et al, 2014], as does the morphogenetic field [Sheldrake R, 1981], with no diminution over distance. Information may thus be everywhere instantaneously, but it is active only where it is specifically directed - for example, by conscious intent - and may be considered intelligent information, producing a very specific response only where it is intended. Thus, information itself may be considered causal even though it does not always have a physical carrier [Walker SI & Davies PC, 2012].

As described above, the biofield has evolved into a multiscale concept that offers a broader context for understanding biological regulation and information flow than does the currently dominant molecular paradigm of biological systems. As such, a biofield, whether at the level of biophotons, patterns of cell membrane resting potentials, EEG of brain, ECG of heart, or the synchronous movements of birds in flight, can succinctly be described as an organizing influence distributed over space and time. While biofields have most often been described as electromagnetic in nature [Rubik B, 2002; Hintz KJ et al, 2003], there have been several proposals of biofields involving quantum information flow [Rein G, 2004; Thaheld FH, 2005; Bischof M & Del Giudice E, 2012]. In their organizing capacity, it seems more useful to speak of biofields in terms of their homeodynamic activities than as individual entities: ie, to describe what they do rather than what they are. As presented earlier, the concept of a field from physics refers to a nonmaterial element that interacts with an object and a field cannot be detected directly but only through its action upon a probe. Thus, biofield interactions can influence and be influenced by a variety of biological pathways including biochemical, cellular, and neurological processes as they modulate activity and information flow across multiple levels of living systems. At this stage, the biofield may be considered as a "massless" or information-based organizing principle in accordance with the original definition proposed by the 1992 NIH advisory committee [Rubik B et al, 1995].

Finally, it is of interest to reflect again on the relation of the biofield concept to *energy medicine*, a term especially in vogue in the latter part of the 20th century. While biofields play a substantive role in guiding health processes, here they are conceived as playing a broader regulatory and informational role in biology than solely as a form of medical intervention as implied by energy medicine. The term *biofield therapy*, which involves healer-based interactions with biofields both within and around living systems [Warber SL et al, 2004; Levin M, 2012], best captures this aspect of healing beyond limited implication of medicine as a treatment for illness.

The biofield concept, emerging initially from vitalist perspectives, offers an increasingly useful approach to explain a variety of physiological phenomena. Its applicability continues to

evolve in terms of empirical inquiry. Endogenous biofield interactions with environmental, geocosmic, and other exogenous fields provide the rudiments of a scientific foundation for a holistic view of life and a *modus operandi* for numerous CAM modalities. The family of energy healing practices that have been widely practiced since antiquity, now called biofield therapies, may involve biocommunication and/or energy transfer through the biofield. While the biofield concept is a useful construct to guide new research on energy healing and other CAM modalities, it is also a requisite for a better understanding of contemporary developments in biophysics and biology. Moreover, information connected with the biofield may serve as a bridge between mind and body, which is fundamental to understanding mind-body interactions [Rubik B et al, 2015].

The biofield is also an important metaphor to guide further research. There are numerous examples from the history of science where metaphor and analogy have been key elements in the construction of successful theories. The use of metaphor in science is especially appropriate and critical for success in the exploratory phase of investigation when detailed descriptions and theories are unavailable. Metaphors provide foundational material for forming hypotheses, conducting studies, and eventually elucidating testable theories. Scientific metaphors can be key elements for posing truly novel questions, which upon experimental testing, advance our knowledge and understanding. The concept of the biofield, while still in its nascent stages, may well serve this purpose as biology moves from a local, chemistry-based model to an interconnected, information-based viewpoint. Further investigations in biofield science and healing, especially those involving multidisciplinary collaborations - including clinical and preclinical trials, physiology, biophysics, device technology, and theoretical and philosophical models - will guide the way to a new paradigm in biology and medicine [Rubik B et al, 2015].

Biofield devices

Muehsam D et al [2015] provide a broad overview of biofield devices, with emphasis on those devices for which solid, peer-reviewed evidence exists. A subset of these devices, such as those based upon EEG- and ECG-based heart rate variability, function via mechanisms that are well understood and are widely employed in clinical settings. Other device modalities, such a gas discharge visualization and biophoton emission, appear to operate through incompletely understood mechanisms and have unclear clinical significance. Device modes of operation include EMF-light, EMF-heat, EMF-nonthermal, electrical current, vibration and sound, physical and mechanical, intentionality and nonlocality, gas and plasma, and other (mode of operation not well-understood). Methodological issues in device development and interfaces for future interdisciplinary research are discussed. Devices play prominent cultural and scientific roles in our society, and it is likely that device technologies will be one of the most influential access points for the furthering of biofield research and the dissemination of biofield concepts. This developing field of study presents new areas of research that have many important implications for both basic science and clinical medicine.

Modalities Using Electromagnetic Fields: Light

One line of research that has yielded a large amount of information on biofield activity is the study of biophoton emission (BE), also called ultraweak photon emission. BE is the spontaneous emission of light which emanates from all living organisms, including humans [Popp FA et al, 1984]. Several studies have reported intercellular BE signaling [Van Wijk R, 2001], and it has been suggested that such signaling by coherent biophotons could explain many regulatory functions [Popp FA & Chang JJ, 1998], including cellular orientation detection [Albrecht-Buehler G, 1992], biophoton-regulation of neurotransmitter release [Galantsev VP et al, 1993], leukocyte respiratory activity [Shen X et al, 2000], and enhanced seed germination [Kuzin AM & Surkenova GM, 1995]. A systematic review has suggested

that detection of BE may be useful as a medical diagnostic approach and as a research tool [Ives JA et al, 2014].

Modalities Using Electromagnetic Fields: Nonthermal

EMF interactions and electric currents, primarily created by ions within the body, are essential for a variety of critical biological functions, including regulation of ion transport, maintenance of membrane electrical potential, nervous system activity, cytoskeletal transport, coordination of cell migration, embryonic development, and wound healing [Funk RH et al, 2006; 2009]. Recent studies have also shown that processes regulating the dynamics of mitosis, meiosis, and a variety of other processes are governed by electric fields generated within the intracellular network of microtubules, centrosomes, chromosomes [Funk RH et al, 2009; Zhao Y & Zhan Q, 2012; Plankar M et al, 2013], and nuclear chromatin [Zhao Y & Zhan Q, 2012a]. Also, EMF signaling in neuronal microtubules has been suggested as a substrate for cognition [Plankar M et al, 2013] and as a source of observed EEG correlates of consciousness [Hameroff S & Penrose R, 2014], suggesting the existence of a system of subtle signaling that relies on rhythm, resonance, and synchronization [Glass L, 2001; Hameroff S et al, 2002].

In addition to these endogenous EMF interactions, biological systems appear to exhibit sensitivity to exogenous EMF exposures for most of the frequencies, field strengths, and amplitudes occurring in natural and man-made environments [Funk RH & Monsees TK, 2006]. These observations have led to the development of a large number of therapeutic applications and clearance from the US Food and Drug Administration (FDA) and regulatory bodies worldwide for EMF treatment of pathologies such as bone repair, pain, and edema [Pilla AA, 2007].

Of particular relevance to biofield science, a large and rapidly growing body of data has demonstrated the existence of nonthermal EMF bioeffects, for which the molecular interaction energies are less than the average thermal energy of the target [Binhi VN & Rubin AB, 2007]. The existence of these extremely weak EMF effects suggests the possibility of bioinformation flow at extremely low energies and could foreshadow a paradigm shift away from the biochemical paradigm and towards an information-oriented model, wherein weak signaling (via EMF, light, or vibration) plays an essential role in biological regulation.

Device employing electrodermal measurement is the apparatus for meridian identification (AMI), which measures electrical characteristics of the skin at acupuncture points located at the base of fingers and toes called Jing-Well points [Tsuchita K & Motoyama H, 2009]. Based on the theory that the "energy" or "strength" of the acupuncture meridians (or energy channels) is reflected by electrodermal characteristics, conductance, capacitance, and polarization, measurements from Jing-Well points are analyzed in order to diagnose a variety of pathologies, as well as to assess overall wellbeing [Deadman P, 1993]. In a controlled study of claustrophobia therapy, increase in AMI-measured prepolarization current at Jing-Well points correlated with a significant reduction in anxiety [Lambrou P et al, 2003]. Similarly, statistically significant differences between electric potential measurements obtained on and off acupoints and between external focus and healing states have been reported in "energy healing" practitioners [Syldona M & Rein G, 1999].

Modalities Based Upon Human Intention

A large and growing research literature has considered the role of human consciousness and intention in biology, psychology, and the physical sciences [Hankey A, 2007; Radin D & Nelson R, 2003]. These human intentionality effects have been reported in a variety of living systems - for example EEG [Wackermann J et al, 2003] and galvanic skin response [Radin D et al 2008] - suggesting that human intention may play a key role in biofield interactions.

Two large-scale projects are currently collecting data on human interactions with global events: (1) the Global Consciousness Project is collecting data on correlations between

statistics of continuously operating random event generators around the world and brief episodes of widespread mental and emotional reaction to major world events [Nelson R & Bancel P, 2011], and (2) the Global Coherence Initiative is seeking to examine interactions of humans with EMFs of terrestrial, solar, and cosmic origin by installing a global network of 12 to 14 ultrasensitive magnetic field detectors around the planet and correlating EMF data with variables such as HRV [McGraty R et al, 2012]. While these global projects involve large numbers of participants around the world, the intention host device (IHD) is another type of device methodology based upon human intention focused more individually [Tiller WA et al, 2000]. The IHD has been reported to broadcast imprinted human intention to condition a laboratory environment and to produce alterations in time-series measurements of temperature, pH, drosophila fitness and energy metabolism, in vitro enzyme activity, and molecular concentration variability [Tiller WA et al, 2000; Kohane MJ & Tiller WA, 2001].

Modalities Using Gas or Plasma

See please INRODUCTION.

Other Device Modalities

In light of observations of nonlocal effects [Hankey A, 2007; Radin D & Nelson R, 2003], which suggest that biofield interactions may involve means of information transfer that cannot be easily described via well-understood substrates (eg, EMFs), here Muehsam D et al [2015] describe devices that do not fit easily into the categories listed above. Although a vast number of other devices fall into this category, here they list 3 of the more well-known modalities: torsion fields, orgone energy, and scalar waves. These 3 modalities were chosen because of their prominent positions amongst devices purported to act upon the biofield. However, it should be noted that the biophysical substrates are either poorly understood or not generally accepted by the scientific community. Claims of effects and efficacy for these modalities have not been verified, and further research is needed to establish not only the veracity of the claims but also to fully confirm the existence of the specific effects reported.

Torsion Fields

The notion of a torsion field is generally credited to the Russian professor Myshkin NP [Yurth DG, 2000] and is based upon the theory that particles with spin are coupled via torsion fields. A collection of relevant experiments is reviewed in a volume by Swanson C [2011]. Torsion fields are of interest to biofield science in that they could provide a theoretical framework for explaining non-EMF interactions and how these might interact with biological systems.

Orgone Energy

Orgone energy is a purported universal life force originally described in the 1930s by the Austrian psychoanalyst Wilhelm Reich [Gardner M, 1957; Blumenfeld R, 2006]. Reich W believed orgone energy to be a massless, omnipresent substance, closely associated with living energy but also present in inert matter. Orgone energy was thought to create organization on all scales using orgone particles called "bions," from the microscopic to macroscopic levels within organisms, clouds, or even galaxies [Bellis M, 2015]. Reich W designed and built special "orgone energy accumulators" to collect and store orgone energy from the environment and claimed these devices could be used for improvement of general health [Blumenfeld R, 2006].

Scalar Waves

Scalar waves are said to be produced when 2 electromagnetic waves of the same frequency are exactly out of phase and cancel with each other [Patten T & Hutchison M, 1991]. Rather than the waves completely disappearing in the destructive interference, it is hypothesized that a transformation of energy into a scalar wave occurs, with the resulting scalar field "reverting back" to a vacuum state of potentiality [Patten T & HHutchison M, 1991]. Scalar waves are purported to explain homeopathy and lymphatic detoxification; treat

diabetes, nearsightedness, kidney stones, Parkinson's disease, strokes, arthritis, and cancer; and reverse the aging process [Scalar Waves Healing Center].

Although the biofield devices described by Muehsam D et al [2015] operate through a great diversity of mechanisms, these devices all share the common quality of being most clearly understood within a biofield framework, wherein information flow or the capacity to create organization acts across hierarchical levels to coordinate biological activity. Elements of this framework are already well accepted by the biomedical community and have been applied through several device modalities, including ECG, EEG, other electrophysiological techniques, some EMF therapies, ultrasound, thermal imaging, and techniques using light like LT. Extraordinary medical and scientific progress has occurred as a result of these modalities and the elucidation of their underlying principles. Further progress is likely to be informed by the recent demonstration of endogenous EMF regulation of a variety of biological processes and indications of quantum information processing in the cytoskeleton [Havelka D et al, 2011; Hameroff S & Penrose, 2014]. These recent results suggest a biophysical basis for biofield coordination of activities across the molecular, cellular, and organismic levels [Glass L, 2001] and may provide testable hypotheses regarding biofield regulation of homeodynamics and mind-body interactions.

In contrast to this growing knowledge of biofield mechanisms, several biofield modalities appear to operate according to principles that are not currently well understood or accepted by mainstream medical science. Further study of those modalities for which there is strong experimental evidence - eg, BE, consciousness and nonlocal interactions, GDV, TCM - may substantially advance our understanding of biofield interactions and their biological and health implications [Shupak NM, 2003]. The growing basic science data and existence of devices operating via consciousness or intention [Hankey A, 2007; Radin D & Nelson R, 2003], which may act through nonlocal quantum correlations, must be taken seriously. Despite long-lasting taboos proscribing study of these phenomena, researchers must have the courage and self-awareness necessary to assess the veracity, specific properties, and general significance of the large and important body of research in this area.

The current existence of biofield devices is a demonstration of the clear, specific, and tangible knowledge that has been gained thus far in biofield science. Devices play prominent cultural and scientific roles in our society, and it is likely that device technologies will be one of the most influential access points for the furthering of biofield research and the dissemination of biofield concepts. Comprehensive study of biofield devices will require a concerted research effort, interdisciplinary collaborations, and sufficient funding. Systematic studies are needed to deepen our understanding of the nature of biofield interactions and to move biofield device development and experimentation forward. This developing field of study presents new areas of research that have many important implications for basic science, clinical medicine, and potentially, the forward progress and evolution of our species. The ever-growing understanding of biofield science holds promise to foster a more humane and personalized form of medicine and an expansion of our scientific viewpoint to include the importance of each individual's interconnectedness with communities, the immediate environment, the earth, and the cosmos [Muehsam D et al, 2015].

Application of electrophoton capture (EPC) analysis based on gas discharge visualization (GDV) technique in medicine

It so happened that our pilot study of the relationship between GDV and neuro-endocrine-immune parameters in March 2010 was preceded by the publication in January 2010 of a systematic review "Application of electrophoton capture (EPC) analysis based on gas discharge visualization (GDV) technique in medicine" [Korotkov KG et al, 2010]. The reader may get the impression that it was precisely the lack in the review of data about the GDV/EEG relationships, not to mention the relationship of GDV with hormones and immune

parameters, determined the topic of our research. In fact, this was not the case. The author of the idea of the project (Popovych IL) is ashamed to admit that in 2010 he still did not know how to use a computer, not to mention the Internet (just like the president of a neighboring state until now). But let's return to the systematic review. In our opinion, the presence of the name of the author of the GDV method in the list of authors of a systematic review about its diagnostic value looks at least unethical, if not to say a conflict of interests. A good overall evaluation of the method, given by third-party authors, would only increase. And now for the essence of the review.

The authors declare that the objective of this study was to evaluate the scale and scope of implementing electrophoton capture (EPC) analysis based on gas discharge visualization (GDV) technique in diverse medical applications and psychophysiology; to identify the range of applications in medicine; and to show in which areas the procedure can be useful to health professionals.

The literature search yielded 136 sources published in peer-reviewed journal articles, theses, monographs, study aids, and proceedings of scientific conferences during the years 2003–2008, each using the GDV method in medicobiological and psychophysiologic investigations. Many doctors and researchers who use GDV cameras or EPC technology in their work are united in the International Union of Medical and Applied Bioelectrography (IUMAB). IUMAB has organized an annual conference called ''Science, Information, Spirit'', held in Saint-Petersburg, Russia, since 1995. Proceedings from this conference provided an initial base for the literature search. Articles related to application of EPC in medicine were also included from proceedings of international scientific conferences such as ''Measuring energy fields'', ''Measuring the human energy field: State of the science'', and some other sources directly related to the EPC (GDV) technology.

Search restrictions were human subjects, English or Russian language, and publication date from 2003 till 2008 (the last 5 years). From all of the articles that were found, reviewers selected only those related to medicine and psychology. Articles were also excluded if they did not present original data or an analysis of original data (excluding commentaries, editorials, or expert opinion pieces), or if they were descriptive surveys. The search yielded a total of 136 articles. Applying the exclusion criteria reduced the collection to 79 papers. Thirteen (13) of 19 RCTs and 19 of 26 SRRs were rated high in both standard checklists. Reviewers have chosen two groups of articles to show the evidence of efficiency of the EPC/GDV method application in the four fields of studies, because they represent the most extensive studies. These are the systematic research reports or articles (SRR) and randomized controlled studies (RCT). These types of articles were chosen because they present results of systematic studies of some group of scientists in one exact medical case, studies that are being carried out for a long period of time, and at the present moment are the most serious, professional, and describe science-based experiments.

Considering the results of all studies listed below, reviewers can conclude that the GDV method or EPC technique can be used in diverse applications in conventional medicine (e.g., preventive assessment of allergic reaction risk, investigation of infectious pathologies, detecting different pathologic processes, anesthesiology and reanimatology, assessment of hirudotherapy effects, monitoring the functional state of patients in postoperative period, and others). The GDV method has shown that it can be implemented as an express method for assessments of treatment rocedure effectiveness.

Results in the psychophysiologic field of study show many different significant correlations between psychophysiologic parameters and parameters of GDV-grams (i.e., processes in the autonomic nervous system, anxiety, neuroticism, functional reserve capacity, emotional and nervous excitation). These results show that the GDV method is a very useful

and quick (express) technique for evaluating emotional and physical conditions in human beings.

In alternative medicine, the GDV technique can be used as an express method for evaluating impact from various treatment procedures. Numerous correlations were found during this research between GDV parameters and the patients' states after treatment procedures.

The GDV method can be applied almost everywhere humans are and in whatever they do. Examples given in these articles show that such human activities as polar expeditions, alcohol drinking, listening to music, focused meditation, and so on are not exceptions from the large field of applications of the EPC technique, and that there are significant correlations in these fields.

The authors of the review admit that there are several limitations to this study. First, the number of studies based on EPC/GDV technique in medicine and psychophysiology is relatively small. The number of all studies based on the GDV technique is not large, because this technique is comparatively young in the scientific world. Reviewers literature search was limited to Russian and English articles. It is possible that some studies were missed because they were not presented during the last 5 years. Despite its young age, the EPC/GDV technique shows very good results in the surveyed fields of study and becomes increasingly popular every year. Another limitation is the possibility of bias in evaluating the studies. Reviewers attempted to avoid this bias by using accepted checklists.

Reviewers have made several conclusions regarding EPC analysis based on the GDV technique in conventional medicine, psychophysiology, alternative medicine, and research studies.

1. Systematic review has revealed that the EPC/GDV method is being used in many different applications in these fields of study and shows excellent or very good results.

2. Researchers have already found diverse correlations between EPC/GDV parameters and various medical, psychologic, and physiologic parameters in humans. Furthermore, they continue their research with an aim to find other correlations.

3. The software and equipment EPC/GDV-complex is a convenient and easy-to-use device, which allows examination of patients with various pathologies and, therefore, offers a wide range of applications. The GDV method has already shown itself to be an express method for evaluating the human organism's psychophysiologic state.

4. The investigations showed that the GDV method delivers valuable diagnostic information on the functional state of patients, allows their state to be monitored, and constitutes a convenient and easy method for conducting preventive examinations of individuals, professional training, and control in various areas of application.

5. All RCTs and SRRs reviewed suggest the GDV method as a prospective and effective method for different nosological and psychophysiologic applications and investigations.

6. There are no negative or undesirable characteristics identified for the GDV method in all reviewed articles.

Also, there are no contraindications to application of the EPC technique.

Among the studies reviewed by the authors, the Cioca GH et al [2004] study is of the greatest retrospective interest to us. GDV and HRV measures were taken in healthy volunteers before and after three different physiological conditions: the orthostatic test consisting of deep breathing followed by rapid standing; ten minutes of strenuous exercise and consumption of chocolate. Statistical significance relationships observed between certain GDV and HRV parameters for all three conditions. In particular, in background was revealed correlation between normalized Area GDI fingers 5R and RRNN (r=0,68), Area 5L-5R fingers and VLF (r=0,64), Area 5L-5R fingers and LF/HF (r=0,61), Entropy 5L-5R fingers and LF (r=0,64), Brightness 5L-5R fingers and RMSSD (r=0,61); in orthostatic test between

Brightness 5L-5R fingers and VLF (r=0,71), Entropy 5L deviation and VLF (r=0,65); in ortho-background test between Brightness 5L-5R fingers and VLF (r=0,71), Entropy 5L deviation and VLF (r=0,66); in exercise test between Stresss Index 10 fingers and LF/HF (r=0,85), Entropy 10 fingers and VLF/HF (r=0,41); in dark chocolate test (three hours after the consumption) between Stresss Index 10 fingers and LF/HF (r=0,81), Entropy 10 fingers and HF (r=0,56), normalized Area GDI of 10 fingers and LF/HF (r=0,51). Cioca GH et al [2004] concluded that these correlations indicate that GDV measures can be used as a measure of well-being in different physiological conditions.

A few more publications on this topic are mentioned in the review, but only in the format of proceedings, moreover, they are not available to us, so we only broadcast them. In particular, Bundzen PV et al [2003] found that basic and integral parameters of optoelectronic emission correlates with humoral-metabolic and reflex regulation processes on the level of the vegetative nervous system. Increase in activity of central (neurohumoral) part of autoregulative mechanisms correspondes with power increase in the optoelectronic emission processes, increase of stress tolerance parameters, and an overall functional index, and corresponds with decrease in an index of energetic deficiency. In the study of Lovygina ON [2005] data obtained by HRV analysis was compared with the GDV results. Statistical correlations between central mechanisms of heart regulation and GDV area parameter were found. According to Krashenuk AI et al [2006], systematic action of hirudotherapy harmonizes functioning of regulative processes in the autonomic nervous system. Therapeutic effects of hirudotherapy were clearly confirmed by the use of monitoring and GDV signals analysis, and also confirmed by nonlinear, fractal and specific analysis of HRV.

Regarding the relationship between GDV and psychophysiological parameters, the authors of the review cite only three works, also in the format of proceedings. According to Polushin US et al [2004], the parameters of ''dynamic'' gas discharge images correlate with the assessment of anxiety by the Spielberger-Khanin scale, which enables using the GDV technique for objective assessment of anxiety for patients before surgical operations. According to O'Keeffe E [2006], excessively high level of the GDV parameter Entropy can indicate mental disorders (e.g., schizophrenia, etc.). If the level of GDV entropy is excessively low, it points to the prospect that this individual may be ''running out of options'' and he is in danger of ''burning out''. Dobson P & O'Keeffe E [2007] discovered significant relationships between GDV parameters and state anxiety and less significant relationships with trait anxiety and neuroticism. Korotkova AK [2006] showed that GDV-gram patterns of right and left hands correlate with parameters of psycho-emotional state and psychophysiologic readiness for sports competitions [Korotkova AK, 2006].

Regarding the connection of GDV with the general adaptive response of the organism, only one work is mentioned [Bykov AT et al, 2006]. The aim of the work was to evaluate the efficiency of using laser therapy on fields and biologically active points under a complex of sanatorium-and-spa treatment for children's diseases of upper air passages based on parametric dynamics of GDV bioelectrography combined with clinical and functional methods of research. The achieved data correlate with figures of cardiointervalogram (neurohumoral activity spectre increase), with nonspecific adaptive responses according to Garkavi LKh et al [1998], and is the evidence of stabilization of the energoinformatic state of organism, formation of long-term adaptation, and allows use of indices of GDV bioelectrography as a method characterizing adaptive mechanisms against a background of sanatorium-and-spa treatment. Thus, the research carried out allows recommendation of GDV bioelectrography as a method of complex diagnostics of an organism's functional state, characterizing alteration of adaptive mechanisms against a background of rehabilitation treatment.

As you can see, on the eve of our research on the relationship between GDV parameters, on the one hand, and parameters of the neuro-endocrine-immune complex, on the other hand, only a few works were published, and even those were only related to HRV and anxiety.

In 2018, Korotkov KG published a "Review of EPI papers on medicine and psychophysiology published in 2008-2018" [Korotkov K, 2018]. However, only two publications turned out to be the focus of our interest.

Sorokin OV [2009] discovered that Area GDI of V right finnger in patients with ischemic heart disease correlate direct with the plasma levels of creatinphosphokinase, protein, direct bilirubin, and glucose. The decrease in Area accompanied with the increase in centralization HRV. The increase in total power HRV associated with the increase in intensity of luminescence of skin.

In the study of Korobka IE et al [2017], to assess the state of the autonomic nervous system of healthy and hypertensive patients the methods of HRV and GDV were applied. In this paper authors used two main parameters. The integral area is an amount of light quanta generated by the subject in computer unit's pixels (the number of pixels in the image having brightness above the threshold). Authors used both the total area of all 10 fingers and the area of fingers of the left and right hands separate. Stress coefficient (unlike to Activation coefficient!?) calculated as the ratio between the total area of the particular subject and the total area of the ideal healthy person, calculated from statistics of 8000 people.

It was revealed that the hypertensive patients differed from the control group in the **HRV Stress index**, and, for hypertensive patients, it exceeded the normal value. The same result was found for the **GDV Stress index**. Men had a shift in the autonomic balance toward the predominance of the sympathetic nervous system, while in women the autonomic balance is shifted toward predominance of the parasympathetic nervous system. This is valid both for healthy and hypertensive people. Moreover, for men lower activity of the parasympathetic center of the autonomic nervous center was observed. There were significant differences in GDV indexes. The integral area of luminescence of fingers of right and left hands, and the total area of the image, had lower values for men compared to women, which also indicates a bias in men of autonomic balance toward the sympathetic nervous system, and confirms the **dependence of the GDV indexes on the activity of the autonomic nervous system.** Hypertensive women differed from healthy ones by lower GDV parameters, which indicate the decrease in functional reserves of the organism and autonomic imbalance.

However, it would be desirable for the authors to support their conclusions with a correlational analysis, which, unfortunately, was not conducted.

We were even more disappointed by a recent article by our compatriots [Nevoit GV et al, 2020], in which the HRV and GDV parameters registered in 82 people were not compared at all (!?). Hopefully this is just a pilot study.

Despite the fact that as of 2018, we already had 20 publications (including 8 articles) on the topic of the review by colleague Korotkov KG, none of them was honored to be cited. In our humble opinion, the author of the review deprived himself.

But in May 2022, when this monograph was being prepared for publication, we received through the Researce Gate resource (to which a special big thank you for everything!) a good systematic review by Indian colleagues Bista S et al [2022; Epub ahead of print], which we quote with undisguised pleasure.

The research team screened 99107 research articles, and 98 999 articles were excluded due to the following reasons: (1) didn't deal with a GDV device, (2) didn't deal with human participants, (3) were published before the year 2000, and (4) were published in a language other than English.

After excluding duplicates, the research team extracted 108 publications that dealt with the application of GDV in human participants. Of these 108 articles, 66 were further excluded for

being either review articles, case studies, letters to the editor, or articles with an unclear methodology. Forty- two studies satisfied the selection criteria and were included in the review.

The 42 studies included eight randomized controlled trials (RCTs), five nonrandomized controlled studies, 17 cross-sectional studies, 10 single-group pre-post studies, and **two correlational studies.**

In the subsections below, the research team has divided the studies into three broad categories for ease of discussion: (1) applications of GDV in health; (2) diagnostic applications of GDV in disease; and (3) applications of GDV in monitoring the effects of therapeutic interventions.

Applications in Health

One study developed normative data for GDV variables for the Indian population that was generated by acquiring GDV-grams of 584 males and 296 females aged 18 to 60 years [Kushwah KK et al, 2016]. Those researchers found that EPI norms for a healthy Indian population were different from European norms, especially for the EPI parameter for IA. The normative range for various GDV variables was as follows: (1) AC, 2.0 to 3.5; (2) IA with a filter, 0.2 to 0.6; (3) IE with a filter, 1.7 to 2.1; (4) IA without a filter, -0.3 to +0.4; and (5) IE without a filter, 1.6 to 2.1.

GDV and gender differences. In a cross-sectional study, the GDV parameters IA and total area had lower values for men than for women [Korobka I et al, 2017]. Another study conducted with an Indian population showed that males had higher values than females in some GDV parameters, the IAR and IAL without a filter and the IAL with a filter [Kushwah KK et al, 2015]. Other studies have reported similar gender differences among meditators and nonmeditators [Deo G et al, 2015; 2016].

Correlation with neuroendocrinological variables. Sone studies have demonstrated that GDV parameters can be influenced by the functions of the neuroendocrinal axis. A study involving 10 women and 10 men aged 33 to 76 years, with a dysfunction of the neuro-endocrine-immune complex and no conclusive clinical diagnosis, displayed correlations, using canonical correlation analysis, between GDV variables and some hormone levels [Babelyuk VY et al, 2017]. These were testosterone, cortisol, calcitonin, triiodothyronine, and aldosterone. The coefficient of canonical correlation between the neuroendocrine constellation and the GDV variables was 0.970.

Another study on remote intercessory prayer (IP) demonstrated a significant correlation between several baseline GDV parameters and the Symptom Index, a quantitative measure developed for assessing the relationship between gastroesophageal reflux and symptoms [Dunlap JH, 2004]. The study found that the area value for the filtered left fourth (4L) finger negatively correlated with the dehydroepiandrosterone (DHEA) at baseline (r = -0.28, *P* = .01).

Correlation with heart rate variability (HRV) and electroencephalography (EEG). One study was conducted to assess the correlation between GDV and HRV variables in three tests of physiological conditions: (1) an orthostatic test with deep breathing for 5 minutes (n = 24), (2) strenuous exercise for 10 minutes (n = 43), and (3) consumption of chocolate (n = 12) [Cioca G et al, 2004]. The study found that some baseline parameters of GDV and HRV had a significant correlation: (1) the NA for the fifth right-hand finger (5R) and the mean RR normal-to-normal intervals (RRNN), with r = 0.68; (2) the areas for the fifth left-hand finger (5L) and the 5R and the very low frequency (VLF) from the HRV with r = 0.64; (3) the areas for the 5L and 5R and the ratio of the low frequency (LF) to the high frequency (HF) from the HRV, with r = 0.61; (4) the entropy for the 5L and 5R and the LF, with r = 0.64; and (5) the brightness for the 5L and 5R and the root mean square of successive differences (RMSSD), with r = 0.61.

Another study conducted with 20 volunteers with dysfunction of the neuro-endocrine-immune complex, demonstrated that the GDV constellation correlated with Baevsky's Stress Index (SI), with r = 0.80 and $P <$ .00001, and with the LF/HF ratio, with r = 0.76 and $P <$ .0001 of the HRV [Babelyuk VY et al, 2017].

In another recent study with children with spastic forms of cerebral palsy, the changes in GDV parameters, including the area of the image in the frontal projection (energy field in the frontal area, both sides) and the entropy (degree of disorder or randomness in the system) in the frontal and left projections, after two weeks of use of the intensive neurophysiological rehabilitation system (Kozyavkin© method) were closely related to changes in the parameters for both the HRV ($R^2 = 0.999$) and the EEG ($R^2 = 0.998$) [Kozyavkina OV et al, 2018].

The following studies cited in the review are not directly related to the topic of our monograph. However, in the next monograph, which is being prepared for publication, GDV will be at least an equal, if not the main, method of researching the effects on the body of Prayer, Reiki, kata of Kyokushin Karate, as well as Holy water. So the next block of review is quite appropriate.

Applications to Monitor the Effects of Interventions

The sensitivity of GDV in assessing subtle changes in energy systems has opened up a new dimension for monitoring the effects of ultrasensitive interventions, such as yoga, including pranayama and meditations; acupuncture; massage; osteopathy; and music.

Massage and osteopathic treatments and neurophysiological rehabilitation. A study with 23 healthy adults investigating the effects of 50-minute, Swedish, full-body massage on GDV parameters showed a significant reduction in some variables: average of IAR and IAL, from 0.13 to 0.3 ($P =$ .004) and left integral entropy, from 2.04 to 1.88 ($P =$ .002) [Haun J et al, 2015].

Korotkov KG et al [2012] studied the effects of a single session of an osteopathic treatment on GDV variables and blood pressure in 33 healthy adults. The study found a reduction in the AC after the osteopathic session, from 86% to 83%. Participants' average systolic blood pressure decreased from 122±14 to 117±12 mm Hg; their diastolic blood pressure decreased from 74±10 to 73±8 mmHg; and their pulse rates decreased from 74±10 to 71±10 bpm.

Another study evaluating the effects of use of an Kozyavkin© method for two weeks for 14 children with spastic form of cerebral palsy showed an increase postintervention in the area of the image in the frontal projection and a decrease in its entropy in the frontal and left projections [Kozyavkina OV et al, 2018].

Acupuncture. In a randomized cross-over study with 34 healthy participants, with 18 receiving authentic acupuncture (AA) and 16 receiving sham acupuncture (SA) during the first session [Roberts NR et al, 2004]. The study's assessments were performed at baseline and at 5 minutes and 30 minutes after needle removal. The 15 minutes of needling occurred at five acupuncture points: bilaterally at large intestine-4, bilaterally at liver-3, and at the governor vessel-20. The S-integer or "symmetry" value (a quantifiable value of the balance depicted in the GDV imagery) on the right side showed a significant increase for the AA at 5 minutes, which was sustained until 30 minutes after the needle removal, whereas the SA showed no significant changes on the S-integer on either side.

Dietary interventions. A recent RCT investigated the influence of diet on GDV variables for 58 healthy adults, 31 males and 27 females [Shankar NR et al, 2016]. The participants were randomly allocated to one of two groups: coconut (C) and groundnut (G). For 90 days, the C group ate a coconut diet that included dishes with raw coconut, and the G group ate a groundnut diet that included roasted and boiled groundnuts served in various forms. The results showed no significant changes in the GDV parameters postintervention, but the

hemoglobin (Hb) value was significantly higher for the C group than for the G group postintervention.

Music therapy.- One study compared the immediate effects of 45 minutes of an active music intervention (AMI) and a silent music intervention (SMI) for 29 patients with T2DM [Rao IT & Nagendra RH, 2014]. The study found a statistically greater increase in the AC and in the reduction in the integral entropy variables after the AMI as compared to the SMI.

Another study with 49 participants, 19 HCs and 30 people suffering from chronic noncommunicable diseases (NCDs), reported a significant increase for the NCDs in the GDV anxiety (a psychological variable reported by GDV device based on activation of sympathetic nervous system), area, and brightness after listening to music (Pachelbel's Canon) for 15 minutes [Gibson SS, 2004]. The same group of participants also performed focused meditation for 15 minutes and reported a further significant increase in the brightness parameter of the GDV-gram.

Another similar study found an increase in the overall area and intensity for 16 students after listening to Indian devotional music for 2.5 hours [Rao TI et al, 2014].

Meditation and other yogic practices. Yoga is an ancient and traditional science that includes the practice of specific postures, regulated breathing, and meditation. Yoga practices are known to enhance the physical and psychological well-being of practitioners. Studies have observed variations in various GDV parameters after different types of spiritual practices across gender, different stages of yoga practice, and expertise.

Meditation. A single-group, pre-post study investigated the effects of 3.5 hours of Anapanasati meditation daily for 5 days on GDV variables for 51 healthy adults, 32 males and 19 females [Deo G et al, 2015]. A significant reduction in the IAR and IAL was found postintervention.

Another study compared the impact of meditation on 184 long-term meditators (LTM), with experience of more than five years, and 248 short-term meditators (STM), with experience from six months to five years [Deo G et al, 2016]. The study showed significant differences between genders. In both LTM and STM, lower values of stress (activation coefficient) were found in woman meditators as compared to men. In both groups, highly significant gender-related differences were observed in integral area parameter, which measures the overall health of an individual. The AC was smaller and the integral entropy was greater for the LTM women than the STM women.

Another similar study contrasted GDV parameters between an LTM group (n = 105) and a naive meditator (NM) group (n = 53) and showed a significantly higher integral entropy for the LTM group [Deo G et al, 2015]. Another RCT with 66 male managers, 33 who practiced cyclic meditation (CM) and 33 who practiced supine rest (SR) for 35 minutes, revealed that the integral entropy and stress level decreased and the IA variable increased significantly more after CM than after SR [Kushwah KK et al, 2016].

Integrated Yoga Program (IYP). The effects of a four-week residential IYP on GDV measures were studied with 152 healthy volunteers ranging in age between 18 and 60 years [Kushwah KK et al, 2015]. The study recruited and enrolled individuals having an IA value between -0.6 and +1, the normal health-index range as per the GDV manual. The yoga program comprised cleansing techniques; yoga postures; breathing practices; meditation; devotional songs; yogic games; the satwik diet, a vegetarian diet described in yoga science; and spiritual discourses. The study found a significant reduction in the AC postintervention. Both the IAL and the IAR without filters had increased significantly postintervention.

Bhat BK et al [2017] studied the effects of a similar seven-day, residential IYP with 37 patients with T2DM, with a mean age of 54.46±7.21 years. Significant mean differences were found postintervention: (1) for the IA, 630.465 (P = .0004); (2) for the FC, -1.783 (P = .0001); (3) for entropy, -0.029 (P = .0012); (4) for the energy levels of the liver, 0.247 (P = .0001); (5)

for the pancreas, 0.176 (p=0.0250); (6) for the coronary vessels, 0.142 (P = .0001); (7) for the cerebral vessels, 0.192 (P = .0002); (8) for the left kidney, 0.157 (P = .0042); and (9) for the right kidney, 0.248 (P = .0001).

Yogasana. One study following a single arm self-as-control design assessed the acute effects of a series of eight yogic postures - ardha chakrasana, padahasthasana, ustrasana, paschimatanasana, sarvangasana, matysyasana, bhujangasana, and salabhasana - on GDV variables for 21 healthy male volunteers aged between18 and 30 years [Sahoo S & Pradhan B, 2015]. Four relaxation postures were given for a control session: tadasana, sithila dandasana, savasana, and makarasana. No significant changes were found after the yoga practice for the intervention or control session. Another similar study with 18 healthy volunteers, 6 females and 12 males, also showed no significant changes in the GDV variables after a Yogasana session [Sushrutha S et al, 2014].

Yajna. Two studies assessed the effects of yajnas on GDV variables. One study found that Bhaishajya Maha Yajna exposure could reduce the IA, whereas no change occurred in entropy [Sushrutha S et al, 2014a]. In another study, these authors compared the effects of 70 minutes of Saraswathi yajna and 60 minutes of a yogasana session on GDV variables for 18 healthy volunteers and demonstrated a significant reduction in the AC after the yajna session (P = .021) [Sushrutha S et al, 2014].

Mudras. An RCT investigating the effects of mudra practice on GDV variables was conducted with 61 volunteers [Kumar K et al, 2018]. The mudra group practiced prana mudra with closed eyes for five minutes in a sitting posture. The control group sat quietly with eyes closed for five minutes. In the second part of the study, the mudra practice was graduated to 10 minutes on the first day, 15 minutes on the second day, and 20 minutes on the third day. The results showed no differences in the GDV variables between the groups. However, significant differences were found in the average intensity and entropy between the effects of mudra practiced for 10 minutes and that practiced for 20 minutes.

Dayan qigong. Rubik B & Brooks AJ [2005] investigated the effects on GDV variables for 16 adults, aged 48 to 80 years, of a one-day qigong workshop that included intense Dayan qigong (wild goose form). The GDV analysis showed a significant increase in the density on the GDV-grams after a qigong session, from 0.40±0.04 to 0.43±0.04 (P < .01).

Prayer. The effects of remote intercessory prayer (IP) once a week for 12 weeks, was studied on GDV variables with 85 healthy male volunteers [Dunlap JH, 2004]. Participants were divided into two groups randomly: a remote IP group (n = 42) and acontrol group (n = 43). The study found no significant differences in the changes in the GDV parameters between the IP and control groups postintervention.

Bista S et al [2022] conclude the review as follows.

Though more studies with a robust methodology are needed to make definitive conclusions, current literature review suggests a potential clinical role for GDV in the diagnosis and monitoring of patients suffering from various disorders, especially those related to ***endocrine and immune systems*** [*highlighted by us*], and for assessing wellness of healthy subjects. GDV may also be useful in monitoring the effects of ultrasensitive interventions, such as yoga, including pranayama and meditation; acupuncture; qigong; music therapy; and massage. Values of GDV variables outside a defined range indicate a disturbance in homeostasis that may predispose people to different disorders. The interventions should aim at bringing the values of the variables back to a normal range. Normative data for a few GDV variables is available for the Indian population, but research is needed to provide normative data for other variables and to validate GDV variables with the gold-standard diagnostic tools in medicine.

Chapter 2

PILOT RESEARCH

The first study was carried out by us in March 2010. The subjects of the study were 8 volunteers (5 women aged 24÷69 years and 3 men aged 35÷57 years). The main subject of research is the bioelectrogram (kirlianogram) of the tips of all fingers.

In the morning we registered bioelectrogram by the method of GDV by the device of "GDV Chamber" ("Biotechprogress", SPb, RF). The first base parameter of GDV is Area (A) of gas discharge/electrophotonic imaging (GDI/EPI) in Right, Frontal and Left projections registered both with and without polyethylene filter (F). The second base parameter is the Shape Coefficient (SC, ratio of square of length of external contour of GDI toward his area), which characterizes the measure of serration/fractality of external contour. The third base parameter of GDI is the Entropy (E), id est measure of chaos. It is considered that GDI, taken off without filter, characterizes the functional changes of organism, and with a filter characterizes organic changes [Korotkov KG, 2001; 2007; 2014].

Then we recorded during 7 min electrocardiogram in II lead to assess the parameters of heart rate variability (HRV) (by hardware-software complex "CardioLab+HRV" produced by "KhAI-Medica", Kharkiv, Ukraine). For further analysis the following parameters HRV were selected.

Baevskiy's parameters: the Mode (Mo), the Amplitude of Mode (AMo), the Variation Scope (MxDMn) [Baevskiy RM, Ivanov GG, 2001].

Temporal parameters (Time Domain Methods): heart rate (HR), the standart deviation of all NN intervals (SDNN), the square root of the mean of the sum of the squares of differences between adjacent NN intervals (RMSSD), the percent of interval differences of successive NN intervals greater than 50 ms (pNN$_{50}$), triangular index (TINN).

Spectral parameters (Frequency Domain Methods): power spectral density (PSD) bands of HRV: high-frequency (HF, range 0,40÷0,15 Hz), low-frequency (LF, range 0,15÷0,04 Hz), very low-frequency (VLF, range 0,040÷0,015 Hz) and ultralow-frequency (ULF, range 0,015÷0,003 Hz) [HRV, 1996; Berntson GG et al, 1997; Shaffer F & Ginsberg JP, 2017].

Calculated classical indexes: LF/HF, LFnu=100%•LF/(LF+HF), Baevskiy's Stress Index (BSI=AMo/2•Mo•MxDMn) and Baevskiy's Activity Regulatory Systems Index (BARSI) [Baevskiy RM & Ivanov GG, 2001].

Blood pressure simultaneously with HR was measured by the "Omron M4-I" device (Netherlands). Based on the obtained data, the Kerdoe's vegetative index [Kerdö I, 1966; Fajda OI et al, 2015] was calculated according to the equation: KVI = 100•(1-BPd/HR).

At the end of the day, all tests were repeated. The digital material was processed using the methods of factor, correlation-regression and canonical analyzes using the "Statistica 5.5" software package.

The interpretation of HRV parameters is outlined in an excellent review by Shaffer F & Ginsberg JP [2017]. Here are the main provisions.

Both sympathetic (SNS) and parasympathetic (PNS) nervous system activity contribute to SDNN and it is highly correlated with ULF, VLF and LF band power, and total power. The pNN$_{50}$ is closely correlated with PNS activity. It is correlated with the RMSSD and HF power. However, the RMSSD typically provides a better assessment of respiratory sinus arrhythmia (RSA) (especially in older subjects) and most researchers prefer it to the pNN$_{50}$. The RMSSD reflects the beat-to-beat variance in HR and is the primary time-domain measure used to estimate the vagally mediated changes reflected in HRV. The RMSSD is more influenced by the PNS than SDNN. The TINN is the baseline width of a histogram displaying NN intervals. Like SDNN and RMSSD, contamination by only two artifacts within a 5-min segment can significantly distort its value.

The ULF band (0,015÷0,003 Hz) registered by complex "CardioLab+HRV" is actually the lower zone of the VLF band (0,040÷0,0033 Hz) in foreign devices (perhaps by analogy with the width of a railway track?). Within a 5-min sample, there are about 0–12 complete periods of VLF oscillation. The VLF rhythm may be fundamental to health. Low VLF power has been shown to be associated with arrhythmic death and PTSD.

There is uncertainty regarding the physiological mechanisms responsible for activity within this band.

Akselrod S et al [1981] in pioneering experiment on seven trained, conscious, unanesthetized dogs illustrated that after adequate parasympathetic blockade the LF (then it was nominated as mid-frequency) and HF peaks are abolished, while the amplitude of the VLF (was nominated as low-frequency) peak is reduced. Combined β-sympathetic and parasympathetic blockade abolishes all HR fluctuations leading to a metronome-like heartbeat. β-sympathetic blockade alone tends to reduce the VLF peak's amplitude, but this effect is not consistent because of the low tonic level of sympathetic activity in the resting dog. Increasing the activity of either the sympathetic (by vasodilator-induced decreasing arterial pressure) or parasympathetic (by vasoconstrictor-induced increasing blood pressure) nervous system augments the area under the VLF peak. Therefore, the PSNS mediates HR fluctuations at frequencies corresponding to the LF and HF peaks of the power spectrum, whereas both SNS and PSNS may mediate the VLF fluctuations. Selective adequate blockade of renin-angiotensin system (by converting enzyme inhibitor) lead to 2-4,5-fold increase in the area under the VLF peak. The authors concluded that sympathetic and parasympathetic nervous activity make frequency-specific contribution to the heart rate power spectrum, and that renin-angiotensin-[aldosterone] system activity strongly modulates the amplitude of the spectral peak located at 0,04 Hz. Taylor JA et al [1998] used blocking drugs to evaluate potential contribution of sympathetic and vagal mechanisms and the renin-angiotensin-aldosterone system to VLF (0,003÷0,03 Hz) HRV in 10 young healthy subjects. Beta-adrenergic blockade had no significant effect on VLF or LF (0,05÷0,15 Hz) power but increased HF (0,2÷0,3 Hz) power 2-fold. ACE blockade had no significant effect on LF or HF power but modestly (approximately 21%) increased VLF power in the supine (but not upright tilt) position. The most profound effects were exerted by parasympathetic blockade: atropine, given alone or with atenolol, abolished nearly all HRV and decreased VLF HRV by 92%. Authors concluded that although VLF band are influenced by the renin-angiotensin-aldosterone system, as LF and HF bands, they depend primarily on the presence of parasympathetic outflow. Therefore, the prognostic value of VLF oscillations may derive from the fundamental importance of parasympathetic mechanisms in cardiovascular health. Recently Del Valle-Mandragon L et al [2022] showing that during hemodialysis angiotensin II had a positive correlation with VLF (r=0,390) and with LF/HF (r=0,359) and a negative correlation with LF (r=-0,262) and HF (r=-0,383) bands. Low power in VLF band has been associated with high level of inflammation markers in several studies [Carney RM et al., 2007; Lampert R et al., 2008]. Finally, low VLF power has been correlated with low levels of testosterone, while other biochemical markers, such as those mediated by the hypothalamic–pituitary–adrenal axis (e.g., cortisol), have not [Theorell T et al., 2007; Hasson D et al., 2009]. So, the ambiguity of judgments about VLF continues.

The heart's intrinsic nervous system appears to contribute to the VLF rhythm and the SNS influences the amplitude and frequency of its oscillations. The VLF rhythm appears to be generated by the stimulation of afferent sensory neurons in the heart. This, in turn, activates various levels of the feedback and feed-forward loops in the heart's intrinsic cardiac nervous system, as well as between the heart, the extrinsic cardiac ganglia, and spinal column. This experimental evidence suggests that the heart intrinsically generates the VLF rhythm and

efferent SNS activity due to physical activity and stress responses modulates its amplitude and frequency [Shaffer F & Ginsberg JP, 2017].

The LF band (0,04÷0,15 Hz) is typically recorded over a minimum 2 min period. This region was previously called the baroreceptor range because it mainly reflects baroreceptor activity during resting conditions. LF power may be produced by both the PNS and SNS, and blood pressure regulation *via* baroreceptors, primarily by the PNS, or by baroreflex activity alone. The SNS does not appear to produce rhythms much above 0,1 Hz, while the parasympathetic system can be observed to affect heart rhythms down to 0,05 Hz (20 s rhythm). In resting conditions, the LF band reflects baroreflex activity and not cardiac sympathetic innervation. During periods of slow respiration rates, vagal activity can easily generate oscillations in the heart rhythms that cross over into the LF band. Therefore, respiratory-related efferent vagally mediated influences are particularly present in the LF band when respiration rates are below 8,5 bpm or 7 s periods or when one sighs or takes a deep breath [Shaffer F & Ginsberg JP, 2017].

The HF or respiratory band (0,15÷0,40 Hz) is conventionally recorded over a minimum 1 min period. For infants and children, who breathe faster than adults, the resting range can be adjusted to 0,24÷1,04 Hz. The HF band reflects parasympathetic activity and is called the respiratory band because it corresponds to the HR variations related to the respiratory cycle. These phasic HR changes are known as RSA and may not be a pure index of cardiac vagal control. Heart rate accelerates during inspiration and slows during expiration. During inhalation, the cardiovascular center inhibits vagal outflow resulting in speeding the HR. Conversely, during exhalation, it restores vagal outflow resulting in slowing the HR via the release of acetylcholine. Total vagal blockage virtually eliminates HF oscillations and reduces power in the LF range. HF power is highly correlated with the pNN_{50} and RMSSD time-domain measures. HF band power may increase at night and decrease during the day. Lower HF power is correlated with stress, panic, anxiety, or worry. The modulation of vagal tone helps maintain the dynamic autonomic regulation important for cardiovascular health. Deficient vagal inhibition is implicated in increased morbidity [Thayer JF et al, 2010].

While HF power indexes vagal modulation of HR, it does not represent vagal tone. If shifts in HF power mirrored shifts in vagal tone, they should produce corresponding changes in average HR. But, breathing at different rates within the 9–24 bpm range, which changes HF power, does not change mean HR. RSA and vagal tone are dissociated during large-scale changes in SNS activity, chemical blockade of the SA node, and when intense vagal efferent traffic dramatically slows HR during inhalation and exhalation. Shifts in respiration rate and volume can markedly change HRV indices (HF power, RSA, pNN_{50}, RMSSD) without actually affecting vagal tone, but under controlled conditions while breathing at normal rates, we can use HF power to estimate vagal tone.

The ratio of LF to HF power (LF/HF ratio) was originally based on 24 h recordings, during which both PNS and SNS activity contribute to LF power, and PNS activity primarily contributes to HF power. The intent was to estimate the ratio between SNS and PNS activity. The assumptions underlying the LF/HF ratio is that LF power may be generated by the SNS while HF power is produced by the PNS. In this model, a low LF/HF ratio reflects parasympathetic dominance. This is seen when we conserve energy and engage in tend-and-befriend behaviors. In contrast, a high LF/HF ratio indicates sympathetic dominance, which occurs when we engage in fight-or-flight behaviors or parasympathetic withdrawal. Other authors challenged the belief that the LF/HF ratio measures "sympatho-vagal balance". First, LF power is not a pure index of SNS drive. Half of the variability in this frequency band is due to the PNS and a smaller proportion is produced by unspecified factors. Second, PNS and SNS interactions are complex, non-linear, and frequently non-reciprocal. Third, confounding by respiration mechanics and resting HR creates uncertainty regarding PNS and SNS

contributions to the LF/HF ratio during the measurement period. Shaffer F & Ginsberg JP [2017] warned that the LF/HF ratio is controversial because different processes appear to generate 24 h and 5 min values, and these values correlate poorly. Furthermore, the SNS contribution to LF power varies profoundly with testing conditions. For example, when LF is calculated while sitting upright during resting conditions, the primary contributors are PNS activity and baroreflex activity - not SNS activity. Therefore, interpretation of 5 min resting baseline LF/HF ratios depends on specific measurement conditions.

It is time to present the obtained results.

At the first stage, the HRV, BP and GDV matrix was subjected to factor analysis (by principal components method [Kim JO & Mueller ChW, 1989]). Principal components (PC) are linear combinations of observed variables that possess orthogonality properties, i.e., they are natural orthogonal functions. The essence of the PC method is the linear transformation and condensation of the initial information. In order to find the matrix of the factor mapping closest to the simplest ideal structure, the procedure of orthogonal rotation by the varimax method was carried out.

The summary of the factor analysis by the PC method of the field of variables is shown in the Table 2.1, which is, in essence, a factor mapping matrix, the elements of which are factor loadings - correlation coefficients between PC and variables. It was found that 93,4% of the variance of the information field is explained by eight PCs, and the minimally sufficient (critical) share of variability (2/3) is explained by three PCs (70,3%). Therefore, to study the factor structure of the field under study, one can limit oneself to the consideration of the first three GCs.

Table 2.1. Factor loadings (Varimax normalized) of HRV, blood pressure and GDV parameters

Variables	PC1	PC2	PC3	PC4	PC5	PC6	PC7	PC8
TINN	**0,97**							
Total Power	**0,96**							
MxDMn	**0,95**							
LF	**0,95**							
ULF	**0,95**							
pNN$_{50}$	**0,94**							
SDNN	**0,93**							
HF	**0,88**							
AMo	**0,84**							
RMSSD	**0,75**							
AFWF	**0,74**							
Baevskiy's SI	0,69							
Korotkov's AI	0,67							
SCRWF	0,66							0,64
ARWF	0,63							
VLF	0,63		-0,58					
SCFWF	0,57		-0,56					
AFF		**0,95**						
ALF		**0,90**						
MRR		**0,81**						
Mode	0,51	**0,80**						
HR		**0,72**						
ARF		0,69						
LF%		0,64						
SCLWF			**0,84**					
VLF%			**0,82**					
HF%		0,55	**0,77**					
ALWF			**0,71**					
LF/HF		0,58	0,65					
SCLF			0,49					
EFF				**0,90**				
ELF				**0,78**				
SCRF				**0,75**				
ELWF				**0,70**				
EFWF				0,64				

SCFF			0,51				
SymWF				0,88			
SymF				0,79			
BARSI				0,72			
ERF					0,80		
BPd					0,77		
BPs					0,71		
KVI=1-BPd/HR		-0,54			0,61		
ULF%						0,88	
ERWF					-0,49	0,51	0,61

The first PC, by definition, reproduces the maximum share of the variability of the information field – 41,2%, it is very closely and closely correlated, on the one hand, with 19 HRV parameters, and on the other - closely and significantly with 5 GDV parameters, which immediately proves the existence of a significant relationship between these HRV and GDV parameters, because only interconnected variables are combined in each PC.

So, the first PC contains information about the activity of cholinergic-adrenergic regulatory influences at different levels of the nervous system. At the same time, the GDV parameters were also found in the composition of this PC: the area (A) of the frontal (F) projection of the GDI taken without a filter (WF), the area of the right (R) projection, the shape coefficients (C) of the right and frontal projections, also without filter This is in excellent agreement with one of the fundamental principles of bioelectrography, that the GDV-grams without a filter reflect the peculiarities of the vegetative status at the moment of time, in particular, the activity of cholinergic sympathetic fibers of the skin, which stimulate sweating.

Here is the calculated Korotkov's activation index (KAI), which, according to our data, is closely inversely correlated with AFWF (r=-0,82) and ARWF (r=-0,78) and directly with CFWF (r=0,82) and CRWF (r=0,67), while the correlation is weaker with parameters of the left (L) projection (r= -0,54 and 0,54 with ALWF and CLWF, respectively).

The second PC explains 18,5% of the variability of the information field and contains, on the one hand, indicators characterizing the level of circulating catecholamines. On the other hand, there are indicators of the area of the frontal, left and right projections of the GDI taken with the filter (F).

The third PC (absorbs 10,6% of the variance), unlike the previous ones, contains information about the left GDI projection without a filter, associated with the relative levels of sympathetic (VLF%) and vagal (HF%) activities and their balance (LF/HF).

The fourth PC (7,0% variability) does not deserve attention in the context of our presentation, since it contains information only about the GDI entropy.

Instead, the fifth PC, explaining only 6,0% of the variance, again combines the parameters of both methods - the symmetry of the frontal projection of the GDI without filter and with the filter and Baevsky's activity regulatory systems index (BARSI), which is almost equally strongly correlated with both of them (r= 0,68 and 0,52, respectively).

Finally, the sixth PC (4,0% variability) combines the entropy of the unfiltered GDI in right projection with blood pressure and the calculated Kerdoe's autonomic index (KVI). By the way, the latter gives a moderate factor load on the second PC, which characterizes the GDI areas of various projections without a filter.

So, even at the stage of factor analysis, it was possible to identify regular relationships between the HRV&BP and GDV parameters, the presence of which is evidenced by the fact that the parameters belong to common main components.

In preparation for the second stage of the analysis of HRV/GDV relationships, we will first consider the matrix of correlations between the GDV parameters themselves (Table 2.2).

According to the equation: $|r| \geq \{exp[2t/(n-1,5)^{0,5}] - 1\}/\{exp[2t/(n-1,5)^{0,5}] + 1\}$,

for a sample with 16 observations, the critical value of the modulus of the correlation coefficient at p<0,05 (t>2,14) is |0,51|, at p<0,01 (t>2,98) is |0,65|.

It has been established that the connections between the area of the GDI and its entropy and between the entropy and the shape coefficient are practically absent in all projections and under both conditions of registration, which indicates the independent informativeness of these GDV parameters. The areas of the GDI in all three projections, taken without a filter, practically do not correlate at all with those taken with a filter, and therefore reflect different parameters of the body. The relationships between the shape coefficients and the entropies of the GDI taken under different conditions do not reach significance levels, and only the GDI entropy of the left projection is little affected by the application of the filter (r=0,72).

Table 2.2. Matrix of correlations between parameters of bioelectrography

Variable	ARWF	ERWF	CRWF	AFWF	SyFWF	EFWF	CFWF	ALWF	ELWF	CLWF	ARF	ERF	CRF	AFF	SyFF	EFF	CFF	ALF	ELF
ARWF																			
ERWF	0,29																		
SCRWF	**-0,75**	0,24																	
AFWF	**0,87**	0,16	**-0,72**																
SyFWF	0,53	0,16	-0,22	0,43															
EFWF	-0,34	0,09	0,37	-0,19	-0,42														
SCFWF	**-0,75**	-0,14	**0,69**	**-0,81**	-0,23	0,20													
ALWF	0,54	0,47	-0,27	**0,70**	0,23	0,12	**-0,72**												
ELWF	-0,51	0,23	0,46	-0,44	-0,53	**0,69**	0,47	-0,02											
SCLWF	-0,50	-0,32	0,32	-0,62	-0,14	-0,03	**0,79**	**-0,88**	0,16										
ARF	-0,12	0,28	0,31	0,06	-0,07	0,17	0,09	0,37	0,11	-0,32									
ERF	0,16	0,34	-0,20	0,15	-0,09	-0,16	-0,08	0,14	0,26	0,03	-0,26								
SCRF	0,30	-0,11	-0,41	0,20	-0,14	-0,38	-0,52	-0,01	-0,60	-0,25	-0,21	0,02							
AFF	-0,05	-0,22	-0,07	0,14	-0,15	0,01	0,25	-0,10	0,04	0,19	0,51	-0,18	-0,36						
SyFF	0,15	0,34	0,28	0,14	0,64	-0,02	-0,08	0,30	-0,17	-0,27	0,33	-0,23	-0,14	-0,30					
EFF	0,05	-0,08	-0,22	0,11	0,02	0,44	0,01	0,14	0,49	0,06	-0,39	0,13	-0,57	0,00	-0,28				
SCFF	0,36	-0,30	-0,31	0,25	0,50	-0,56	-0,12	-0,38	**-0,72**	0,26	-0,40	-0,12	0,35	0,00	0,20	-0,34			
ALF	-0,26	0,00	0,22	-0,08	-0,40	0,11	0,23	0,06	0,15	**0,85**	-0,25	-0,15	**0,78**	-0,16	-0,35	-0,35			
ELF	-0,27	0,03	0,19	-0,11	-0,15	0,42	0,40	0,02	**0,72**	0,25	0,18	0,13	**-0,86**	0,46	-0,07	0,62	-0,41	0,25	
SCLF	-0,01	0,00	0,23	-0,19	0,44	-0,49	0,24	-0,43	-0,34	0,39	-0,39	0,14	0,07	-0,32	0,40	-0,39	**0,72**	-0,47	-0,27

Notes: A - area, E - entropy, SC - shape coefficient of right (R), frontal (F) and left (L) projections without filter (WF) and with filter (F). Highlighted modules with significance **p<0,01** and p<0,05 and *insignificant*.

The filter does not affect the connections, or rather their absence, between the entropies of the GDI of the lateral projections. The areas of the lateral projections under normal conditions are very moderately correlated (r=0,54), on the other hand, when the filter is used, their correlation significantly increases (r=0,85), therefore, the filter, leveling the effect on GDI of perspiration, sweating and gas production skin, reduces the lateral asymmetry of areas of light.

Correlation between the areas of the GDI and their jaggedness (fractality) under normal conditions of registration is almost equally strong inverse in all projections, while the filter reduces it to nothing in the right and frontal projections and minimizes it to the limit of significance - in the left projection.

The serrations (shape coefficients) of the lateral projections of the GDI taken without a filter correlate weakly (r=0,32), but not at all (r=0,07) with the filter, that is, the filter contributes to the manifestation of the lateral asymmetry of the fractality of the GDI. The relations of the symmetry of the frontal projection GDI are significant only with the area of light of the right projection and the entropy of the left projection under conditions without a filter.

Let's move on to the analysis of correlations between GDV and HRV&BP parameters. In the Table 2.3 shows the results of screening coefficients of linear correlation under normal conditions, and in Table. 2.4 - under the conditions of filter application.

It was found that, firstly, there is a significant predominance of both the number and strength of connections with the HRV&BP parameters of the GDI area and its fractality

(jaggedness) of the right projection compared to the left (the central projection is much more similar to the right than to the left); secondly, the use of a polyethylene filter "cuts off" all previous connections, at the same time, causes the appearance of new connections in the central and, to a lesser extent, in the left projections; third, left projection GDI entropy is significantly correlated with only a few HRV parameters.

Table 2.3. Coefficients of linear correlation between the parameters of bioelectrography without a filter and the heart rate variability and blood pressure

Parameter	RIGT PROJECTION			FRONTAL PROJECTION			LEFT PROJECTION		
	Area	Entropy	Shape coeff	Area	Entropy	Shape coeff	Area	Entropy	Shape coeff
BPs	**0,76**	*0,45*	-0,57	**0,72**	*-0,30*	-0,59	*0,50*	-0,29	-0,51
BPd	**0,66**	*0,30*	-0,61	**0,71**	*-0,32*	-0,55	0,52	-0,21	*-0,46*
HR	*0,32*	*-0,31*	-0,46	*0,35*	*-0,42*	-0,13	-0,17	-0,51	0,12
1-BPd/HR	*-0,31*	*-0,49*	0,13	*-0,32*	*-0,08*	0,35	-0,57	-0,18	0,47
MRR	*-0,22*	*0,25*	0,33	*-0,39*	*0,07*	-0,03	0,02	0,14	-0,06
SDNN	-0,63	*0,22*	**0,71**	**-0,79**	*0,27*	0,58	-0,35	0,53	0,39
RMSSD	-0,57	*0,42*	**0,74**	-0,57	*0,39*	0,33	0,12	0,57	-0,06
pNN$_{50}$	**-0,67**	*0,21*	**0,77**	**-0,78**	*0,19*	0,58	-0,33	0,49	0,38
Total Pow	**-0,68**	*0,19*	**0,75**	**-0,79**	*0,25*	0,60	-0,35	0,52	0,40
ULF	**-0,65**	*0,15*	**0,76**	**-0,67**	*0,23*	0,51	-0,20	0,44	0,24
ULF%	-0,52	*-0,47*	0,32	-0,39	*-0,04*	0,33	-0,24	-0,07	0,20
VLF	-0,53	*0,11*	0,53	**-0,75**	*0,14*	**0,72**	-0,59	0,44	**0,77**
VLF%	*0,25*	*-0,02*	-0,14	*0,06*	*-0,29*	0,24	-0,33	-0,34	0,51
LF	**-0,73**	*0,12*	**0,73**	**-0,84**	*0,30*	**0,66**	-0,44	0,56	0,48
LF%	*-0,21*	*-0,41*	-0,13	*0,03*	*0,15*	0,17	-0,26	0,14	0,26
HF	-0,54	*0,24*	*0,68*	-0,56	*0,21*	0,31	0,04	0,39	0,00
HF%	*-0,02*	*0,32*	0,15	*-0,02*	*0,16*	-0,35	0,46	0,21	-0,61
LF/HF	*0,14*	*-0,33*	-0,28	*0,14*	*-0,02*	0,24	0,36	-0,18	0,50
HRVTI	**-0,67**	*0,08*	**0,68**	**-0,83**	*0,26*	**0,65**	-0,44	0,51	0,46
Mode	*-0,17*	*0,20*	0,31	*-0,36*	*0,06*	0,07	-0,14	0,05	0,14
AMo	*0,50*	*-0,01*	-0,45	**0,76**	*-0,22*	-0,54	0,54	-0,37	-0,53
MxDMn	**-0,70**	*0,02*	**0,65**	**-0,75**	*0,30*	0,60	-0,32	0,51	0,34
BSI	0,55	*0,14*	-0,42	**0,76**	*-0,20*	-0,51	0,50	-0,33	*-0,42*
BARSI	0,57	*0,40*	-0,24	**0,67**	*-0,07*	**-0,52**	0,63	-0,29	-0,55

Table 2.3. Coefficients of linear correlation between the parameters of bioelectrography with a filter and the heart rate variability and blood pressure

Parameter	RIGT PROJECTION			FRONTAL PROJECTION			LEFT PROJECTION		
	Area	Entropy	Shape coeff	Area	Entropy	Shape coeff	Area	Entropy	Shape coeff
BPs	*0,08*	*0,47*	*0,32*	*-0,08*	*-0,14*	*0,22*	*-0,14*	*-0,25*	*0,03*
BPd	*0,13*	0,52	*0,21*	*0,00*	*-0,02*	*0,12*	*-0,08*	*-0,07*	*-0,08*
HR	*0,18*	*-0,13*	*0,21*	**0,70**	*-0,33*	*0,50*	*0,46*	*-0,06*	*0,02*
1-BPd/HR	*0,04*	*-0,48*	*0,01*	*0,55*	*-0,24*	*0,27*	*0,45*	*0,05*	*0,06*
MRR	*-0,30*	*0,15*	*0,17*	**-0,90**	*-0,07*	*-0,19*	*-0,56*	*-0,27*	*0,29*
SDNN	*-0,02*	*0,00*	*-0,38*	*-0,37*	*0,03*	*-0,34*	*-0,12*	*0,27*	*0,25*
RMSSD	*0,32*	*0,05*	*-0,35*	*-0,33*	*-0,03*	**-0,67**	*0,11*	*0,22*	*-0,06*
pNN$_{50}$	*0,05*	*-0,07*	*-0,41*	*-0,27*	*-0,03*	*-0,34*	*-0,01*	*0,29*	*0,26*
Total Pow	*0,05*	*-0,06*	*-0,42*	*-0,26*	*0,00*	*-0,35*	*-0,01*	*0,32*	*0,24*
ULF	*0,26*	*-0,13*	*-0,44*	*-0,13*	*-0,13*	*-0,33*	*0,16*	*0,32*	*0,22*
ULF%	*0,20*	*-0,12*	*0,05*	*-0,01*	*-0,34*	*-0,04*	*0,19*	*-0,18*	*0,13*
VLF	*-0,31*	*0,14*	*-0,34*	*-0,20*	*0,20*	*-0,19*	*-0,19*	*0,28*	*0,25*
VLF%	*-0,19*	*0,15*	*0,02*	*0,31*	*-0,09*	*0,40*	*0,01*	*-0,13*	*0,28*
LF	*0,02*	*-0,08*	*-0,42*	*-0,19*	*0,04*	*-0,35*	*0,03*	*0,36*	*0,18*
LF%	*0,12*	*-0,27*	*-0,25*	**0,73**	*0,25*	*0,04*	*0,46*	*0,49*	*-0,35*
HF	*0,26*	*-0,15*	*-0,34*	*-0,28*	*-0,15*	*-0,34*	*0,07*	*0,22*	*0,19*
HF%	*0,06*	*0,05*	*0,13*	**-0,69**	*-0,03*	*-0,35*	*-0,30*	*-0,15*	*-0,05*
LF/HF	*-0,04*	*-0,08*	*-0,20*	**0,69**	*0,17*	*0,33*	*0,26*	*0,27*	*-0,05*
TINN	*0,04*	*-0,10*	*-0,40*	*-0,19*	*-0,01*	*-0,32*	*0,03*	*0,32*	*0,21*

Mode	-0,43	0,18	0,03	**-0,83**	-0,03	0,10	**-0,69**	-0,17	0,58
AMo	0,19	0,00	0,19	0,34	-0,02	0,14	0,20	-0,15	-0,29
MxDMn	0,34	-0,17	-0,39	0,03	-0,12	-0,44	0,35	0,37	0,00
BSI	0,08	-0,05	-0,05	0,33	0,20	0,22	0,04	0,05	-0,18
BARSI	0,18	-0,13	-0,21	0,02	0,20	0,13	-0,15	0,05	-0,03

It is significant that strong connections with BP parameters of the area (direct) and, somewhat weaker, fractality (inverse) of the GDI of the right and central projections are associated with similar connections with markers of sympathetic and vagal regulatory influences, which, in turn, are associated with associated with BP.

In particular, systolic BP - with sympathetic marker AMo (r=0,41) and Baevskiy's stress index (r=0,40) and vagal markers - LF (r=-0,60), pNN$_{50}$ (r=-0,56) and MxDMn (r=-0,54). With regard to diastolic BP, the respective relationships are somewhat weaker (r= 0,42; 0,40; -0,58; -0,53 and -0,46 respectinely).

Therefore, the size of the GDI area (directly) and the degree of its jaggedness (inversely) in the right and frontal projections without a filter reflect both the state of adrenergic-cholinergic vasomotor regulation and the result of this regulation - blood pressure.

The degree of influence of HRV&BP parameters on GDV parameters can be expressed by coefficients of multiple correlation and determination:
ALF: R=0,93; R^2=0,86; CLWF: R=0,92; R^2=0,85; AFF: R=0,91; R^2=0,83; ERWF: 0,89; R^2=0,80; CLF: R=0,89; R^2=0,79; AFWF: R=0,88; R^2=0,78; ARWF: R=0,84; R^2=0,70; CFF: R=0,83; R^2=0,69; ALWF: R=0,81; R^2=0,65; ARF: R=0,79; R^2=0,63; CRWF: R=0,79; R^2=0,62; CFWF: R=0,78; R^2=0,61; ELWF: R=0,75; R^2=0,56; SymFF: R=0,75; R^2=0,56; SymFWF: R=0,71; R^2=0,50; ELF: R=0,69; R^2=0,48; p=0,04.

The rest of the GDV parameters are insignificantly determined by the HRV&BP parameters:
EFF: R=0,68; R^2=0,46; p=0,12; ERF: R=0,55; R^2=0,31; p=0,21; CRF: R=0,55; R^2=0,31; p=0,21; EFWF: R=0,56; R^2=0,31; p=0,21.

Connections of the Korotkov's activation index, proposed by the author as a stress criterion, deserve special attention. According to our data, this index is indeed significantly related to the parameters of adreno- and cholinergic regulatory influences, but in the **opposite** way - with sympathetic markers inversely, and with vagal - directly, in particular with Baevsky's stress index r=-0,66, and with Baevsky's regulatory system activity index r=-0,53. So, physiologically, the Korotkov's activation index is an index of relaxation, not stress. Looking ahead, we note that in our subsequent studies the contradiction was ironed out: the correlation is still positive, but on the border of significance

In Fig. 2.1. visualized 3D diagrams of relationships between some parameters of bioelectrography and HRV&BP.

At the last stage, a canonical correlation analysis was carried out, which allows to find out the relationship between the set of HRV&BP parameters (accepted as a factor characteristic) and GDV parameters (accepted as a result characteristic). 4 pairs of canonical radicals were identified (Fig. 2.2).

The factor structure of the first pair is formed, on the one hand, by the average value of the cardio intervals (MRR) (r=-0,83) and Kerdoe's VI (IK) (r=0,50), and on the other hand by the area of the frontal projection taken with the filter (SFF) (r=0,97). As you can see, the dependence is almost complete. A somewhat weaker, but still very strong connection was established between the roots of the second pair, formed respectively from the average values of VLF (r=-0,92) and LF (r=-0,74) bands of HRV and the area of the frontal projection without a filter (SFWF) (r=-0,68) and the shape coefficient of the left projection without filter (CLWF) (r=0,68). The factor structure of the third pair of radicals is formed, on the one hand, by the vagal marker RMSSD (r=0,63), and on the other hand by the entropy of the right projection taken without a filter (ERWF) (r=0,77) and again by CLWF (r= -0,71). The

canonical connection is also very strong. The last canonical pair is formed, respectively, from systolic BP (r=0,81), LF (r=-0,61), RMSSD (r=-0,53) and WN1 (r=-0,52) and, and on the other hand, from SFWF (r=0,72) and ERWF (r=0,49). The connection is much weaker than the previous ones, but still significant: R=0,827; R^2=0,684; χ^2=10; Λ Prime=0,31; p=0,03.

Fig. 2.1. 3D diagrams of relationships between GDV and HRV&BP parameters (top left: X - LF; Y - Ps; Z - SRWF; top right: X - WN1; Y - VLF; Z - CLWF; bottom left: X - MRR; Y - LF; Z - SFF; bottom right: X - MxDMn; Y - Ps; Z - IA

R=0,990; R^2=0,981; χ^2=86; Λ Prime<10^{-4}; p<10^{-6}

R=0,965; R^2=0,930; χ^2=51 Λ Prime=0,004; p<10^{-4}

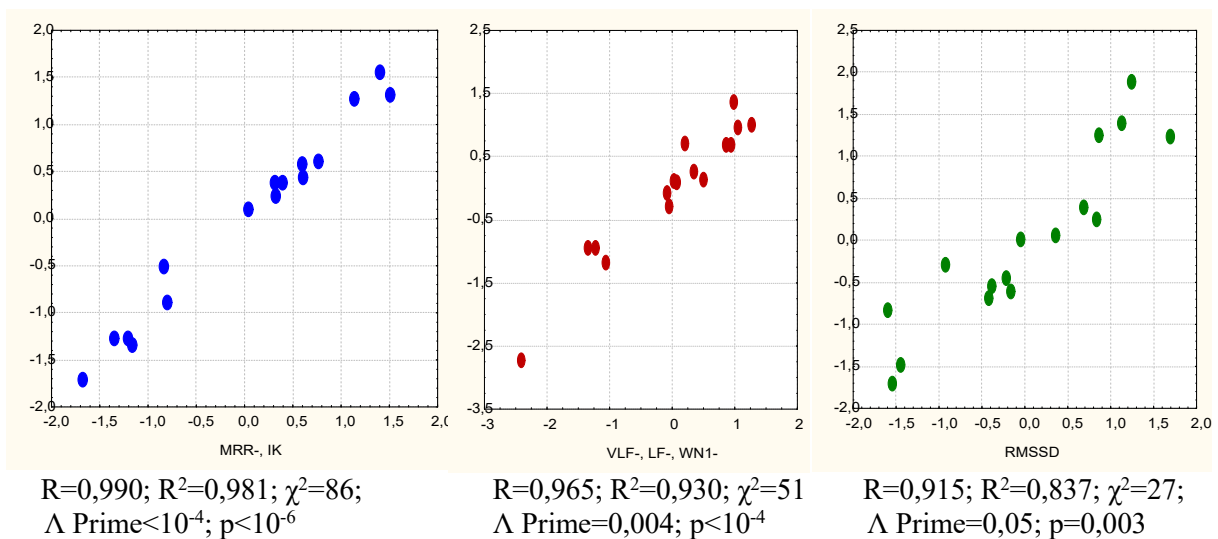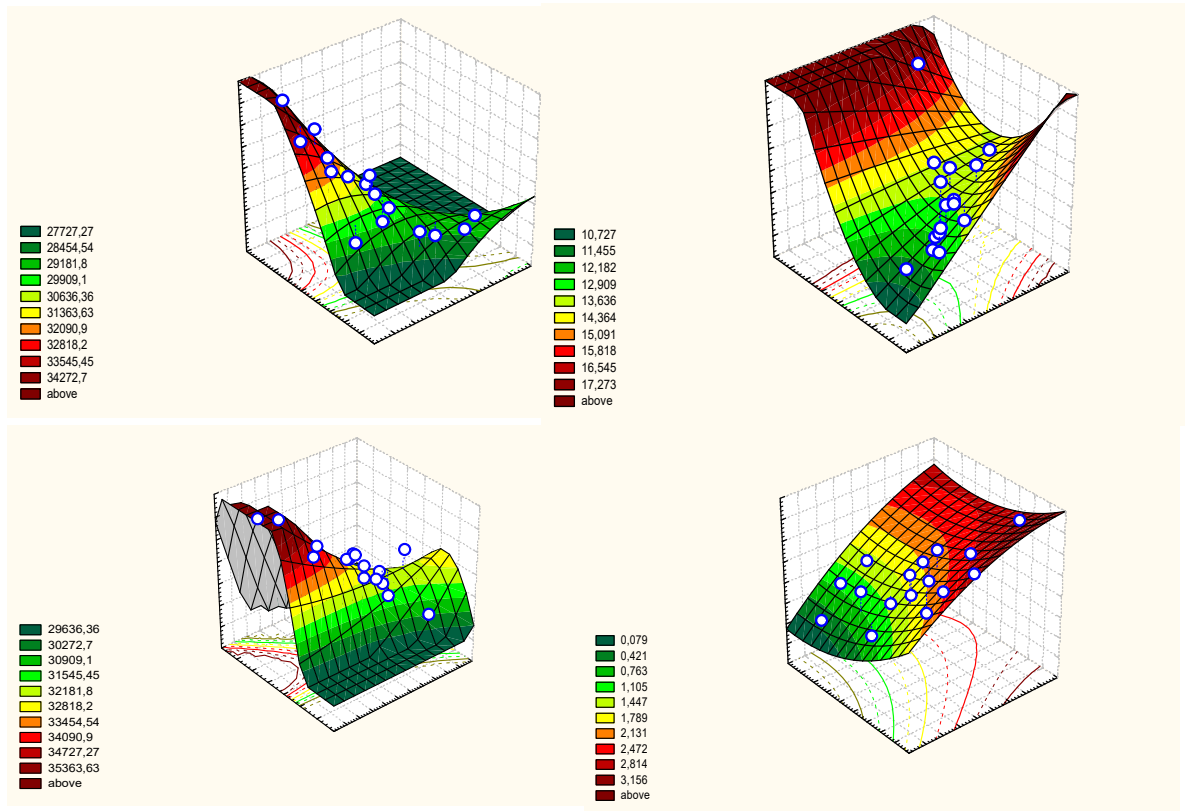R=0,915; R^2=0,837; χ^2=27; Λ Prime=0,05; p=0,003

Fig. 2.2. Canonical relationship between heart rate variability and blood pressure parameters (X axis) and bioelectrography (Y axis)

Therefore, both the individual parameters of bioelectrography and the bioelectrogram as a whole reflect, at least, the state of different levels of cholinergic-adrenergic regulatory effects

on the cardiovascular system and their consequence - blood pressure, that is, the method of gas-discharge visualization of the photoelectron emission of the skin surface induced by a high-frequency electromagnetic field, registers real physiological processes.

The obtained results, despite, to put it mildly, the not very favorable attitude of the Institute's administration, inspired us to continue the search for physiological correlates of bioelectrography.

The object of the second pilot study conducted in August 2010, were 10 practically healthy volunteers - men by age 26-56 years (including two authors). In the morning in basale terms at first registered kirlianogram, whereupon took from an ulnar vein the blood for determination of plasma levels of main adaptive hormones: cortisol, triiodothyronine and testosterone by the ELISA method with the use of analyzer of "Tecan" (Oesterreich) and corresponding sets of reagents of JSC "Alkor Bio" (St-Pb., RF) as well as sodium and potassium (by the method of flaming photometry on the device ПФМ У 4.2), with the purpose of estimation of mineralocorticoid activity after Na/К-ratio. After it volunteers filled a questionnaire with the purpose of estimation of level of the trait and reactive anxiety (by STAI of Spielberger ChD [1983] in modification of Khanin YL [1998]). Through 1,5 hours all tests repeated.

According to a mentioned equation, for a sample with n=20 the critical size of the module of coefficient of correlation at $p<0,05$ ($t>2,1$) is 0,45.

It is educed (Table 2.4) that area of GDI, taken off **without** polyethylene **filter** in a **right** projection, statistically the meaningful does not correlate with any psychophysiological or endocrine parameters.

Table 2.4. A matrix of coefficients of correlation between the parameters of gas discharge image in right (R), frontal (F) and left (L) projections and psychophysiological and endocrine parameters

Parameters of gas discharge image in different projections		Area A		Shape Coefficient C		Entropy E		Symmetry Sym	
Psychophysiological &endocrine paramet	Proje ction	without filter	with filter	without filter	with filter	without filter	with filter	without filter	with filter
Trait anxiety	R	0,26	0,04	0,16	-0,37	0,12	0,02	0,39	0,15
	F	0,35	-0,03	-0,07	-0,28	0,04	-0,31		
	L	0,36	0,00	-0,24	-0,14	-0,06	0,01		
Reactive anxiety	R	0,27	0,32	-0,18	-0,20	-0,00	0,11	0,22	0,00
	F	0,26	0,23	-0,05	-0,17	-0,09	-0,15		
	L	0,16	0,27	-0,19	-0,03	-0,24	-0,04		
Triiodothyronine	R	0,25	**0,47**	-0,29	-0,15	-0,35	-0,08	0,40	0,20
	F	0,35	**0,53**	-0,19	-0,35	-0,34	-0,21		
	L	0,26	**0,51**	-0,29	-0,35	**-0,52**	**-0,46**		
Testosterone	R	0,19	-0,09	-0,19	-0,25	0,03	-0,39	0,30	0,13
	F	0,18	-0,23	-0,44	-0,20	-0,06	**-0,45**		
	L	0,35	-0,11	-0,41	-0,35	-0,12	-0,39		
Cortisol	R	0,15	0,07	0,29	-0,12	-0,17	0,06	-0,29	-0,33
	F	-0,12	-0,10	0,13	0,15	0,07	0,09		
	L	-0,06	0,01	-0,10	0,12	0,02	0,23		
Sodium	R	0,10	-0,07	-0,36	-0,15	0,10	-0,31	0,13	-0,27
	F	0,07	-0,02	-0,10	-0,17	0,20	-0,21		
	L	-0,10	-0,07	-0,31	0,22	-0,23	-0,28		
Potassium	R	0,11	0,22	-0,28	0,01	-0,06	0,23	0,15	-0,15
	F	0,16	0,25	0,12	-0,06	-0,17	0,09		
	L	-0,21	0,26	0,04	0,22	-0,23	0,18		
Mineralocorticoid activity (Na/K)	R	-0,11	-0,25	0,25	0,00	0,09	-0,21	-0,21	0,01
	F	-0,22	-0,29	-0,11	0,10	0,24	-0,08		
	L	0,14	-0,29	-0,09	-0,15	0,25	-0,17		

Positive connections are however noteworthy with the levels of the trait (TA) and reactive (RA) anxiety and triiodothyronine (T_3). In a result the coefficient of canonical

correlation R arrives at 0,43 ($\chi^2_{(3)}$=3,3; p=0,34). At the terms of registration **with the filter** connection of area with T$_3$ it appears meaningful, with RA some increases, but with TA fades away, at the same time, a loosely-coupled negative interface appears with mineralocorticoid activity (MCA). Accordingly the coefficient of canonical correlation grows to 0,51 ($\chi^2_{(3)}$=5,0; p=0,17).

The Shape coefficient, being taken off without filter, correlates with TA and PA mildly and poorly negatively, as well as with testosterone. Canonical correlation appears moderate: R=0,43; $\chi^2_{(2)}$=3,6; p=0,17. At the terms of registration with a filter moderate correlation is educed with T$_3$ and weak - with cortisol, so that R=0,47 ($\chi^2_{(2)}$=4,3; p=0,12).

The entropy, registered without filter, mildly negatively correlates with testosterone and sodium and poorly positively - with potassium, however canonical correlation with these parameters appeared considerable: R=0,62 ($\chi^2_{(3)}$=7,9; F$_{(3,2)}$=3,3; p=0,048). Equalization of multiple regression looks like:

ER = 6,23 - 0,010•T(nM/l) - 0,018•Na(mM/l) + 0,101•K(mM/l).

Application of filter does not influence on connection of entropy with sodium, weakens considerably - with testosterone, but assists appearance of connection with cortisol and reverses character of connection with potassium. On the whole the canonical correlation is somewhat weakened: R=0,51 ($\chi^2_{(3)}$=5,0; p=0,17).

The area of GDI, taken off **without filter** in a **frontal** projection, correlates straight mildly with T$_3$ and TA and poorly with RA. Canonical correlation appears moderate: R=0,59 ($\chi^2_{(3)}$=7,1; p=0,07). Application of filter does not influence on connection with RA, connection takes on it is not with TA, does noticeable connections with testosterone and MCA and substantially strengthens connection with T$_3$ (Fig. 2.3).

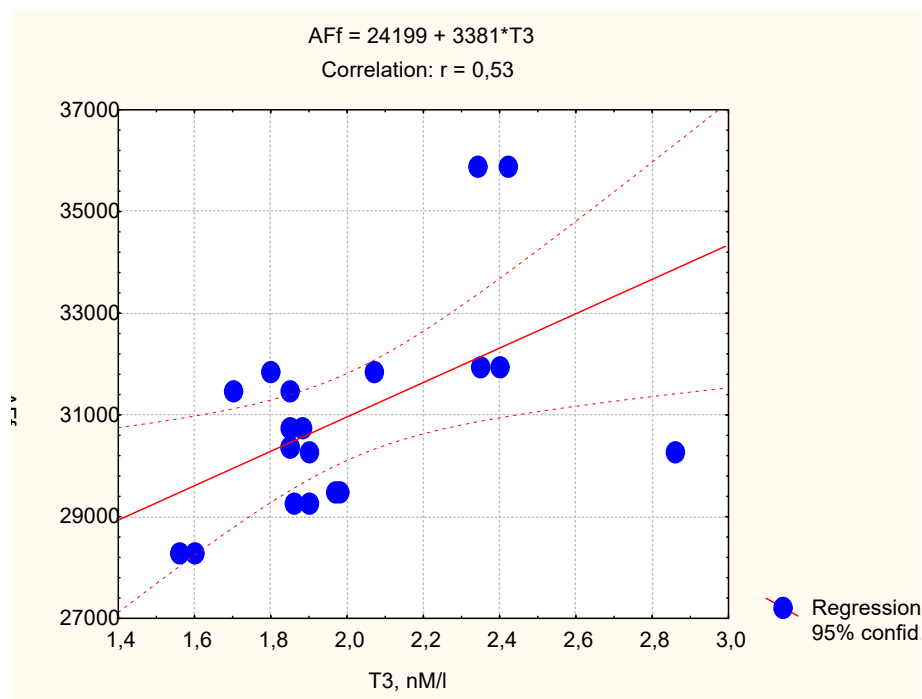**Fig. 2.3. Cross-correlation connection between plasma triiodothyronine (axis of X) and Area of GDI in frontal projection, taken off with filter (AFf) (axis of Y)**

Thus something grows force of canonical cross-correlation connection: R=0,61 ($\chi^2_{(3)}$=7,6; F$_{(3,2)}$=3,1; p=0,056) (Fig. 2.4).

Equalization of multiple regression:

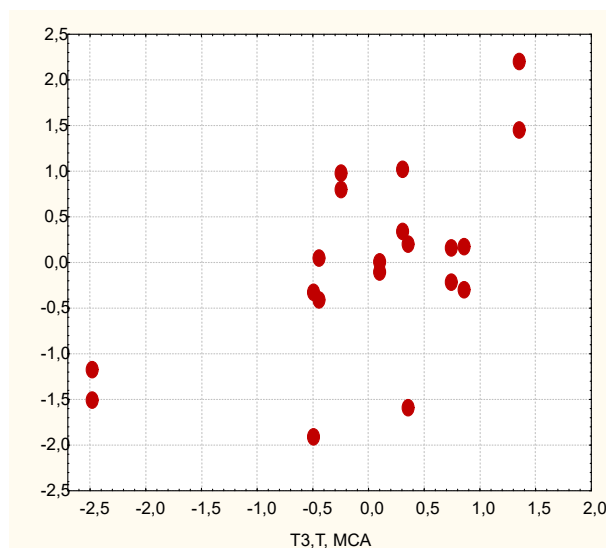AFf = 26973 + 3397•T$_3$(nM/l) - 65,2•T(nM/l) - 25,9•MCA.

Fig. 2.4. Canonical cross-correlation connection between plasma triiodothyronine (T₃), testosterone (T) and mineralocorticoid activity (MCA) (axis of X) and Area GDI in frontal projection, taken off with filter (AFf) (axis of Y)

Connections with the Shape coefficient of GDI have negative character and some more weak: $R=0,53$ ($\chi^2_{(2)}=5,5$; $p=0,063$), and a filter weakens them yet in a greater degree: $R=0,36$ ($\chi^2_{(2)}=2,4$; $p=0,29$). In default of filter Entropy of GDI correlates negatively mildly with testosterone and TA: $R=0,54$ ($\chi^2_{(2)}=5,7$; $p=0,056$), and a filter, not influences on connection with testosterone, completely eliminates connection with TA.

In the **left** projection the area of GDI in default of filter correlates mildly with TA and testosterone and poorly with T₃: $R=0,58$ ($\chi^2_{(3)}=7,0$; $p=0,07$). The filter does not affect the connections with the first two parameters, but does noticeable connections with RA and MCA and considerably strengthens connection with T₃, however it this does not significantly affect the strength of the canonical correlation: $R=0,53$ ($\chi^2_{(3)}=5,6$; $p=0,13$). The relationships of shape coefficient are similar after a structure and force, but opposite after character. At presence of filter $R=0,53$ ($\chi^2_{(3)}=5,6$; $p=0,13$), at his absence canonical correlation is analogical, but some more credible: $R=0,53$ ($\chi^2_{(2)}=5,6$; $F_{(2,2)}=3,3$; $p=0,061$) (Fig. 2.5).
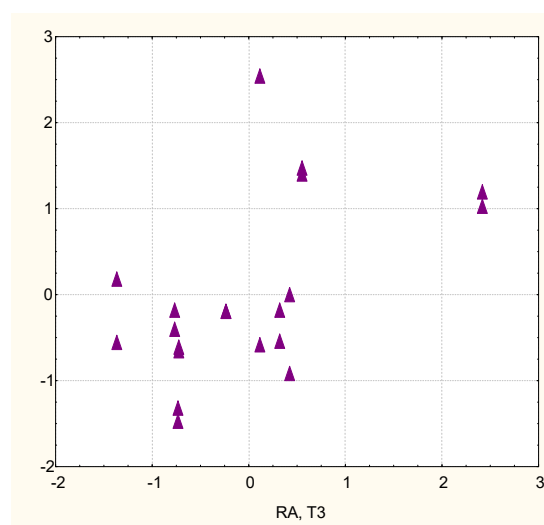

Fig. 2.5. Canonical cross-correlation connection between plasma triiodothyronine (T₃) and reactive anxiety (RA) (axis of X) and coefficient of form of GDI in the left projection, taken off with filter (CLf) (axis of Y)

Equalization of multiple regression:

$CLf = 14,9 - 1,07 \cdot T_3(nM/l) - 0,013 \cdot RA$.

To the investigated parameters entropy of GDI appeared closer in all related in the left projection. In default of filter she correlates negatively mildly from T_3 and testosterone, poorly - from sodium and positively poorly - from cortisol. Her dependence on compatible influence of triiodo-thyronine and testosterone, traced on Fig. 2.6, described by equalization:

$EL = 4,61 - 0,237 \cdot T_3(nM/l) - 0,007 \cdot T(nM/l)$;
$R=0,58; F_{(2,2)}=4,2; p=0,032$.

■	3,473
■	3,546
■	3,62
■	3,693
■	3,766
■	3,839
■	3,913
■	3,986
■	4,059
■	4,132
■	above

Fig. 2.6. Cross-correlation dependence of entropy of GDI in the left projection, taken off without filter (axis of Z) from levels in plasma of triiodothyronine (axis of X) and testosterone (axis of Y)

And on Fig. 2.7 traced dependence of this parameter of GDI on compatible influence of triiodothyronine, testosterone, cortisol and sodium, which is described by equalization:

$EL = 6,79 - 0,144 \cdot T_3(nM/l) - 0,03 \cdot T(nM/l) + 0,00025 \cdot C(nM/l) - 0,0175 \cdot Na(mM/l)$;
$R=0,76; \chi^2_{(4)}=13,8; F_{(4,2)}=5,1; p=0,008$.

A filter, not affecting influences on entropy in left projection from the side of testosterone and sodium, weakens influence on her T_3 and cortisol and strengthens connection with the trait anxiety. In a result force of canonical correlation does not change practically. Compatible influence of testosterone and sodium, traced on Fig. 2.8, described by equalization:

$Elf = 5,62 - 0,008 \cdot T(nM/l) - 0,012 \cdot Na(mM/l)$;
$R=0,60; F_{(2,2)}=4,7; p=0,024$.
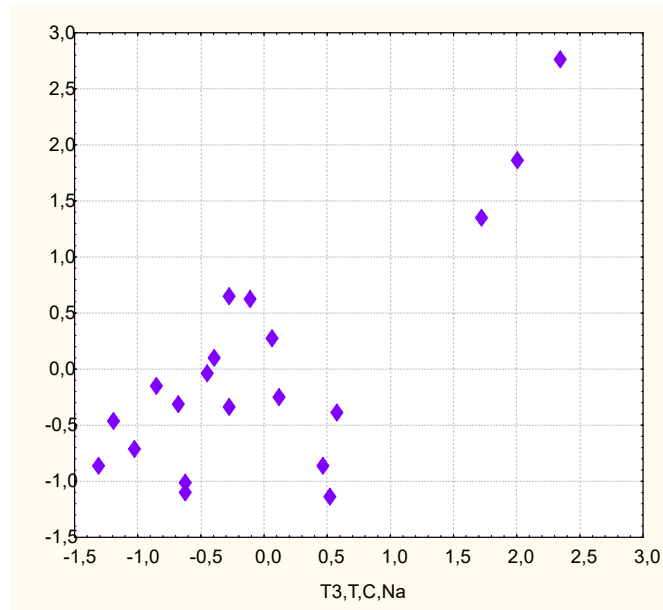
Fig. 2.7. Canonical cross-correlation connection between a plasma triiodo-thyronine (T₃), testosterone (T), cortisol (C) and sodium (axis of X) and by entropy of GDI in the left projection, taken off without a filter (EL) (axis of Y)

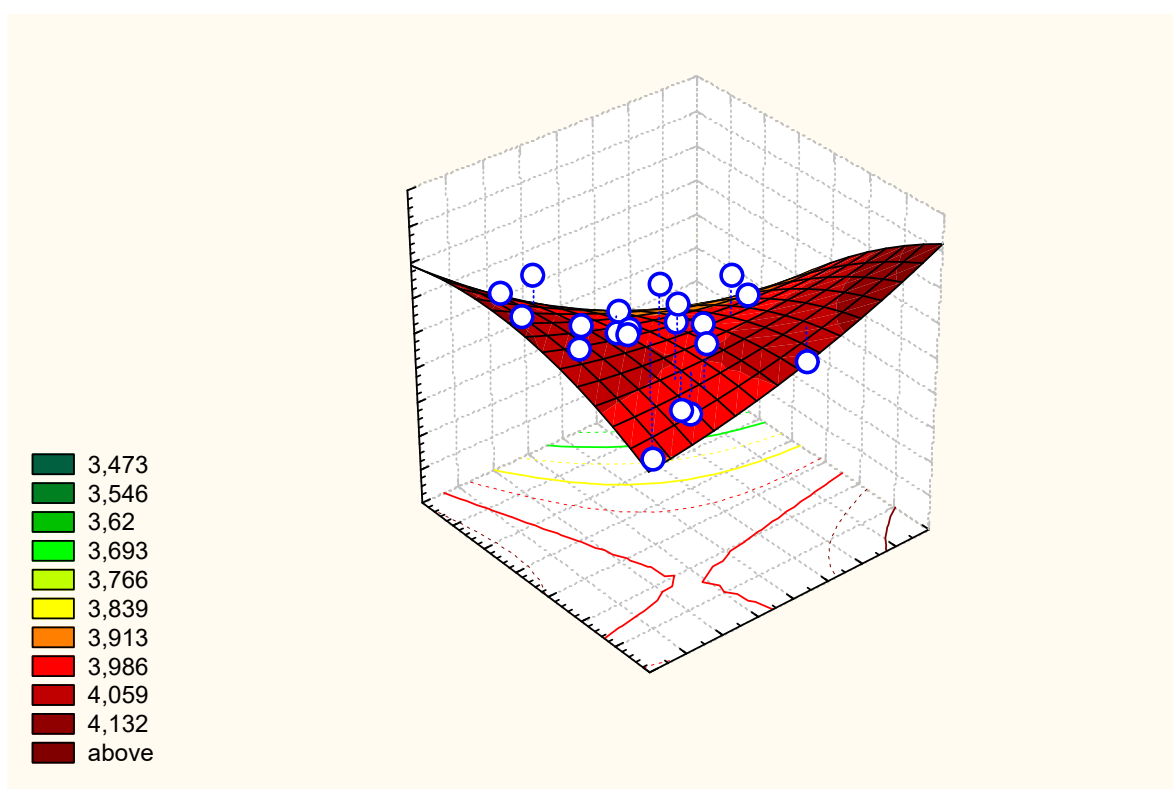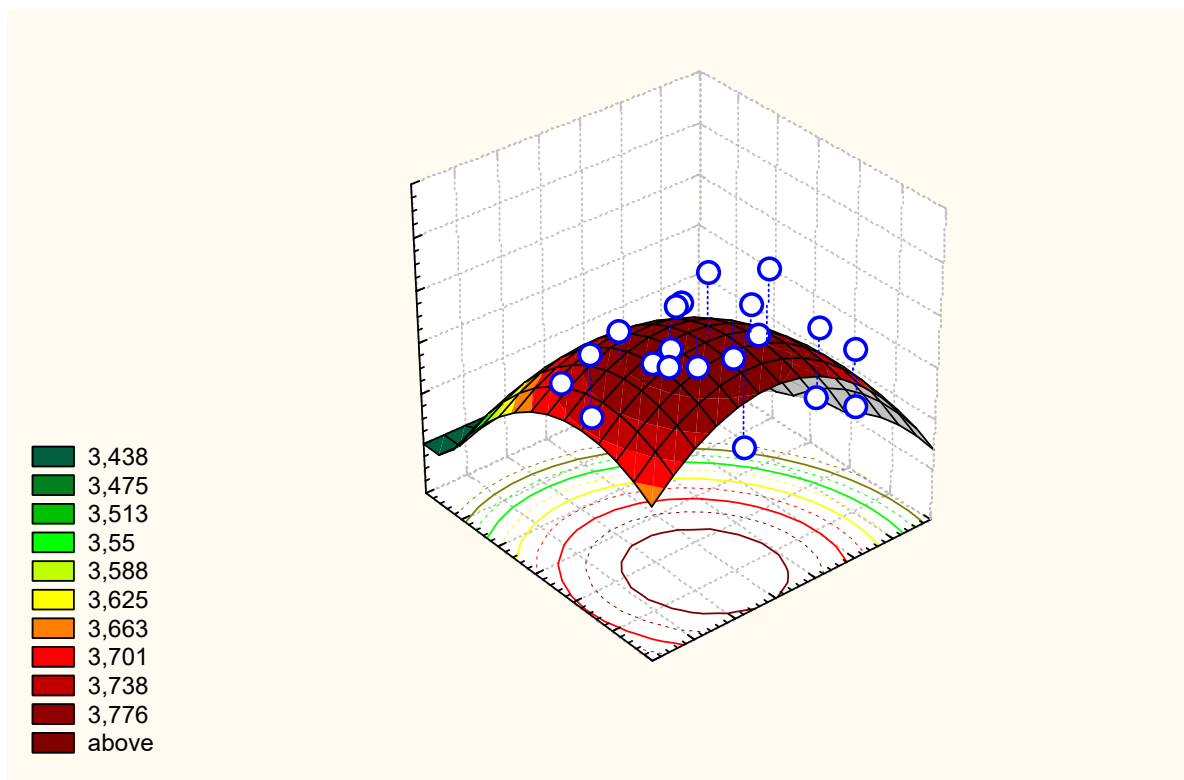**Fig. 2.8. Cross-correlation dependence of entropy of GDI in the left projection, taken off with a filter (axis of Z) from levels in plasma of testosterone (axis of X) and sodium (axis of Y)**

Canonical cross-correlation connection is traced on Fig. 2.9.

$Elf = 6,63 - 0,008 \cdot T(nM/l) - 0,016 \cdot Na(mM/l) - 0,148 \cdot T_3(nM/l) - 0,006 \cdot TA$;

$R = 0,77$; $\chi^2_{(4)} = 14,5$; $F_{(4,2)} = 5,5$; $p = 0,006$.
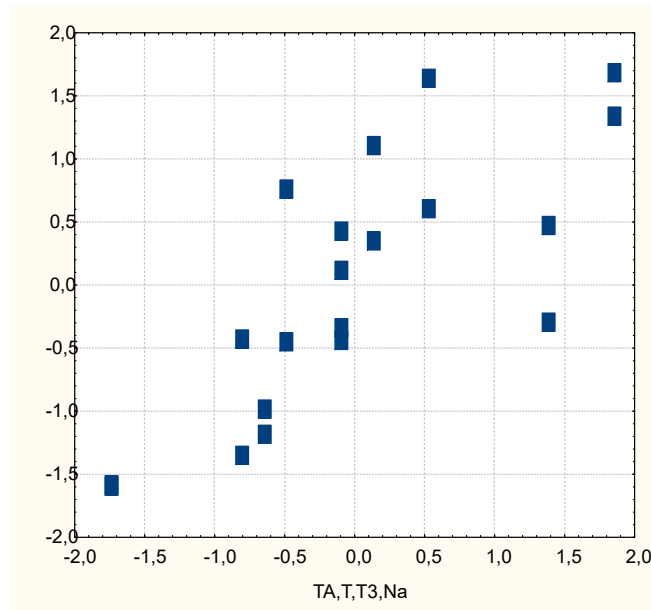
Fig. 2.9. Canonical cross-correlation connection between the trait anxiety (TA) and level in plasma of testosterone (T), triiodothyronine (T$_3$), sodium (axis of X) and by Entropy of GDI in the left projection, taken off with filter (ELf) (axis of Y)

Canonical dependence of Symmetry (Sym) of GDI appeared the same strong at the terms of absence of filter:

Sym = 72,6 + 0,132•T(nM/l) - 0,0042•C(nM/l) + 3,95•T$_3$(nM/l) + 0,170•TA;

R=0,74; $F_{(4,2)}$=4,7; p=0,012.

At the same time, a filter considerably weakens this dependence:

Sym f = 101,7 - 0,0011•C(nM/l) - 0,051•Na(mM/l);

R=0,41; $F_{(2,2)}$=1,8; p=0,20.

On the next stage of research influence of separate psychophysiologic and endocrine parameters on GDI on the whole was analysed.

It is educed (Fig. 2,10) that trait anxiety determines the state of GDI on 44% (R=0,66; $\chi^2_{(6)}$=8,7; p=0,19), but reactive anxiety only on 23% (R=0,48; $\chi^2_{(5)}$=4,2; p=0,53). Compatible influence TA and RA on GDI, judging after the coefficient of canonical correlation, estimated in 59% (Fig. 2.11).
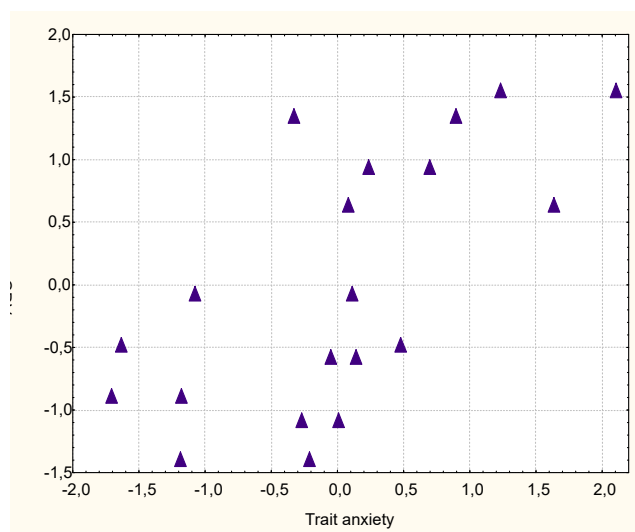
Fig. 2.10. Canonical cross-correlation connection between the trait anxiety (axis of X) and parameters of gas discharge visualization (axis of Y)
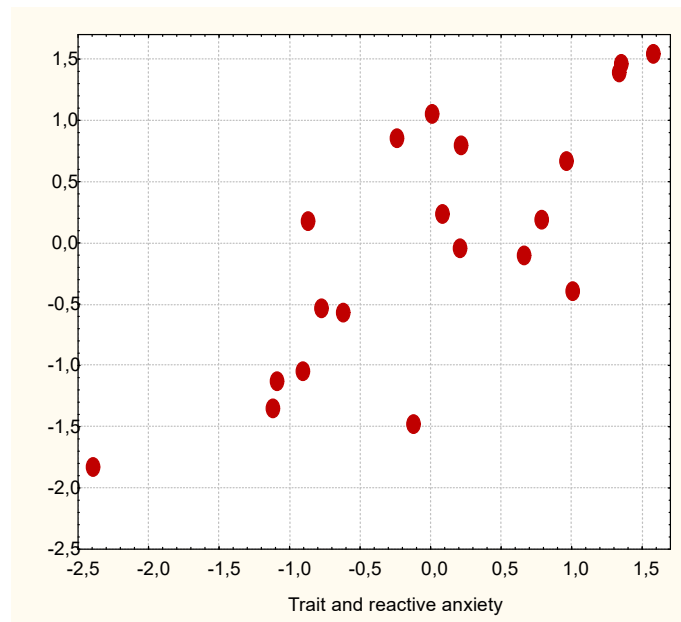
Fig. 2.11. Canonical cross-correlation connection between the trait and reactive anxiety (axis of X) and parameters of gas discharge visualization (axis of Y)

The plasma level of triiodothyronine determines the integral state of GDI on 64% (R=0,80; $\chi^2_{(6)}$=15,3; p=0,018) (Fig. 2.12).
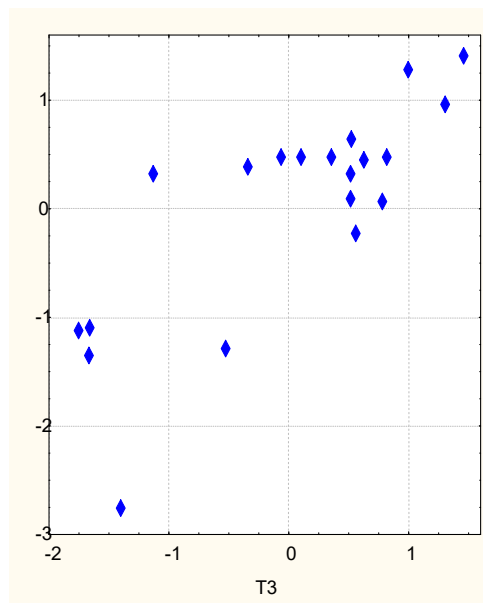
Fig. 2.12. Canonical cross-correlation connection between the level in plasma of triiodothyronine (axis of X) and parameters of gas discharge visualization (axis of Y)

At the same time the plasma level of testosterone influences a considerably less measure (on 23%) on the parameters of GDV (R=0,48; $\chi^2_{(3)}$=4,3; p=0,23) (Fig. 2.13).
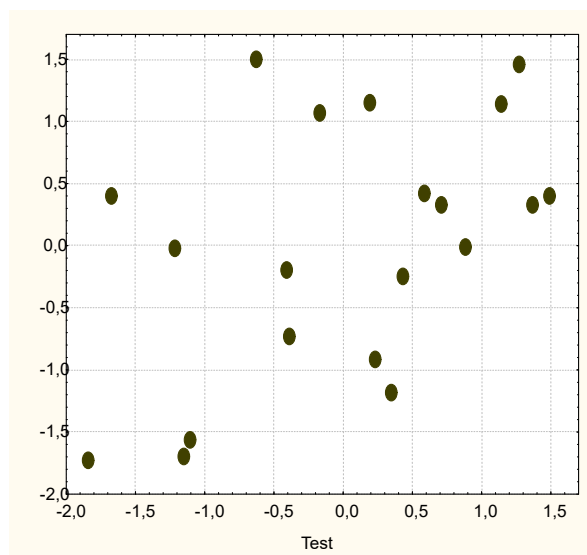
Fig. 2.13. Canonical cross-correlation connection between the level in plasma of testosterone (axis of X) and parameters of gas discharge visualization (axis of Y)

Yet weaker is determination of parameters of GDI from the side of mineralocorticoid activity (R=0,40; $\chi^2_{(2)}$=2,9; p=0,23) and cortisol (R=0,35; $\chi^2_{(3)}$=2,1; p=0,54).

But the **combined** influence of the transferred four endocrine factors on the integral state of GDI appears very strong: the measure of determination presents 90%: R=0,95; R^2=0,90; $\chi^2_{(40)}$=58,7; p=0,028 (Fig. 2.14).
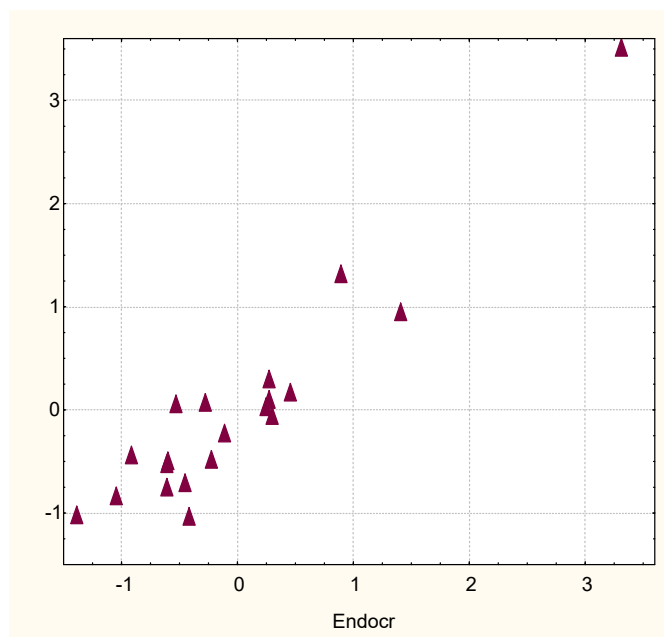
Fig. 2.14. Canonical cross-correlation connection between endocrine parameters (axis of X) and parameters of gas discharge visualization (axis of Y)

Thus the endocrine canonical root gets the positive factor loading from MCA (R=0,82), cortisol (R=0,81) and testosterone (R=0,36) while the negative factor loading from the plasma level of triiodothyronine (R=-0,48). On the other hand, the canonical root of GDV is presented by direct character by the entropy of GDI in a right projection, taken off with filter (R=0,34) and shape coefficient of GDI in the left projection at the same terms (R=0,22) while by reverse character by the area GDI in frontal (R=-0,32), left (R=-0,25) and right (R=-0,18) projections, also at presence of filter.

It is considered that GDI, taken off without filter, characterizes the functional changes of organism, while with filter - organic changes. Thus a right projection represents the bodily condition of human, and left projection - her emotional state. But the results of cross-correlation analysis are got by us ground to us to disagree with these claims of Korotkov KG. In fact the level of trait and reactive anxiety mildly correlates with some parameters of GDI both in the left and in right projections. Endocrine parameters also correlate both with a right projection and with the left projection parameters of GDI, thus with the last even some more frequent and stronger. We can't accept and the first position of Korotkov KG in relation to the role of polyethylene filter during registration of GDI. Moreover, parameters of the functional state of main adaptive glands closer and more frequent correlate with the parameters of GDI exactly at the terms of presence of filter.

At the same time, it is educed by us, that the parameters of GDI on the whole are appropriately related to the functional state, foremost, thyroid, and also testis and adrenal cortex, which in an aggregate characterize the state of adaptation and nonspecific resistibility of organism. Momentously, that the combined influence of endocrine parameters on the state of GDI considerably prevails them partial influences, that testifies in behalf on GDI as a marker of the integral state of adaptations.

It is known that the level of trait anxiety is predefined by the functional state of such nervous structures as orbito-frontal cortex, amygdala, hippocampus and others like that [Tolkunov D et al, 2010]. The appropriate connection of the state of GDI educed by us with the level of the trait anxiety characterizes GDI and as the marker of processes of neurodynamics.

The stated results were published in:

1. Popovych IL, Babelyuk VYe, Dubkova GI. Parameters of bioelectrography (kirlianography) is closely correlated with parameters of heart rate variability and blood pressure [in Ukrainian]. In: IX VV Podvysotskyi reading: Bulletin Materials Scientic Conference (Odesa, 27-28 May 2010). Odesa. OSMU; 2010: 143-144.

2. Popovych IL, Babelyuk VYe, Dubkova GI. Relations between the parameters bioelectrography (kirlianography) and heart rate variability and blood pressure [in Ukrainian]. Medical Hydrology and Rehabilitation. 2010; 8(1): 4-16.

3. Babelyuk VYe, Dubkova GI, Popovych IL. Correlation parameters of electrophotonics (kirlianogram) with neuroendocrine parameters [in Ukrainian]. In: Materials of V scientific-practical conference "Issues of pathology in conditions of extreme factors action on the body" (Ternopil', 1-2 November 2012): Achievements of Clinical and Experimental Medicine. 2012; 2(17): 158-158.

4. Babelyuk VYe, Popovych IL. Some biophysical and hematological correlates testosteronemia levels in healthy men [in Ukrainian]. Zdorovye muzhchiny. Health males. 2013; 2(45): 180-181.

5. Babelyuk VYe. The parameters of gaz discharge visualization (kirlianogram) appropriately associated with some psychophysiological and endocrine parameters of healthy men. Medical Hydrology and Rehabilitation. 2013; 11(1): 21-30.

CHAPTER 3

CAUSAL RELATIONSHIPS BETWEEN THE PARAMETERS OF GAS DISCHARGE VISUALIZATION AND PRINCIPAL NEUROENDOCRINE FACTORS OF ADAPTATION

Previously we showed that at practically **healthy** men the parameters of gas discharge visualization are appropriately related to their trait and reactive anxiety, plasma levels of triiodothyronine, testosterone and cortisol, as well as mineralocorticoid activity, appraised by plasma Na/K-ratio. Most determined from the side of psychophysiological and endocrine parameters is entropy of gas discharge image in the left projection with a filter and without filter, symmetry and area of GDI in a frontal projection with a filter and coefficient of form of GDI in the left projection with a filter and in a frontal projection without filter. On the whole endocrine status determines kirlianogram on 90%. Thus, the parameters of GDI represent the registered psychophysiological and endocrine parameters of organism of human objectively.

The object of third observation in November 2015 were 20 volunteers: ten women and ten men aged 33-76 years without clinical diagnose but with dysfunction of neuro-endocrine-immune complex and metabolism, characteristic for premorbid (intermediate between **health and illness**) state.

In the morning on an empty stomach we already usual registered kirlianogram. Then we recorded during 7 min electrocardiogram in II lead to assess the parameters of HRV. At last in portion of venous blood we determined levels of Cortisol, Testosterone, Triiodothyronine as well as Aldosterone and Calcitonin (by the ELISA with the use of analyzers "Tecan" and "RT-2100C" and corresponding sets of reagents from "Алкор Био" Ltd, XEMA Co Ltd and DRG International Inc). Every day four people were tested. A week later, all the tests were repeated.

As noted Korotkov KG [2001; 2007; 2014], the GDV method is a bridge between the logical science of the West and the intuitive science of the East. It allows us to represent the same phenomena in different languages, in different systems, to look at the same things from different points of view. Korotkov KG put forward the concept that each Chakra is associated with a part of the finger. This approach is embodied in the "GDV Chakras" program, which allows us to quantify the state of virtual Chakras.

The cornerstone of Eastern medicine in general and Ayurveda in particular is the concept of CHAKRAS and Ki/Qi energy. Unfortunately, this concept is categorically not accepted by **academic** (fortunately, not all) Ukrainian (as well as Russian) science, which thereby robs itself of its prospects (for a moment, China is now the second power in the world; and journals indexed in Scopus publish articles on Ki/Qi energy and the biofield, for the discovery of which the Jewish-Ukrainian Genius **Gurvich AG** was repressed). Thank God, officials stopped calling acupuncture a pseudoscience. The infamous VASKhNIL 1948 session with the criminal surrender of advanced positions in world genetics did not teach anything. Readers will understand why the results obtained in 2015 were published only in 2017, after the retirement of the author-generator of ideas of this study.

A short tour about Chakras from the
https://lifescriptdoctor.com/wp-content/uploads/2015/06/the-seven-chakras.jpg

Chakras are the energy centers that are a part of a human energy shell or body (also known as the human aura). They are responsible for absorbing vital energy-informational particles of different spectrum from the surrounding environment and for releasing energy-informational particles from a human body. **Chakras are like energy-informational routers that receive and transmit energy** as well as information which makes it possible for us to interact with the surrounding environment (energy-informational field) and people.

Energy centers or Chakras filter and supply human body with needed energy from the Chaos of the surrounding Environment. Each Charka has its own frequency spectrum and its own energy coding. Excessive or used energy is released from a human body through the work of Chakras. They are also responsible for transmitting coded energy that is used to connect and interact with other people.

Let's put it in simple terms and see **how energy of life is related to the Chakra system**. We all get our energy of life from the food we eat, but only partially. Our food consumption cannot cover all the energy frequencies we need to live during a day. If we take into account the whole spectrum of energy frequencies the human body needs to really live (not just mere thoughtless material survival) then there has to be another energy source which can simply be described as the energy field. Chakra system is like an energy-informational digestive system. It consumes energy from without and releases used or unnecessary energy that is utilized by other living or non-living systems of the surrounding environment (the field). The work of energy centers or Chakras is an **integral part of living a healthy life**. It is commonly accepted that there are seven Chakras in the human energy shell or the human aura (there are other Chakra systems that use 9, 12, 16, 22, etc., energy centers to explain how human energy body works, the key is to find the one that resonates with you and the one that works for you in practice).
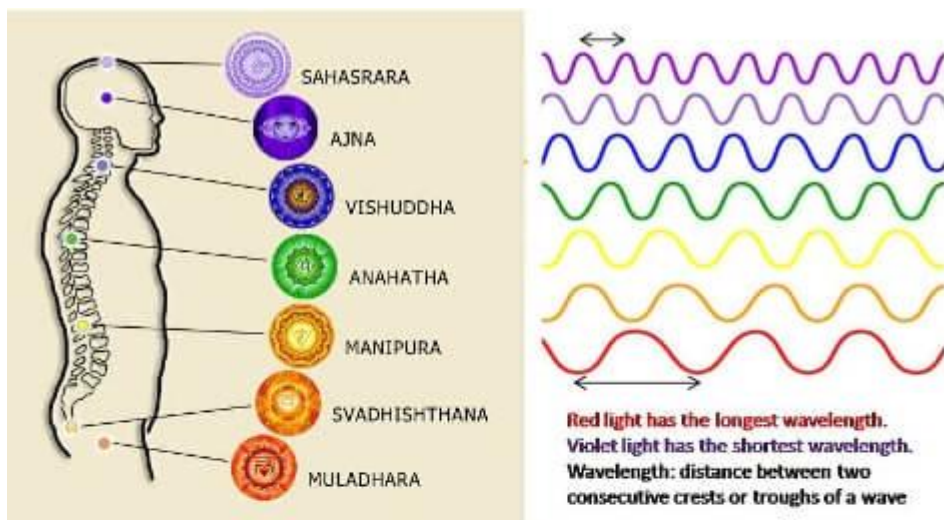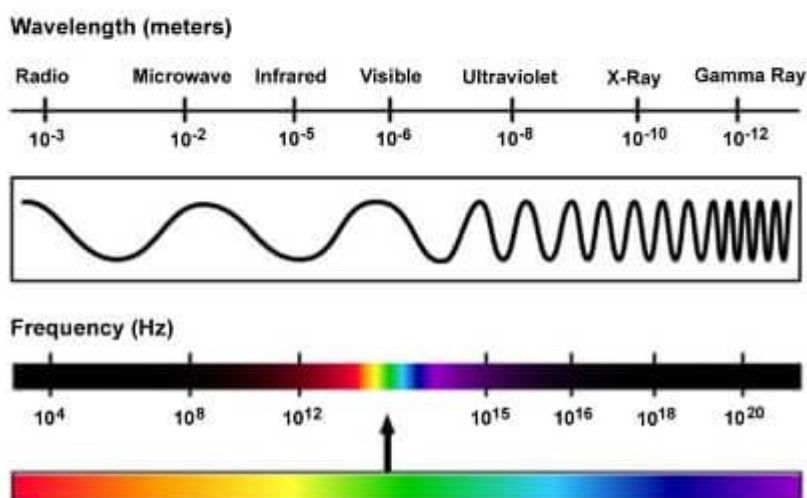
Fig. 3.1. The seven Chakras and a model of the energy-informational frequency spectrum

Information is coded and carried by the energy wave through modulation. That is the way **chakras receive and transmit information**. Energy wave can be modulated by an informational wave.

Lower three human Chakras are dominated by energy rather than information, while upper two Chakras have more information than energy. The two energy centers in the middle 4th and 5th Chakras serve as adapters of information into energy and vice versa.

Any of **the seven Chakras can work in two phases**: absorbing energy and information from the surrounding space; emitting or releasing energy and information from the human body.

The phases of chakra energy flow alternate. Here is where the seven chakras are located on the human body:
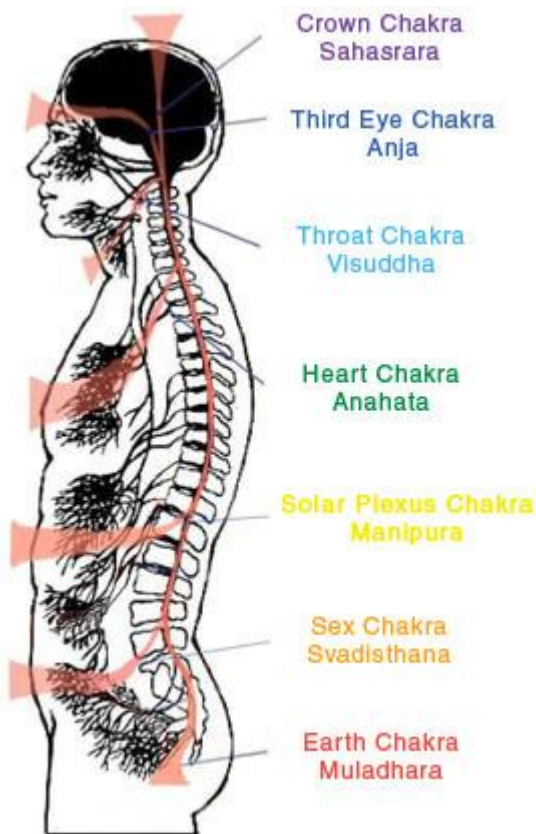
Fig. 3.2. The seven Chakras and the human spine
7th chakra, Crown Chakra or Sahasrara – top of a head
6th chakra, Third Eye Chakra or Ajna – forehead, pineal gland
5th chakra, Throat Chakra or Visuddha – throat area (thyroid gland)
4th chakra, Heart Chakra or Anahata – on the heart level, center of a chest
3rd chakra, Solar Plexus Chakra or Manipura – stomach or navel area
2nd chakra, Sex Chakra or Svadisthana – pubic area, lower abdomen
1st chakra, Earth Chakra or Muladhara – perineum area, the base of the spine
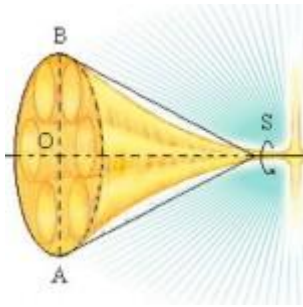
Fig. 3.3. Human Chakra structure

The structure of a human Chakra can be visualized as a spinning cone with a diameter of 3-5 cm (Fig. 3.3). These "energy cones" converge as they enter the human body and then "connect" to the main energy pillar – the spine (system bus in computer terminology, Fig. 3.4).

Main Components of a Computer System
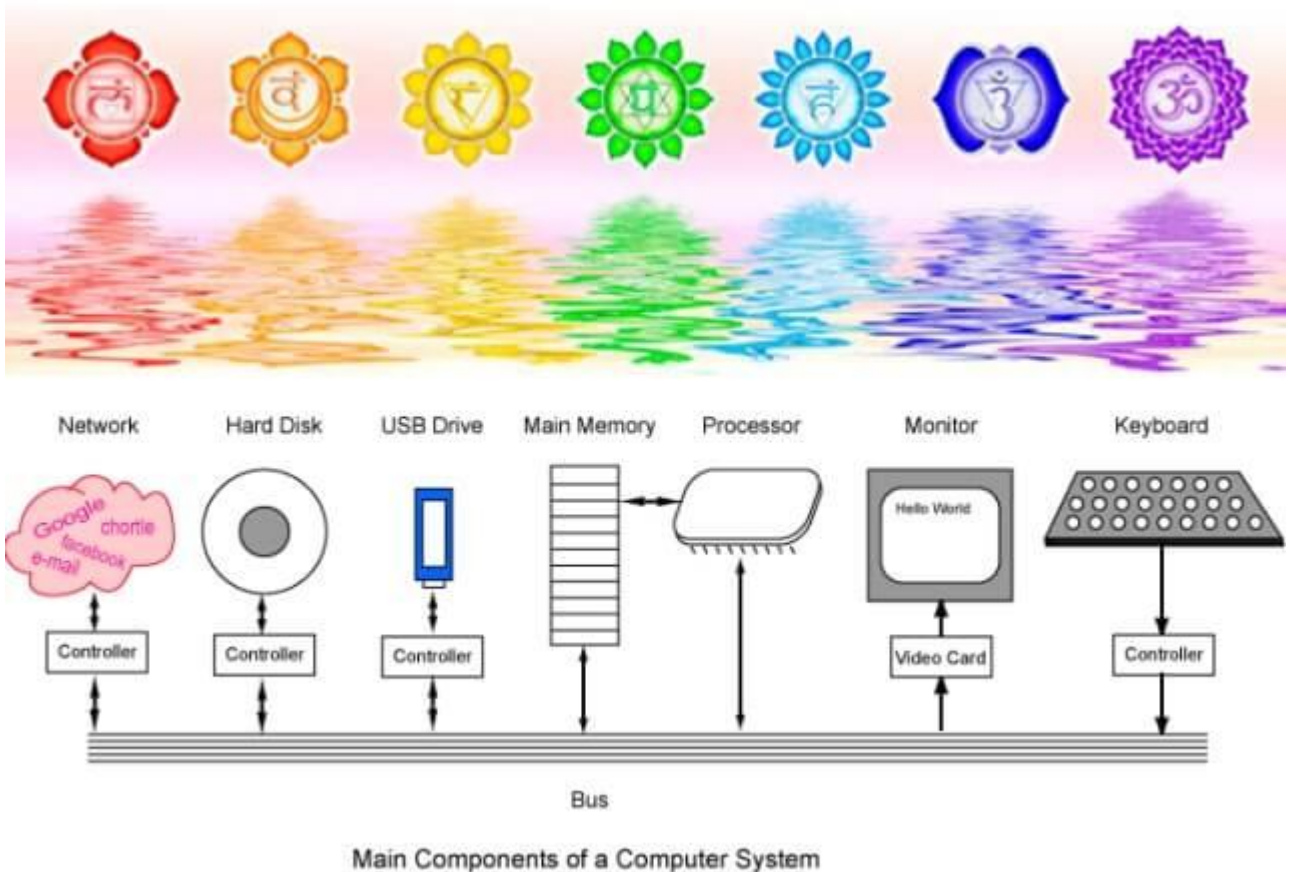
Fig. 3.4. Chakras and computer system bus analogy

Human Chakras depending on their location in the human body facilitate the work of certain organs and body systems by supplying energy (and information) from without and emitting used energy (and information) from within the certain organs and body systems. **That is the way energy is kept in balance in the human organism.** Just like with breathing: you breathe in the oxygen and breathe out carbon dioxide. You also eat food and drink water, and then, well, you release whatever is left over. By analyzing the quality of the energy and

the frequency of each Chakra energy "breathing" process it is possible to evaluate what is happening in the inner organs of your body.

How seven Chakras are connected with nervous and endocrine systems of a human body?

In Puchko LG [2004] we read that the **first** Chakra is related to the testicles and sacral plexus, **second** Chakra to the ovaries, adrenals and kidneys, **third** Chakra to **spleen**, liver and solar plexus, **fourth** Chakra to **thymus**, heart and cardial plexus, **fifth** Chakra to thyroid and parathyroid glands, **sixth** Chakra to pituitary gland and brain, **seventh** Chakra to pineal gland.

Chase CR [2018] provides a table according to which the **first** Chakra is associated with adrenals, pelvic nerve plexus, spine, kidneys, bladder, large intestine; **second** Chakra with testes/ovaries, inferior mesenteric ganglion, ileum, organs of reproduction; **third** Chakra with [endocrine] pancreas, celiac plexus ganglion, liver, gall bladder, stomach, duodenum, pancreas, **spleen**; **fourth** Chakra with **thymus**, celiac plexus, heart, circulation, vagus nerve; **fifth** Chakra with thyroid and parathyroid glands, inferior cervical ganglion, lungs, bronchus, larynx, pharynx, large intestine, vagus nerve; **sixth** Chakra with pituitary and pineal glands, thalamus, hypothalamus, superior cervical ganglion, left brain, lower brain, ears/nose, left eye; **seventh** Chakra with pineal gland, right brain, upper brain, right eye.

49
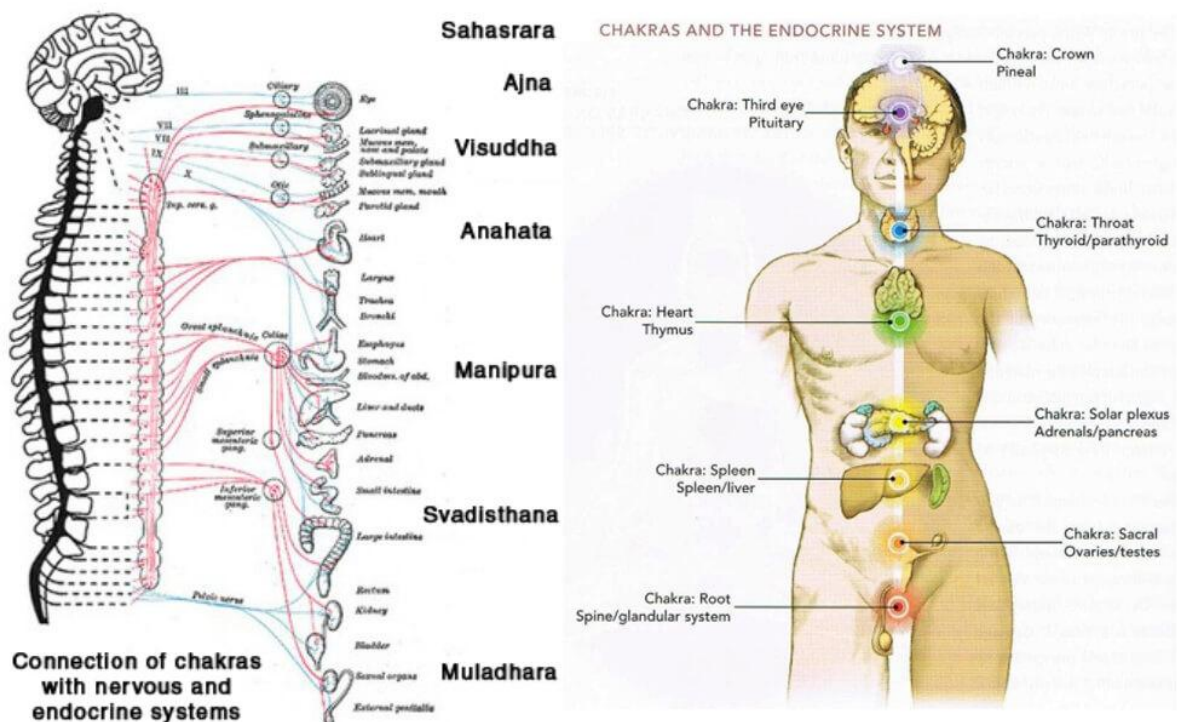
Fig. 3.5. Connection of Chakras with nervous and endocrine systems of a human body
https://lifescriptdoctor.com/wp-content/uploads/2015/06/the-seven-chakras.jpg

After such a retreat, it is time to move on to the presentation of our own results.

To visualize correlationship we should decide concerning factor (argument) and effective (function) parameters. In terms of mathematics it does not matter, while in terms of physiology there is the perennial problem of cause and effect. Accordingly, and based on the biblical postulate that "The beginning was the Word ...", that is, information/energy, we have chosen as a factor GDV parameters.

For a sample of 40 observations critical value of correlation coefficient module at $p<0,05$ ($t>2,02$) is 0,31, at $p<0,01$ ($t>2,70$) is 0,41, at $p<0,001$ ($t>3,55$) is 0,52.

Revealed that Testosterone level moderately positively correlated, especially, with Entropy GDI in Left projection (Fig. 3.6).

It should be noted that men plasma Testosterone was in range 6,4÷19,2 nM/L (norm 9,5÷20,1 nM/L), in one case it was 4,5 nM/L (norm 9,5 nM/L), while in women plasma Testosterone was in range 1,6÷4,8 nM/L (norm 0,05÷4,6 nM/L). Thus at women Entropy Left in 16 of 20 tests was less than 3,8.

Also found a moderate positive correlation Testosterone with Area GDI in Frontal projection with filter and with Shape coefficient GDI in Left projection.

Contrary to expectation, we found no connection Testosterone level with Chakra 1 or 2, while detected with Chakra 3 Asymmetry as well as Chakras 5 and 7 Energy (Table 3.1).

Taken together, these parameters GDV determine plasma Testosterone level by 65% (Table 3.1 and Fig. 3.7).

Test = -45,8 + 13,9*EL
Correlation: r = 0,466
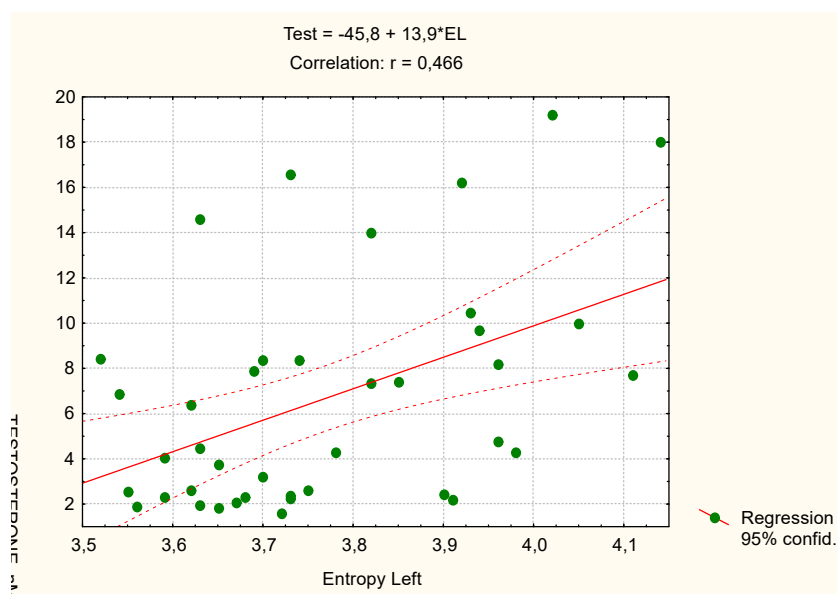
Fig. 3.6. Relationship between Entropy Gas Discharge Image in Left projection (axis X) and serum Testosterone (axis Y)

Table 3.1. Regression Summary for Dependent Variable: Testosterone
R=0,805; R^2=0,648; Adjusted R^2=0,571; $F_{(7,3)}$=8,4; $p<10^{-5}$; Std. Error of estimate: 3,2 nM/L

		Beta	St. Err. of Beta	B	St. Err. of B	$t_{(32)}$	p-level
	r		Intercpt	-109	28,9	-3,76	,001
EL	0,47	,197	,132	5,88	3,94	1,49	,145
AF f	0,42	,481	,140	,00092	,00027	3,44	,002
Ch3A	0,38	,294	,109	4,62	1,72	2,69	,011
SL	0,29	,770	,235	,896	,273	3,28	,003
Ch5E	0,25	,309	,166	5,05	2,71	1,87	,071
Ch7E	-0,30	-,303	,183	-6,25	3,78	-1,65	,108
Sym	-0,26	,583	,201	,583	,201	2,90	,007

Abbreviations of GDV parameters: A - Area, E - Entropy, Sym – Symmetry, S – Shape coefficient, R – Right projection, F – Frontal projection, L – Left projection, f – with filter, Chakras (Ch) Energy [E=(R+L)/2] and Asymmetry (A=R-L).
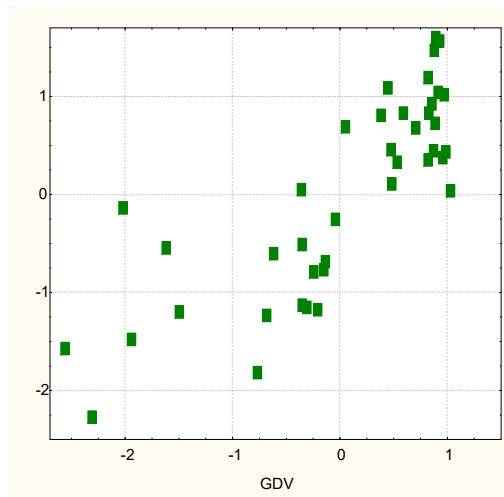
Fig. 3.7. Canonical correlation between GDV parameters (axis X) and plasma Testosterone (axis Y)

Instead, were met expectations regarding the key adaptation hormone Cortisol, which plasma level moderately but significantly correlated with Chakra 2 Asymmetry, which, as noted, is related to the adrenals, as well as with Chakra 6 Asymmetry and Energy, which is related to pituitary gland (ACTH) and brain (CRH) (Fig. 3.8 and Table 3.2).
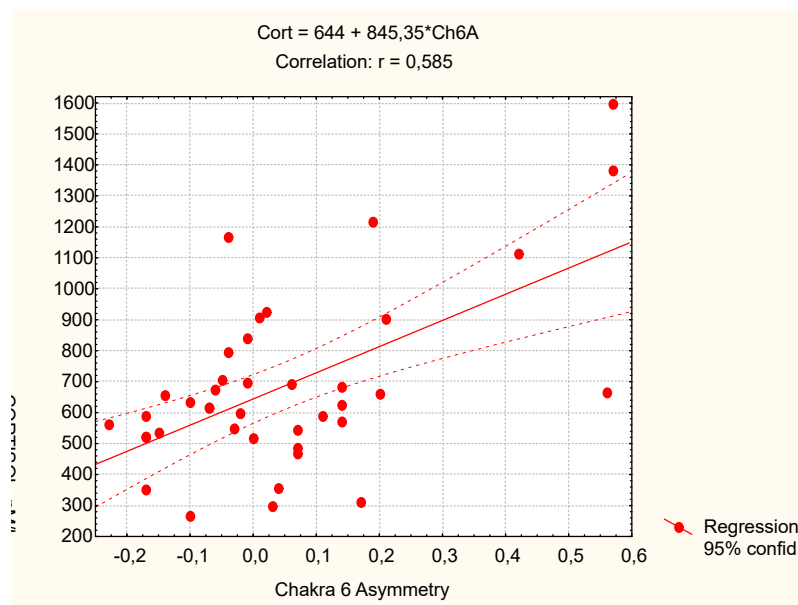
Fig. 3.8. Relationship between Chakra 6 Asymmetry (axis X) and plasma Cortisol (axis Y)

Table 3.2. Regression Summary for Dependent Variable: Cortisol

R=0,663; R^2=0,440; Adjusted R^2=0,393; $F_{(3,4)}$=9,4; $p<10^{-4}$; Std. Error of estimate: 223 nM/L

		Beta	St. Err. of Beta	B	St. Err. of B	$t_{(36)}$	p-level
	r		Intercpt	688	46	15,0	10^{-6}
Ch6A	0,59	,476	,136	688	197	3,50	,001
Ch6E	0,39	,208	,135	204	133	1,54	,133
Ch2A f	-0,31	-,261	,126	-304	146	-2,08	,045

Both Chakras together determine Cortisol level by 44% (Table 3.2 and Fig. 3.9).
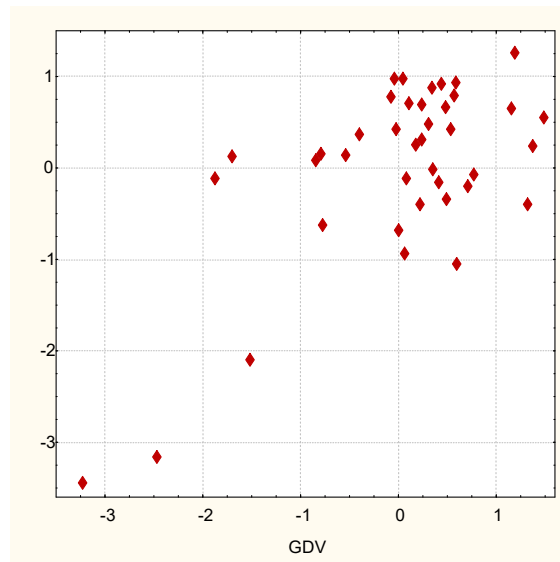
Fig. 3.9. Canonical correlation between GDV parameters (axis X) and plasma Cortisol (axis Y)

Once fully consistent with the concept of Chakras regulatory role Calcitonin plasma level, which source is as C-cells of the thyroid gland (related to Chakra 5) and thymus (related to Chakra 4). Both Chakras together determine Calcitonin plasma level by 37,5% (Table 3.3 and Fig. 3.10).

Table 3.3. Regression Summary for Dependent Variable: Calcitonin

$R=0,613$; $R^2=0,375$; Adjusted $R^2=0,323$; $F_{(3,4)}=7,2$; $p<10^{-3}$; Std. Error of estimate: 2,8 ng/L

		Beta	St. Err. of Beta	B	St. Err. of B	$t_{(36)}$	p-level
	r		Intercpt	-24,2	11,95	-2,02	,050
Ch5A	0,38	,354	,132	5,83	2,17	2,68	,011
Ch4A f	0,37	,341	,132	4,48	1,74	2,58	,014
EF f	0,34	,338	,132	8,39	3,27	2,56	,015
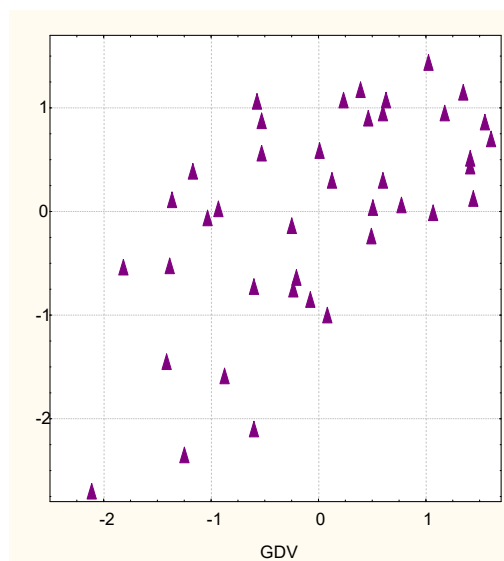
Fig. 3.10. Canonical correlation between GDV parameters (axis X) and plasma Calcitonin (axis Y)

Instead, for the main thyroid hormone Triiodothyronine we have not found connections with Chakra 5, but only with Chakras 1 and 7 (Table 3.4) as well as with Area GDI in Frontal and Left projections, which together determine Triiodothyronine plasma level by 36% (Table 3.4 and Fig. 3.11).

Table 3.4. Regression Summary for Dependent Variable: Triiodothyronine
R=0,603; R^2=0,364; Adjusted R^2=0,270; $F_{(5,3)}$=3,9; p=0,007; Std. Error of estimate: 0,77 nM/L

		Beta	St. Err. of Beta	B	St. Err. of B	$t_{(34)}$	p-level
	r		Intercpt	7,84	2,39	3,28	,002
Ch1A	-0,40	-,257	,150	-1,021	,595	-1,71	,096
Sym	-0,32	-,398	,185	-,0726	,0337	-2,15	,038
AF	-0,27	-,605	,417	-,00016	,00011	-1,45	,156
AL	-0,26	,639	,436	,00020	,00013	1,47	,152
Ch7A	0,28	,492	,188	1,527	,584	2,62	,013
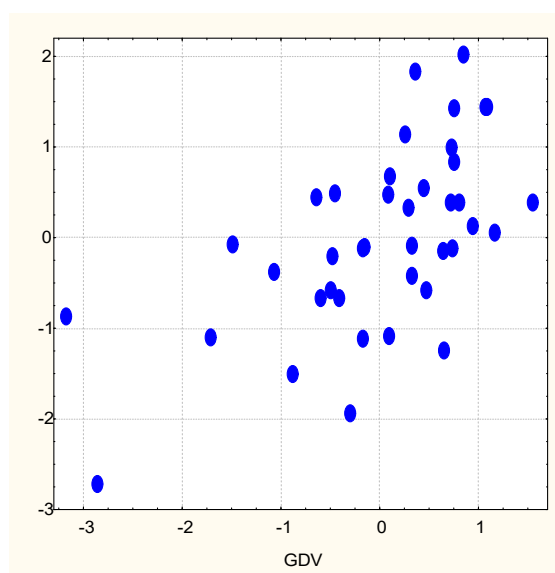
Fig. 3.11. Canonical correlation between GDV parameters (axis X) and plasma Triiodothyronine (axis Y)

And absolutely poorly, but significantly was associated with GDV parameters Aldosterone plasma level (Table 3.5 and Fig. 3.12).

Table 3.5. Regression Summary for Dependent Variable: Aldosterone
R=0,481; R^2=0,232; Adjusted R^2=0,168; $F_{(3,4)}$=3,6; p=0,022; Std. Error of estimate: 15 pM/L

		Beta	St. Err. of Beta	B	St. Err. of B	$t_{(36)}$	p-level
	r		Intercpt	117	251	0,47	,64
EF	-0,40	-,314	,157	-32,1	16,0	-2,00	,05
Ch6A f	-0,26	-,231	,147	-12,9	8,3	-1,56	,13
Sym f	0,27	,173	,156	2,65	2,39	1,11	,28
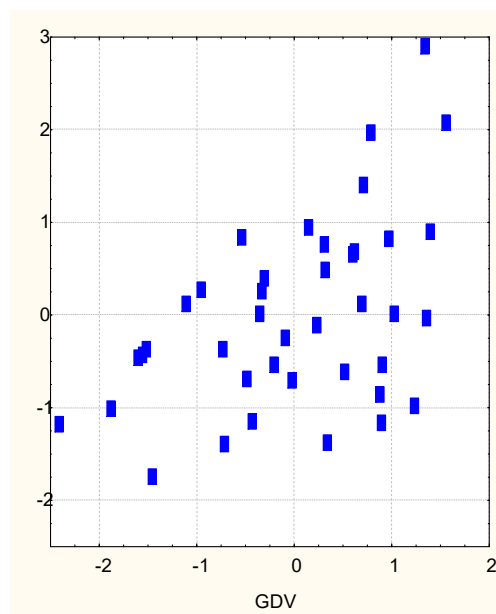
Fig. 3.12. Canonical correlation between GDV parameters (axis X) and plasma Aldosterone (axis Y)

Baevskiy's Stress Index is an integral parameter of the autonomic nervous system. Established that it is closely correlated with a number of options EEG, including power spectral density of δ-rhythm in the loci: O1 (r=0,68); Fp1 (r=0,67); T5 (r=0,66); T6 (r=0,66); O2 (r=0,49) as well as with amplitude of δ-rhythm (r=0,54) and modal frequency of α-rhythm (r=-0,44); Canonical R=0,80 [Popovych IL et al, 2014].

It is not surprising that Baevskiy's Stress Index is related to Chakra 6 (Fig. 3.13 and Table 3,6), which, in turn, is connected with brain.
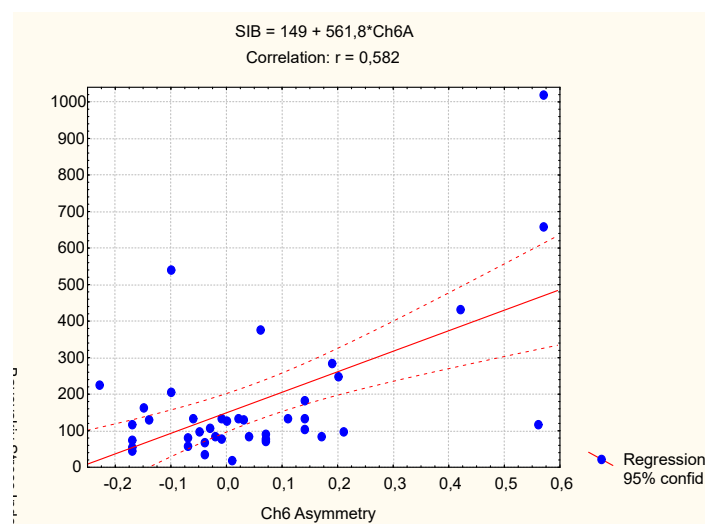
Fig. 3.13. Relationship between Chakra 6 Asymmetry (axis X) and Baevskiy's Stress Index (axis Y)

Interestingly, the components of Baevskiy's Stress Index associated with GDV parameters less crowded. Canonical correlation coefficients are for the Mode 0,617 (R^2=0,381; AdjR^2=0,329; $F_{(3,4)}$=7,4; p<10^{-3}), for AMo as sympathetic marker 0,701 (R^2=0,491; AdjR^2=0,417; $F_{(5,3)}$=6,6; p<10^{-3}), for MxDMn as vagal marker 0,630 (R^2=0,397; AdjR^2=0,347; $F_{(3,4)}$=7,9; p<10^{-3}). Triangular Index as marker of vagal tone associated with GDV parameters even weaker: R=0,483; R^2=0,234; AdjR^2=0,170; $F_{(3,4)}$=3,7; p=0,021.

Temporal HRV parameters as others markers of vagal tone on the strength of canonical correlation with GDV parameters were ranked in the following order: SDNN ($R=0,505$; $R^2=0,255$; $AdjR^2=0,193$; $F_{(3,4)}=4,1$; $p=0,013$); RMSSD ($R=0,341$; $R^2=0,116$; $AdjR^2=0,093$; $F_{(1,4)}=5,0$; $p=0,031$; pNN_{50} ($R=0,331$; $R^2=0,110$; $AdjR^2=0,086$; $F_{(1,4)}=4,7$; $p=0,037$).

Chakra 6 together with Chakras 5, 2 and 3 determines Baevskiy's Stress Index by 63% (Table 3.6 and Fig. 3.14).

Table 3.6. Regression Summary for Dependent Variable: Stress Index
$R=0,795$; $R^2=0,633$; Adjusted $R^2=0,566$; $F_{(6,3)}=9,5$; $p<10^{-5}$; Std. Error of estimate: 126 units

		Beta	St. Err. of Beta	B	St. Err. of B	$t_{(33)}$	p-level
	r			Intercpt	3593	1878	1,91	,064
Ch6A	0,58	,339	,120	327	115	2,83	,008
Ch6E	0,48	,982	,419	643	274	2,35	,025
Ch5E	0,35	-,705	,419	-443	263	-1,68	,102
Ch2A f	-0,39	-,219	,126	-170	98	-1,74	,091
Ch3A f	-0,35	-,189	,111	-153	90	-1,71	,097
Sym f	-0,33	-,197	,111	-36	20	-1,77	,085
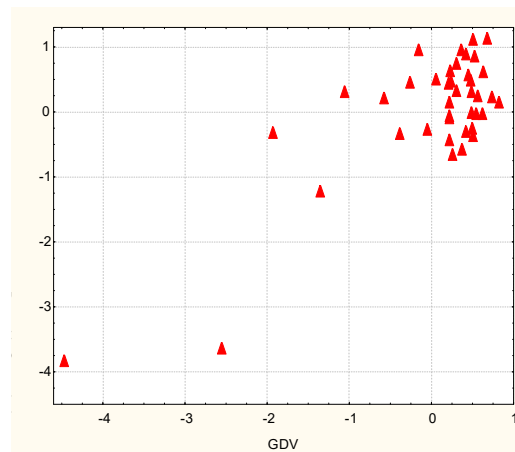
Fig. 3.14. Canonical correlation between GDV parameters (axis X) and Baevskiy's Stress Index (axis Y)

PSD of HF band HRV as spectral marker of vagal tone is also poorly associated with GDV parameters, and the correlation is stronger for the relative PSD ($R=0,568$; $R^2=0,323$; $AdjR^2=0,245$; $F_{(4,3)}=4,2$; $p=0,007$) than absolute PSD ($R=0,408$; $R^2=0,166$; $AdjR^2=0,121$; $F_{(2,4)}=3,7$; $p=0,034$).

We will remind that it is speculated that absolute PSD of LF band HRV reflects mainly Sympathetic outflow or both Sympathetic and Vagal origin, while relative PSD is seen as more likely marker of sympathetic tone. As mentioned fourth Chakra is related to thymus, **heart and cardial** plexus. It is noteworthy that absolute PSD of LF band correlates with Asymmetry and Energy of fourth Chakra, which together with Area of GDI in the Right projection determines its by 39% (Table 3.7).

Table 3.7. Regression Summary for Dependent Variable: LF absolute
$R=0,623$; $R^2=0,388$; Adjusted $R^2=0,337$; $F_{(3,4)}=7,6$; $p<10^{-3}$; Std. Error of estimate: 851 msec^2

		Beta	St. Err. of Beta	B	St. Err. of B	$t_{(36)}$	p-level
Intercpt	r			4239	1147	3,69	,001
Ch4A	-0,39	-,200	,140	-651	456	-1,43	,162
Ch4E f	0,32	,548	,164	2585	775	3,33	,002

AR	-0,25	-,526	,159	-,168	,051	-3,31	,002

Stronger and more numerous links with GDV parameters found for relative PSD of LF band, primarily with the Area of GDI in the Left projection (Fig. 3.15 Table 3.8).
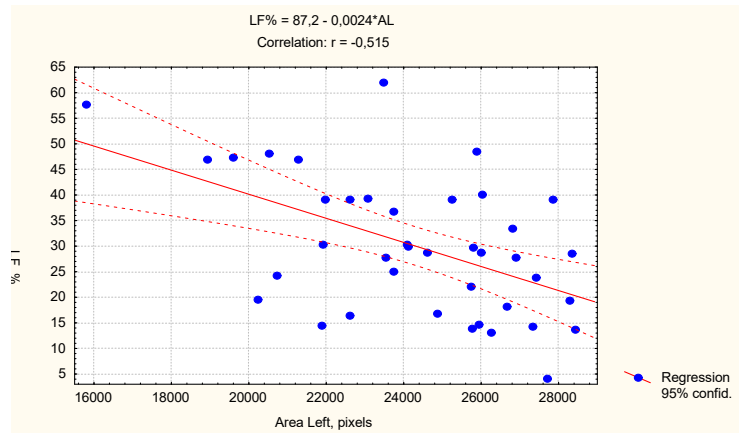
Fig. 3.15. Relationship between Area GDI in Left projection (axis X) and relative PSD of LF band HRV (axis Y)

In general, the higher sympathetic tone, the smaller the area of GDI and the higher its Shape coefficient and Korotkov's Activation Coefficient (CAK). Taken together these GDV parameters determines relative SPD LF band HRV by 53% (Table 3.8).

Table 3.8. Regression Summary for Dependent Variable: LF relative
R=0,729; R^2=0,531; Adjusted R^2=0,428; $F_{(7,3)}$=5,2; p<10^{-3}; Std. Error of estimate: 10 %

		Beta	St. Err. of Beta	B	St. Err. of B	$t_{(32)}$	p-level
	r		Intercpt	220	61	3,63	,001
AL	-0,51	-1,141	,365	-,0052	,0017	-3,13	,004
AF	-0,37	1,280	,457	,0050	,0018	2,80	,009
AF f	-0,34	-,875	,288	-,0045	,0015	-3,04	,005
KAC	0,41	,885	,255	11,34	3,26	3,48	,001
SR f	0,36	-,313	,246	-3,079	2,417	-1,27	,212
SF f	0,33	-,174	,225	-1,267	1,640	-,77	,446
SR	0,30	-,242	,293	-,826	1,001	-,82	,415

Regarding the absolute PSD of VLF band we found connection with Chakras 5 and 6 related to Thyroide gland, Hypophyse and Brain as well as with Chakras 3, 1 and 4, whith together determines its by 44% (Table 3.9 and Fig. 3.16).

Table 3.9. Regression Summary for Dependent Variable: VLF absolute
R=0,661; R^2=0,437; Adjusted R^2=0,314; $F_{(7,3)}$=3,55; p=0,006; Std. Err. of estimate: 2042 $msec^2$

		Beta	St. Err. of Beta	B	St. Err. of B	$t_{(32)}$	p-level
	r		Intercpt	-15759	9034	-1,74	,091
Ch3A f	0,39	,288	,171	2989	1781	1,68	,103
Ch1E	0,38	,370	,157	2915	1239	2,35	,025
CH6A f	0,32	,810	,504	6909	4302	1,61	,118
CH5A f	0,28	-,853	,500	-6749	3952	-1,71	,097
EF	0,27	,562	,219	8754	3415	2,56	,015
EL	0,27	-,285	,235	-4226	3472	-1,22	,232
Ch4 A	-0,28	-,325	,153	-2500	1175	-2,13	,041
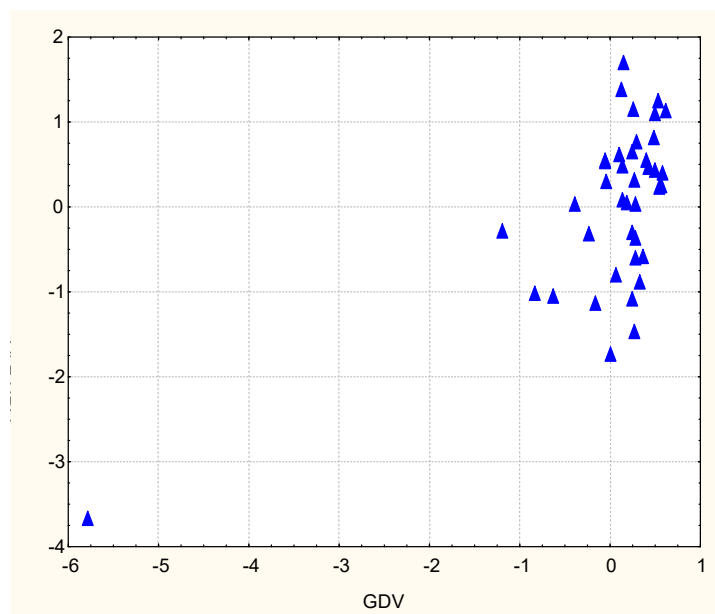
Fig. 3.16. Canonical correlation between GDV parameters (axis X) and PSD of VLF band HRV (axis Y)

There is speculation that VLF band ($0,04 \div 0,015$ Hz) HRV associated with oscillation blood levels of **renin** (0,04 Hz) and epinephrine (0,025 Hz) as well as reflects **thermoregulatory** cycles [cyt: Kotelnikov SA et al, 2002]. In support of these assumptions prove identified in this cohort links between absolute PSD of VLF and **Aldosterone** (r=-0,33) as well as **Triiodethyronine** (r=0,24). Instead, relative PSD of VLF band is associated with both Chakras 5 and 6, and with Chakra 2, whith together with Chakra 4 determines its by 45% (Table 3.10).

Table 3.10. Regression Summary for Dependent Variable: VLF relative
R=0,669; R^2=0,448; Adjusted R^2=0,367; $F_{(5,3)}$=5,5; $p<10^{-3}$; Std. Error of estimate: 14 %

		Beta	St. Err. of Beta	B	St. Err. of B	$t_{(34)}$	p-level
	r		Intercpt	59,2	2,7	21,8	10^{-6}
Ch1A f	0,39	,351	,139	33,5	13,3	2,53	,016
Ch4A f	0,30	,232	,129	15,7	8,7	1,80	,081
Ch6E	0,29	,333	,132	20,4	8,1	2,52	,017
Ch5A f	0,28	,245	,130	14,1	7,5	1,89	,067
Ch2A f	-0,33	-,233	,135	-16,9	9,8	-1,72	,095

It is speculated that ULF band ($0,015 \div 0,003$ Hz) HRV associated with oscillation blood level of norepinephrine (0,002 Hz) as well as 17-OCS (0,0019 Hz) [cyt: Kotelnikov SA et al, 2002]. In support of these assumptions prove identified in this cohort links between ULF and Cortisol (r=0,23). We found no connection its with Chakra 2, instead found with Chakras 4 and 6 related to cardiac plexus, Hypophyse and Brain, whith together with Chakra 5 determines absolute PSD of ULF band by 43% (Table 3.11 and Fig. 3.17).

Table 3.11. Regression Summary for Dependent Variable: ULF
R=0,658; R^2=0,433; Adjusted R^2=0,349; $F_{(5,3)}$=5,2; p=,0012; Std. Error of estimate:123 $msec^2$

		Beta	St. Err. of Beta	B	St. Err. of B	$t_{(34)}$	p-level
	r		Intercpt	-4632	1847	-2,51	,017
Ch5E	0,34	,241	,140	121	70	1,72	,095
Ch6A f	0,34	,268	,133	142	70	2,01	,052

Ch6A	0,28	,261	,141	201	109	1,84	,074
Sym f	0,30	,349	,137	50	20	2,55	,015
Ch4A f	-0,31	-,267	,132	-154	76	-2,03	,051
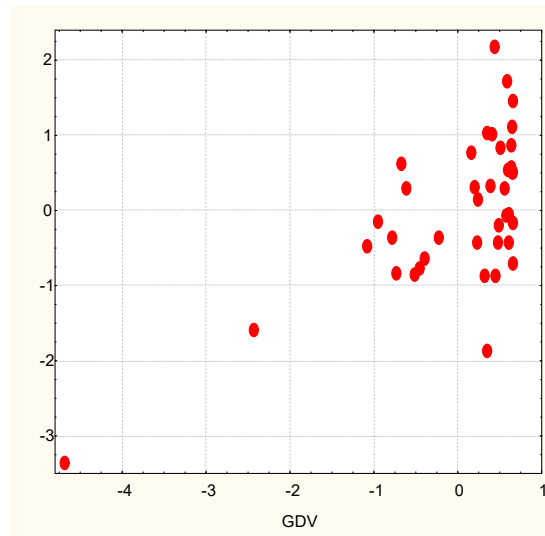
Fig. 3.17. Canonical correlation between GDV parameters (axis X) and PSD of ULF band HRV (axis Y)

LF/HF ratio is another integral parameter of the autonomic nervous system reflecting sympathetic-vagal balance. Established that it is correlated with a number of options EEG, including index of α-rhythm (r=-0,32) and its asymmetry (r=0,30), modal frequency of θ-rhythm (r=-0,34), relative PSD P4-β (r=0,37), C3-β (r=0,36), P3-α (r=-0,33) as well as absolute PSD C3-α (r=-0,32), F3-α (r=-0,31), F4-α (r=-0,3) and T5-θ (r=0,31); Canonical R=0,56 [Popovych IL et al, 2014]. Nevertheless, we found no connection LF/HF ratio with Chakra 6, while it is determined by Shape coefficients in Left and Frontal projections as well as by Entopy GDI in Frontal projection by 57% (Table 3.12 and Fig. 3.18).

Table 3.12. Regression Summary for Dependent Variable: LF/HF
R=0,755; R^2=0,570; Adjusted R^2=0,507; $F_{(5,3)}$=9,0; $p<10^{-4}$; Std. Error of estimate: 3,9

		Beta	St. Err. of Beta	B	St. Err. of B	$t_{(34)}$	p-level
	r		Intercpt	-89,4	21,3	-4,19	,0002
SL	0,49	1,648	,380	2,148	,496	4,33	,0001
EF f	0,39	,294	,119	11,71	4,74	2,47	,0186
SF	0,37	-,714	,294	-,750	,309	-2,43	,0205
AL	-0,29	,679	,254	,0013	,0005	2,68	,0114
Ch1A	-0,28	-,377	,122	-9,19	2,96	-3,11	,0038
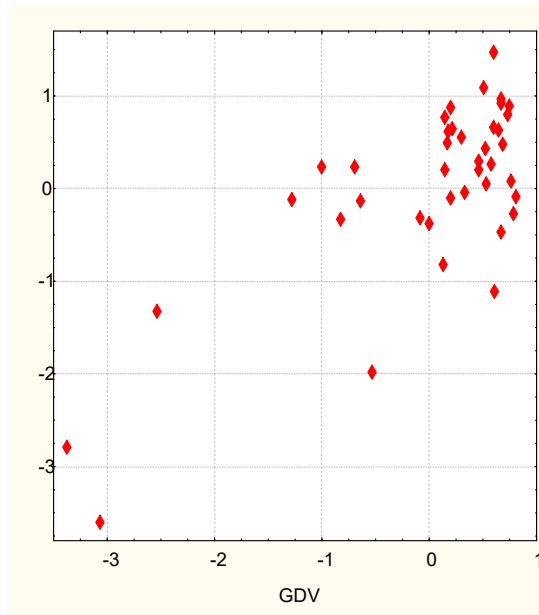
Fig. 3.18. Canonical correlation between GDV parameters (axis X) and LF/HF ratio HRV (axis Y)

At the final stage, we analyzed the relationships between the two constellations parameters.

The program has selected 22 GDV parameters (right set) and 9 neuro-endocrine parameters (left set), information of which condensed to three pairs of canonical roots (Table 3.13).

Table 3.13. Chi-Square Tests with Successive Roots Removed

	R	R^2	χ^2	df	p	Λ Prime
0	**,970**	**,941**	**264**	**198**	**,001**	**$<10^{-4}$**
1	,958	,918	198	168	,055	$<10^{-3}$
2	*,918*	*,842*	*141*	*140*	*,462*	*,002*

As seen in Table 3.14, GDV Root 1 (major) receives positive factor load from eight options, including Chakras 3, 2 and 7, while negative load from six settings, including the Chakras 6, 7 and 5. Corresponding neuro-endocrine Root includes information on key factors of adaptation, which is determined GDV parameters by 94% (Table 3.13 and Fig. 3.19).

Table 3.14. Canonical Analysis Summary. Factor Structure

Right set	Root 1	Root 2	Root 3	**Left set**	Root 1	Root 2	Root 3
Ch3 Asymmetry	**,47**	,21	-,05	Testosterone	**,77**	-,07	-,44
Entropy Left	**,40**	-,12	-,36	Cortisol	**-,69**	,24	-,44
Ch3 Asymmetry f	**,37**	,07	-,07	Stress Index	**-,58**	-,00	-,52
Ch2 Asymmetry f	**,36**	,09	,21	Aldosterone	,08	**,65**	-,09
Shape coeffic. Left	**,36**	-,15	-,00	T3	,06	**,34**	-,01
Ch7 Asymmetry	**,30**	,19	-,17	VLF	-,09	**,19**	-,39
Area Frontal f	**,25**	,03	-,47	LF/HF	,34	**-,36**	-,36
Shape coeff Frontal	**,24**	-,04	-,09	Calcitonin	-,09	**-,28**	-,45
Ch6 Asymmetry	**-,39**	-,04	-,62	ULF	,00	,11	**-,68**
Ch7 Energy	**-,35**	-,02	,00				
Ch5 Asymmetry	**-,32**	,12	-,35				
Area Left	**-,24**	,14	-,20				
Ch6 Energy	**-,23**	,14	-,55				

Symmetry	-,22	-,03	,13				
Entropy Frontal f	,09	-,46	-,29				
Entropy Frontal	,11	-,30	-,28				
Ch4 Asymmetry f	-,05	-,19	,13				
Ch6 Asymmetry f	,11	-,19	-,36				
Ch1 Asymmetry	-,01	-,06	,05				
Symmetry f	,13	,37	,04				
Ch5 Energy	-,02	,08	-,57				
Area Frontal	-,00	,02	-,33				
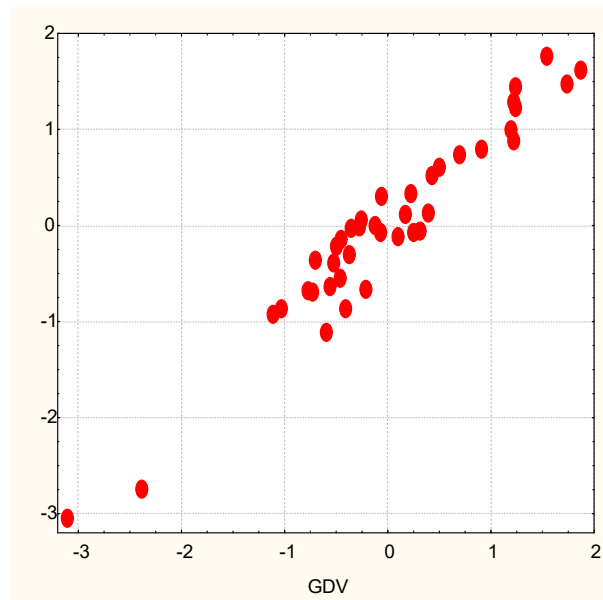
Fig. 3.19. Correlation between the first canonical roots of GDV parameters (axis X) and neuro-endocrine parameters (axis Y)

GDV Root 2 (minor) receives factor load from six others settings, which determines others neuro-endocrine parameters by 92% (Table 3.13 and Fig. 3.20).
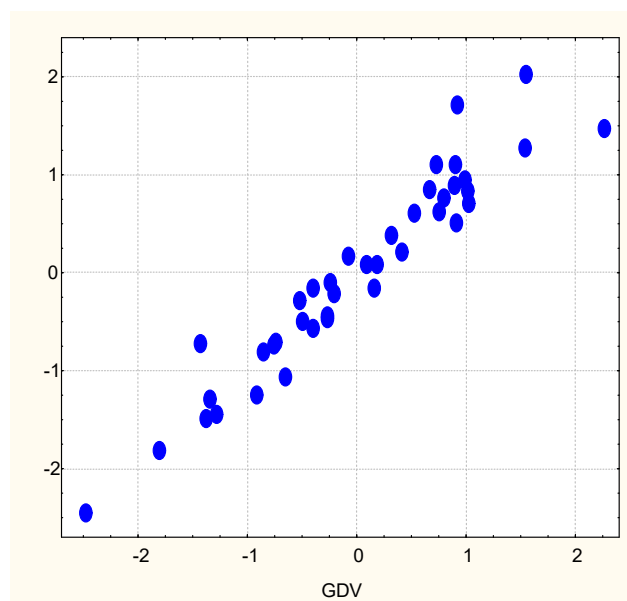
Fig. 3.20. Correlation between the second canonical roots of GDV parameters (axis X) and neuro-endocrine parameters (axis Y)

The third pair of canonical roots is not worthwhile because of the nonsignificant p-level. We consider it necessary to bring the correlation matrix (Table 3.15).

Table 3.15. Matrix of GDV-Neuroendocrine Correlations
p<0,05; p<0,01; p<0,001

Neuro-endocrine parameters	GDV parameters: A - Area, E - Entropy, Sym – Symmetry, S – Shape coefficient, F – Frontal projection, L –Left projection, f – with filter									
	AF	AFf	Sym	Symf	EF	EFf	SF	AL	EL	SL
Testosterone		,42	-,26			,25			,47	,29
Cortisol										
Stress Index				-,33						
LF/HF			-,35	-,38	,25	,39	,37	-,29	,36	,49
Aldosterone				,27	-,40	-,28				
T3	-,27		-,32				,25	-,26		,28
Calcitonin				-,29		,34				
ULF	,25	,25		,30					,26	
VLF					,27				,27	

Prolongation of table 3.15

| Neuro-endocrine parameters	Gas Discharge Visualization parameters: virtual Chacras Asymmetry (A) and Energy (E)										
	Ch1 A	Ch2 Af	Ch3 A	Ch3 Af	Ch4 Af	Ch5 A	Ch5 E	Ch6 A	Ch6 Af	Ch6 E	Ch 7A E	Ch7 E
Testosterone			,38	,25			,25				,27	-,30
Cortisol		-,31				,43		,59		,39		
Stress Index		-,39	-,33	-,35		,46	,35	,58		,48		
LF/HF	-,28											
Aldosterone									-,26			
T3	-,40										,28	
Calcitonin					,37	,38		,37				
ULF				,26	-,31		,34	,28	,34	,34		
VLF				,39					,32	,28		

We cherish the hope that confirmed that between principal neuroendocrine factors of adaptation and parameters of GDV exist strong canonical correlation suggesting informativenes this method for estimation at least adaptation and its changes.

The stated results were published in:

1. Babelyuk VYe, Dubkova GI, Popovych IL. Gas discharge visualization parameters correlate with some psycho-physiological and endocrine parameters of healthy men [in Ukrainian]. In: "Actual problems of biophysical medicine". Materials VII International symposium (Kyïv, 14-17 May 2014). Kyïv. OO Bohomolets' Institute of Physiology; 2014: 11-13.

2. Babelyuk VYe, Dubkova GI, Kikhtan VV, Korolyshyn TA, Popovych IL. The relationship between the parameters of gas discharge visualization and neuro-endocrine regulation [in Ukrainian]. In: Valeology: current status, trends and prospects development. Abstracts XIV International scientific and practical conference (Kharkiv-Drohobych, 14-16 April 2016). Kharkiv. VN Karazin KhNU; 2016: 360-361.

3. Babelyuk VYe, Dubkova GI, Kikhtan VV, Korolyshyn TA, Zukow W, Popovych IL. The parameters of gas discharge visualization and principal neuroendocrine factors of adaptation closely correlated. In: IX International symposium "Actual problems of biophysical medicine" (Kyïv, 12-15 May 2016). Kyïv. OO Bohomolets' Institute of Physiology; 2016: 9-10.

4. Babelyuk VYe, Dubkova GI, Korolyshyn TA, Zukow W, Popovych IL. The correlationships between parameters of gas discharge visualization and principal neuroendocrine factors of adaptation. In: Pathophysiology and Pharmacy: ways of integration. Abstracts VII National Congress of Pathophysiologists Ukraine with international participation (5-7 October 2016). Kharkiv. NPhU; 2016: 8-8.

5. Babelyuk VE, Gozhenko AI, Dubkova GI, Babelyuk NV, Zukow W, Kovbasnyuk MM, Popovych IL. Causal relationships between the parameters of gas discharge visualization and

principal neuroendocrine factors of adaptation. Journal of Physical Education and Sport. 2017; 17(2): 624-637.

CHAPTER 4

CAUSAL RELATIONSHIPS BETWEEN THE PARAMETERS OF GAS DISCHARGE VISUALIZATION AND IMMUNITY

Considering the close interaction of the neural and endocrine systems with the immune system [Solomon GF, 1987; Korneva EA, 1993; 2020; Akmayev PG, 1996; Chrousos GP, 2000; Neuroimmunomodulation, 2000; Tracey KJ, 2002; Nance DM & Sanders VM, 2007; Thayer JF & Sternberg EM, 2010; Chavan SS et al, 2017; Chavan SS & Tracey KJ, 2017; Pavlov VA et al, 2018; Chang EH et al, 2019], it was quite logical to study the relationship between the parameters of the latter and GDV parameters.

The object of observation were members of the same cohort: 10 women and 10 men aged 33-76 years without clinical diagnose but with dysfunction of neuro-endocrine-immune complex and metabolism, characteristic for premorbid (intermediate between health and illness) state. Immune status evaluated on a set of I and II levels recommended by the WHO as described in handbook [Lapovets' LYe & Lutsyk BD, 2004]. For phenotyping subpopulations of lymphocytes used the methods of rosette formation with sheep erythrocytes on which adsorbed monoclonal antibodies against receptors CD3, CD4, CD8, CD22 and CD16 from company "Granum" (Kharkiv) with visualization under light microscope with immersion system. We carried out also test of "active" rosette formation. The state of humoral immunity judged by the concentration in plasma of immunoglobulins classes G, A, M (ELISA, analyser "Immunochem", USA) and circulating immune complicis (with polyethylene glycol precipitation method).

We calculated also the Entropy (h) of Immunocytogram (relative contents subpopulations of lymphocytes) using Popovych's IL [2022] equation, which is based on Shannon's CE [1948] equation:

$$h = - [CD4 \cdot \log_2 CD4 + CD8 \cdot \log_2 CD8 + CD22 \cdot \log_2 CD22 + CD16 \cdot \log_2 CD16]/\log_2 4.$$

Educated in the spirit of Western medicine, we decided to look at the results through the eyes of adherents of Eastern medicine, ie the parameters of GDV were considered as an argument (cause), and the parameters of Immunity as a function (consequence).

Among the parameters of cellular immunity, the relative level of T-killers in the blood correlates most closely with the parameters of GDV, in particular with Entropy of GDI in Left projection (Fig. 4.1).
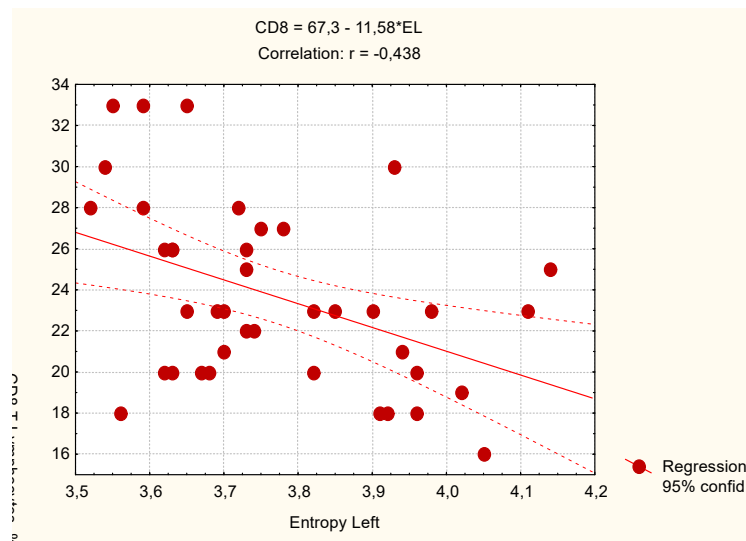
Fig. 4.1. Scatterplot of correlation between Entropy of GDI in Left projection (X-line) and CD8$^+$CD3$^+$ T-lymphocytes level (Y-line)

By stepwise exclusion to reach the maximum value of adjusted R^2, the regression model included six GDV parameters, the total impact of which on the level of T-killers is estimated at 42% (Table 4.1 and Fig. 4.2).

Table 4.1. Regression Summary for Dependent Variable: CD8⁺CD3⁺ Tc-lymphocytes
R=0,646; R^2=0,418; Adjusted R^2=0,312; $F_{(6,3)}$=3,9; $\chi^2_{(6)}$=18,9; p=0,004; SE: 3,6 %

	r	Beta	St. Err. of Beta	B	St. Err. of B	$t_{(33)}$	p-level
				Intercpt	-15,52	63,03	-,25	,81
EL	-0,44	-,265	,148	-7,01	3,92	-1,79	,08
EL f	-0,37	-,146	,157	-3,59	3,86	-,93	,36
Ch5 E	-0,33	-,126	,143	-1,83	2,08	-,88	,39
Ch4 A	-0,30	-,199	,148	-2,73	2,03	-1,35	,19
Sym f	0,38	,202	,149	,84	,62	1,36	,18
Ch1 A f	0,36	,195	,153	4,59	3,59	1,28	,21

Abbreviations of GDV parameters: A – Area (pixels), E - Entropy, Sym – Symmetry (%), S – Shape coefficient, R – Right projection, F – Frontal projection, L – Left projection, f – with filter, ChE - Chakra Energy [E=(R+L)/2], ChA – Chakra Asymmetry (A=R-L).
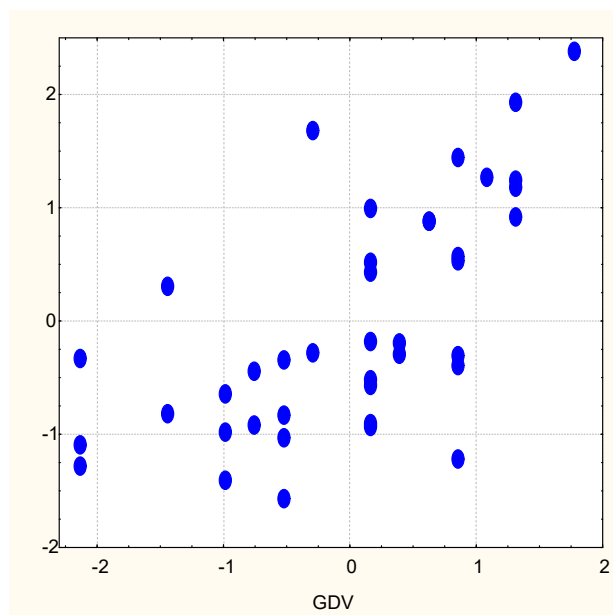
Fig. 4.2. Scatterplot of canonical correlation between GDV parameters (X-line) and CD8⁺CD3⁺ Tc-lymphocytes level (Y-line)

The level of T-helpers is upregulated by the symmetry of the GDI registered with the filter and the asymmetry of the seventh Chakra, while it is downregulated by the energy of the sixth Chakra. The degree of determination is 26% (Table 4.2 and Fig. 4.3).

Table 4.2. Regression Summary for Dependent Variable: CD4⁺ CD3⁺Th-lymphocytes
R=0,566; R^2=0,320; Adjusted R^2=0,264; $F_{(3,4)}$=5,7; $\chi^2_{(3)}$=14,1; p=0,003; SE: 4,4 %

	r	Beta	St. Err. of Beta	B	St. Err. of B	$t_{(36)}$	p-level
				Intercpt	-127,1	63,6	-2,00	,053
Sym f	0,35	,361	,140	1,75	,68	2,57	,014
Ch7 A f	0,30	,351	,139	8,42	3,32	2,53	,016
Ch6 E f	-0,32	-,265	,139	-5,16	2,71	-1,91	,065
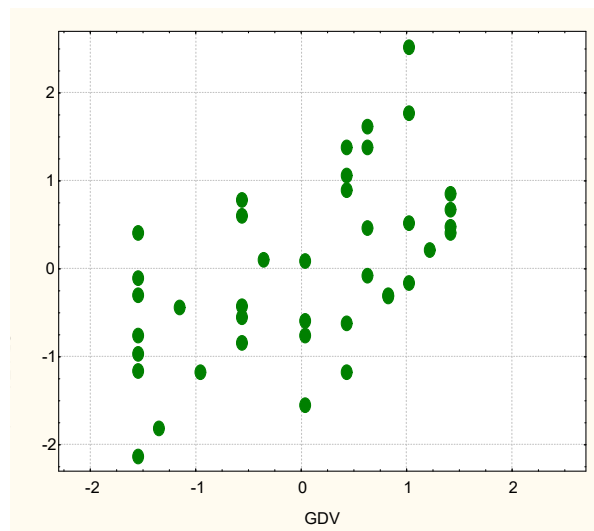
Fig. 4.3. Scatterplot of canonical correlation between GDV parameters (X-line) and CD4+CD3+Th-lymphocytes level (Y-line)

The level of T-lymphocytes with high affinity ("active") is subject to downregulation by the asymmetry of the fifth and fourth Chakras, as well as the energy of the seventh Chakra. The degree of determination is 33% (Table 4.3 and Fig. 4.4).

Table 4.3. Regression Summary for Dependent Variable: "active" T Lymphocytes
R=0,572; R^2=0,327; Adjusted R^2=0,250; $F_{(4,3)}$=4,3; $\chi^2_{(4)}$=14,3; p=0,007; SE: 3,7 %

	r	Beta	St. Err. of Beta	B	St. Err. of B	$t_{(35)}$	p-level
			Intercpt	30,65	,64	48,2	10^{-6}
Ch5 A	-0,37	-,255	,147	-5,15	2,95	-1,74	,090
Ch4 A f	-0,34	-,289	,140	-4,65	2,25	-2,07	,046
Ch4 A	-0,31	-,249	,147	-3,30	1,95	-1,69	,099
Ch7 E	-0,25	-,235	,141	-4,15	2,49	-1,67	,105
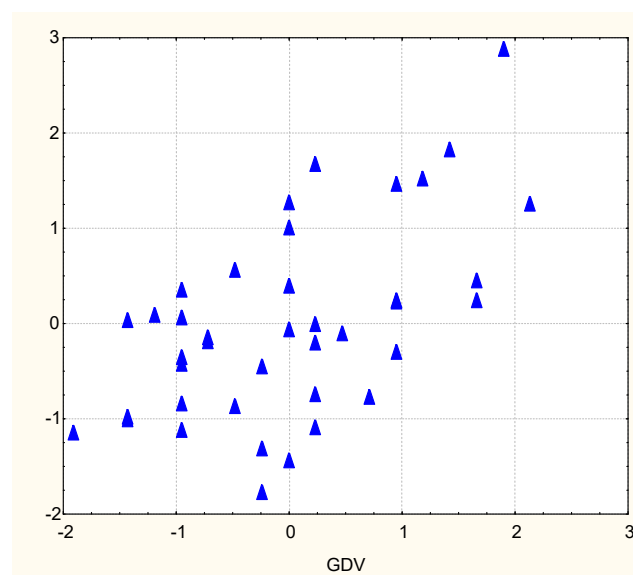
Fig. 4.4. Scatterplot of canonical correlation between GDV parameters (X-line) and "active" T-lymphocytes level (Y-line)

Downregulation by the third and sixth Chakras of the level of natural killers is very weak (16%), but statistically significant (Table 4.4 and Fig. 4.5).

Table 4.4. Regression Summary for Dependent Variable: NK-Lymphocytes
R=0,396; R^2=0,156; Adjusted R^2=0,111; $F_{(2,4)}$=3,4; p=0,043; SE: 4,5 %

		Beta	St. Err. of Beta	B	St. Err. of B	$t_{(37)}$	p-level
	r		Intercpt	18,95	,85	22,39	10^{-6}
Ch3 A f	-0,28	-,307	,152	-6,19	3,06	-2,02	,050
Ch6 E	-0,25	-,280	,152	-4,58	2,49	-1,84	,073
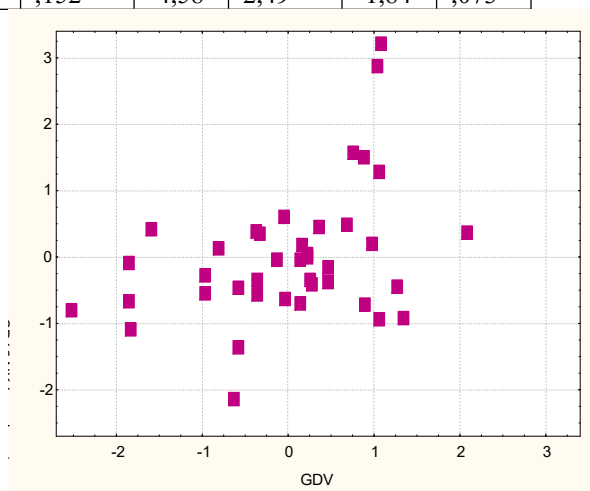
Fig. 4.5. Scatterplot of canonical correlation between GDV parameters (X-line) and NK-lymphocytes level (Y-line)

66

Instead, the relationship between B-lymphocyte levels and Chakras is insignificant (Table 4.5 and Fig. 4.6).

Table 4.5. Regression Summary for Dependent Variable: CD22+ B-lymphocytes
R=0,438; R^2=0,192; Adjusted R^2=0,099; $F_{(4,3)}$=2,1; $\chi^2_{(4)}$=7,7; p=0,105; SE: 4,0 %

|		Beta	St. Err. of Beta	B	St. Err. of B	$t_{(35)}$	p-level
	r		Intercpt	23,14	,66	35,0	10^{-6}
Ch4 A f	-0,21	-,301	,156	-4,84	2,52	-1,92	,063
Ch7 A	-0,16	-,270	,158	-3,93	2,29	-1,71	,096
Ch3 A	0,17	,284	,158	3,82	2,12	1,80	,080
Ch2 E	0,16	,227	,154	3,05	2,07	1,48	,149
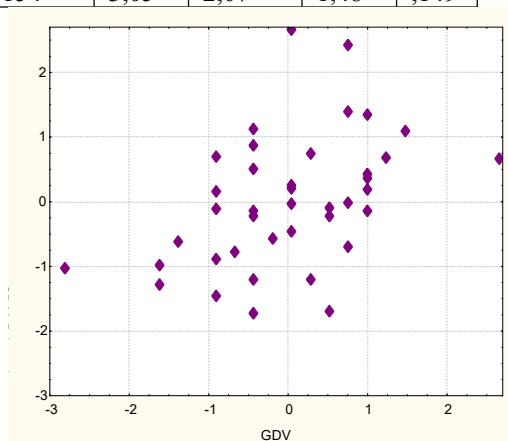
Fig. 4.6. Scatterplot of canonical correlation between GDV parameters (X-line) and CD22+ B-lymphocytes level (Y-line)

The level of 0-lymphocytes calculated by the balance method (100-Tc-Th-B-NK) was associated with the symmetry of GDI and the energy of the sixth Chakra, determined by these parameters by 21% (Table 4.6 and Fig. 4.7).

Table 4.6. Regression Summary for Dependent Variable: 0-Lymphocytes
R=0,457; R^2=0,209; Adjusted R^2=0,143; $F_{(3,4)}$=3,2; $\chi^2_{(3)}$=8,5; p=0,036; SE: 12,1 %

		Beta	St. Err. of Beta	B	St. Err. of B	$t_{(36)}$	p-level
	r		Intercpt	286,9	181,5	1,58	,123
Sym f	-0,34	-,202	,170	-2,52	2,11	-1,19	,240
Sym	-0,29	-,222	,169	-,59	,45	-1,32	,196
Ch6 E	0,28	,270	,151	12,14	6,81	1,78	,083
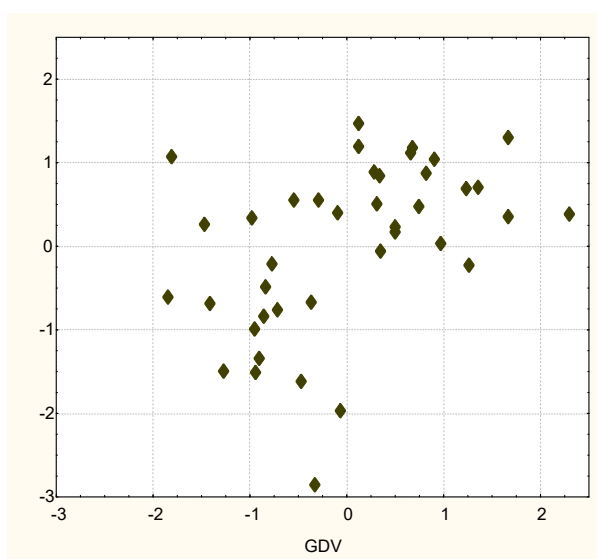
Fig. 4.7. Scatterplot of canonical correlation between GDV parameters (X-line) and 0-lymphocytes level (Y-line)

Immunocytogram entropy correlates with three GDV parameters at the limit significance (Table 4.7 and Fig. 4.8).

Table 4.7. Regression Summary for Dependent Variable: Entropy of Immunocytogram
R=0,429; R^2=0,184; Adjusted R^2=0,116; $F_{(3,4)}$=2,7; $\chi^2_{(3)}$=7,4; p=0,059; SE: 0,034

		Beta	St. Err. of Beta	B	St. Err. of B	$t_{(36)}$	p-level
	r		Intercpt	,162	,520	,31	,757
Sym f	0,30	,297	,154	,010	,005	1,93	,061
EL f	-0,26	-,175	,155	-,035	,031	-1,13	,268
Ch3 A f	-0,23	-,225	,155	-,034	,023	-1,45	,155
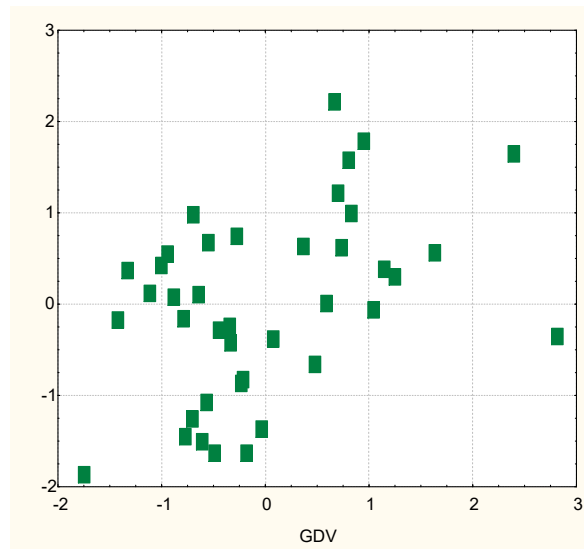
Fig. 4.8. Scatterplot of canonical correlation between GDV parameters (X-line) and Entropy of Immunocytogram (Y-line)

At the next stage, the analysis of the canonical correlation between the registered parameters of cellular immunity, on the one hand, and the parameters of GDV selected at the previous stage, on the other hand, was performed.

As a result, a pair of canonical roots were formed (Table 4.8). The program did not include B-lymphocytes in the structure of the immune root, apparently due to the insignificant coefficient of canonical correlation, but under the same conditions the entropy of the immunocytogram was still found in the factor structure of the root.

Table 4.8. Factor Structure of GDV and Cellular Immunity Canonical Roots

Left set	Root 1
Symmetry GDI f	,64
Ch7 Asymmetry f	,35
Symmetry GDI	,33
Ch6 Energy f	-,50
Ch6 Energy	-,49
Ch5 Energy	-,40
Ch4 Asymmetry	-,32
Ch4 Asymmetry f	-,17
Ch3 Asymmetry f	-,15
Ch5 Asymmetry	-,15
Entropy GDI Left	-,11
Right set	Root 1
$CD4^+CD3^+$ Th	,86
NK-Lymphocytes	,59
Entropy ICG	,46
$CD8^+CD3^+$ Tc	,41
CD3 T "active"	,18
0-Lymphocytes	-,65

The GDV-root represents 11 parameters, three of which give positive factor loads, which reflects their enhancing immunotropic effect, while the other 8 parameters have an immunosuppressive effect. Downregulation of 0-lymphocyte levels is physiologically favorable because it reflects the activation of receptor expression by immature immunocytes.

In general, the canonical correlation between the parameters of GDV and cellular immunity was strong, but it is unclear why statistically insignificant (Fig. 4.9).

R=0,809; R²=0,657; χ²$_{(84)}$=104; p=0,07; Λ Prime=0,026
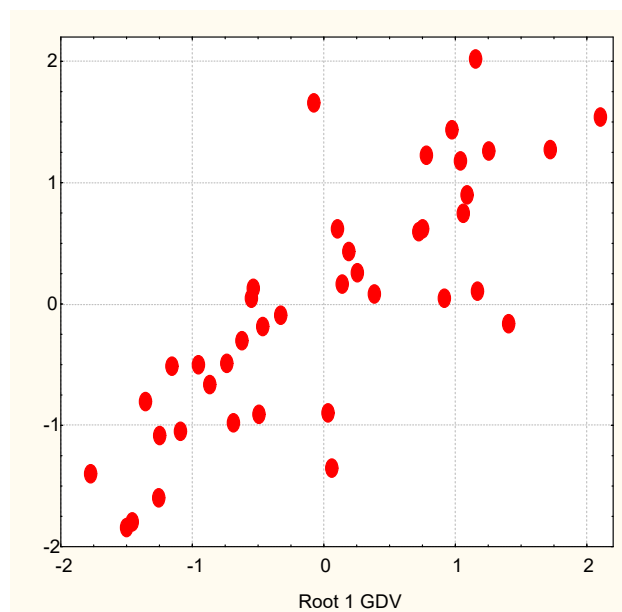
Fig. 4.9. Scatterplot of canonical correlation between GDV parameters (X-line) and Cellular Immunity parameters (Y-line)

Among the parameters of humoral immunity, IgA was most closely related to the parameters of GDV. First of all, it is the energy of the fifth and sixth Chakras (Fig. 4.10-4.11).
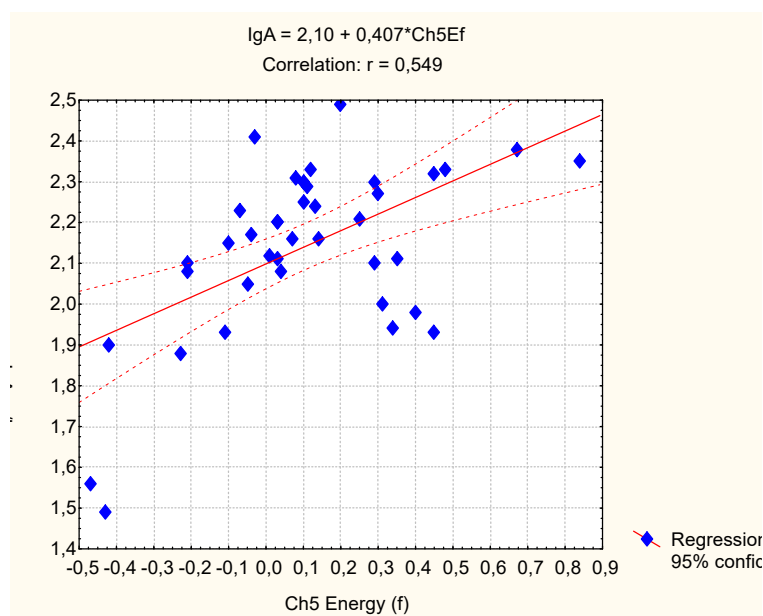
Fig. 4.10. Scatterplot of correlation between Chakra 5 Energy (f) (X-line) and IgA plasma level (Y-line)

Significant influence on the level of IgA also have other parameters of GDV, in total determining it by 51% (Table 4.9 and Fig. 4.12).

Levels of Iggs of other classes are determined by the parameters of GDV less, in particular IgG by 42% (Table 4.10 and Fig. 4.13) and IgM by 39% (Figs. 4.14-4.15 and Table 4.11).
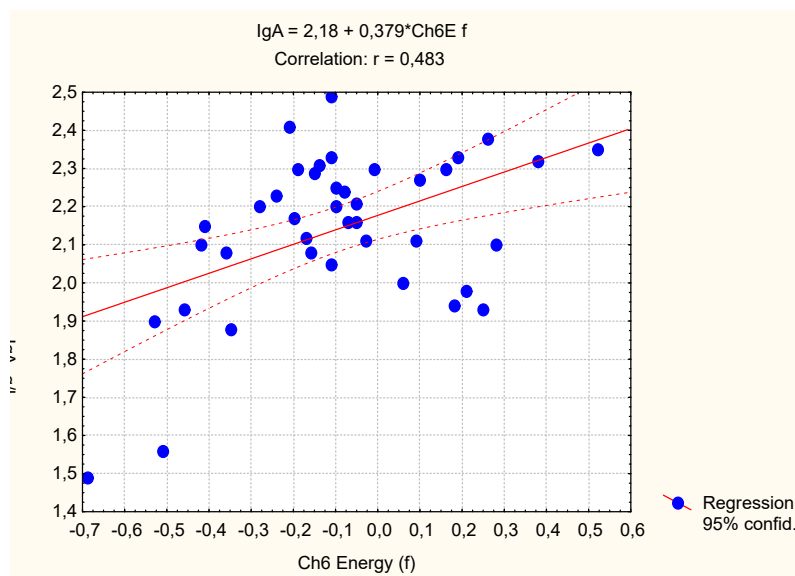
Fig. 4.11. Scatterplot of correlation between Chakra 6 Energy (f) (X-line) and IgA plasma level (Y-line)

Table 4.9. Regression Summary for Dependent Variable: IgA
R=0,716; R^2=0,512; Adjusted R^2=0,366; $F_{(9,3)}$=3,5; $\chi^2_{(9)}$=24,0; p=0,005; SE: 0,16 g/L

		Beta	St. Err. of Beta	B	St. Err. of B	$t_{(30)}$	p-level
	r		Intercpt	1,890	1,319	1,43	,162
Ch6 E f	0,48	,526	,242	,413	,190	2,18	,038
Ch1 E f	0,44	,478	,332	,433	,301	1,44	,160
ER f	0,41	,463	,155	,623	,209	2,99	,006
Ch3 E f	0,34	-,384	,299	-,309	,241	-1,28	,210
Ch1 E	0,29	-,519	,264	-,343	,174	-1,97	,058
AL f	0,28	-,501	,296	-,00005	,00003	-1,69	,102
Ch7 E	0,27	,287	,208	,246	,178	1,38	,177
SL f	-0,27	-,319	,258	-,046	,037	-1,24	,226
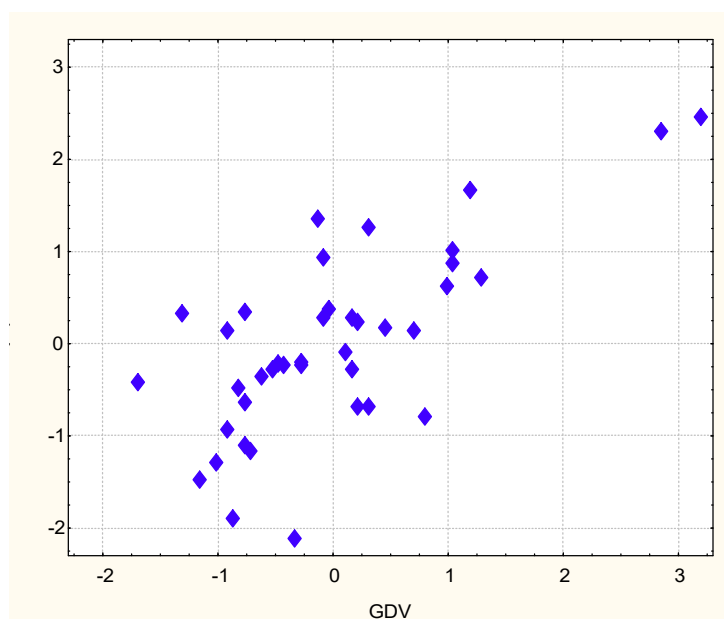
Fig. 4.12. Scatterplot of canonical correlation between GDV parameters (X-line) and IgA plasma level (Y-line)

Table 4.10. Regression Summary for Dependent Variable: IgG

R=0,645; R^2=0,416; Adjusted R^2=0,331; $F_{(5,3)}$=4,9; $\chi^2_{(5)}$=19,1; p=0,002; SE: 2,7 g/L

		Beta	St. Err. of Beta	B	St. Err. of B	$t_{(34)}$	p-level
	r		Intercpt	8,93	5,29	1,69	,100
AF	0,40	,319	,220	,00031	,00021	1,45	,156
Ch7 E	0,35	1,005	,396	13,72	5,41	2,53	,016
Ch1 A	0,35	,313	,136	4,50	1,96	2,29	,028
Ch3 A	0,31	,320	,135	3,33	1,40	2,38	,023
Ch2 E	0,28	-,960	,434	-9,97	4,51	-2,21	,034
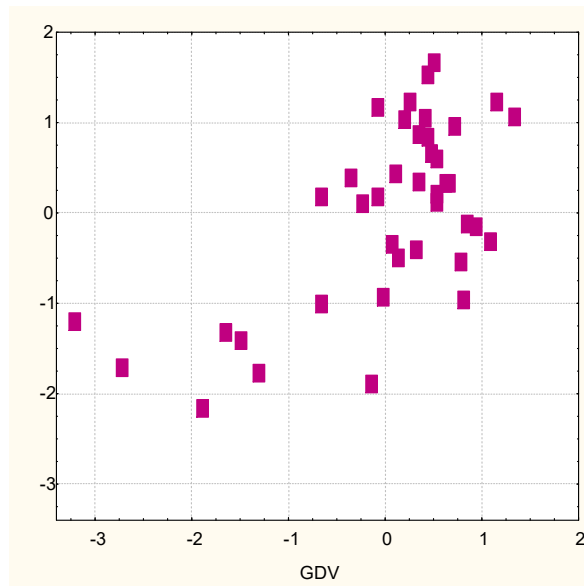
Fig. 4.13. Scatterplot of canonical correlation between GDV parameters (X-line) and IgG plasma level (Y-line)
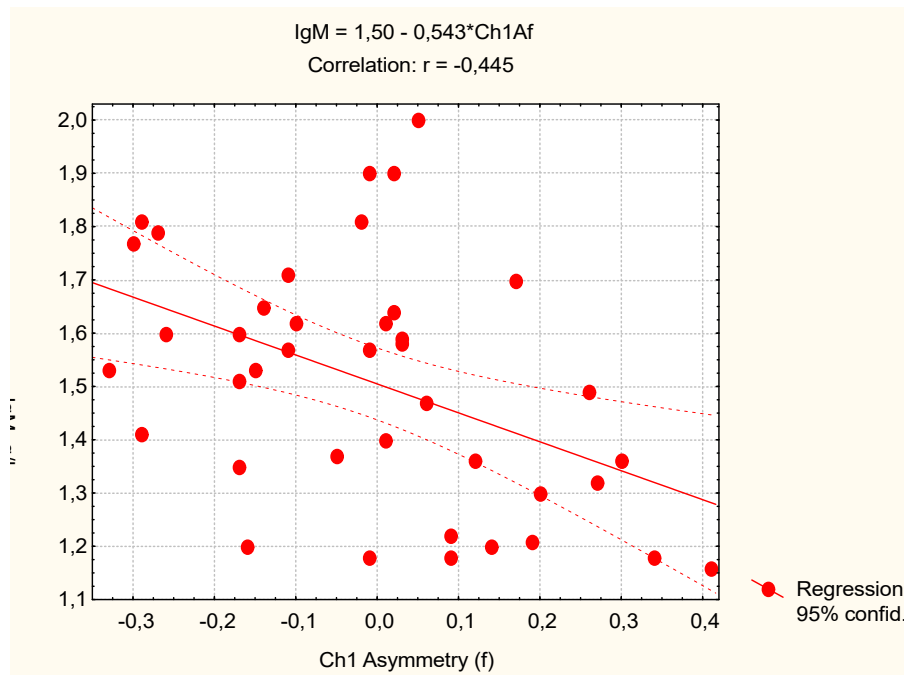
Fig. 4.14. Scatterplot of correlation between Chakra 1 Asymmetry (f) (X-line) and IgM plasma level (Y-line)

Table 4.11. Regression Summary for Dependent Variable: IgM
R=0,622; R^2=0,387; Adjusted R^2=0,353; $F_{(2,4)}$=11,7; $\chi^2_{(2)}$=18,1; p=0,0001; SE: 0,18 g/L

	r	Beta	St. Err. of Beta	B	St. Err. of B	$t_{(37)}$	p-level
			Intercpt	1,511	,029	51,66	10^{-6}
Ch1 A f	-0,44	-,547	,132	-,668	,162	-4,13	,0002
Ch7 E f	-0,32	-,447	,132	-,546	,162	-3,38	,002
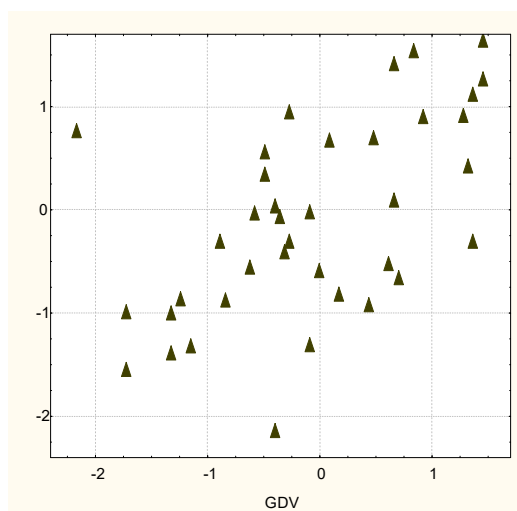
Fig. 4.15. Scatterplot of canonical correlation between GDV parameters (X-line) and IgM plasma level (Y-line)

And the weakest were the links between the parameters of GDV and the level of circulating immune complexes (Table 4.12 and Fig. 4.16).

Table 4.12. Regression Summary for Dependent Variable: CIC
R=0,491; R^2=0,241; Adjusted R^2=0,178; $F_{(3,4)}$=3,8; $\chi^2_{(3)}$=10,1; p=0,018; SE: 12 units

	r	Beta	St. Err. of Beta	B	St. Err. of B	$t_{(36)}$	p-level
			Intercpt	148,9	46,7	3,19	,003
EF	-0,37	-,347	,146	-29,45	12,39	-2,38	,023
Ch6 A f	-0,31	-,187	,161	-8,68	7,51	-1,16	,255
Ch1 E	-0,28	-,192	,161	-8,24	6,89	-1,20	,240
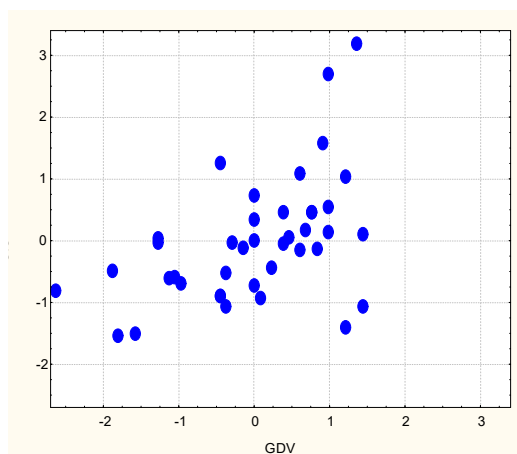
Fig. 4.16. Scatterplot of canonical correlation between GDV parameters (X-line) and CIC plasma level (Y-line)

The result of the canonical correlation analysis shows that the determination by the GDV parameters of humoral immunity is much stronger than cellular: 81% vs 66% (Table 4.13 and Fig. 4.17).

Table 4.13. Factor Structure of GDV and Humoral Immunity Canonical Roots

Left set	Root 1
Ch1 Asymmetry	**,40**
Area Frontal	**,37**
Ch7 Energy	**,34**
Ch3 Asymmetry	**,34**
Ch2 Energy	**,25**
Area Left f	**,22**
Ch1 Energy f	**,19**
Ch5 Energy	**,18**
Ch2 Energy f	**,08**
Ch6 Energy f	**,08**
Ch7 Energy f	**,06**
Ch3 Energy f	**,03**
Entropy Frontal	**-,32**
Shape Left f	**-,15**
Ch6 Asymmetry f	**-,10**
Right set	Root 1
IgG	**,85**
IgM	**,57**
CIC	**,28**
IgA	**,24**

73

R=0,897; R²=0,807; χ²(68)=104; p=0,003; Λ Prime=0,024
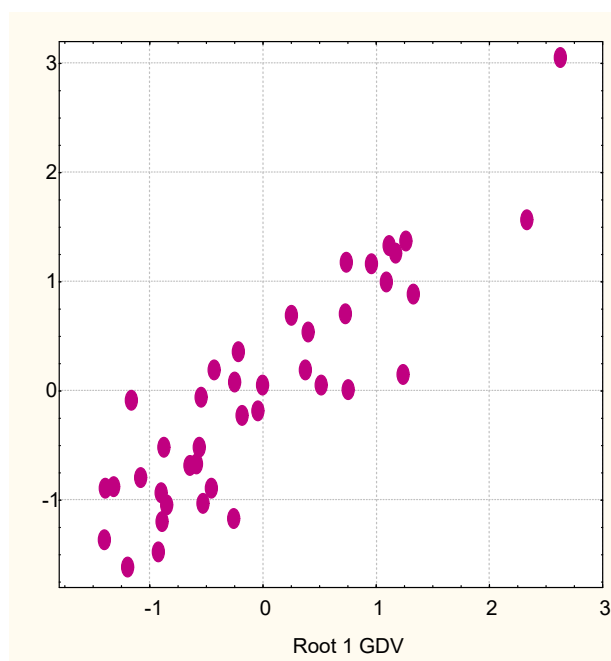
$R=0{,}897; R^2=0{,}807; \chi^2_{(68)}=104; p=0{,}003; \Lambda\ Prime=0{,}024$

Fig. 4.17. Scatterplot of canonical correlation between GDV parameters (X-line) and Humoral Immunity parameters (Y-line)

At the final stage, the analysis of the canonical correlation of cellular and humoral immunity parameters with GDV parameters was performed.

According to the results of the canonical analysis, two pairs of roots are formed, which are almost identical in the coefficients R and R^2, but differ significantly in the factor structure

(Tables 4.14 and 4.15). Judging by the coefficients of determination (Figs. 4.18 and 4.19), the parameters of GDV almost totally regulate the state of immunity.

Table 4.14. Factor Structure of GDV and Immunity Canonical Roots

Left set	Root 1	Root 2
Ch7 Energy f	**-,48**	-,10
Ch2 Energy f	**-,46**	-,12
Ch7 Energy	**-,38**	,04
Ch2 Energy	**-,38**	-,05
Ch4 Asymmetry f	**-,31**	,23
Symmetry	**-,27**	-,22
Area Frontal	**-,26**	,17
Area Left f	**-,26**	,15
Ch5 Energy	**-,25**	,21
Ch4 Asymmetry	**-,23**	,21
Ch6 Energy f	**-,23**	,20
Ch3 Energy f	**-,21**	-,03
Ch1 Energy f	**-,20**	,01
Entropy Left f	**,28**	**,24**
Ch5 Asymmetry	**-,23**	**,24**
Ch6 Energy	**-,22**	**,25**
Ch1 Asymmetry	-,16	**,37**
Symmetry f	,10	**-,43**
Ch1 Asymmetry f	**-,30**	**-,34**
Right set	Root 1	Root 2
CD3 T "active"	**,60**	-,41
IgM	**,43**	,37
CIC	**,16**	,06
IgA	**-,33**	-,01
CD4$^+$CD3$^+$ Th	,07	**-,46**
CD8$^+$CD3$^+$ Tc	-,22	**-,40**
Entropy ICG	-,17	**-,36**
CD16$^+$ NK	-,11	**-,14**
0-Lymphocytes	,11	**,44**
IgG	-,21	**,37**
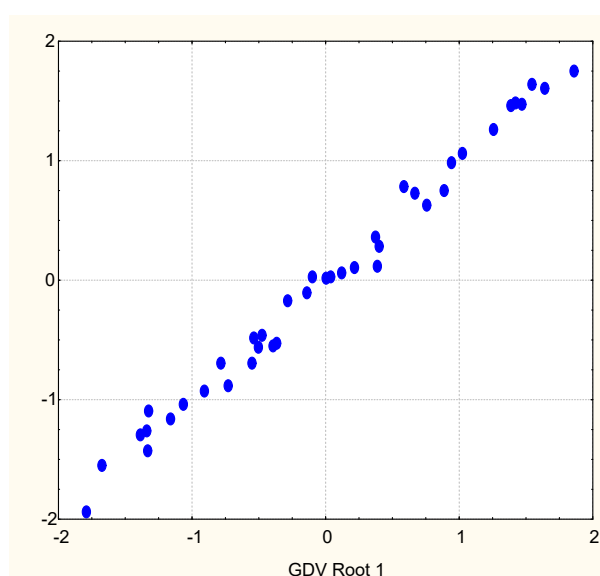
R=0,994; R^2=0,988; $\chi^2_{(280)}$=388; p<10^{-4}; Λ Prime<10^{-6}

Fig. 4.18. Scatterplot of canonical correlation between GDV parameters (X-line) and all Immunity parameters (Y-line). The first pair of roots
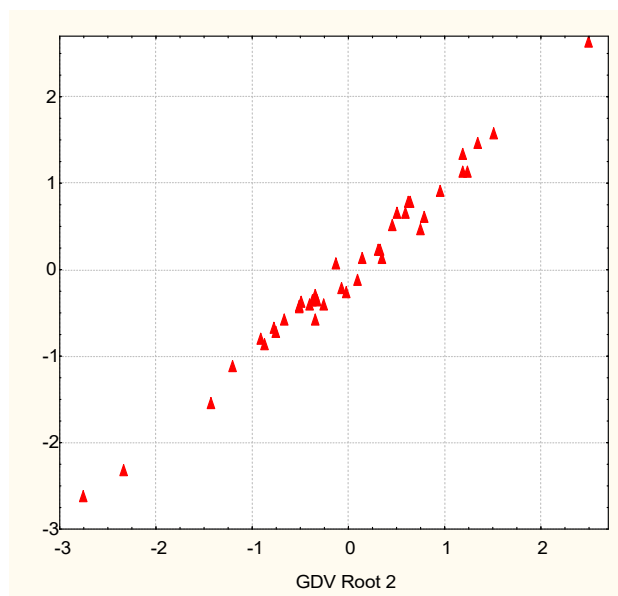
R=0,992; R^2=0,984; $\chi^2_{(243)}$=341; p=0,007; Λ Prime<10^{-6}

Fig. 4.19. Scatterplot of canonical correlation between GDV parameters (X-line) and all Immunity parameters (Y-line). The second pair of roots

Contrary to expectations, the parameters of the **fourth** and **third** Chakras, which are associated with the thymus and spleen, respectively, give only moderate factor loads, while the top positions are occupied by the parameters of the **seventh** and **second** Chakras.

However, our shock quickly turns into antishock, given that these Chakras represent the pineal gland and brain and adrenals or sexual glands, respectively. The immunomodulatory effect of adrenal and gonadal hormones has long been known, as well as thyroid and parathyroid hormones [reviews: Sternberg EM, 2006; Uchakin PN et al, 2007; Popovych IL et al, 2020] associated with the **fifth** Chakra, also present in the factor structure of the root. Now it became known about the immunomodulatory activity of the pineal gland [Markus RP et al, 2007; Csaba G, 2016; Markus RP et al, 2018; Rezzani A et al, 2020]. Finally, one of the trends in modern neuroimmunology is the role of immunomodulation of the vagus [reviews: Marques-Deak A et al, 2005; Sternberg EM, 2006; Tracey KJ, 2009; Thayer JF & Sternberg EM, 2010; Popovych IL et al, 2020] associated with the **fourth** and **fifth** Chakras, the activity of which, in turn, is controlled by the neural network [Tracey KJ, 2009; Thayer JF & Sternberg EM, 2010]. The presence in the factor structure of the parameters of symmetry and asymmetry is perfectly consistent with the lateralization of cortical regulatory structures.

The materials of the chapter are published in the article:

Babelyuk VYe, Gozhenko AI, Dubkova GI, Zukow W, Hubyts'kyi VY, Ruzhylo SV, Fedyayeva SI, Kovalchuk HY, Popovych IL. Causal relationships between the parameters of gas discharge visualization and immunity. Pedagogy and Psychology of Sport. 2021; 7(1): 115-134.

75

CAUSAL RELATIONSHIPS BETWEEN THE PARAMETERS OF GAS DISCHARGE VISUALIZATION AND PHAGOCYTOSIS AS WELL AS LEUKOCYTOGRAM

In portion of the venous blood of the same patients we estimated parameters of phagocytic function of neutrophils as described by Douglas SD & Quie PG [1981] with moderately modification by Kovbasnyuk MM.

Here is the author's description of the method. 5 drops of blood immediately after collection, made in glass centrifuge tubes with 2 ml of 4% solution of sodium citrate. Blood samples were stored in a refrigerator at a temperature of 4^0C. Further samples were centrifuged (5000 rev/min for 5 min). The supernatant was removed with the help of the Pasteur's pipette. We used a fraction of leukocytes with traces of erythrocytes. The objects of phagocytosis served daily cultures of Staphylococcus aureus (ATCC N 25423 F49) as typical specimen for Gram-positive Bacteria and Escherichia coli (O55 K59) as typical representative of Gram-negative Bacteria. Both cultures obtained from Laboratory of Hydro-Geological Regime-Operational Station JSC "Truskavets'kurort". To prepare the suspension microbes did wipes with relevant shoals sterile saline, immersed tubes in boiling water for 3 seconds, cooled to room temperature. Integrity microbes controlled with the aid of a microscope. To do this, drop the suspension of microbes applied to skimmed substantive piece of glass, fixed in alcohol lamp flame. Ready preparations stained by Papenheim, microscoped during immersion, lense h90, eyepiece x10. The test samples were prepared as follows. In Vidal's plastic tubes made in the following order of 0,05 mL of heparin, 0,05 mL of sterile saline, 0,1 mL suspension of leukocytes, 0,05 mL suspension of microbial bodies. Samples shaked and placed in thermostat at 37^0C for 30 min, shaking them with every 10 mins. Then, to stop phagocytosis, the sample was cooled under running water for 10 min. In further samples are centrifuged (5000 rev/min, for 5 min), the supernatant removed with the help of the Pasteur's pipette. From the suspension of leukocytes (with traces of red blood cells) prepared strokes, dried in air at room temperature and stained by Papenheim. Microscoped during immersion lens h90, x10 eyepiece.

Take into account the following parameters of phagocytosis: activity (percentage of neutrophils, in which found microbes - Hamburger's Phagocytosis Index, **PhI**), intensity (number of microbes absorbed one phagocytes - Microbial Count **MC** or Right's Index) and completeness (percentage of dead microbes - Killing Index **KI**).

Microbial number and index their digestion is determined for each phagocyte and fixed in phagocytic frame.

The integrated evaluation of phagocytic function of neutrophils is made by the number of microbes that are able to neutralize neutrophils contained in 1 liter of blood, named as Bactericidal Capacity of Neutrophils (BCCN) and calculated by equation [Popovych IL et al, 2003]:

$$BCCN(10^9 Bac/L) = Leukocytes(10^9/L) \cdot Neutrophils(\%) \cdot PhI(\%) \cdot MC(Bac/Phag) \cdot KI(\%)/10^6$$

Every day four people were tested. A week later, all the tests were repeated.

The activity of phagocytosis by neutrophils of E. coli as a typical representative of gram-negative microbes is most closely related to GDV (Table 5.1). It is significant that the top position is occupied by the energy just of the **fourth** Chakra associated with **thymus** as well as cardiac and celiac plexus and vagus nerve. It is also expected that among the Chakras that activate this parameter of phagocytosis, the **third** Chakra was found, which is associated with **spleen** and **celiac plexus ganglion** (which carries out nervous control of spleen within the framework of the well-known cholinergic anti-inflammatory reflex/pathway [Tracey KJ, 2002; 2009; 2010]).

Table 5.1. Regression Summary for Dependent Variable: Phagocytosis Index vs E. coli
R=0,616; R^2=0,380; Adjusted R^2=0,244; $F_{(7,3)}$=2,80; p=0,022; SE: 0,47%

		Beta	St. Err. of Beta	B	St. Err. of B	$t_{(32)}$	p-level
	r		Intercpt	99,50	,206	484	10^{-6}
Ch4E f	0,45	,473	,261	1,153	,636	1,81	,079
Ch7E f	0,45	,774	,396	2,228	1,139	1,96	,059
Ch6E	0,39	,244	,195	,451	,361	1,25	,220
Ch1E f	0,38	,291	,305	,689	,722	,95	,347
Ch2E f	0,36	-,535	,394	-1,475	1,088	-1,36	,185
Ch3E f	0,31	-,362	,323	-,761	,679	-1,12	,270
Ch4E	0,27	-,322	,243	-,707	,534	-1,32	,195

Despite the **seventh** Chakra does not directly affect the immune system, its location among the first two is quite natural, because it is associated with the pineal gland as well as the right and upper brain. The pineal gland, in turn, is closely linked to immunity through melatonin [Markus RP et al, 2007; Markus RP et al, 2018; Rezzani A et al, 2020]. According to Tracey's KJ [2007] conception of immunological homunculus the CNSs structures that are projected onto certain EEG loci are responsible for certain immune functions. In developing this concept, we have previously shown that certain EEG loci are responsible for the regulation of phagocytosis [Kul'chyns'kyi AB et al, 2016; Popovych IL et al, 2018; Popovych IL et al, 2022].

The **sixth** Chakra is associated with pituitary and pineal glands, left and lower brain, thalamus, hypothalamus, superior cervical ganglion. Therefore, its presence in this constellation is also fully consistent with the mentioned above concept of neuro-immunomodulation.

The **first** Chakra is associated with adrenals and pelvic nerve plexus; **second** Chakra with testes/ovaries and inferior mesenteric ganglion. Immunomodulatory action of hormones of adrenals and testes/ovaries is well documented [reviews: Sternberg EM, 2006; Uchakin PN et al, 2007; Popovych IL et al, 2020].

Korotkov KG [2001; 2007; 2014] believes that GDI, taken off without filter, characterizes the **functional** changes of organism, while taken with a filter characterizes **organic** changes. With regard to the fourth Chakra, we confirm this by finding a lower correlation coefficient.

Taken together, the six Chakras positively determine the activity of phagocytosis by neutrophils the most represented bacterium in the human microbiota by 38% (Fig. 5.1).
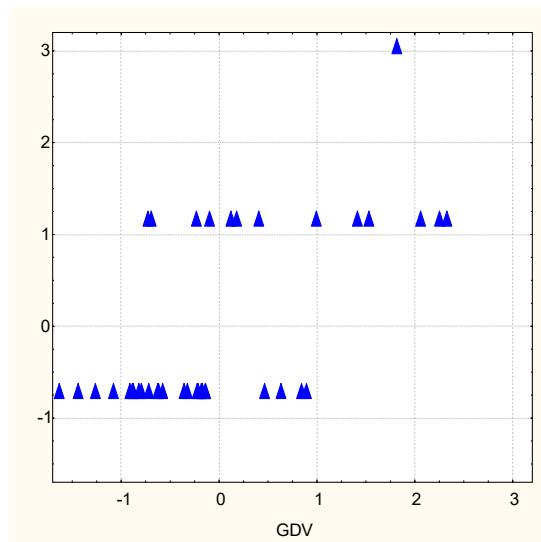
R=0,616; R²=0,380; χ²$_{(7)}$=16,5; p=0,021; Λ Prime=0,620
Fig. 5.1. Scatterplot of canonical correlation between GDV parameters (X-line) and the Phagocytosis Index vs E. coli (Y-line)

The intensity of phagocytosis of E. coli is determined by the **fourth** Chakra also positively, but only by 23% (Table 5.2).

Table 5.2. Regression Summary for Dependent Variable: Microbial Count of E. coli
R=0,484; R²=0,234; Adjusted R²=0,147; F$_{(4,3)}$=2,68; p=0,048; SE: 6,4 Bac/Phag

		Beta	St. Err. of Beta	B	St. Err. of B	t$_{(35)}$	p-level
	r		Intercpt	2,338	28,861	,08	,936
Entropy F f	0,30	,164	,182	8,108	8,989	,90	,373
Entropy F	0,28	,199	,182	8,669	7,953	1,09	,283
Ch4A f	0,28	,263	,150	6,880	3,935	1,75	,089
Ch4E f	0,27	,207	,150	6,482	4,686	1,38	,175

Instead, the completion of phagocytosis of E. coli is determined by 24% negatively (Table 5.3).

Table 5.3. Regression Summary for Dependent Variable: Killing Index vs E. coli
R=0,489; R²=0,241; Adjusted R²=0,176; F$_{(3,4)}$=3,78; p=0,019; SE: 5,9%

		Beta	St. Err. of Beta	B	St. Err. of B	t$_{(36)}$	p-level
	r		Intercpt	39,71	1,27	31,2	10⁻⁶
Ch7E	-0,39	-,954	,444	-25,72	11,98	-2,15	,039
Ch3E f	-0,37	-,220	,185	-5,57	4,68	-1,19	,242
Ch2E	-0,29	,744	,434	15,25	8,90	1,71	,095

The **fifth** Chakra was found to be involved in the downregulation of Bactericidal Capacity vs E. coli (Table 5.4).

Table 5.4. Regression Summary for Dependent Variable: Bactericidal Capacity vs E. coli
R=0,494; R²=0,244; Adjusted R²=0,203; F$_{(2,4)}$=5,96; p=0,006; SE: 17•10⁹ Bac/L

		Beta	St. Err. of Beta	B	St. Err. of B	t$_{(37)}$	p-level
	r		Intercpt	158,2	23,4	6,76	10⁻⁶
Area L	-0,37	-,401	,144	-,0049	,0017	-2,80	,008
Ch5A	-0,29	-,324	,144	-29,98	13,28	-2,26	,030

The **fifth** Chakra is associated with thyroid and parathyroid glands, vagus nerve and inferior cervical ganglion. This is consistent with data on the effect of triiodothyronine, calcitonin, parathyroid hormone and vagus on phagocytosis [reviews: Sternberg EM, 2006; Thayer JF & Sternberg EM, 2010; Popovych IL et al, 2020].

In the Tables 5.5-5.8 show regression models for GDV parameters and phagocytosis of Staph. aureus as a typical representative of gram-positive microbes. As you can see, the number of GDV parameters included in the model is much smaller, the connections are weaker and also have the opposite direction.

Table 5.5. Regression Summary for Dependent Variable: Killing Index vs St. aureus
R=0,482; R²=0,232; Adjusted R²=0,191; F$_{(2,4)}$=5,60; p=0,008; SE: 4,5%

		Beta	St. Err. of Beta	B	St. Err. of B	t$_{(37)}$	p-level
	r		Intercpt	45,1	,771	58,5	10⁻⁶
Ch7A f	0,44	,416	,145	9,743	3,388	2,88	,007

| Ch7E | 0,25 | ,205 | ,145 | | 4,260 | 3,007 | 1,42 | ,165 |

Table 5.6. Regression Summary for Dependent Variable: Microbial Count of Staph. aureus

R=0,338; R^2=0,114; Adjusted R^2=0,091; F$_{(1,4)}$=4,91; p=0,033; SE: 6,6 Bac/Phag

		Beta	St. Err. of Beta	B	St. Err. of B	t$_{(38)}$	p-level
	r		Intercpt	60,8	1,22	49,7	10^{-6}
Ch6E	-0,34	-,338	,153	-7,95	3,59	-2,22	,033

Table 5.7. Regression Summary for Dependent Variable: Phagocytosis Index vs Staph. aureus

R=0,365; R^2=0,133; Adjusted R^2=0,086; F$_{(2,4)}$=2,84; p=0,071; SE: 0,70%

		Beta	St. Err. of Beta	B	St. Err. of B	t$_{(37)}$	p-level
	r		Intercpt	99,3	,115	862	10^{-6}
Ch2E	-0,28	-,278	,153	-,644	,355	-1,81	,078
Ch2A	-0,24	-,233	,153	-,539	,354	-1,52	,137

Table 5.8. Regression Summary for Dependent Variable: Bactericidal Capacity vs Staph. aureus

R=0,448; R^2=0,201; Adjusted R^2=0,134; F$_{(3,4)}$=3,02; p=0,042; SE: 16•10^9 Bac/L

		Beta	St. Err. of Beta	B	St. Err. of B	t$_{(36)}$	p-level
	r		Intercpt	57,0	27,0	2,11	,042
Ch5A	-0,27	-,337	,151	-27,38	12,30	-2,22	,032
Ch3A f	-0,23	-,246	,154	-17,81	11,12	-1,60	,118
Shape R f	0,23	,218	,152	2,74	1,92	1,43	,162

This is more clearly illustrated by the factor structure of canonical roots (Table 5.9). In particular, the Completion of phagocytosis and Bactericidal Capacity versus Escherichia coli **downregulated** by GDV parameters, instead the same parameters for Staphylococcus aureus **upregulated**. And vice versa, Intensity and Activity of phagocytosis **upregulated** for Escherichia coli but **downregulated** for Staphylococcus aureus.

Table 5.9. Factor Structure of GDV and Phagocytic Canonical Roots

Left set	R
Ch6E	,682
Ch3E f	,627
Ch7E	,563
Ch4E	,550
Ch1E f	,525
Area L	,500
Ch2E	,377
Ch7E f	,368
Entropy F f	,360
Ch2E f	,331
Ch5A	,301
Ch7A f	,175
Shape R f	-,386
Right set	R
KI E. coli	-,734

BCCN E. coli	-,513
MC St. aur.	-,310
PhI St. aur.	-,179
BCCN St. aur.	-,212
MC E. coli	,384
PhI E. coli	,240
KI St. aur.	,114

This state of affairs is consistent with the known data that the regulation of phagocytosis of gram-negative and gram-positive microbes is carried out by various neuro-endocrine mechanisms [Straub RH et al, 2005; Straub RH et al, 2006], which, as shown in this study, are associated with the Chakras.

In general, GDV parameters determine the parameters of phagocytosis by neutrophils of gram-negative and gram-positive microbes by 72% (Fig. 5.2).
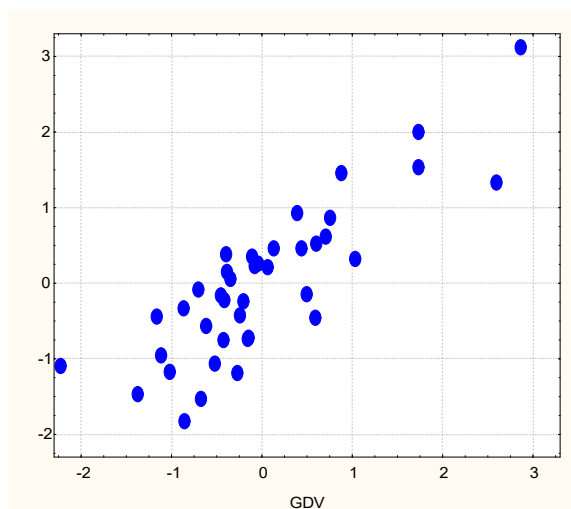
R=0,847; R²=0,717; χ²(104)=130; p=0,044; Λ Prime=0,0097

Fig. 5.2. Scatterplot of canonical correlation between parameters of the GDV (X-line) and the Phagocytosis (Y-line)

In portion of the capillary blood we counted up Leukocytogram (LCG) (Eosinophils, Stub and Segmentonucleary Neutrophils, Lymphocytes and Monocytes) and calculated its Entropy (h) using Popovych's IL [2001] equation, which is based on classical Shannon's CE [1948] equation:

$hLCG = -[Lymph \cdot log_2 Lymph + Mon \cdot log_2 Mon + Eos \cdot log_2 Eos + SNN \cdot log_2 SNN + StubN \cdot log_2 StubN]/log_2 5.$

The percentage of monocytes in the Leukocytogram was most closely related to GDV parameters, which is quite expected given the role of monocytes in immunity as an antigen-presenting cells and macrophages. It is noteworthy that **all seven** Chakras were involved in the downregulation of the level of monocytes in the blood, and to approximately the same extent, judging by the correlation coefficients (Table 5.10).

It seems that the level of monocytes is downregulated by the **fourth** Chakra (associated with **thymus)** and the **third** Chakra (associated with **spleen**) directly and by others through hormones and nerve structures. In particular, due to hormones of adrenal (**first** Chakra), testes/ovaries (**second** Chakra), thyroid and parathyroid (**fifth** Chakra), pituitary and pineal (**sixth** Chakra) glands as well as vagus nerve, inferior and superior cervical ganglion and celiac plexus (**fifth, fourth, sixth** and **third** Chakras), which innervate the thymus and spleen [Nance DN & Sanders VM, 2007].

According to mentioned above conception of immunological homunculus the CNSs structures that are projected onto certain EEG loci are responsible for certain immune functions. On the other hand, believe that **sixth** Chakra is associated with left and lower brain, and the **seventh** Chakra with right and upper brain.

Table 5.10. Regression Summary for Dependent Variable: Monocyte proportion
R=0,769; R^2=0,592; Adjusted R^2=0,411; $F_{(12)}$=3,27; p=0,005; SE: 1,5%

	r	Beta	St. Err. of Beta	B	St. Err. of B	$t_{(27)}$	p-level
				Intercpt	-1,263	8,037	-,16	,876
Ch4E f	-0,46	-,392	,211	-3,465	1,866	-1,86	,074
Ch6E f	-0,45	-1,419	,472	-10,542	3,506	-3,01	,006
Ch1E f	-0,44	-,296	,241	-2,542	2,062	-1,23	,228
Ch7E	-0,43	,508	,482	4,128	3,913	1,05	,301
Ch2E	-0,42	-1,005	,705	-6,205	4,352	-1,43	,165
Ch2E f	-0,42	-,487	,286	-4,876	2,862	-1,70	,100
Ch3E	-0,36	-,367	,329	-2,231	1,998	-1,12	,274
Ch5E f	-0,32	1,654	,549	11,605	3,852	3,01	,006
Shape F f	0,45	-,426	,291	-,453	,309	-1,47	,154
Shape L	0,36	,598	,430	,274	,197	1,39	,176
Shape F	0,34	-1,605	,780	-,593	,288	-2,06	,049
Entropy F	0,34	,436	,177	5,381	2,192	2,46	,021

Taken together, all Chakras determine the level of monocytes by 59% (Fig. 5.3).
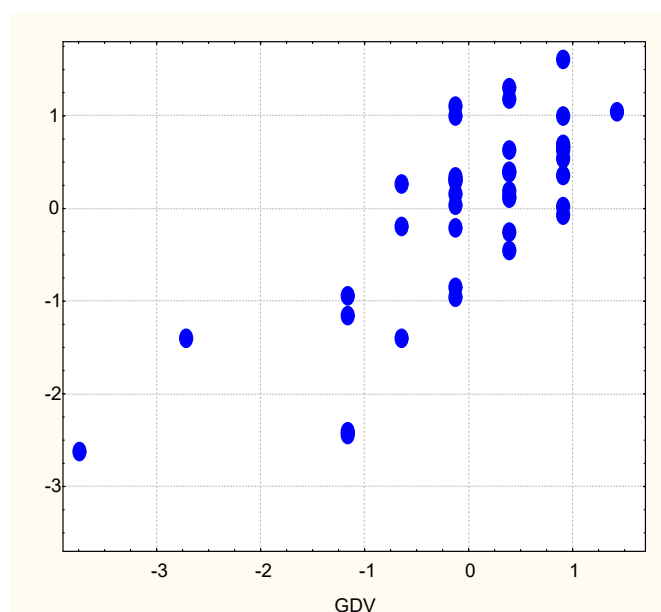
R=0,769; R^2=0,592; $\chi^2_{(12)}$=28,7; p=0,004; Λ Prime=0,408
Fig. 5.3. Scatterplot of canonical correlation between GDV parameters (X-line) and the Monocytes level (Y-line)

The level in the blood of eosinophils is regulated by the Chakras less (Table 5.11 and Fig. 5.4).

Table 5.11. Regression Summary for Dependent Variable: Eosinophils proportion
R=0,703; R^2=0,494; Adjusted R^2=0,436; $F_{(4,4)}$=8,53; p=0,0001; SE: 1,7%

	r	Beta	St. Err. of Beta	B	St. Err. of B	$t_{(35)}$	p-level
				Intercpt	51,2	25,8	1,99	,055

		Beta	St. Err. of Beta	B	St. Err. of B	t	p-level
Ch6A	0,50	,447	,126	5,167	1,457	3,55	,001
Ch4E	0,33	,407	,122	3,793	1,143	3,32	,002
Ch2A f	-0,29	-,243	,122	-2,262	1,131	-2,00	,053
Symmetry f	-0,27	-,239	,127	-,518	,276	-1,88	,069
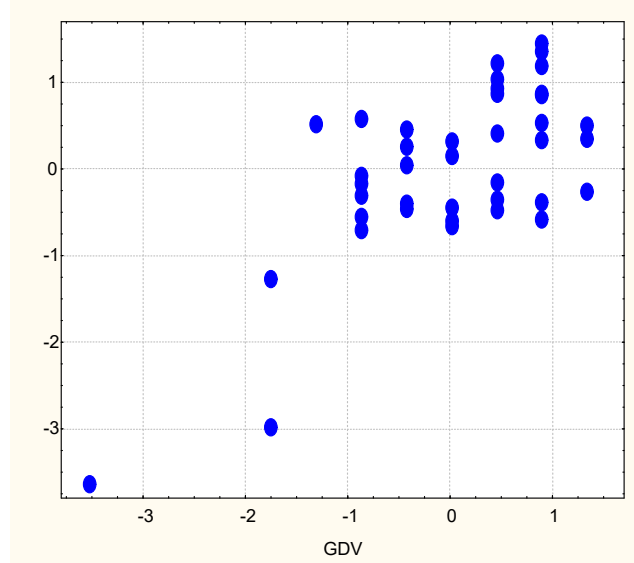
R=0,703; R²=0,494; $\chi^2_{(4)}$=24,5; p<10⁻⁴; Λ Prime=0,506

Fig. 5.4. Scatterplot of canonical correlation between GDV parameters (X-line) and the Eosinophils level (Y-line)

The level of pan-lymphocytes in the blood is even weaker, but statistically significantly related to the Chakras (Table 5.12).

Table 5.12. Regression Summary for Dependent Variable: Lymphocytes proportion
R=0,492; R^2=0,242; Adjusted R^2=0,155; $F_{(4,4)}$=2,79; p=0,041; SE: 3,8%

		Beta	St. Err. of Beta	B	St. Err. of B	$t_{(35)}$	p-level
	r		Intercpt	28,7	,647	44,3	10⁻⁶
Ch1A	-0,29	-,225	,151	-4,120	2,768	-1,49	,146
Ch6A	-0,27	-,210	,149	-4,436	3,158	-1,40	,169
Ch1A f	0,26	,268	,147	5,991	3,291	1,82	,077
Ch3A f	0,25	,195	,151	3,442	2,661	1,29	,204

In contrast, the associations of both neutrophil populations with GDV parameters were insignificant (Tables 5.13 and 5.14).

Table 5.13. Regression Summary for Dependent Variable: Stub Neutrophils proportion
R=0,374; R^2=0,140; Adjusted R^2=0,093; $F_{(2,4)}$=3,01; p=0,061; SE: 1,1%

		Beta	St. Err. of Beta	B	St. Err. of B	$t_{(37)}$	p-level
	r		Intercpt	3,39	,247	13,7	10⁻⁶
Ch1E	-0,34	-,214	,195	-,764	,697	-1,10	,280
Ch4E	-0,33	-,201	,195	-,916	,888	-1,03	,309

Table 5.14. Regression Summary for Dependent Variable: PMN Neutrophils proportion
R=0,307; R^2=0,094; Adjusted R^2=0,070; $F_{(1,4)}$=3,94; p=0,054; SE: 4,4%

		Beta	St. Err. of Beta	B	St. Err. of B	$t_{(38)}$	p-level
	r		Intercpt	71,9	6,25	11,5	10⁻⁶
Shape F f	-0,31	-,307	,154	-,757	,381	-1,99	,054

Interestingly, the Entropy of the Leukocytogram as an information parameter also correlates with the information parameters of GDV, in particular its entropy (Table 5.15).

Table 5.15. Regression Summary for Dependent Variable: Entropy of Leukocytogram
R=0,636; R^2=0,404; Adjusted R^2=0,274; F$_{(7,3)}$=3,10; p=0,013; SE: 0,035

	r	Beta	St. Err. of Beta	B	St. Err. of B	t$_{(32)}$	p-level
				Intercpt	-,233852	,370506	-,63	,532
Shape F f	0,41	,489	,232	,011023	,005233	2,11	,043
Ch6A	0,36	,344	,145	,072039	,030356	2,37	,024
Activation Coef	0,29	,369	,228	,014629	,009039	1,62	,115
Entropy F	0,26	,266	,175	,069710	,045830	1,52	,138
Ch3E	-0,38	-,315	,238	-,040605	,030730	-1,32	,196
Area L	-0,29	,441	,279	,000006	,000004	1,58	,124
Symmetry	-0,26	,338	,246	,002812	,002050	1,37	,180

The last smear of the picture is Table 5.15 on the total content of leukocytes in the blood.

Table 5.16. Regression Summary for Dependent Variable: Leukocytes level
R=0,559; R^2=0,312; Adjusted R^2=0,255; F$_{(3,4)}$=5,44; p=0,003; SE: 0,63 G/L

	r	Beta	St. Err. of Beta	B	St. Err. of B	t$_{(36)}$	p-level
				Intercpt	4,942	,426	11,6	10^{-6}
Ch1A	-0,43	-,378	,145	-1,199	,461	-2,60	,014
Ch1A f	0,31	,319	,138	1,233	,535	2,30	,027
Shape R	0,28	,179	,146	,033	,027	1,23	,227

Taken together, the parameters of the Leukocytogram are determined by the parameters of GDV by 82% (Table 5.17 and Fig. 5.5).

Table 5.17. Factor Structure of GDV and Leukocytogram's Canonical Roots

Right set	R
Ch6A	,752
Ch5A	,538
Ch1A	,460
Shape F f	,273
Entropy F	,252
Shape L	,233
Shape F	,206
Shape R	,081
Ch7E	,071
Ch6E f	,065
Ch1A f	-,270
Ch1E f	-,260
Ch1E	-,248
Ch4E f	-,205
Ch2E f	-,204
Ch3E	-,180
Ch4E	-,110
Ch2E	-,057
Left set	R
Eosinophils	,510
Entropy LCG	,488
Monocytes	,373
Stub Neutrophils	,162

Lymphocytes	**-,461**
Leukocytes	**-,396**
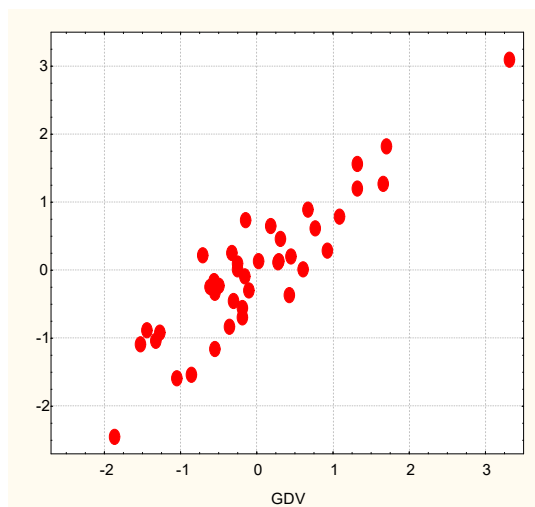
R=0,904; R^2=0,818; χ$^2_{(108)}$=138; p=0,027; Λ Prime=0,005

Fig. 5.5. Scatterplot of canonical correlation between parameters of the GDV (X-line) and the Leukocytogram (Y-line)

Next based on Leukocytogram elements we calculated its Adaptation Index as well as Strain Index by Popovych IL [2000; 2021]. The informativeness of these indices was demonstrated by other authors [Hubyts'kyi VY et al, 2013], as well as its advantage over the Lymphocytes/Segmentonucleary Neutrophils ratio [Garkavi LKh et al, 2000].

We remind that the algorithm of quantization of the Popovych's indexes is based on the proposed Garkavi LKh et al [1990; 1998] ranges of relative content in the Leukocytogram of lymphocytes, which determines the type of General Adaptation Reaction of Organism (GARO) as well as other components of Leukocytogram and total leukocyte levels indicating harmonic or disharmonious character of GARO (Table 5.18).

Table 5.18. Quantification of General Adaptation Reaction of Organism (first version)

Leukocyto-gram Lymphocy-tes level, %	**G**eneral **A**daptation **R**eaction of **O**rganism	Eosinophils and Stub Neutrophils: 1÷6 %; Monocytes: 4÷7 %; Leukocytes: 4÷8 G/l	Eosinophils and Stub Neutrophils: <1; >6; Monocytes: <4; >7; Leukocytes: <4; >8 G/l
<21	Stress	1,22	0,02
21÷27	Training	1,46	0,74
28÷33	Quiet Activation	1,95	0,98
34÷43,5	Heightened Activation	1,70	0,50
≥44	Overactivation		0,26

Strain Index-1 = [(Eo/3,5-1)^2 + (SN/3,5-1)^2 + (Mon/5,5-1)^2 + (Leu/6-1)^2]/4.

Later, Garkavi LKh et al [2000] proposed some other boundaries of ranges, on the basis of which we calculated the second version of the indices (Table 2).

Table 5.19. Quantification of General Adaptation Reaction of Organism (second version)

Leukocyto-gram Lymphocy-tes level, %	**G**eneral **A**daptation **R**eaction of **O**rganism	Eosinophils: 1÷4,5 %; Stub Neutrophils: 3÷5,5 %; Monocytes: 5÷7 %; Leukocytes: 4÷6 G/l	Eosinophils: <1;>4,5% Stub Neutrophils: <3; >5,5; Monocytes: <5; >7; Leukocytes: <4; >6 G/l
<21	Stress	1,22	0,02
21÷27	Training	1,46	0,74
28÷33	Quiet Activation	1,95	0,98

| 34÷43,5 | Heightened Activation | 1,70 | | 0,50 |
| ≥44 | Overactivation | | | 0,26 |

Strain Index-2 = $[(Eo/2,75-1)^2 + (SN/4,25-1)^2 + (Mon/6-1)^2 + (Leu/5-1)^2]/4$.

As expected, the links between Leukocytary Indices and Chakras, which represent the endocrine glands that secrete adaptive hormones, have been found. It is stated that the second version of the indices is somewhat more informative than the first: determination coefficiens constitute 61% vs 57% (Tables 5.20-5.25 and Figs. 5.6 and 5.7).

Table 5.20. Regression Summary for Dependent Variable: Popovych's Strain Index-1
R=0,740; R^2=0,548; Adjusted R^2=0,481; $F_{(5,3)}$=8,2; $p<10^{-4}$; SE: 0,10

		Beta	St. Err. of Beta	B	St. Err. of B	$t_{(34)}$	p-level
	r			Intercpt	0,238	0,038	6,21	10^{-6}
Ch6A	0,63	0,420	0,133	0,293	0,093	3,16	0,003
Ch6E	0,46	1,512	0,477	0,716	0,226	3,17	0,003
Ch5E	0,35	-0,977	0,407	-0,444	0,185	-2,40	0,022
Ch6E f	0,20	-0,256	0,193	-0,135	0,101	-1,33	0,193
Ch7E	0,11	-0,144	0,142	-0,083	0,081	-1,02	0,315

Table 5.21. Regression Summary for Dependent Variable: Popovych's Adaptation Index-1
R=0,497; R^2=0,247; Adjusted R^2=0,184; $F_{(3,4)}$=3,94; p=0,016; SE: 0,40

		Beta	St. Err. of Beta	B	St. Err. of B	$t_{(36)}$	p-level
	r			Intercpt	-0,842	1,584	-0,53	0,598
Ch6A	-0,33	-0,355	0,147	-0,796	0,329	-2,42	0,021
Entropy R f	0,29	0,211	0,149	0,611	0,430	1,42	0,164
Ch1A	0,26	0,266	0,150	0,516	0,291	1,77	0,085

Table 5.22. Factor Structure of GDV and Strain&Adaptation Indices-1 Canonical Roots

Right set	R
Ch6A	-0,832
Ch6E	-0,628
Ch5E	-0,486
Ch6E f	-0,280
Ch7E	-0,147
Entropy R f	0,153
Ch1A	0,082
Left set	R
Strain Index-1	-0,997
Adaptation Index-1	0,541
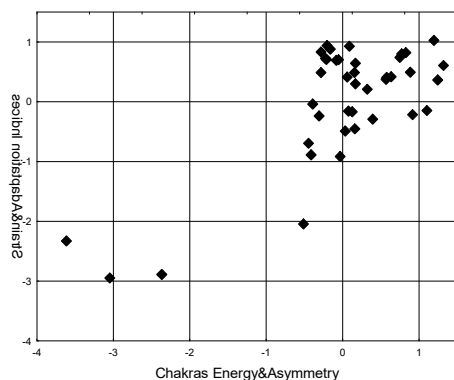
R=0,756; R^2=0,572; $\chi^2_{(14)}$=37; p=0,0007; Λ Prime=0,336

Fig. 5.6. Scatterplot of canonical correlation between parameters of the GDV (X-line) and the Leukocytary Indices-1 (Y-line)

Table 5.23. Regression Summary for Dependent Variable: Popovych's Strain Index-2
R=0,781; R^2=0,611; Adjusted R^2=0,553; $F_{(5,3)}$=10,7; $p<10^{-5}$; SE: 0,186

		Beta	St. Err. of Beta	B	St. Err. of B	$t_{(34)}$	p-level
	r		Intercpt	0,387	0,113	3,41	0,002
Ch6A	0,59	0,447	0,129	0,627	0,180	3,48	0,001
Ch6E	0,52	1,540	0,427	1,466	0,406	3,61	0,001
Ch5E	0,37	-1,242	0,388	-1,135	0,354	-3,20	0,003
Ch4E	0,26	0,208	0,183	0,235	0,207	1,14	0,263
Ch7E	0,21	-0,212	0,172	-0,244	0,198	-1,23	0,226

Table 5.24. Regression Summary for Dependent Variable: Popovych's Adaptation Index-2
R=0,465; R^2=0,216; Adjusted R^2=0,174; $F_{(2,4)}$=5,11; p=0,011; SE: 0,29

		Beta	St. Err. of Beta	B	St. Err. of B	$t_{(37)}$	p-level
	r		Intercpt	0,964	0,046	20,8	10^{-6}
Ch5A	-0,37	-0,430	0,149	-0,652	0,225	-2,89	0,006
Ch5E	0,20	0,286	0,149	0,301	0,156	1,93	0,062

Table 5.25. Factor Structure of GDV and Strain&Adaptation Indices-2 Canonical Roots

Right set	R
Ch6A	-0,754
Ch6E	-0,681
Ch5A	-0,587
Ch5E	-0,495
Ch4E	-0,327
Ch7E	-0,277
Left set	R
Strain Index-2	-0,998
Adaptation Index-2	0,191
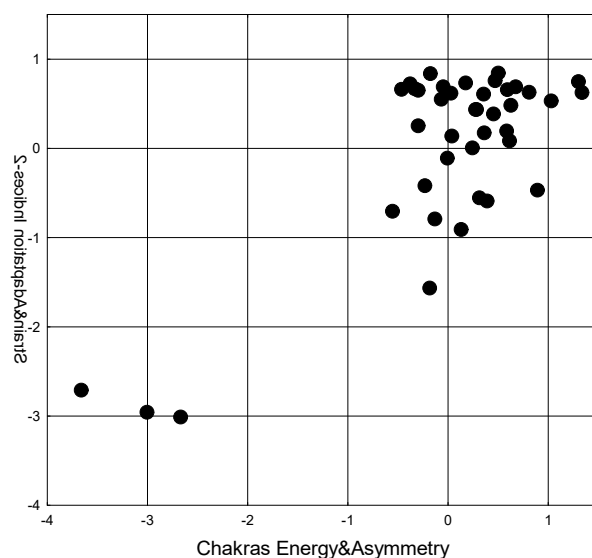
R=0,783; R^2=0,613; $\chi^2_{(12)}$=44; $p<10^{-4}$; Λ Prime=0,280

Fig. 5.7. Scatterplot of canonical correlation between parameters of the GDV (X-line) and the Leukocytary Indices-2 (Y-line)

Since leukocytes secrete cytokines, it is appropriate to analyze the relationship with GDV parameters of Interleukin-1 plasma level (determined by ELISA, analyzer "RT-2100C", USA, reagents from "Vector-Best", RF).

It was found that Interleukin-1 level is determined by the Entropy of GDV in the Left projection and the parameters of the five Chakras by 64% (Table 5.26 and Fig. 5.8).

Table 5.26. Regression Summary for Dependent Variable: IL-1
R=0,798; R^2=0,638; Adjusted R^2=0,477; $F_{(12,3)}$=3,96; p=0,0015; SE: 0,81 ng/L

	r	Beta	St. Err. of Beta	B	St. Err. of B	$t_{(27)}$	p-level
			Intercpt	-20,9	5,17	-4,04	,0004
Entropy L	0,40	,533	,145	3,586	,973	3,69	,0010
Entropy L f	0,30	,540	,170	3,374	1,062	3,18	,0037
Ch6E f	0,31	1,079	,343	4,590	1,460	3,14	,0040
Ch6E	0,27	-,867	,355	-3,324	1,359	-2,45	,0213
Ch1E	0,24	,747	,349	2,676	1,252	2,14	,0417
Ch3A	0,23	,441	,156	1,562	,554	2,82	,0089
Ch6A f	0,23	-,660	,235	-2,560	,910	-2,81	,0090
Ch4A	0,22	,440	,144	1,537	,501	3,07	,0049
Ch1E f	0,21	-,743	,281	-3,649	1,381	-2,64	,0135
Ch4E f	0,18	-,757	,308	-3,834	1,557	-2,46	,0205
Ch4E	0,17	,908	,315	4,142	1,436	2,88	,0076
Ch7A	-0,19	-,373	,149	-1,430	,572	-2,50	,0187
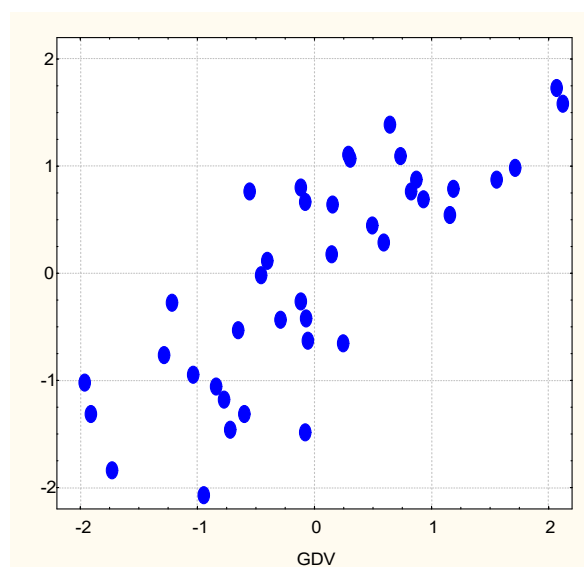
R=0,798; R^2=0,638; $\chi^2_{(12)}$=32,5; p=0,0012; Λ Prime=0,362
Fig. 5.8. Scatterplot of canonical correlation between GDV parameters (X-line) and the Interleukin-1 level (Y-line)

The materials of the chapter are published in the articles:
1. Babelyuk VY, Gozhenko AI, Dubkova GI, Babelyuk NV, Zukow W, Kindzer BM, Kovbasnyuk MM, Popovych IL. Causal relationships between the parameters of gas discharge visualization and phagocytosis. Journal of Education, Health and Sport. 2021; 11(6): 268-276.

2.   Babelyuk VY, Tserkovnyuk RG, Ruzhylo SV, Dubkova GI, Babelyuk NV, Zukow W, Popovych IL. Causal relationships between the parameters of gas discharge visualization and leukocytogram. Journal of Education, Health and Sport. 2021; 11(7): 258-269.

CHAPTER 6

PARAMETERS OF GAS DISCHARGE VISUALIZATION CORRELATED WITH PARAMETERS OF ACUPUNCTURE POINTS, EEG, HRV AND HORMONES

Thus, we have been shown that exist strong canonical correlation between parameters of GDV and principal neuroendocrine factors of adaptation as well as parameters of leukocytogram, immunity and phagocytosis.

Final evaluation study study, conducted on a much expanded contingent, will analyze the relationships between GDV parameters, on the one hand, and the parameters of acupuncture points, EEG, HRV and adaptation hormones, on the other.

The object of observation were 60 volunteers: 31 women and 29 men aged 26-76 years with dysfunction of neuro-endocrine-immune complex and dysmetabolism.

In the morning we registered primarily the kirlianogram (Dubkova GI) by the method of GDV by the device of "GDV Chamber" ("Biotechprogress", SPb, RF).

Electrical conductivity recorded (Hubyts'kyi VY) in follow acupuncture points: Pg(ND), TR(X) and MC(AVL) at Right and Left side. Used complex "Medissa". For each pair, the Laterality Index (LI) was calculated according to the equation:

LI, % = [200•(Right – Left)/(Right + Left)].

To assess the parameters of heart rate variability (HRV) recorded during 7 min electrocardiogram in II lead (software and hardware complex "CardioLab+HRV", KhAI-MEDICA, Kharkiv). For further analysis the following parameters HRV were selected. Temporal parameters (Time Domain Methods): the standard deviation of all NN intervals (SDNN), the square root of the mean of the sum of the squares of differences between adjacent NN intervals (RMSSD), the percent of interval differences of successive NN intervals greater than 50 msec (pNN$_{50}$); Triangular Index (TNN). Spectral parameters (Frequency Domain Methods): power spectral density (PSD) bands of HRV - high-frequency (HF, range 0,4÷0,15 Hz), low-frequency (LF, range 0,15÷0,04 Hz), very low-frequency (VLF, range 0,04÷0,015 Hz) and ultralow-frequency (ULF, range 0,015÷0,003 Hz). Calculated classical indexes: LF/HF; (VLF+LF)/HF; LFnu=100%•LF/(LF+HF). Baevsky's parameters. Heart rate (HR), Mode (Mo), the Amplitude of Mode (AMo), Variational Scope (MxDMn), Stress Index (BSI=AMo/2•Mo•MxDMn) as well as Baevsky's Activity of Regulatory Systems Index (BARSI).

Simultaneosly EEG recorded a hardware-software complex "NeuroCom Standard" (KhAI MEDICA, Kharkiv) monopolar in 16 loci (Fp1, Fp2, F3, F4, F7, F8, C3, C4, T3, T4, P3, P4, T5, T6, O1, O2) by 10-20 international system, with the reference electrodes A and Ref tassels on the ears. The duration of the epoch was 25 sec. Among the options considered the average EEG amplitude (μV), average frequency (Hz), frequency deviation (Hz), index (%) as well as absolute (μV^2/Hz) and relative (%) PSD of basic rhythms: β (35÷13 Hz), α (13÷8 Hz), θ (8÷4 Hz) and δ (4÷0,5 Hz) in all loci, according to the instructions of the device. In addition, calculated coefficient of Asymmetry (As) and Laterality Index (LI) for PSD each Rhythm using equations:

As, % = 100•(Max – Min)/Min;

LI, % = Σ [200•(Right – Left)/(Right + Left)]/8

We calculated also for each locus EEG and HRV Shannon's CE [1948] Entropy (h) of normalized PSD using Popovych's equations:

hEEG = - [PSDα•log$_2$ PSDα + PSDβ•log$_2$ PSDβ + PSDθ•log$_2$ PSDθ + PSDδ•log$_2$ PSDδ]/log$_2$ 4

hHRV=- [PSHF•log$_2$PSHF+PSLF•log$_2$PSLF+PSVLF•log$_2$PSVLF+PSULF•log$_2$PSULF]/log$_2$ 4

Among hormones determined (Kikhtan VV) major adaptation hormones Cortisol, Testosterone and Triiodothyronine (by the ELISA with the use of analyzer "RT-2100C" and corresponding sets of reagents from "Алкор Био", XEMA Co, Ltd and DRG International Inc).

At the first stage of the analysis, a matrix of correlations between the parameters of acupuncture points (AP) and gas-discharge image (GDI) was created (Table 6.1).

The next step was to calculate the canonical correlation between the two sets of parameters. The factor structure of acupuncture root is formed by indicators of electrical conductivity, but not its lateralization. GDI-root represents the shape coefficients of the image recorded without a filter in all three projections, and the entropy of the image also in all projections, but taken using a polyethylene filter, as well as the Korotkov's activation coefficient. These parameters carry factor loads with the same sign as the conductivity parameters. Instead, the symmetry of GDI and its area in all projections are related to electrical conductivity in the opposite way. The canonical correlation between the two constellations is significant (Table 6.2 and Fig. 6.1).

Following the accepted algorithm, the canonical analysis of the relationship between the parameters of AP and virtual Chakras was performed (Tables 6.3 and 6.4). This time, the acupuncture root factor structure included AP MC(AVL) lateralization, which negatively correlates with the Asymmetry of the fifth and sixth virtual Chakras registered with the filter. Interestingly, the Energy of the fifth Chakra was outside the structure of the root. In general, the strength of the canonical correlation between AP and Chakras was at the previous level (Fig. 6.2).

Table 6.1. Matrix of correlations between the parameters of acupuncture points and gas-discharge image

Variable	Correlations N=119								
	Pg(ND) R	Pg(ND) L	Pg(ND) LI	MC(AVL) R	MC(AVL) L	MC(AVL) LI	TR(X) R	TR(X) L	TR(X) LI
KAC	0,28	0,26	0,09	0,17	0,20	-0,04	0,24	0,32	0,00
Area R	-0,09	-0,09	0,00	-0,02	-0,09	0,02	-0,17	-0,21	0,02
Area RF	0,07	0,02	0,07	0,15	0,07	-0,03	-0,00	-0,00	0,01
Entropy R	0,02	-0,03	0,09	-0,01	-0,07	-0,00	0,09	0,05	-0,05
Entropy RF	0,11	0,10	0,02	0,16	0,20	-0,10	0,08	0,14	-0,13
CR	0,15	0,16	0,03	0,05	0,15	-0,05	0,19	0,29	-0,02
CRF	0,02	0,05	-0,01	-0,10	-0,02	-0,05	0,08	0,07	-0,04
Area F	-0,09	-0,12	0,06	-0,04	-0,12	0,01	-0,19	-0,24	0,02
Area FF	0,08	0,03	0,08	0,14	0,07	-0,02	0,05	0,04	0,02
Symmetry	-0,23	-0,25	-0,08	-0,16	-0,27	0,04	-0,26	-0,39	-0,01
Symmetry F	-0,11	-0,10	-0,02	-0,00	-0,07	0,05	-0,07	-0,10	0,07
Entropy F	0,07	0,03	0,09	-0,04	-0,09	-0,03	0,05	0,02	-0,05
Entropy FF	0,18	0,19	-0,10	0,24	0,28	-0,05	0,16	0,21	-0,18
CF	0,19	0,22	-0,01	0,12	0,24	-0,06	0,24	0,36	0,01
CFF	0,06	0,08	-0,05	-0,02	0,04	-0,02	0,13	0,12	0,01
Area L	-0,12	-0,15	0,02	-0,09	-0,18	0,01	-0,23	-0,29	0,00
Area LF	0,06	0,01	0,08	0,07	-0,03	0,04	-0,06	-0,08	0,01
Entropy L	0,06	0,02	0,04	0,09	0,03	0,02	0,04	-0,02	0,05
Entropy LF	0,17	0,20	-0,12	0,19	0,25	-0,16	0,17	0,22	-0,18
CL	0,19	0,22	-0,00	0,14	0,24	-0,00	0,24	0,35	0,02
CLF	0,00	0,04	-0,09	-0,05	0,05	-0,11	0,12	0,14	0,00

Note. For a sample with n = 119 $_{0,05}|r|>0,18$; $_{0,01}|r|>0,24$; $_{0,001}|r|>0,31$

Table 6.2. Factor structure of AP electrical conductivity and gas-discharge image

Left set	R
TR(X) L	-0,739
MC(AVL) L	-0,633
TR(X) R	-0,500
Pg(ND) L	-0,455
MC(AVL) R	-0,385
Pg(ND) R	-0,384
Right set	**R**
Shape Coeff F	-0,773
Shape Coeff L	-0,731
Shape Coeff R	-0,617
Korotkov's AC	-0,538
Entropy L (f)	-0,409
Entropy F (f)	-0,395
Entropy R (f)	-0,380
Symmetry	0,850
Area Left	0,567
Area Frontal	0,471
Area Right	0,407
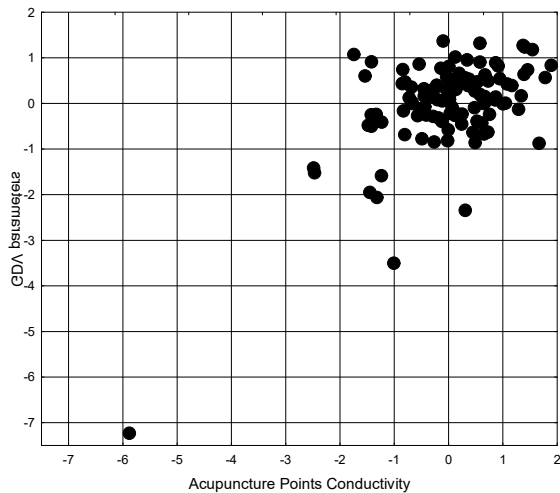
R=0,635; R^2=0,404; $\chi^2_{(88)}$=135; p=0,001; Λ Prime=0,288

Fig. 6.1. Scatterplot of canonical correlation between electrical conductivity of Acupuncture Points (X-line) and GDI parameters (Y-line)

Table 6.3. Matrix of correlations between the parameters of acupuncture points and virtual Chakras

Root Variable	Correlations, left set with right set								
	CH1E	CH2E	CH3E	CH4E	CH6E F	CH7E	CH5A F	CH6 A	CH6A F
Pg(ND)R	-0,06	-0,134	-0,08	-0,09	0,20	-0,05	-0,04	0,10	0,00
Pg(ND)L	-0,06	-0,147	-0,11	-0,14	0,17	-0,05	0,03	0,13	0,07
MC(AVL)R	-0,02	-0,138	-0,07	-0,13	0,10	-0,06	0,03	0,14	0,05
MC(AVL)L	-0,09	-0,227	-0,16	-0,23	0,05	-0,12	0,16	0,20	0,16
TR(X)R	-0,13	-0,264	-0,22	-0,19	0,07	-0,21	0,17	0,18	0,20
TR(X)L	-0,21	-0,342	-0,28	-0,28	0,05	-0,23	0,19	0,18	0,22
MC(AVL)LI	0,01	0,070	0,02	0,03	-0,02	0,05	-0,26	-0,01	-0,24

Table 6.4. Factor structure of AP electrical conductivity and virtual Chakras

Left set	R
TR(X) L	-0,718
MC(AVL) L	-0,605
TR(X) R	-0,481
Pg(ND) L	-0,410
MC(AVL) R	-0,346
Pg(ND) R	-0,293
MC(AVL) LI	0,330
Right set	**R**
Ch2 E	0,653
Ch4 E	0,633
Ch3 E	0,550
Ch1 E	0,466
Ch7 E	0,415
Ch6 E (f)	0,124
Ch6 A	-0,530
Ch5 A (f)	-0,570
Ch6 A (f)	-0,530

$R=0,614$; $R^2=0,377$; $\chi^2_{(63)}=114$; $p<10^{-4}$; Λ Prime$=0,353$

Fig. 6.2. Scatterplot of canonical correlation between electrical conductivity of Acupuncture Points (X-line) and virtual Chakras parameters (Y-line)

If the GDI and Chakras parameters are **combined in one set**, its canonical correlation with APs is stronger than in a separate analysis (Table 6.5 and Fig. 6.3).

Table 6.5. Factor structure of AP electrical conductivity and virtual Chakras Roots

Left set	R
TR(X) L	-0,706
MC(AVL) L	-0,620
TR(X) R	-0,485
Pg(ND) L	-0,366
MC(AVL) R	-0,365
Pg(ND) R	-0,289
MC(AVL) LI	0,349
Right set	R
Symmetry	0,682
Ch2 E	0,579
Ch4 E	0,546
Ch3 E	0,483
Area Left	0,469
Ch1 E	0,416
Korotkov's AC	0,414
Area Frontal	0,387
Ch7 E	0,378
Area Right	0,334
Ch6 E (f)	0,117
Shape Coeff F	-0,629
Shape Coeff L	-0,586
Ch5 A (f)	-0,499
Shape Coeff R	-0,496
Ch6 A (f)	-0,457
Entropy L (f)	-0,361
Entropy F (f)	-0,334
Entropy R (f)	-0,326
Ch6 A	-0,281

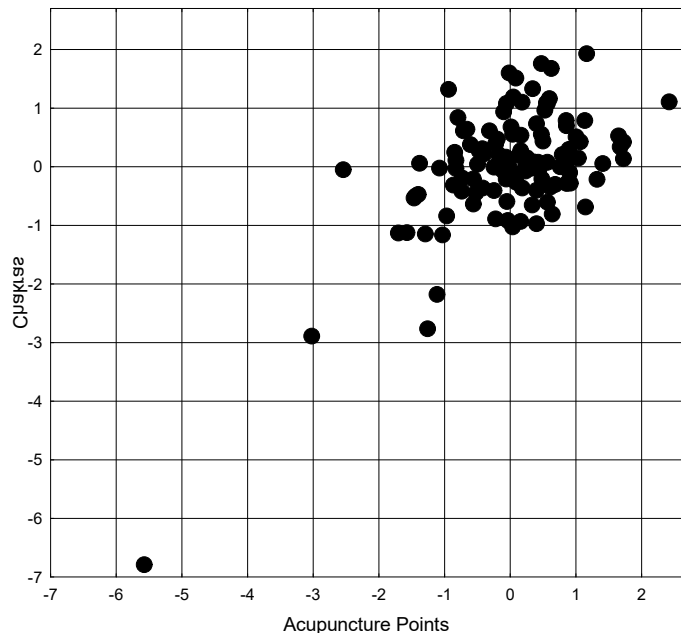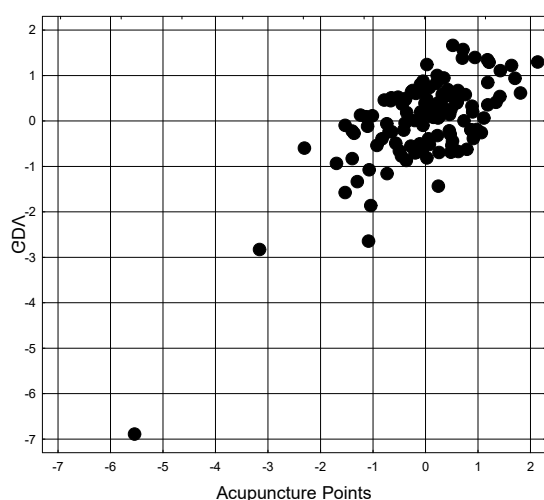R=0,707; R^2=0,499; $\chi^2_{(140)}$=178; p=0,016; Λ Prime=0,180

Fig. 6.3. Scatterplot of canonical correlation between electrical conductivity of Acupuncture Points (X-line) and total GDV parameters (Y-line)

In our view, this is perfectly consistent with the proposition that each one of the 7 Chakras originates from AP on the physical body [cyt. by Chase CR, 2018].

Screening of correlations between GDI and HRV parameters revealed (Table 6.6) that the old good rhythm frequency (Heart Rate) has the maximum coefficients for sampling, correlating positively with GDI entropy in all projections under both recording conditions. Negative correlation with entropy was found for markers of vagal tone (RMSSD, pNN_{50}, HF), with the maximum with the entropy of GDI recorded with a filter in frontal projection. Markers of sympathetic tone (LFnu, LF/HF, LF%) correlate, naturally, positively. In addition, the latter correlate positively with the shape coefficients and negatively with the GDI area in the left projection.

Among the detected hormones, only testosterone significantly correlates with GDI parameters. Interestingly, actual testosterone levels correlate positively with the area of GDI recorded with the filter, while standardized by sex and age with the entropy of GDI recorded without the filter in the left projection.

The activation coefficient proposed by Korotkov KG as a GDV Stress Index, according to our data, does not correlate with the Baevsky's HRV Stress Index, and the correlation with markers of sympathetic-vagal balance and sympathetic tone, although statistically significant, is not convincing enough.

**Table 6.6. Matrix of correlations between the autonomic-endocrine and GDI parameters**

Variable	Correlations N=119												
	Test act	Test stand	BSI In	HR	RMS SD	pNN 50	LF	HF	LF/ HF	CI	LF %	LFnu	VLF %
KAC	0,04	-0,05	-0,05	0,14	-0,02	-0,01	0,15	-0,04	0,24	0,09	0,25	0,26	-0,16
ER	-0,09	0,18	0,17	0,33	-0,13	-0,13	-0,10	-0,09	0,17	0,06	0,20	0,06	-0,18
ER f	-0,03	0,02	0,09	0,28	-0,17	-0,22	-0,12	-0,15	0,09	0,04	0,20	0,05	-0,19
SCR	0,05	-0,02	-0,09	0,06	-0,00	-0,01	0,16	-0,04	0,19	0,06	0,18	0,22	-0,08
SCR f	0,01	0,05	0,01	0,04	-0,08	-0,10	0,02	-0,14	0,14	0,02	0,12	0,20	-0,04
AF	0,13	0,06	0,14	0,01	-0,09	-0,06	-0,20	-0,04	-0,10	0,02	0,15	-0,12	0,11
AF f	0,27	-0,03	0,11	0,08	-0,11	-0,07	-0,17	-0,07	0,03	0,07	0,02	-0,02	0,02
EF	-0,06	0,06	0,09	0,22	-0,12	-0,14	-0,07	-0,12	0,10	0,06	0,11	0,08	-0,08
EF f	-0,08	-0,12	0,19	0,32	-0,22	-0,23	-0,15	-0,24	0,21	0,20	0,20	0,22	-0,13
SCF	0,07	-0,07	-0,09	0,09	-0,03	-0,04	0,14	-0,07	0,20	0,07	0,19	0,23	-0,09
SCF f	0,07	-0,07	0,01	0,07	-0,08	-0,10	0,03	-0,12	0,18	0,09	0,10	0,21	-0,02
AL	0,02	0,16	0,13	0,01	-0,03	-0,03	-0,20	-0,01	-0,22	-0,05	0,22	-0,23	0,13
EL	0,05	0,21	0,03	0,26	-0,18	-0,21	-0,16	-0,20	0,20	0,14	0,09	0,10	-0,05
ELF	-0,06	0,11	0,02	0,22	-0,15	-0,20	-0,11	-0,19	0,05	0,07	0,08	0,08	-0,05
SCL	0,10	-0,09	-0,09	0,11	-0,04	-0,05	0,15	-0,07	0,24	0,08	0,25	0,27	-0,14

In general, the canonical correlation between the analyzed constellations is strong (Table 6.7 and Fig. 6.4).

Table 6.7. Factor structure of HRV&endocrine and GDI Roots

Left set	R
Testosterone, nM/L	**-0,616**
LFnu, %	**-0,283**
LF/HF	**-0,214**
(VLF+LF)/HF	**-0,208**
(VLF+ULF)/TP	**-0,145**
Heart Rate	**-0,142**

Stress Index, ln un	**-0,093**
Testosterone, Z	**0,525**
RMSSD, msec	**0,123**
HF, msec^2	**0,097**
LF, msec^2	**0,052**
pNN$_{50}$, %	**0,009**
Right set	**R**
Entropy R	**0,370**
Entropy L	**0,266**
Entropy L (f)	**0,250**
Entropy F	**0,201**
Entropy R (f)	**0,159**
Area Left	**0,109**
Shape Coeff R (f)	**0,022**
Entropy F (f)	**0,019**
Area Frontal (f)	**-0,331**
Shape Coeff L	**-0,122**
Area Frontal	**-0,120**
Shape Coeff F (f)	**-0,115**
Shape Coeff F	**-0,079**
Korotkov's AC	**-0,037**
Shape Coeff R	**-0,021**
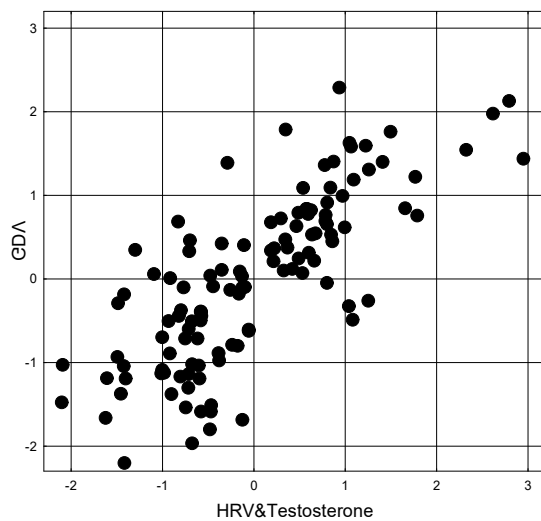
R=0,769; R^2=0,591; $\chi^2_{(210)}$=282; p=0,0007; Λ Prime=0,065

Fig. 6.4. Scatterplot of canonical correlation between HRV&Endocrine (X-line) and GDV (Y-line) parameters

Instead, as a result of the canonical correlation with the parameters of the virtual Chakras, cortisol and triiodothyronine were included in the factor structure of the autonomic-endocrine root (Tables 6.8 and 6.9). The prominent place in it of the VLF band encourages us to dwell in more detail on the interpretation of its physiological essence.

As noted Shaffer F & Ginsberg JP [2017], the heart's intrinsic nervous system appears to contribute to the VLF rhythm and the sympathetic nervous system influences the amplitude and frequency of its oscillations. VLF power may also be generated by physical activity, thermoregulatory, renin–angiotensin, and endothelial influences on the heart. Vagal activity may contribute to VLF power since parasympathetic blockade almost completely abolishes it. In contrast, sympathetic blockade does not affect VLF power. The VLF rhythm appears to be

generated by the stimulation of afferent sensory neurons in the heart. This, in turn, activates various levels of the feedback and feed-forward loops in the heart's intrinsic cardiac nervous system, as well as between the heart, the extrinsic cardiac ganglia, and spinal column. This experimental evidence suggests that the heart intrinsically generates the VLF rhythm and efferent sympathetic nervous system activity due to physical activity and stress responses modulates its amplitude and frequency. Because in our device ULF band (range 0,015÷0,003 Hz) is integrated into the lower zone of VLF band, what has been said about the latter also applies to the former. By the way, the relative PSD of these bands during the analysis were combined into an option (VLF+ULF).

Table 6.8. Matrix of correlations between the autonomic-endocrine parameters and parameters of virtual Chakras

| Chakra E&A	Test raw	Test stand	Cor-tisol	T3	AMo	dX	AMo/dX	BSI	HR	HF %	LF nu	VLF ULF	VLF	TP
1 E f	-0,02	0,15	-0,01	-0,08	-0,04	-0,02	-0,03	0,01	**0,23**	0,10	-0,09	0,12	0,14	0,09
2 E f	**-0,21**	0,08	-0,06	-0,02	-0,06	0,02	-0,06	-0,03	0,15	0,17	-0,13	0,07	0,08	0,05
3 E	-0,13	0,10	-0,04	0,02	0,07	-0,09	0,06	0,06	0,06	0,17	**-0,21**	0,11	0,11	0,07
4 E	**-0,23**	0,13	-0,01	-0,00	0,01	-0,08	0,03	0,04	0,09	0,14	**-0,18**	0,06	0,07	0,02
4 E f	**-0,18**	0,12	-0,07	-0,08	-0,07	0,01	-0,07	-0,03	**0,19**	0,15	-0,08	-0,07	-0,06	-0,07
5 E	0,08	0,11	-0,01	-0,01	**0,19**	-0,18	**0,19**	**0,22**	**0,21**	0,02	-0,04	-0,04	-0,02	-0,08
5 E f	0,07	0,08	-0,02	-0,07	0,14	-0,13	0,12	0,14	**0,20**	0,05	-0,01	-0,06	-0,05	-0,09
6 E	0,01	**0,23**	-0,00	0,01	**0,22**	-0,19	**0,22**	**0,24**	**0,20**	0,04	-0,07	-0,02	-0,01	-0,07
6 E f	-0,01	0,14	-0,02	-0,05	0,16	-0,14	0,15	**0,18**	**0,22**	0,08	-0,04	-0,03	-0,01	-0,05
7 E	-0,16	0,17	-0,01	0,02	0,08	-0,10	0,07	0,07	0,16	0,16	**-0,18**	0,15	0,17	0,10
7 E f	**-0,19**	0,11	-0,07	-0,02	-0,02	-0,02	-0,02	0,03	**0,25**	**0,18**	-0,10	0,04	0,05	0,03
1 A f	0,01	**-0,23**	0,05	-0,04	**0,23**	**-0,28**	**0,24**	**0,24**	0,05	-0,10	0,03	**0,21**	**0,24**	0,14
2 A	0,01	0,07	**-0,20**	0,02	-0,12	0,11	-0,12	-0,13	-0,06	0,13	-0,04	-0,01	-0,01	0,01
2 A f	0,08	-0,06	0,04	-0,04	-0,10	0,11	-0,14	-0,15	-0,10	**0,32**	-0,28	0,07	0,07	0,11
3 A	**0,19**	0,02	-0,17	-0,03	-0,12	0,07	**-0,18**	-0,16	-0,09	-0,07	0,10	-0,13	-0,11	-0,12
4 A	0,15	0,10	0,07	-0,03	0,15	**-0,22**	0,14	0,13	0,11	-0,12	0,05	0,16	0,16	0,07
4 A f	-0,06	0,00	0,03	0,00	-0,05	0,01	-0,05	-0,06	0,09	-0,06	-0,02	**0,25**	**0,26**	**0,24**
5 A	-0,02	**-0,24**	0,09	**0,24**	0,15	-0,10	**0,20**	0,18	-0,01	-0,07	0,11	-0,05	-0,05	-0,06
5 A f	0,04	**-0,31**	0,02	0,07	0,08	-0,09	0,07	0,05	-0,01	-0,03	0,02	-0,02	-0,01	-0,02
6 A	-0,09	**-0,34**	0,08	0,20	0,14	-0,13	0,19	0,17	-0,00	-0,04	0,11	-0,02	-0,01	-0,03
6 A f	0,07	**-0,35**	-0,00	0,03	0,06	-0,07	0,04	0,03	0,01	-0,04	0,05	-0,01	0,00	0,00
7 A	0,06	-0,02	**-0,22**	0,03	-0,13	0,11	-0,13	-0,13	-0,11	0,12	-0,03	0,03	0,03	0,06
7 A f	0,04	-0,11	0,11	-0,01	0,01	0,02	-0,03	-0,03	-0,08	**0,24**	-0,22	0,10	0,10	0,12

The above is consistent with the view that **fourth** Chakra is related to heart, cardiac plexus and vagus nerve, and the **first** Chakra is associated with adrenals. In our opinion, the significant connections between the levels of cortisol and testosterone and the parameters of the **first** and **second** Chakras, and triiodothyronine - the **fifth** Chakra, are quite natural.

In general, the canonical correlation between the HRV&endocrine and virtual Chakras parameters is strong (Table 6.9 and Fig. 6.5).

Table 6.9. Factor structure of HRV&endocrine and virtual Chakras Roots

Left set HRV&Hormones	R
VLF, msec^2	**0,489**
VLF+ULF, msec^2	**0,476**
Total Power HRV, msec^2	**0,449**
Testosterone, Z	**0,427**
HF/TP	**0,250**
MxDMn HRV, msec	**0,130**
Cortisol, nM/L	**0,077**
Heart Rate	**-0,320**
Testosterone, nM/L	**-0,287**
LFnu, %	**-0,243**
Amplitude Mode HRV, %	**-0,232**

Vegetative Balance Index	**-0,199**
Baevsky's Stress Index, un	**-0,190**
Triiodothyronine, nM/L	**-0,117**
Right set Chakras	**R**
7 E	0,474
7 E f	0,398
1 E f	0,395
4 E	0,368
2 E f	0,364
4 A f	0,364
4 E f	0,313
3 E	0,279
6 E	0,197
6 E f	0,195
4 A	0,161
2 A	0,062
5 E f	0,056
5 E	0,052
2 A f	0,028
6 A	-0,327
3 A	-0,327
5 A f	-0,308
5 A	-0,294
6 A	-0,273
1 A f	-0,179
7 A	-0,069
7 A f	-0,045
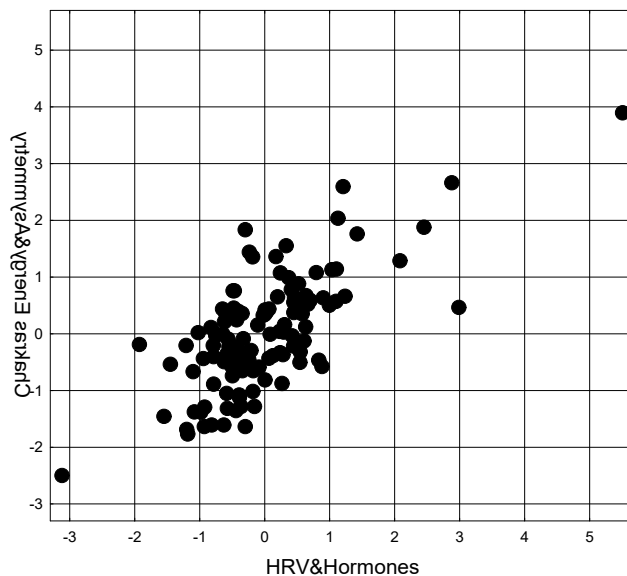
R=0,712; R^2=0,507; $\chi^2_{(345)}$=404; p=0,015; Λ Prime=0,016

Fig. 6.5. Scatterplot of canonical correlation between HRV&Endocrine (X-line) and virtual Chakras (Y-line) parameters

In the final stage, based on the screening of the relationships between the GDI and EEG parameters, a correlation matrix was created, limited only by variables with significant coefficients (Table 6.10).

Table 6.10. Matrix of correlations between the EEG and GDI parameters

Variabl	CAK	AR	ER	ERF	CR	CRF	AF	SYM	Sym	EF	CF	CFF	AL	ALF	EL	CL	CLF
	Correlations N=120																
IRA	-0,10	0,04	-0,15	-0,20	0,09	0,10	-0,03	0,17	0,11	-0,05	-0,06	0,10	-0,00	-0,15	-0,12	-0,06	0,12
FP1H	-0,18	0,19	0,08	0,07	0,16	-0,09	0,16	0,21	0,05	0,07	-0,21	-0,13	0,25	0,12	0,03	-0,23	-0,13
F3A	-0,08	-0,01	-0,03	-0,25	0,03	0,10	-0,06	0,09	0,07	-0,04	-0,01	0,06	-0,04	-0,05	-0,22	-0,02	0,08
F7T%	-0,18	0,22	0,14	0,11	0,19	-0,12	0,17	0,16	-0,00	0,17	-0,22	-0,13	0,25	0,09	0,02	-0,24	-0,11
F8T%	-0,13	0,21	0,14	0,03	0,15	-0,18	0,17	0,10	0,08	0,10	-0,16	-0,17	0,25	0,10	0,12	-0,19	-0,14
T3B%	-0,12	0,08	0,26	0,18	0,06	-0,01	0,07	0,07	-0,05	0,16	-0,07	-0,04	0,09	0,05	0,15	-0,12	-0,08
T4H	-0,13	0,22	0,12	0,07	0,22	-0,16	0,19	0,26	0,13	0,21	-0,26	-0,22	0,27	0,16	0,01	-0,28	-0,19
C3A	-0,11	0,04	-0,03	-0,25	0,07	0,11	-0,02	0,12	0,11	-0,04	-0,04	0,07	0,00	-0,04	-0,21	-0,04	0,09
C4A	-0,13	0,07	-0,03	-0,27	0,09	0,07	0,01	0,12	0,10	-0,07	-0,08	0,04	0,04	-0,02	-0,25	-0,09	0,07
C4D	-0,14	0,03	-0,06	-0,09	0,04	0,07	0,05	-0,02	-0,25	0,05	-0,06	0,11	0,01	0,01	0,07	-0,04	0,08
T5D%	0,07	-0,11	-0,28	-0,05	0,06	-0,03	-0,03	-0,10	0,03	-0,19	0,06	0,00	-0,07	0,01	-0,07	0,08	0,02
P3B%	0,01	0,05	0,27	0,25	0,02	-0,05	0,08	-0,03	-0,12	0,16	-0,02	-0,07	0,05	0,13	0,22	-0,03	-0,13
P3A	-0,13	0,06	-0,04	-0,23	0,07	0,08	0,00	0,13	0,10	-0,06	-0,05	0,06	0,01	-0,06	-0,26	-0,04	0,08
P3D	-0,07	-0,03	-0,19	-0,30	0,02	0,05	0,00	0,04	0,03	-0,14	-0,05	0,07	0,05	-0,01	-0,10	-0,05	0,06
P4B%	0,02	0,02	0,32	0,25	0,01	-0,05	0,03	-0,04	-0,13	0,24	-0,03	-0,03	0,02	0,11	0,25	-0,01	-0,05
P4D	-0,05	0,01	-0,20	-0,31	0,00	0,06	0,04	0,03	-0,03	-0,20	-0,01	0,06	0,01	-0,01	-0,11	-0,02	0,02
O2B%	-0,01	0,08	0,30	0,08	0,01	-0,14	0,11	-0,00	-0,07	0,20	-0,07	-0,14	0,13	0,19	0,18	-0,09	-0,23
O2D	0,12	-0,15	-0,23	-0,12	0,15	0,12	-0,14	-0,18	-0,16	-0,22	0,21	0,15	-0,20	-0,11	-0,11	0,22	0,18

According to the canonical correlation analysis (Table 6.11), the factor structure of the neuro-endocrine root was headed by real testosteronemia. Next are variables with similar in sign, but much lower factor loads. Significantly, the markers of **sympathetic** tone are interspersed with PSD of **δ-** and **α-**rhythms of EEG parameters.
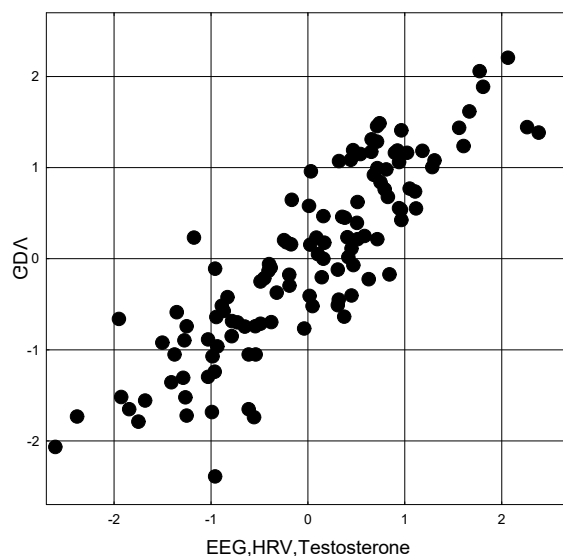
Table 6.11. Factor structure of neuro-endocrine and GDI canonical Roots

Left set	R
Testosterone, nM/L	0,557
LFnu, %	0,275
O2-δ PSD, μV²/Hz	0,253
P4-δ PSD, μV²/Hz	0,242
LF/HF	0,228
C4-δ PSD, μV²/Hz	0,225
T5-δ PSD, %	0,222
(VLF+LF)/HF	0,190
Heart Rate	0,162
P3-α PSD, μV²/Hz	0,140
(VLF+ULF)/TP	0,138
C3-α PSD, μV²/Hz	0,104
C4-α PSD, μV²/Hz	0,101
P3-δ PSD, μV²/Hz	0,077
F3-α PSD, μV²/Hz	0,068
Index α, %	0,063
Baevsky's Stress Index, ln un	0,043
Testosterone standard, Z	-0,399
F7-θ PSD, %	-0,381
F8-θ PSD, %	-0,359
Entropy T4	-0,306

Entropy Fp1	**-0,293**
P4-β PSD, %	**-0,165**
T3-β PSD, %	**-0,156**
P3-β PSD, %	**-0,145**
O2-β PSD, %	**-0,145**
RMSSD, msec	**-0,095**
HF, msec^2	**-0,083**
LF, msec^2	**-0,028**
Right set	**R**
Entropy R	**-0,339**
Entropy L	**-0,232**
Entropy L (f)	**-0,298**
Entropy F	**-0,241**
Entropy R (f)	**-0,290**
Area Left	**-0,168**
Entropy F (f)	**-0,132**
Area Frontal (f)	**0,249**
Shape Coeff F (f)	**0,199**
Shape Coeff L	**0,142**
Shape Coeff F	**0,110**
Shape Coeff R (f)	**0,106**
Shape Coeff R	**0,089**
Area Frontal	**0,056**
Korotkov's AC	**0,037**

The constellation of variables with opposite loads is headed by testosterone, standardized by sex and age. It is accompanied by markers of **vagal** tone and PSD **θ**- and **β**-rhythm of EEG, as well as **Entropy** at the loci T4 and Fp1.

The canonical correlation between neuroendocrine and GDV parameters is very strong (Fig. 6.6).

R=0,869; R^2=0,755; χ$^2_{(480)}$=565; p=0,005; Λ Prime=0,002

Fig. 6.6. Scatterplot of canonical correlation between Neuro-Endocrine (X-line) and GDV (Y-line) parameters

Interestingly, the factor structure of GDI Roots is also represented by Entropy. We have previously shown that the Entropy of GDI correlates with the entropy of both EEG and

leukocytogram and immunocytogram [Gozhenko AI et al, 2021]. Another constellation of GDI parameters is formed by Shape Coefficients, which give the opposite sign of the load. The last element of the factor structure is the GDI Area in the left and front projections.

Unfortunately, our possibilities for identifying cortical and subcortical regions are limited. It is traditionally believed that loci C3/C4 projected hippocampus, and loci T3/T4 reflect the activity of the amygdala [Romodanov PD, 1993]. In practice, transcranial magnetic and direct current stimulation of the T3/T4 scalp position is used to reach the insular cortex, and F3/F4 loci - to activate the dorsolateral prefrontal cortex nuclei [review: Iseger TA et al, 2020]. The figures presented by Winkelmann T et al [2017] and Yoo HJ et al [2018] give us reason to assume that the loci C3/C4 projected precentral gyrus, T3/T4 – inferior temporal gyrus, F3/F4 - caudal anterior cingulate cortex or rostral middle frontal gyrus or superior frontal gyrus, P3/P4 – supramarginal gyrus, T5/T6 – caudal anterior cingulate cortex. These cortical structures affect the activity of the vagus and sympathetic nuclei.

Now consider the connections between EEG parameters and Chakras energy.

Table 6.12. Matrix of correlations between the virtual Chakras Energy and EEG parameters

Variable	Ch1E	Ch1Ef	Ch2E	Ch2Ef	Ch3E	Ch3Ef	Ch4E	Ch4Ef	Ch5E	Ch5Ef	Ch6E	Ch6Ef	Ch7E	Ch7Ef
DF	0,16	0,27	0,11	0,16	0,11	0,24	0,13	0,14	0,10	0,18	0,14	0,22	0,15	0,22
AF	0,24	0,22	0,24	0,22	0,17	0,16	0,19	0,21	0,14	0,12	0,19	0,14	0,19	0,19
LIA	0,17	0,19	0,23	0,21	0,21	0,17	0,20	0,17	0,23	0,16	0,28	0,17	0,24	0,20
FP1H	0,20	0,16	0,26	0,18	0,25	0,18	0,26	0,15	0,09	0,11	0,17	0,14	0,28	0,15
FP2H	0,18	0,12	0,21	0,14	0,22	0,12	0,24	0,15	0,09	0,12	0,19	0,14	0,17	0,10
FP2B%	0,21	0,26	0,16	0,19	0,17	0,19	0,17	0,20	0,10	0,21	0,20	0,24	0,15	0,17
F3H	0,21	0,19	0,19	0,16	0,23	0,15	0,25	0,14	0,18	0,23	0,24	0,22	0,17	0,16
F3B%	0,19	0,22	0,15	0,16	0,12	0,18	0,13	0,18	0,14	0,19	0,23	0,23	0,14	0,17
F3T%	0,25	0,22	0,24	0,20	0,22	0,20	0,35	0,25	0,17	0,17	0,19	0,19	0,25	0,18
F3A	-0,07	-0,21	-0,08	-0,15	-0,06	-0,18	-0,13	-0,22	-0,04	-0,11	-0,01	-0,08	-0,10	-0,13
F4H	0,25	0,19	0,29	0,23	0,28	0,21	0,28	0,18	0,15	0,18	0,24	0,22	0,28	0,25
F4T%	0,19	0,14	0,25	0,19	0,19	0,17	0,31	0,24	0,09	0,08	0,12	0,12	0,27	0,18
F7T%	0,22	0,13	0,28	0,18	0,24	0,10	0,33	0,23	0,06	0,01	0,11	0,07	0,28	0,15
F8H	0,15	0,18	0,22	0,23	0,20	0,18	0,22	0,19	0,12	0,14	0,18	0,19	0,27	0,22
F8T%	0,21	0,13	0,23	0,16	0,16	0,10	0,26	0,19	0,09	0,05	0,14	0,09	0,28	0,15
T3H	0,18	0,13	0,23	0,16	0,23	0,11	0,25	0,15	0,12	0,10	0,20	0,13	0,21	0,15
T4H	0,21	0,20	0,29	0,24	0,30	0,21	0,28	0,25	0,12	0,13	0,23	0,21	0,29	0,28
T4A	0,05	-0,06	0,06	0,02	0,08	-0,03	0,03	-0,08	0,11	0,01	0,17	0,09	0,07	0,05
T4D	-0,08	-0,17	-0,12	-0,20	-0,15	-0,24	-0,12	-0,19	-0,08	-0,14	-0,14	-0,17	-0,13	-0,21
C3T%	0,15	0,14	0,20	0,12	0,14	0,13	0,27	0,23	0,11	0,11	0,14	0,15	0,23	0,12
T5B%	0,25	0,30	0,15	0,20	0,21	0,24	0,17	0,22	0,23	0,29	0,27	0,30	0,14	0,20
T6H	0,13	0,15	0,19	0,17	0,18	0,14	0,25	0,22	0,09	0,16	0,16	0,21	0,21	0,16
T6B	0,22	0,22	0,26	0,28	0,25	0,27	0,20	0,18	0,24	0,17	0,29	0,21	0,26	0,29
P3A%	-0,08	-0,16	-0,06	-0,14	-0,06	-0,14	-0,18	-0,24	-0,13	-0,15	-0,10	-0,13	-0,06	-0,12
P4A	-0,02	-0,15	-0,03	-0,13	-0,03	-0,12	-0,14	-0,23	-0,02	-0,11	-0,00	-0,10	-0,04	-0,12
O2B%	0,19	0,28	0,15	0,18	0,20	0,27	0,18	0,20	0,20	0,27	0,27	0,29	0,14	0,18
O2D	-0,21	-0,17	-0,21	-0,15	-0,24	-0,15	-0,21	-0,15	-0,07	-0,12	-0,14	-0,13	-0,17	-0,15

Screening revealed the closest link between relative PSD of β-rhythm in locus T5 and virtual Chakras 1 and 6 Energy registered with filter (Figs. 6.7 and 6.8).
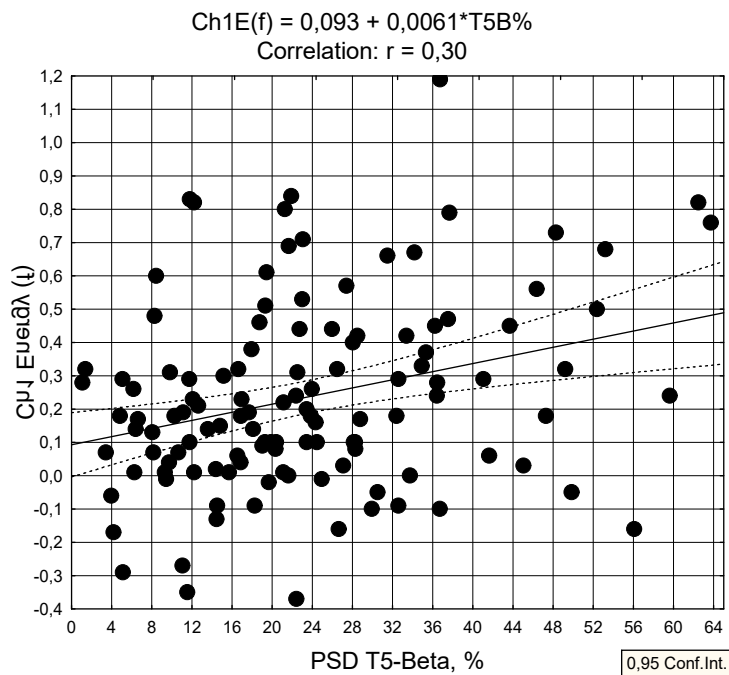
Ch1E(f) = 0,093 + 0,0061*T5B%
Correlation: r = 0,30

Fig. 6.7. Scatterplot of correlation between relative PSD of β-rhythm in locus T5 (X-line) and virtual Chakra 1 Energy (registration with filter) (Y-line)
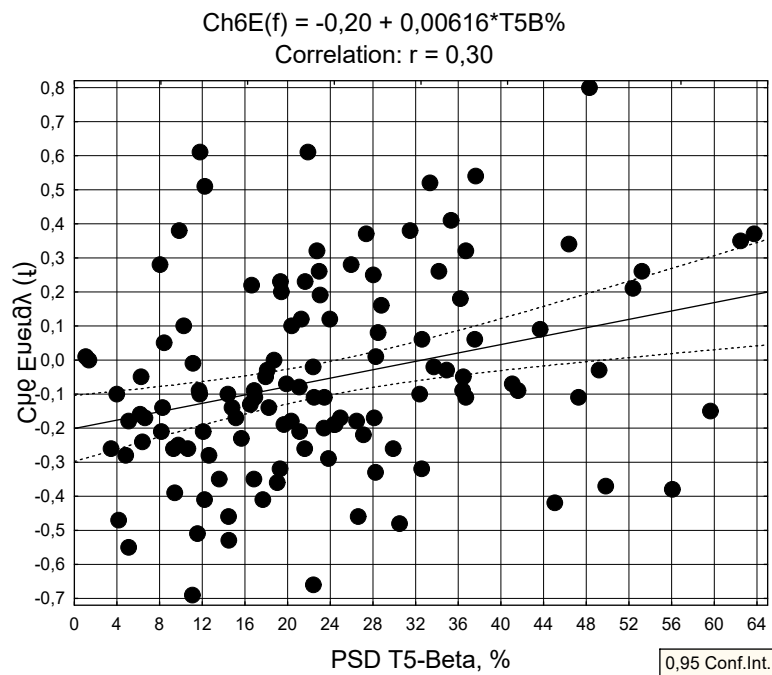
Ch6E(f) = -0,20 + 0,00616*T5B%
Correlation: r = 0,30

Fig. 6.8. Scatterplot of correlation between relative PSD of β-rhythm in locus T5 (X-line) and virtual Chakra 6 Energy (registration with filter) (Y-line)

The coefficients of canonical correlation between the EEG parameters and virtual Chakras Energy are in the interval 0,415÷0,564 and 0,358÷0,528 when registering without a filter and with a filter, respectively (Fig. 6.9).
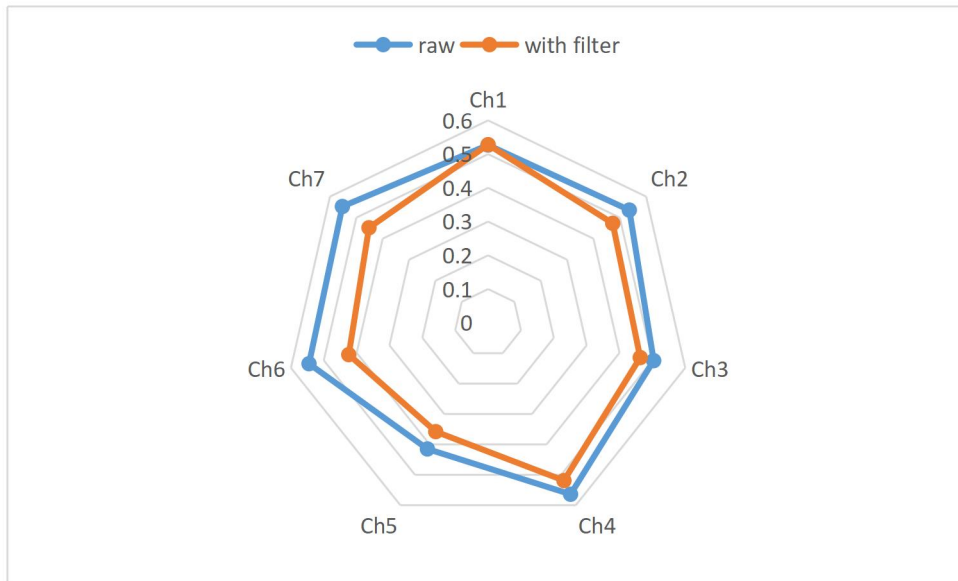
Fig. 6.9. Multiple correlation coefficients between EEG parameters and Energy of raw virtual Chakras and registered with filter

As we can see, the registration with the use of the filter reduces the strength of the connections of the EEG parameters with the Energy of the Chakras, mostly the sixth and seventh, except for the first Chakra. This is in perfect agreement with the classical ideas about the relationship of the former to the nervous system, as well as with the concept of Korotkov KG that GDI, taken off without filter, characterizes the functional changes of organism, while taken with a filter characterizes organic changes.

Further, for canonical analysis, EEG parameters were combined with HRV parameters and hormones.

Interim results are shown in Tables 6.13 and 6.14 and Figures 6.10 and 6.11.

Table 6.13. Factor structure of EEG,HRV&Endocrine and virtual Chakras (without filter) Energy Roots

Left set EEG, HRV&Hormones	R
Entropy T4	0,506
Entropy F8	0,436
Entropy Fp1	0,416
Entropy F4	0,408
Entropy T6	0,361
Testosterone standard, Z	0,356
F8-θ PSD, %	0,353
Entropy Fp2	0,318
Laterality α, Hz	0,305
VLF, msec²	0,302
F4-θ PSD, %	0,301
T6-β PSD, µV²/Hz	0,296
F7-θ PSD, %	0,295
VLF+ULF, msec²	0,287
Entropy T3	0,285
C3-θ PSD, %	0,250
Total Power HRV, msec²	0,233
O2-β PSD, %	0,196
T4-α PSD, µV²/Hz	0,181

|	
F3-θ PSD, %	**0,179**
Entropy F3	**0,155**
Frequency α, Hz	**0,134**
Heart Rate	**0,124**
Amplitude Mode HRV, %	**0,108**
T5-β PSD, %	**0,083**
P3-α PSD, %	**0,081**
Testosterone, nM/L	**-0,315**
LFnu, %	**-0,229**
O2-δ PSD, μV²/Hz	**-0,215**
Right set *Chakras Energy*	**R**
7 E	**0,694**
2 E	**0,600**
4 E	**0,467**
3 E	**0,446**
6 E	**0,387**
1 E	**0,282**
5 E	**0,155**
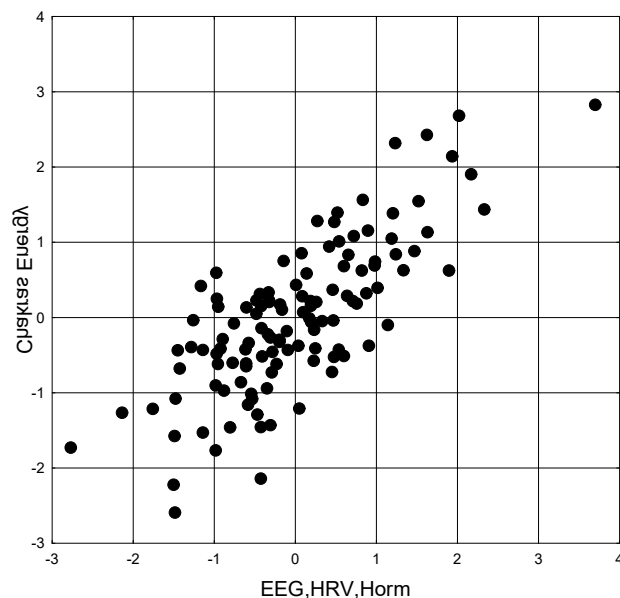
R=0,768; R²=0,590; χ²(245)=313; p=0,002; Λ Prime=0,039

Fig. 6.10. Scatterplot of canonical correlation between Neuro-endocrine parameters (X-line) and virtual Chakras Energy (registration without filter) (Y-line)

Table 6.14. Factor structure of EEG,HRV&Endocrine and virtual Chakras (with filter) Energy Roots

Left set *EEG, HRV&Hormones*	**R**
Entropy T4	**0,416**
HF/TP	**0,237**
Testosterone standard, Z	**0,235**
Frequency α, Hz	**0,216**
F3-θ PSD, %	**0,209**
T6-β PSD, μV²/Hz	**0,209**
Heart Rate	**0,192**
F3-β PSD, %	**0,168**
Laterality α, Hz	**0,159**

Fp2-β PSD, %	**0,127**
Frequency δ, Hz	**0,119**
T5-β PSD, %	**0,075**
O1-β PSD, %	**0,073**
O2-β PSD, %	**0,060**
Total Power HRV, msec²	**0,063**
VLF, msec²	**0,043**
Testosterone, nM/L	**-0,468**
P4-α PSD, μV²/Hz	**-0,196**
Amplitude Mode HRV, %	**-0,189**
T4-δ PSD, μV²/Hz	**-0,183**
P3-α PSD, %	**-0,159**
Vegetative Balance Index	**-0,145**
LFnu, %	**-0,143**
F3-α PSD, μV²/Hz	**-0,120**
Cortisol, nM/L	**-0,106**
Right set Chakras Energy	**R**
4 E f	**0,633**
7 E f	**0,586**
2 E f	**0,530**
1 E f	**0,296**
3 E f	**0,283**
6 E f	**0,208**
5 E f	**0,007**
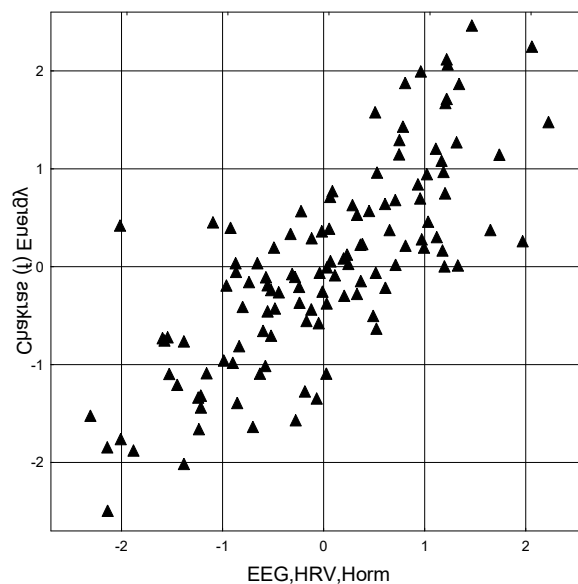
R=0,772; R²=0,596; $\chi^2_{(210)}$=283; p=0,0006; Λ Prime=0,057

Fig. 6.11. Scatterplot of canonical correlation between Neuro-endocrine parameters (X-line) and virtual Chakras Energy (registration with filter) (Y-line)

In the end, it was found (Table 6.15) that the prominent places in the factor structure of the root of Chakra Energies are occupied by the seventh, second and fourth Chakras, which are responsible for: the pineal gland, **right** brain, upper brain; **testes/ovaries**; and heart, circulation, vagal nerve, respectively. On the other hand, the factor structure of the neuro-endocrine root is represented primarily by Entropies and PSD **right**-handed (paired) loci, as well as **testosterone**.

Table 6.15. Factor structure of EEG,HRV&Endocrine and virtual Chakras Energy Roots

EEG, HRV&Hormones	R
Entropy T4	-0,460
Testosterone standard, Z	-0,343
F7-θ PSD, %	-0,320
Entropy F8	-0,318
F8-θ PSD, %	-0,315
T6-β PSD, μV²/Hz	-0,298
F4-θ PSD, %	-0,283
Laterality α, Hz	-0,280
Entropy F4	-0,277
Entropy T6	-0,266
C3-θ PSD, %	-0,233
Entropy T3	-0,230
F3-β PSD, %	-0,226
Frequency α, Hz	-0,220
Heart Rate	-0,213
Entropy Fp1	-0,211
HF/TP	-0,189
Entropy Fp2	-0,172
T4-α PSD, μV²/Hz	-0,165
Fp2-β PSD, %	-0,161
F3-θ PSD, %	-0,154
Frequency δ, Hz	-0,122
O2-β PSD, %	-0,111
O1-β PSD, %	-0,106
VLF, msec²	-0,108
Total Power HRV, msec²	-0,088
T5-β PSD, %	-0,078
Entropy F3	-0,055
Testosterone, nM/L	0,398
T4-δ PSD, μV²/Hz	0,217
O2-δ PSD, μV²/Hz	0,136
LFnu, %	0,124
P4-α PSD, μV²/Hz	0,094
Cortisol, nM/L	0,053
Amplitude Mode HRV, %	0,017
Chakras Energy	R
7 E	-0,583
7 E f	-0,578
2 E	-0,531
2 E f	-0,522
4 E f	-0,544
4 E	-0,487
3 E	-0,333
3 E f	-0,286
6 E	-0,306
6 E f	-0,274
1 E f	-0,283
1 E	-0,259
5 E	-0,111
5 E f	-0,058
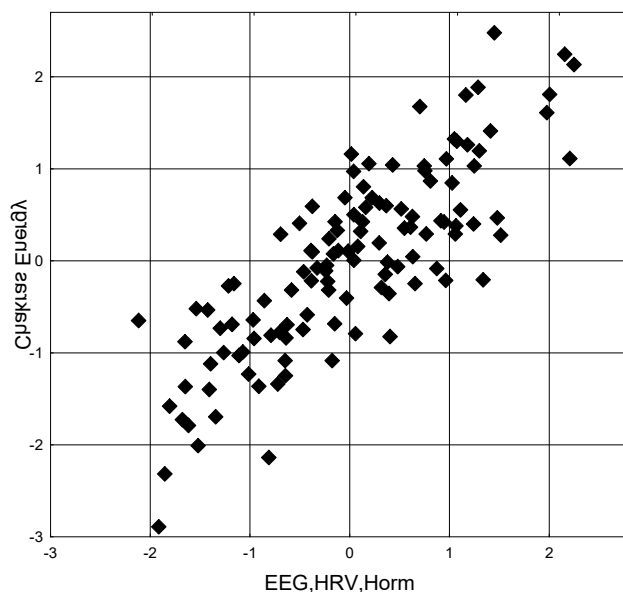
R=0,821; R^2=0,674; $\chi^2_{(490)}$=545; p=0,045; Λ Prime=0,003

Fig. 6.12. Scatterplot of canonical correlation between Neuro-endocrine parameters (X-line) and virtual Chakras Energy (Y-line)

Another basic characteristic of virtual Chakras is their Asymmetry. This is consistent with the position of the existence of morpho-functional asymmetry of many, if not all, paired organs or their halves, including the hemispheres of the brain [Miskovic V & Schmidt LA, 2010; Kruhliy YuZ, 2010; 2012; Balle M et al, 2013; Barylyak LG et al, 2013].

Screening revealed a number of significant correlations, the strongest of which are shown in Figs 6.13 and 6.14.
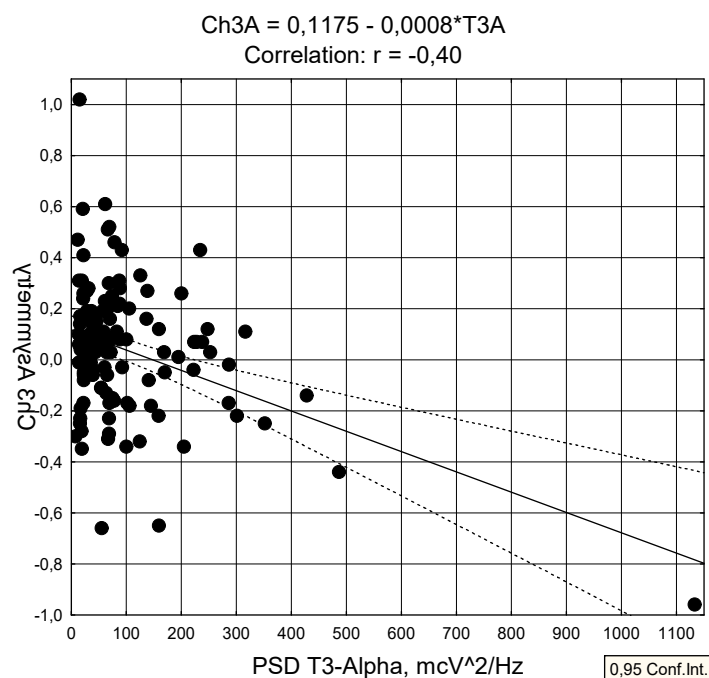
Fig. 6.13. Scatterplot of correlation between PSD of α-rhythm in locus T3 (X-line) and virtual Chakra 3 Asymmetry (Y-line)
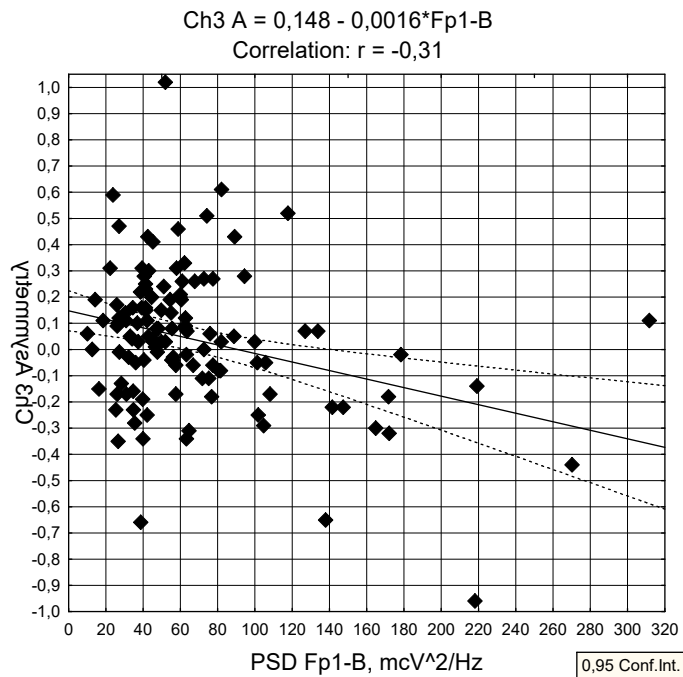
Fig. 6.14. Scatterplot of correlation between PSD of β-rhythm in locus Fp1 (X-line) and virtual Chakra 3 Asymmetry (Y-line)

Interestingly, the effect of the polyethylene filter on the strength of the correlations with the EEG parameters of the Asymmetry of the Chakras was much more noticeable compared to their Energy. This is especially true of the Asymmetry of the third and seventh Chakras, while the EEG connections of the sixth Chakra remain stable (Fig. 6.15).
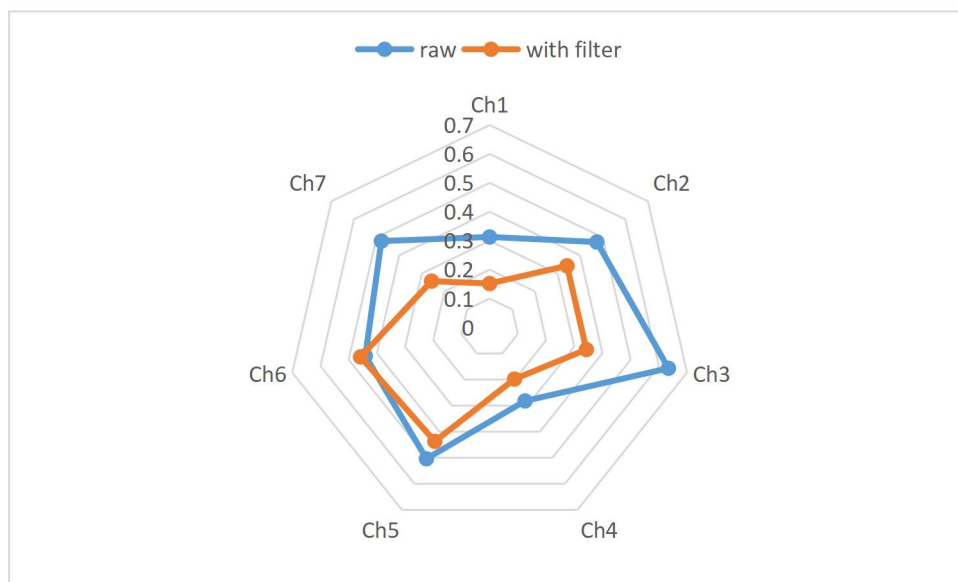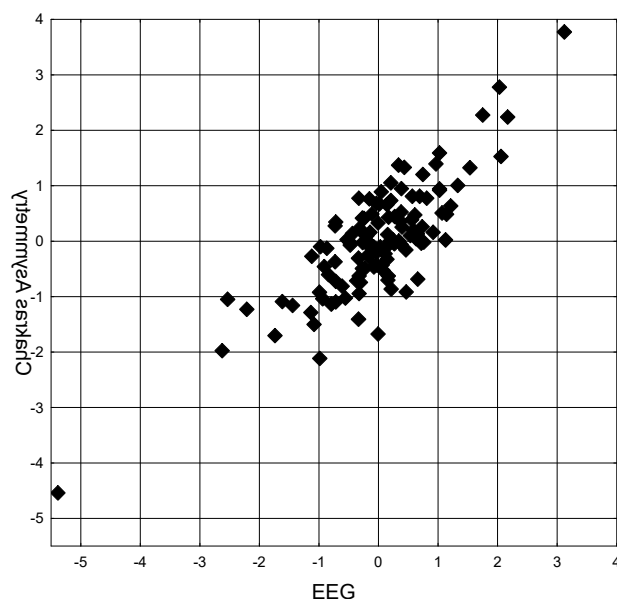
Fig. 6.15. Multiple correlation coefficients between EEG parameters and Asymmetry of raw virtual Chakras and registered with filter

In general, the canonical correlation between EEG parameters and the Asymmetry of virtual Chakras is stated as strong (Table 6.16 and Fig. 6.16).

Table 6.16. Factor structure of EEG and virtual Chakras Asymmetry Roots

Left set EEG, HRV&Hormones	R
T5-θ PSD, μV²/Hz	-0,488
Fp1-θ PSD, μV²/Hz	-0,471
T4-α PSD, μV²/Hz	-0,436
Fp2-α PSD, μV²/Hz	-0,432
F7-α PSD, μV²/Hz	-0,430
C3-θ PSD, μV²/Hz	-0,415
T3-α PSD, μV²/Hz	-0,407
O1-θ PSD, μV²/Hz	-0,404
Index β, %	-0,400
P3-θ PSD, μV²/Hz	-0,337
F4-δ PSD, μV²/Hz	-0,329
T5-δ PSD, μV²/Hz	-0,314
T5-δ PSD, %	-0,245
O1-α PSD, μV²/Hz	-0,313
F7-θ PSD, μV²/Hz	-0,291
C4-δ PSD, μV²/Hz	-0,289
Fp2-θ PSD, μV²/Hz	-0,275
Fp1-β PSD, μV²/Hz	-0,274
T5-α PSD, μV²/Hz	-0,245
F3-α PSD, μV²/Hz	-0,240
C4-α PSD, μV²/Hz	-0,212
T6-β PSD, μV²/Hz	-0,179
Frequency β, Hz	0,397
Fp2-β PSD, %	0,289
Frequency θ, Hz	0,282
F3-β PSD, %	0,278
Laterality δ, %	0,171
P3-β PSD, %	0,120
O2-β PSD, %	0,119
Frequency δ, Hz	0,091
Right set Chakras Asymmetry	R
3 A	0,519
5 A f	0,515
2 A	0,488
6 A f	0,421
3 A f	0,375
2 A f	0,361
7 A	0,343
7 A f	0,260
4 A	-0,162
1 A	-0,147
6 A	-0,053
5 A	-0,048
1 A f	-0,037

R=0,820; R²=0,673; χ²(468)=519; p=0,054; Λ Prime=0,004

Fig. 6.16. Scatterplot of canonical correlation between EEG parameters (X-line) and virtual Chakras Asymmetry(Y-line)

Korotkov KG [2001; 2014], the founder of the GDV method, by analogy with the concept of thermodynamic entropy, introduced the term Entropy of the GDV-gram and created the corresponding software for its calculation. The author introduced the classification of GDV-grams according to the degree of "imbalance", namely: a high Entropy value indicates strongly unbalanced GDV-grams, which corresponds to an unstable state of homeokinesis, on the other hand, equal, "calm" GDV-grams have a lower Entropy value.

The author believes that GDV-grams reflect "the state of internal production of negative entropy". This production depends on the functional state of the organism and on the flows of energy and information from the outside. The experiments of the author's laboratory showed that the entropy of the GDV-gram is an informative characteristic of the state of the organism. High entropy signals chaos and low entropy signals death. Like many of the body's parameters, entropy values must be within the range of norms. In all processes, be they physical, chemical or biological, entropy increases. Living organisms reduce their own entropy by using energy from the environment. It is said that living organisms produce negative entropy or 'neg-entropy.' When therapy is performed correctly, EPI entropy reduces.

However, recent studies of our laboratory proved that the high level of entropy of EEG, HRV, Leukocytogram (LCG) and Immunocytogran (ICG) as well as its increase under the influence of adaptogens are not unequivocally unfavorable, and on the other hand, the low level of entropy as well as its decrease are not unequivocally favorable [Gozhenko AI et al, 2021].

Based on the above, it would be interesting to analyze the relationship between the entropy of the parameters of the neuro-immune complex and gas discharge imaging.

The object of observation were 20 volunteers: ten women and ten men aged 33-76 years, examined twice with an interval of 7 days.

In the first stage of the analysis a correlation matrix is created (Table 6.17).

As a result of the screening, the most significant relationship was found between the GDI entropy (filtered) in the **left** projection and the SPD EEG entropy in the **right** lateral frontal locus (Fig. 6.17). Unfortunately, intrigue about cross-linking such as the corticospinal pyramid tract has been dispelled by other facts.

Table 6.17. Correlation matrix for Entropies of gas-discharge image, power spectral density EEG loci, HRV, Leukocytogram and Immunocytogram

Entropy	Right GDI	Right GDI (f)	Frontal GDI	Frontal GDI (f)	Left GDI	Left GDI (f)
Fp2	,09	,10	,18	,16	,08	,06
F4	,08	-,07	,16	-,04	,07	-,14
F8	-,01	-,19	-,02	**-,24**	-,07	**-,46**
T4	-,22	-,08	-,06	**-,27**	-,02	-,16
C4	,03	-,07	-,06	-,04	-,17	-,19
T6	,17	-,01	,03	-,12	-,05	-,08
P4	**,24**	,20	,19	**,27**	,13	,02
O2	,21	,21	-,02	,06	,04	,11
Fp1	-,00	-,07	-,06	,11	-,15	,05
F3	,19	,14	**,28**	,19	**,25**	-,02
F7	-,03	-,03	,08	,10	-,19	-,11
T3	-,22	-,05	-,07	-,08	-,24	-,22
C3	,01	-,14	-,17	-,11	**-,24**	-,19
T5	,10	-,17	-,07	-,10	-,07	-,14
P3	,20	,12	,09	,20	,04	,05
O1	,16	,24	,13	**,31**	,17	,19
HRV	-,10	-,05	-,08	-,24	-,21	-,10
LCG	**,30**	-,08	**,30**	,18	,18	,14
ICG	-,25	-,18	-,26	-,21	-,27	**-,30**

Note. For a sample of 40 observations critical value of correlation coefficient module at $p<0,05$ (t>2,02) is 0,31, at $p<0,01$ (t>2,70) is 0,41, at $p<0,001$ (t>3,55) is 0,52.
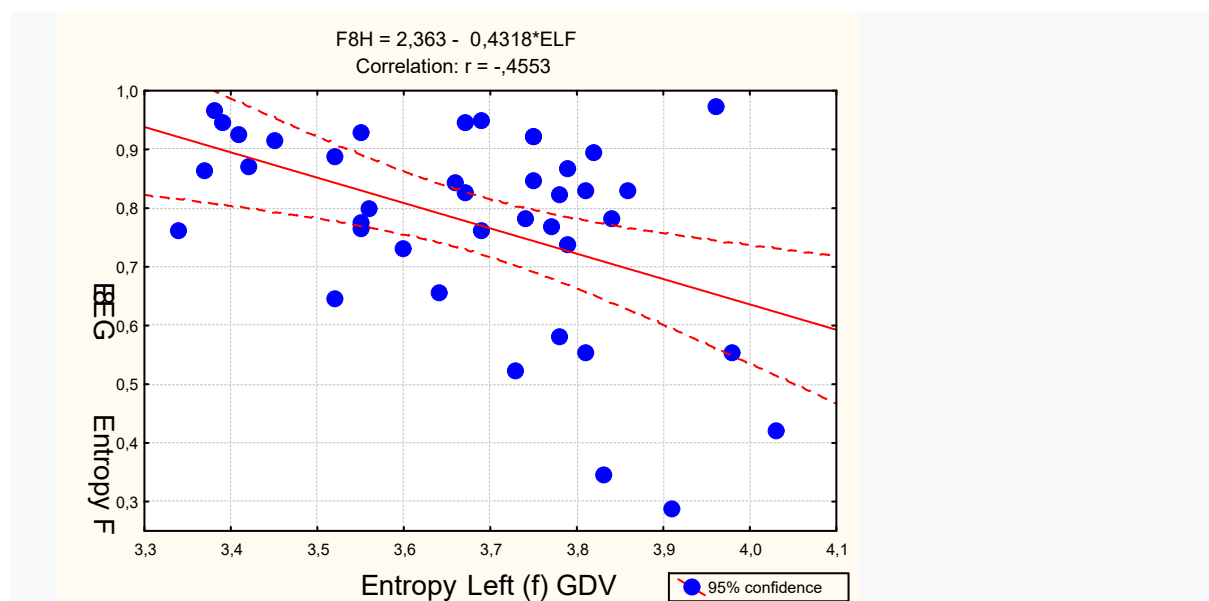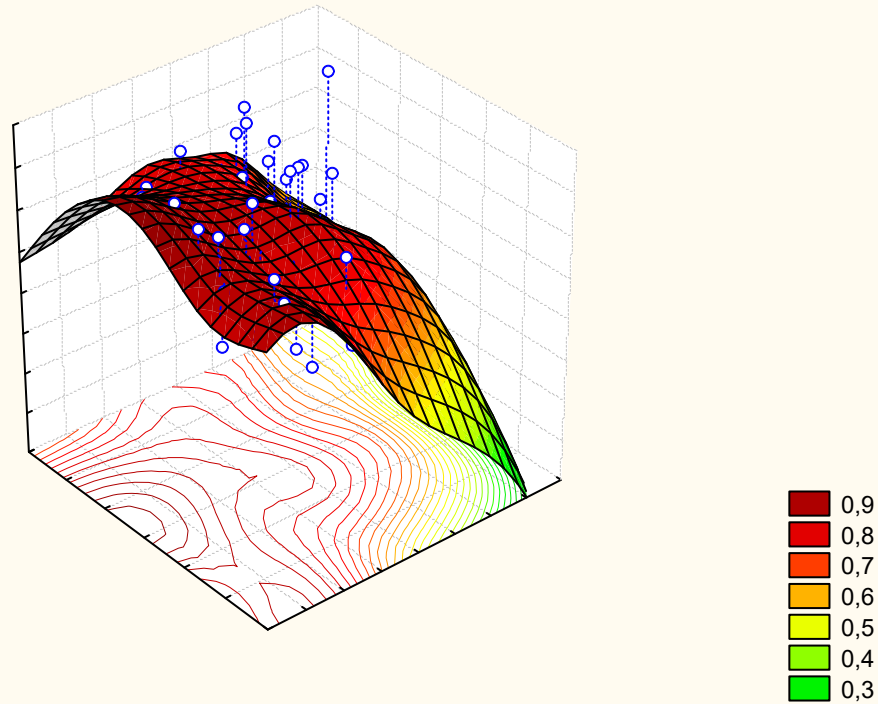
Fig. 6.17. Scatterplot of correlation between the Entropy GDI (filtered) on the Left projection (X-axis) and the Entropy in F8 locus EEG (Y-axis)

The inclusion in the multiple regression model of the second, by the power of the link, variable brought about the aesthetic pleasure of the three-dimensional image (Fig. 6.18), but no more, judging by R.

$F8h=2,22-0,472\cdot ELf+0,081\cdot EFf$; $R=0,458$; $R^2=0,210$; $F_{(2,4)}=4,9$; $p=0,013$

Fig. 6.18. Scatterplot of dependence of entropy in F8 locus EEG (Z-axis) on entropies GDI (filtered) on the Left (X-axis) and Frontal (Y-axis) projections

In the next step, the canonical correlation between the entropy indices of the GDI taken without a filter and with a filter in three projections, on the one hand, and PSD of 16 EEG loci, on the other, was analyzed.

By stepwise exclusion, 5 variables were included in the canonical GDV root structure, and 6 variables were included in the root EEG structure (Table 6.18). Judging by the factor loadings, the causal root represents directly, mainly, the entropy of GDI (with filter) in the left projection, while the entropy of GDI (without filter) in the right projection reflects inversely. On the other hand, the EEG root reflects the PSD entropy at five loci inversely and only one directly. Overall, GDI entropy determines the PSD EEG entropy by 33% (Fig. 6.19).

Table 6.18. Factor structure of canonical correlation between Entropy of GDI (right set) and EEG (left set)

Right set	R
Left GDI (f)	**,536**
Left GDI	**,158**
Right GDI	**-,420**
Frontal GDI (f)	**-,084**
Frontal GDI	**-,055**
Left set	R
F8H	**-,514**
P4H	**-,478**
C3H	**-,454**
F3H	**-,237**
O1H	**-,141**
T4H	**,360**
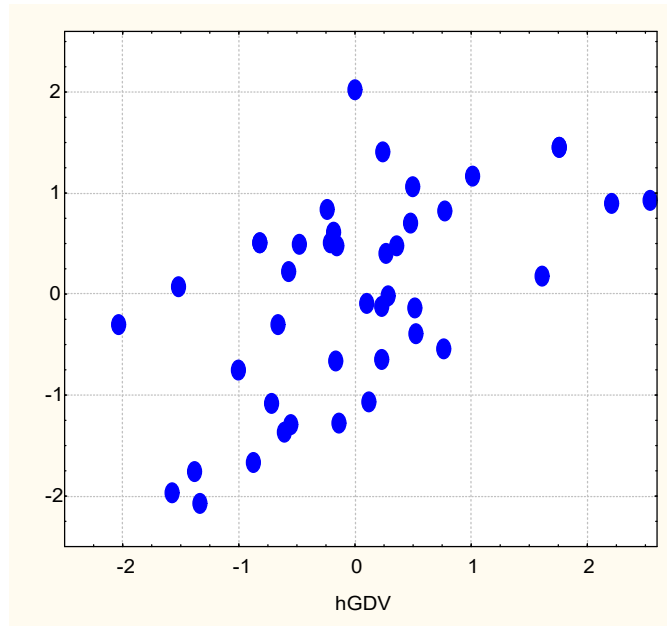
R=0,575; R²=0,330; χ²(30)=38; p=0,158; Λ Prime=0,341

Fig. 6.19. Scatterplot of canonical correlation between Entropy of GDI (X-line) and EEG (Y-line)

The additional inclusion in the left set parameters of HRV, LCG and ICG entropies gives a significant increase in the canonical relationship between the roots. This changes the factor structure of the roots. Contrary to expectations, HRV entropy was found outside the model (Table 6.19 and Fig. 6.20).

Table 6.19. Factor structure of canonical correlation between Entropy of GDI (right set) and EEG,LCG&ICG (left set)

Right set	R
Right GDI	,50
Frontal GDI	,24
Frontal GDI (f)	,24
Left GDI (f)	-,33
Right GDI (f)	-,28
Left GDI	-,03
Left set	R
LCGH	,477
P4H	,335
C3H	,287
F8H	,229
F3H	,183
O1H	,121
T4H	-,440
ICGH	-,006
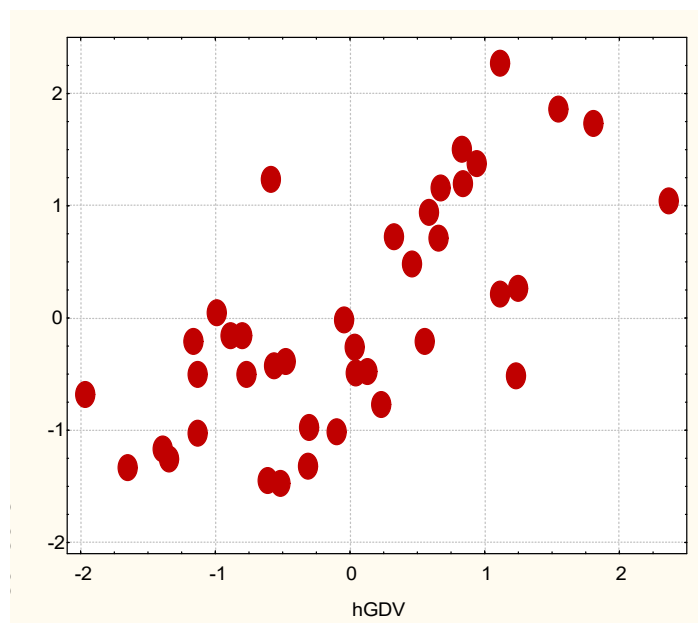
R=0,699; R²=0,489; χ²(48)=54; p=0,262; Λ Prime=0,181

Fig. 6.20. Scatterplot of canonical correlation between Entropy of GDI (X-line) and EEG as well as LCG&ICG (Y-line)

Thus, we have documented the relationship between the Entropy parameters of electroencephalogram, blood leukocytogram and immunocytograms on the one hand, and gas-discharge images on the other. However, the question of the causal nature of this relationship remains open. What is primary: electrical activity of the brain, excretion of cytokines and hormones by immunocytes, or emission of photons and free electrons by acupuncture points (circulation of Qi/Ki-energy)? We will limit ourselves to announcing that this will be the topic of our next monograph.

The materials of the chapter are published in the articles:

1. Babelyuk VY, Babelyuk NV, Popadynets' OO, Dubkova GI, Muszkieta R, Zukow W. Relationships between the entropy of gas-discharge image and the entropies of EEG, HRV, immunocytogram and leukocytogram. In: Mater of the XII All-Ukrainian Sci-Pract conf "Actual issues of pathology under the conditions of action of extraordinary factors on the body". Galician readings II (Ternopil', October 29-30, 2020). Ternopil'; 2020: 119-120.

2. Babelyuk VYe, Popadynets' OO, Dubkova GI, Zukow W, Muszkieta R, Gozhenko OA, Popovych IL. Entropy of gas-discharge image correlates with the entropies of EEG, immunocytogram and leukocytogram but not HRV. Pedagogy and Psychology of Sport. 2020; 6(2): 30-39.

3. Babelyuk VY, Tserkovniuk RG, Babelyuk NV, Żukow X, Ruzhylo SV, Dubkova GI, Korolyshyn TA, Hubyts'kyi VY, Kikhtan VV, Gozhenko AI, Popovych IL. The parameters of gas discharge visualization (biophotonics) correlated with parameters of acupuncture points, EEG, HRV and hormones. Journal of Education, Health and Sport. 2021; 11(12): 359-373.

4. Babelyuk VY, Tserkovniuk RG, Dubkova GI, Kruhliy YS, Korolyshyn TA, Babelyuk NV, Zukow W, Ruzhylo SV, Fihura OA, Gozhenko AI, Popovych IL. Relationships between the neuro-endocrine parameters and virtual chakras energy and asymmetry. Journal of Education, Health and Sport. 2022; 12(1): 235-249.

CHAPTER 7

REACTIONS OF GDV PARAMETERS TO TRANSCUTANEOUS ELECTRICAL STIMULATION BY DEVICES "VEB-1" AND "VEB-2"

The above results, in our humble opinion, quite convincingly demonstrated that GDV parameters objectively reflect the state of at least the neuro-endocrine-immune complex of the body, which is responsible for its adaptation and non-specific resistance. This became the basis for including the GDV method in the arsenal of methods of our laboratory. So, it is time to move on to the applied aspects of GDV.

In 2015, a generator for electrotherapy and stimulation oh human nerve centers was created (**Babelyuk VE, Dobrovolsky YG, Korsunskyi IH)**, called "VEB-1"®. Conceiving and creating our device, we were based on the following provisions. The influence of impulses of a rectangular shape (range 7-18 Hz) made it possible to fix the frequency ranges of each basic nerve node. Low frequency had minimal effects of stimulation on the corresponding nerve node, while high frequency - the maximum. For the effective excitation of nerve centers, the frequency beat method is used. It consists in obtaining oscillations with close frequencies. To obtain the effect of the frequency beats are generated by pulses of rectangular shape to two signal channels. The channels differ in frequency, which is the beat frequency. For example, for obtaining a beat frequency 6 Hz, forming pulses in a first channel to a carrier frequency of 30 Hz, a second channel at a frequency of 36 Hz. When the first pulse is formed on both channels with a phase shift of 0°, we obtain an absolute zero current in the output (Fig. 7.1).
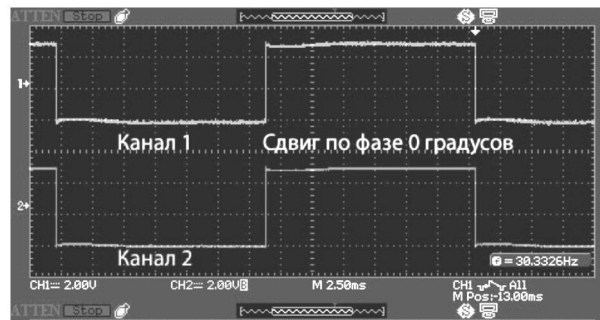
Fig. 7.1. Oscillogram of the first clock pulse

Fig. 7.2 shows a periodic signal generated by frequency beats voltage in the two channels to form a common output signal (a). Also in Fig. 7.2 is a graph of the current of the output signal (б). Such effect creates a shock wave through the object at the desired frequency. He also spins an electromagnetic field in the object.
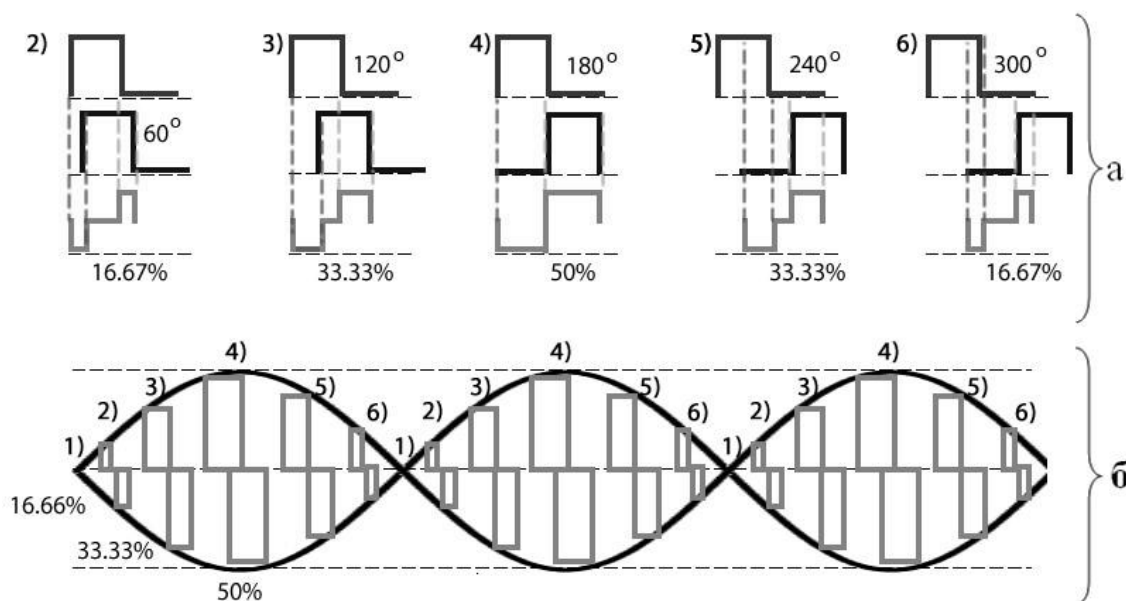
Fig. 7.2. Received by frequency beats a periodic signal (a) and a current diagram of the generated output signal (б)

The generator is assembled on the basis of the patent of Ukraine for utility model 105875 "Portable device for electrotherapy and stimulation" [Babeluk VE, 2016]. Its operation is described [Babeluk VY et al, 2017; Dobrovolsky et al, 2020].

The generator is assembled on the basis of a two-channel circuit using two frequency synthesizers, amplifiers, each of which generates its own frequency.

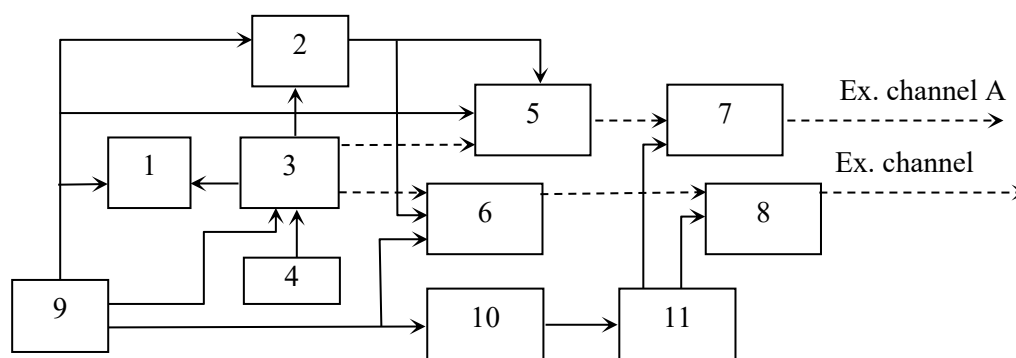Fig. 7.3 shows a block diagram of the device indicating the movement of electric current.

Fig. 7.3. A block diagram of the generator VEB-1
1 - display; 2 - synthesizer of the signal with a sampling frequency up to 0,001 Hz; 3 - micro-controller; 4 - the encoder; 5 - channel A signal synthesizer; 6 - synthesizer of the channel B signal; 7 - channel A signal amplifier; 8 - the amplifier of a signal of the channel B; 9 - battery 5 V; 10 - voltage converter 5-24 V; 11 - voltage regulator; 12 - amplitude control of the output signal.

Transmission of the electrical signal to the patient is carried out by means of contact copper electrodes through the wires. The generator operates as follows. Instrument software sets the operating frequency of the pulse beats 0,01-100 Hz with steps on each channel is not more than 0,001 Hz. Discreteness in each channel is not more than 0,001 Hz is provided by a clock synthesizer (2). It forms the frequency corresponding to the number of filling of the thirty two-bit synthesizer frequency (5,6) divided by 1000.

Table 7.1. The technical characteristics of the generator

Parameter	Parameter norm
The maximum power consumption, W	1,2
Output signal level by amplitude, V	3,6-16,2
The maximum amplitude of the output signal, V	16,2
The maximum possible current impact mA	25
Ripping protection when current exceeds 25 mA	yes
Operating current, mA	8-18
The shape of the output signal	Meander
Frequency range of action, Hz	144-1120
Power battery voltage, V	4,8-5,3
Continuous operation time, hours	8

The appearance of the generator with a set of necessary equipment is shown in Fig. 7.4.

Fig. 7.4. The appearance of the generator with a set of necessary equipment
1 - generator VEB-1; 2 - two cords with JACK connectors and terminal clamps for connection to OUT-A and OUT-B outputs; 3 - contact pads or tubes; 4 - power cable with connectors USB-B and USB-A; 5 - battery 5 V.

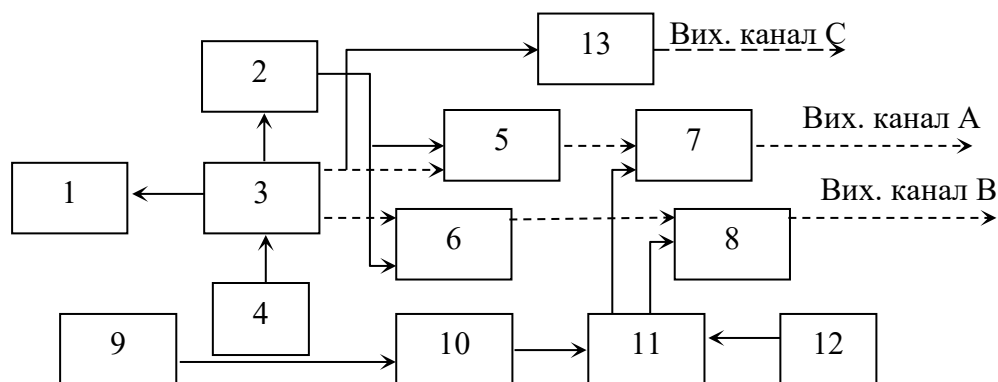In 2019 designed device "VEB-2" (Fig. 7.5).

Fig. 7.5. A block diagram of the generator VEB-2
1 - display; 2 - clock signal synthesizer; 3 - controller; 4 - encoder; 5 - signal synthesizer channel A; 6 - signal synthesizer channel B; 7 - signal amplifier channel A; 8 - signal amplifier channel B; 9 - 5 V battery; 10 - voltage converter 5-24 V; 11 - voltage regulator; 12 - regulator of the amplitude of the output signal; 13 - channel filter C

Unlike the device "VEB-1", designed to stimulate nerve centers, the electrostimulator "VEB-2" implemented an additional channel for input of information impulses into the body -

channel C, whose task is the local concentration of the field, which is formed by two signal channels (A and B) to the point and body of the person as close as possible to the organ affected (heart, liver, spleen, right and left kidneys) at frequencies that contribute to the maximum recovery of the organ.

The first part of the program for adjusting the level of the output signal lasts 20 seconds, after which the main part of the program (generation of pulse current of alternating frequency in the range from 144 Hz to 1120 Hz) lasts for 21 ("VEB-1") or 26 ("VEB-2") minutes.

We have conducted a number of studies with increasing numbers of observed volunteers and applied methods.

The object of the first observation (June 2015) were 14 healthy males aged 24-59 years (including three authors). In the morning registered kirlianogram by the method of GDV by the device of "GDV Chamber" ("Biotechprogress", SPb, RF). After the initial testing, an electrical stimulation session was performed with a VEB-1 device (for 21 minutes) as well as for three consecutive days. The next morning after completing the four-day course, retesting was performed.

Results processed using the software package "Statistica 5.5". The reference values of the parameters are taken from the database of our laboratory.

Among the GDV registered parameters, we restrict ourselves to those that were included in the discriminant model as well as those that were out of the model but changed statistically significantly (Table 7.2).

Table 7.2. Discriminant Function Analysis Summary for parameters of GDV
Step 9, N of vars in model: 9; Grouping: 2 grps; Wilks' Λ: 0,219; approx. $F_{(9,2)}=7,1$; $p<10^{-3}$

Variables currently in the model	Refe-rence (n=88)	Initial level (n=14)	Final level (n=14)	Change after 4 Seanses	Wil ks' Λ	Par tial Λ	F-re move (1,2)	p-le-vel	Tole-ran-cy
Area GDI in Left pro-jection, kPixels	24,5 ±0,5	22,3 ±1,2	23,4 ±0,9	+1,1 ±0,5	,397	,552	14,6	,001	,063
Symmetry GDI (f), %	94,7 ±0,1	93,67 ±0,31	92,62 ±0,47	-1,05 ±0,46	,337	,648	9,8	,006	,352
Chak 2 Asymmetry (f)		+0,06 ±0,04	-0,09 ±0,05	-0,15 ±0,05	,225	,970	,5	,468	,406
Chakra 2 Asymmetry	+0,11 ±0,04	+0,12 ±0,06	0,00 ±0,07	-0,12 ±0,11	,243	,902	2,0	,179	,538
Chak 7 Asymmetry (f)		+0,06 ±0,03	-0,05 ±0,03	-0,11 ±0,04	,269	,813	4,1	,057	,393
Chakra 6 Asymmetry	+0,04 ±0,02	+0,08 ±0,05	-0,02 ±0,05	-0,09 ±0,05	,268	,816	4,1	,059	,550
Chakra 4 Asymmetry (f)		+0,04 ±0,03	-0,03 ±0,05	-0,07 ±0,06	,282	,776	5,2	,035	,499
Chakra 2 Energy	-0,08 ±0,05	-0,32 ±0,16	-0,24 ±0,10	+0,08 ±0,07	,268	,817	4,0	,060	,081
Variable currently not in the model	**Refere nce (n=88)**	**Initial level (n=14)**	**Final level (n=14)**	**Change after 4 Seanses**	**Wil ks' Λ**	**Par tial Λ**	**F to en-ter**	**p-le-vel**	**Tole-ran-cy**
Chakra 7 Energy	+0,04 ±0,03	-0,29 ±0,07	-0,22 ±0,07	+0,08 ±0,03	,217	,99	,141	,71	,161
Chakra 7 Energy (f)		-0,10 ±0,05	-0,05 ±0,06	+0,05 ±0,02	,218	,99	,078	,78	,504
Chakra 3 Asymmetry	+0,22 ±0,04	+0,15 ±0,04	+0,04 ±0,04	-0,10 ±0,04	,212	,97	,527	,48	,401
Chakra 7 Asymmetry	+0,10 ±0,03	+0,12 ±0,04	-0,02 ±0,05	-0,14 ±0,06	,218	1,0	,047	,83	,826

Note. In each column, the top row is the average, the bottom row is the standard error

It has been found that the electrostimulation course increases the reduced area of GDI to the lower normal zone. However, the initial asymmetry of the GDI (f) becomes even more pronounced. Other biophysical parameters do not change significantly.

Instead, changes in the parameters of the virtual Chakras were detected. As you can see, the second, third, fourth, sixth and seventh Chakras were shifted to the right, and after the course of electrostimulation, the asymmetry of the volunteers was leveled out. However, right-side asymmetry of the second Chakra, registered with the filter, reversed to the left-hand side. The decrease of energy deficit of the second and seventh Chakras was also revealed.

Individual changes of GDV recognizable parameters condensed in a discriminant root (Table 7.3) are visualized in Fig. 7.6.

Table 7.3. Standardized, Structural and Raw Coefficients and Constant for GDVs variables

| Variables currently in the model	Standardized	Structural	Raw
Chakra 2 Asymmetry (f)	-,306	-,256	-1,867
Chakra 7 Asymmetry (f)	-,780	-,243	-6,391
Symmetry GDI (f), %	-1,131	-,195	-,763
Chakra 6 Asymmetry	-,654	-,144	-3,630
Chakra 2 Asymmetry	-,483	-,135	-1,985
Chakra 4 Asymmetry (f)	-,759	-,123	-4,671
Area GDI in Left projection, kPixels	3,015	,079	,800
Chakra 2 Energy	-1,701	,045	-3,432
Eigenvalue	3,57	**Constant**	41,74
R=0,884; Wilks' Λ=0,219; $\chi^2_{(9)}$=33; p=10^{-4}			
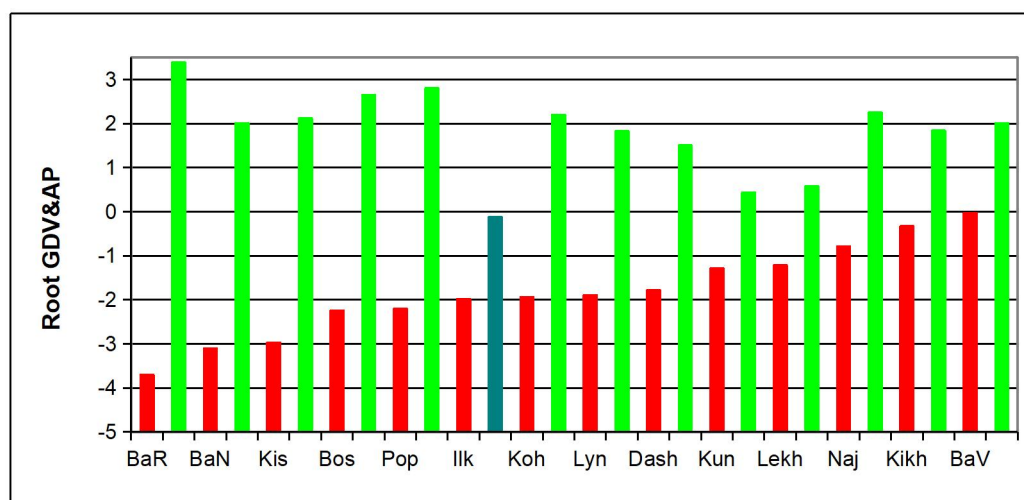
Fig. 7.6. Individual values of the canonical discriminant GDVs root before (red columns) and after (green columns) four-day electrostimulation course with the device "VEB-1"

It is clearly visible that in all volunteers (formally with one exception) the constellation of GDV parameters responds significantly to electrical stimulation by device "VEB-1".

The object of the second observation (Mars 2019) were 18 volunteers (employees of the clinical sanatorium "Moldova"): 11 women aged 33-62 years and 7 men aged 29-62 years (Mean±SD: 51±12) without clinical diagnose but with dysfunction of neuro-endocrine-immune complex documented previously.

In the morning registered kirlianogram by the method of GDV by the device "GDV Chamber" ("Biotechprogress", SPb, RF).

After the initial testing, an electrical stimulation session was performed with a VEB-1 device (for 21 minutes) or a VEB-2 device (for 26 minutes), as well as for three consecutive

days. The next morning after completing the four-day course, retesting was performed. The reference values of the parameters are taken from the database of our laboratory.

At the first stage of the analysis of the results, profiles of GDV parameters were constructed before and after the course of electrical stimulation by both devices.

As you can see (Fig. 7.7), electrical stimulation causes a significant reduction in the area of the GDI taken without a filter in frontal and left projections.
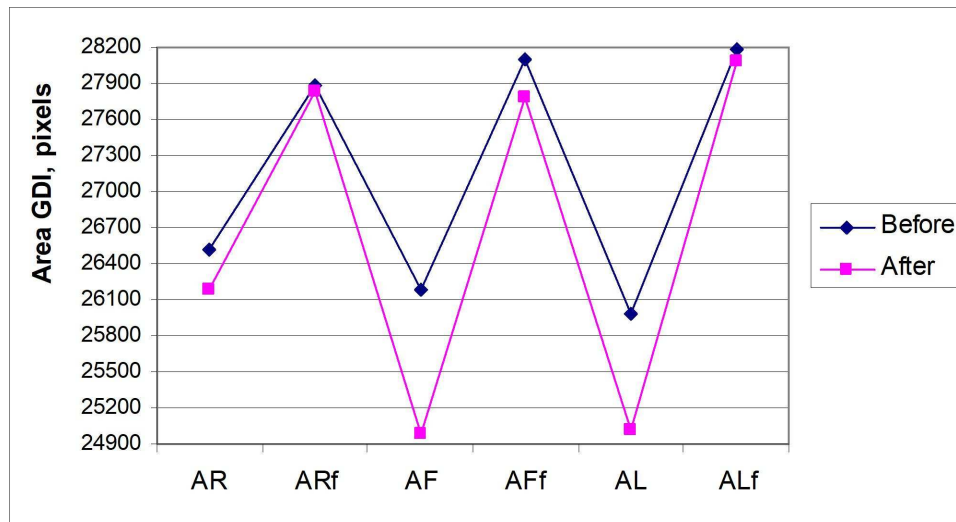

Fig. 7.7. Profiles of the Area of the gas-discharge image taken without the filter and with the filter (f) in the right (R), frontal (F) and left (L) projections before and after a four-day course of electrostimulation by the VEB-1 and VEB-2 devices

The entropy of GDI decreases most noticeably in the left projection and, to a lesser extent, in the right (Fig. 7.8).
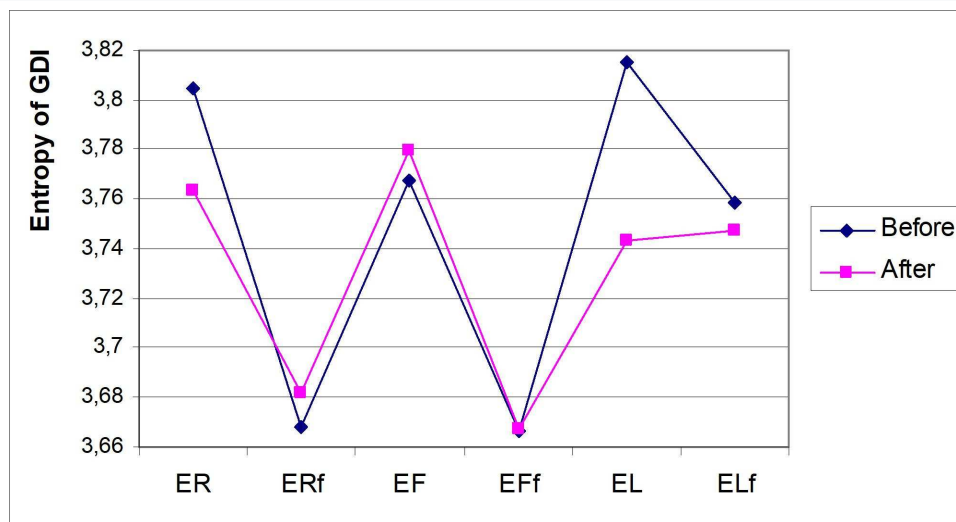

Fig. 7.8. Profiles of the Entropy of the gas-discharge image taken without the filter and with the filter (f) in the right (R), frontal (F) and left (L) projections before and after a four-day course of electrostimulation by the VEB-1 and VEB-2 devices

Instead, the response to electrical stimulation of the GDI form appears visually insignificant (Fig. 7.9).

Fig. 7.9. Profiles of the Shape Coefficient of the gas-discharge image taken without the filter and with the filter (f) in the right (R), frontal (F) and left (L) projections before and after a four-day course of electrostimulation by the VEB-1 and VEB-2 devices

Now consider the effect of electrical stimulation on the energy of the virtual Chakras, calculated by the program based on the GDV parameters of the skin of ten fingers. There is a significant decrease in the energy of the second, third, fifth, sixth and seventh Chakras under the conditions of registration without a filter, as well as an increase in the energy of the seventh Chakra during its registration with a filter (Fig. 7.10).
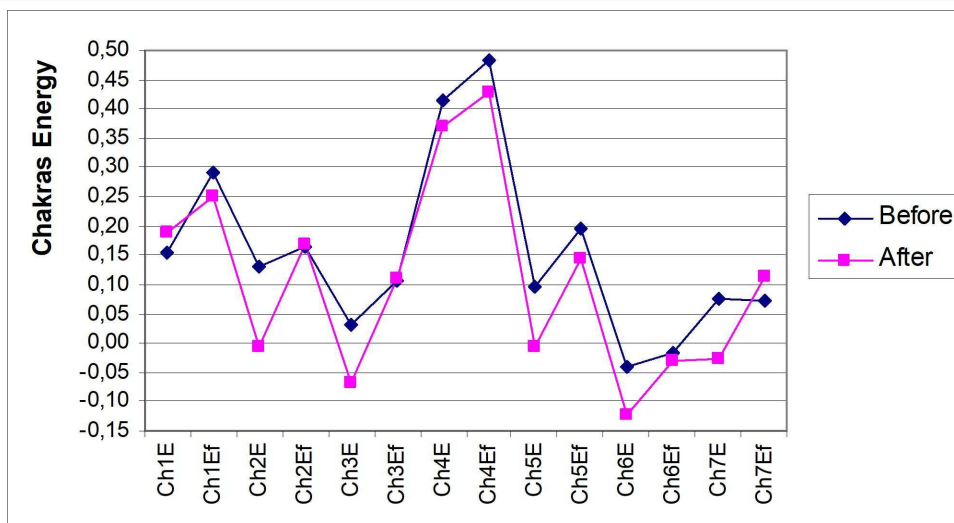
Fig. 7.10. Profiles of the Energy of the virtual Chakras taken without the filter and with the filter (f) in the right (R), frontal (F) and left (L) projections before and after a four-day course of electrostimulation by the VEB-1 and VEB-2 devices

The motley picture of reactions to electrostimulation of symmetry of Chakras is revealed (Fig. 7.11). In particular, the left (negative) asymmetry of the first Chakra (f) is almost completely leveled.
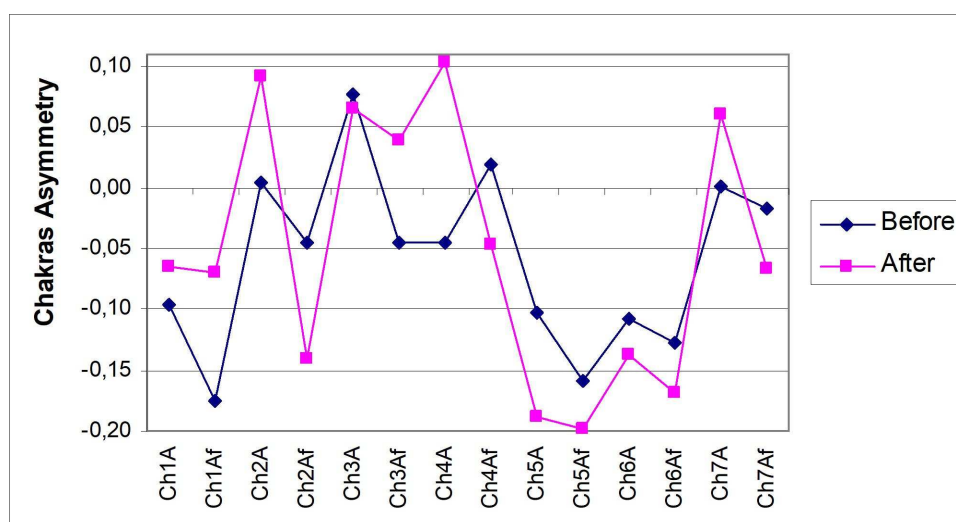
Fig. 7.11. Profiles of the Asymmetry of the virtual Chakras taken without the filter and with the filter (f) in the right (R), frontal (F) and left (L) projections before and after a four-day course of electrostimulation by the VEB-1 and VEB-2 devices

Instead, the initially symmetrical second Chakra becomes asymmetrical, with displacements occurring in opposite directions under different conditions of registration. The right-hand asymmetric shift is detected for the third (f) and fourth Chakras.

To determine which changes in GDV parameters are characteristic of the effects of electrical stimulation, a procedure of discriminant analysis using the forward stepwise method was performed. The program "Statistica 8.0" included 9 parameters in the model. Also noteworthy are three other parameters that turned out to be outside the discriminant model despite statistically significant changes (Tables 7.4 and 7.5).

Table 7.4. Discriminant Function Analysis Summary
Step 9, N of vars in model: 9; Grouping: Before&After electrostimulation
Wilks' Lambda: 0,403; approx. $F_{(9,3)}=4,3$; p=0,002

Variables currently in the model	Refer (36)	Average value Before (18)	After (18)	Wilks' Λ	Partial Λ	F-remove	p-level	Tole-rancy
Area GDI Frontal, kpixels	24,9 0,6	26,2 1,2	25,0 1,0	0,471	0,856	4,37	0,046	0,121
Chakra 2 Energy	-0,07 0,05	0,13 0,11	-0,01 0,10	0,568	0,709	10,65	0,003	0,075
Chakra 3 Asymmetry (f)	0,01 0,03	-0,05 0,04	0,04 0,03	0,449	0,897	2,98	0,096	0,571
Chakra 4 Asymmetry	0,03 0,05	-0,05 0,09	0,10 0,09	0,425	0,948	1,44	0,241	0,591
Chakra 7 Energy (f)	0,02 0,03	0,07 0,07	0,11 0,05	0,753	0,535	22,59	0,0001	0,111
GDI Shape Coefficient Left (f)	11,5 0,1	13,0 0,3	13,6 0,3	0,483	0,835	5,16	0,032	0,268
Entropy of GDI Right	3,85 0,02	3,80 0,02	3,76 0,03	0,403	0,999	0,02	0,900	0,723
Entropy of GDI Left	3,93 0,02	3,82 0,01	3,74 0,04	0,492	0,818	5,77	0,024	0,529

				Wilks' Λ	Partial Λ	F to enter	p-level	Tole-rancy
Chakra 2 Asymmetry (f)	0,02 0,04	-0,04 0,06	-0,14 0,06	0,512	0,786	7,07	0,013	0,680
Variables currently not in the model				**Wilks' Λ**	**Partial Λ**	**F to enter**	**p-level**	**Tole-rancy**
Chakra 3 Energy	-0,09 0,05	0,03 0,14	-0,07 0,08	0,400	0,994	0,15	0,705	0,203
Chakra 7 Energy	-0,11 0,04	0,08 0,10	-0,03 0,08	0,389	0,966	0,87	0,359	0,058
Chakra 1 Asymmetry (f)	-0,01 0,03	-0,17 0,07	-0,07 0,04	0,390	0,968	0,82	0,375	0,522

Note. In each column, the top row is the average, the bottom row is the standard error

Table 7.5. Summary of Stepwise Analysis (Variables ranked by criterion Lambda)

Variables currently in the model	F to enter	p-level	Lambda	F-value	p-level
Chakra 3 Asymmetry (f)	2,49	0,124	0,932	2,49	0,124
Chakra 7 Energy (f)	1,66	0,207	0,887	2,10	0,139
Chakra 2 Energy	7,32	0,011	0,722	4,11	0,014
Entropy of GDI Right	3,19	0,084	0,655	4,09	0,009
Area GDI Frontal, kpixels	1,99	0,169	0,614	3,77	0,009
Chakra 2 Asymmetry (f)	3,53	0,070	0,547	4,00	0,005
GDI Shape Coefficient Left (f)	2,76	0,108	0,498	4,03	0,004
Entropy GDI Left	4,64	0,040	0,425	4,56	0,001
Chakra 4 Asymmetry	1,44	0,241	0,403	4,28	0,002
r*=0,773; Wilks' Λ=0,403; $\chi^2_{(9)}$=26,8; p=0,0015					

The effects of electrical stimulation can be divided into the following networks. First, it is almost complete normalization of the initially increased GDI Area in the frontal projection and Ch3 Energy. Second, it is a normalizing decrease in the initially increased Energy of Ch2 and Ch7 (f). Third, it is a normalizing right-hand shift of more or less pronounced left-sided Asymmetry of Ch1(f) and Ch3(f). These effects should be clearly interpreted as physiologically beneficial.

The second set is created by quasi-normal (Ch4A, Ch7Ef) and elevated (SCLf) parameters, which increase after electrical stimulation, the physiological assessment of changes of which we will leave without comment.

The third set is formed by initially reduced levels of GDI Entropy in the right and left projections, which continue to decrease after electrical stimulation, as well as quasi-symmetric Ch2f, which is transformed into left-asymmetric. If the decrease in Entropy can still be assessed positively [Gozhenko AI et al, 2021], then the price change of the latter parameters will wait.

Information about the GDV parameters is condensed in the canonical discriminant root, which correlates with some of them positively, and with others negatively (Table 7.6). The same table shows the Raw Coefficients and Constant for discriminant variables, based on which as well as on the individual values of the parameters of the GDV, the individual values of the canonical root before and after electrostimulation course were calculated.

The striking changes in GDV are documented by calculating the square of the Mahalanobis distance between the recognition parameters before and after the course of electrostimulation: $D^2_M=5,93$ (F=4,28; p=0,0017).

Table 7.6. Standardized, Structural and Raw Coefficients and Constant for Variables (ranked by Structural coefficient)

Variables currently in the model	Coefficients		
	Standardized	Structural	Raw
Entropy GDI Left	0,758	0,197	4,883
Chakra 2 Asymmetry (f)	0,726	0,160	2,856
Entropy of GDI Right	0,038	0,144	0,312
Chakra 2 Energy	2,547	0,136	5,942
Area GDI Frontal, kpixels	-1,414	0,111	-0,301
Chakra 3 Asymmetry (f)	-0,549	-0,222	-3,464
GDI Shape Coefficient Left (f)	-1,016	-0,170	-0,755
Chakra 4 Asymmetry	-0,386	-0,164	-0,999
Chakra 7 Energy (f)	-2,644	-0,069	-10,36
Eigenvalue	1,48	**Constant**	-0,847

At the final stage of the analysis, the mean values of the canonical discriminant root were calculated separately for women and men who underwent electrical stimulation with "VEB-1" or "VEB-2" devices.

As you can see (Fig. 7.12), the effects on the set of GDV parameters are almost equally pronounced in people of both sexes when using both devices.
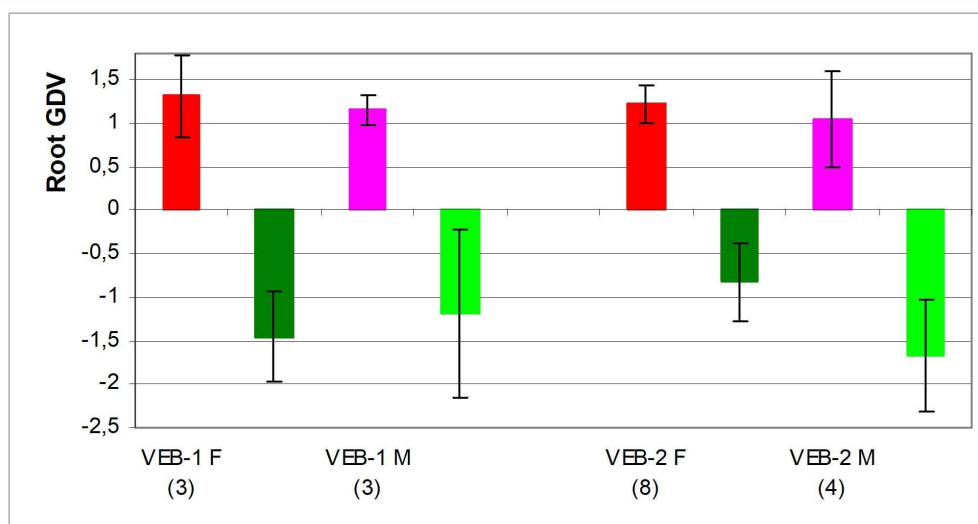
Fig. 7.12. Average values (Mean±SE) of the canonical discriminant root before and after four-day electrostimulation course with the devices "VEB-1" and "VEB-2" at females (F) and males (M)

It seems that the use of an additional electrode for direct impact on individual organs in the device "VEB-2" is excessive, it is enough to affect only the nerve plexuses (or Chakras?!).

Selected 9 parameters can be used to identify initial or final status a particular volunteer. This is achieved through the calculation of classification functions on the basis of the obtained Coefficients and Constants (Table 7.7).

The accuracy of classification is very high (Table 7.8).

Table 7.7. Coefficients and Constants for Classification Functions

Variables currently in the model	Before	After
Chakra 3 Asymmetry (f)	-13,90	-5,700
Chakra 7 Energy (f)	120,7	145,2
Chakra 2 Energy	-110,5	-124,6
Entropy of GDI Right	296,3	295,5
Area GDI Frontal, kpixels	15,80	16,51
Chakra 2 Asymmetry (f)	-14,15	-20,91
GDI Shape Coefficient Left (f)	33,87	35,66
Entropy GDI Left	75,58	64,02
Chakra 4 Asymmetry	-46,17	-43,80
Constants	-1135,2	-1133,2

Table 7.8. Classification Matrix
Rows: Observed classifications
Columns: Predicted classifications

	Percent correct	Before	After
Before	94,4	17	1
After	88,9	2	16
Total	91,7	19	17

The article was ending with a phrase: According to the expectations based on the results of previous studies of our laboratory, the detected changes in GDV parameters are accompanied by changes in parameters of HRV, EEG, acupuncture, immunity and metabolism, which will be published in future articles.

We kept our promise.

The object of last observation were employees of the sanatorium "Moldova": 19 women 30-62 y and 19 men 25-63 y.

In the morning in basal condition registered (**Dubkova GI**) kirlianogram by the method of GDV by the device of "GDV Chamber" ("Biotechprogress", SPb, RF).

Then recorded (**Korolyshyn TA**) simultaneosly electrocardiogram (ECG) and electroencephalogram (EEG).

Electroconductivity recorded (**Hubyts'kyi VY**) in follow points of acupuncture: Pg(ND), TR(X) and MC(AVL) at Right and Left side, which represents the nervous, endocrine and immune systems respectively. Used complex "Medissa". For each pair, the Laterality Index was calculated according to the already mentioned formula.

Next determined (**Musiyenko VY & Kyrylenko IG**) the Elektrokinetic Index (EKI) as rate of electronegative nuclei of buccal epithelium by intracellular microelectrophoresis on the device "Biotest" (Kharkiv State University).

Parameters of immunity and phagocytic function of neutrophils estimated as described above.

At last in portion of venous blood determined (**Kikhtan VV**) plasma levels of main hormones of adaptation; IL-1, IL-6 and C-reactive protein (by the ELISA with the use of analyzer "RT-2100C"); total cholesterol (by a direct method after the classic reaction by Zlatkis-Zack) and content of him in composition of high-density lipoproteins (by the enzyme method) as well as routine biochemical parameters according to instructions with the use of analyzers "Reflotron" (BRD) and "Pointe-180" (USA) and corresponding sets of reagents.

After the initial testing, an transcutaneous electrical stimulation session was performed with the "VEB-1"® (21 patients) or the "VEB-2" (17 patients) devices. The next morning after completing the four-day course, retesting was performed.

Reference values are taken from the database of our laboratory.

Results processed (**Popovych IL**) using the software package "Statistica 6.4".

According to the algorithm of the Truskavetsian Scientific School, to enable a correct comparison of parameters expressed in different units and with different variability, which determines the "physiological price" of parameter changes (the most striking examples: changes by 1% of glomerular filtration and tubular reabsorption or by 0,1 unit of urine and blood pH), registered parameters-variables (V) were transformed into Z-score according to the aquations:

Z = (V-N)/SD = (V/N-1)/Cv, where

N is average norm, SD is standard deviation, Cv is coefficient of variation in norm.

Profiles of their Z-scores before and after a course of transcutaneous electrical stimulation were created as a result of screening for statistically significant (according to the Student's criterion) changes in registered parameters. Running ahead of the train, we note that the profile also included several of those variables that nevertheless appeared in the discriminant model despite insignificant changes (while a number of parameters with significant dynamics were left out of the model).

Since the width of the page does not allow to reproduce the panorama, it is forcibly divided into downregulating (Figs. 7.13 and 7.14) and upregulating (Figs. 7.15 and 7.16) effects of electrical stimulation.
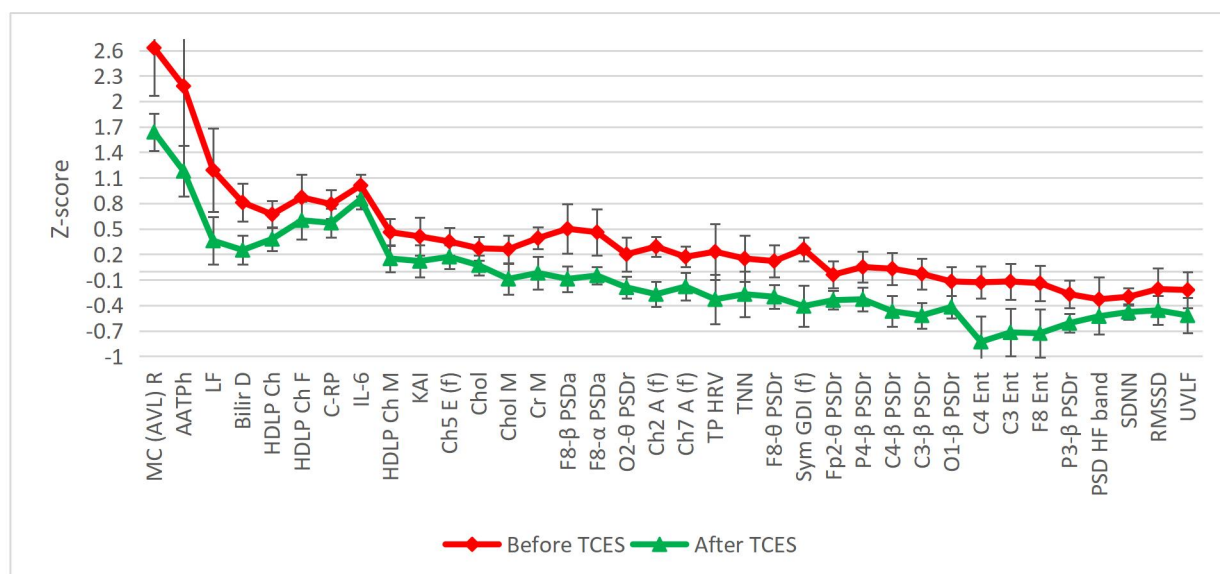
Fig. 7.13. Profiles of parameters whose levels decreased under the influence of transcutaneous electrical stimulation

As can be seen, electrical stimulation reduces to a greater or lesser extent the level of 7 HRV-markers of vagal tone, PSD of beta-rhythm in 6 loci, theta-rhythm in 3 loci, alpha-rhythm in locus F8 as well as PSD entropy in 3 loci. Such changes in the electrical activity of the brain are accompanied by a decrease, first of all, in the electrical conductivity of AP MC(AVL) Right and **5 parameters of GDV**, levels in the blood of asparagine transferase, direct bilirubin, creatinine, cholesterol in general and in the composition of high-density lipoproteins, as well as markers of inflammation: C-RP and IL-6.
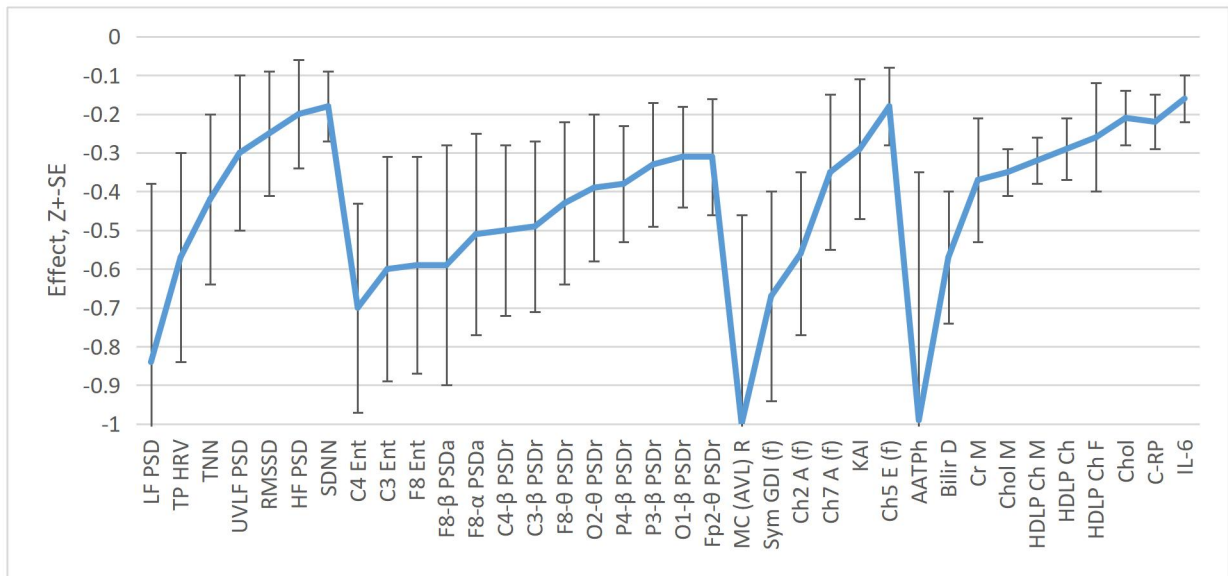

Fig. 7.14. Inhibitory/downregulating effects of transcutaneous electrical stimulation

On the other hand (Figs. 7.15 and 7.16), electrical stimulation causes a drastic increase in PSD of delta-rhythm in 4 loci and less pronounced in the other 5 loci, as well as PSD of theta-rhythm in locus F3, combined with a sympathotonic shift of HRV-markers of sympatho-vagal balance. Such changes in the electrical activity of the brain are accompanied by a increase, first of all, in Strain Index of leukocytogram and 6 parameters of phagocytosis of Gram-positive and Gram-negative bacteria by neutrophils, blood levels of $CD3^+CD25^+$ T-lymphocytes and CIC as well as in **2 GDV parameters**. Separately, a moderate increase in testosterone level should be noted, but only in men.
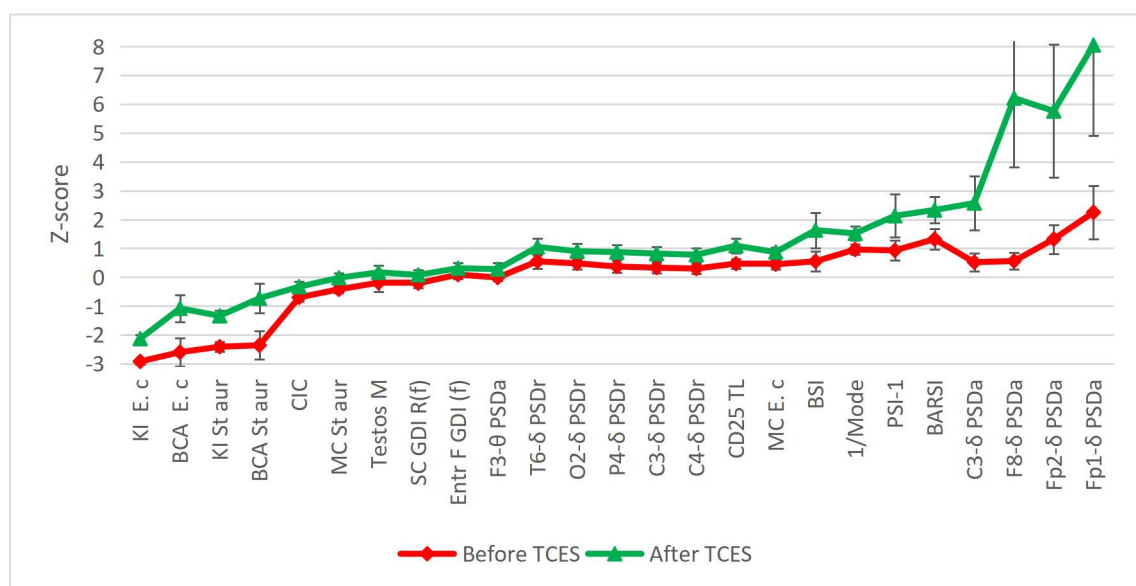
Fig. 7.15. Profiles of parameters whose levels increased under the influence of transcutaneous electrical stimulation
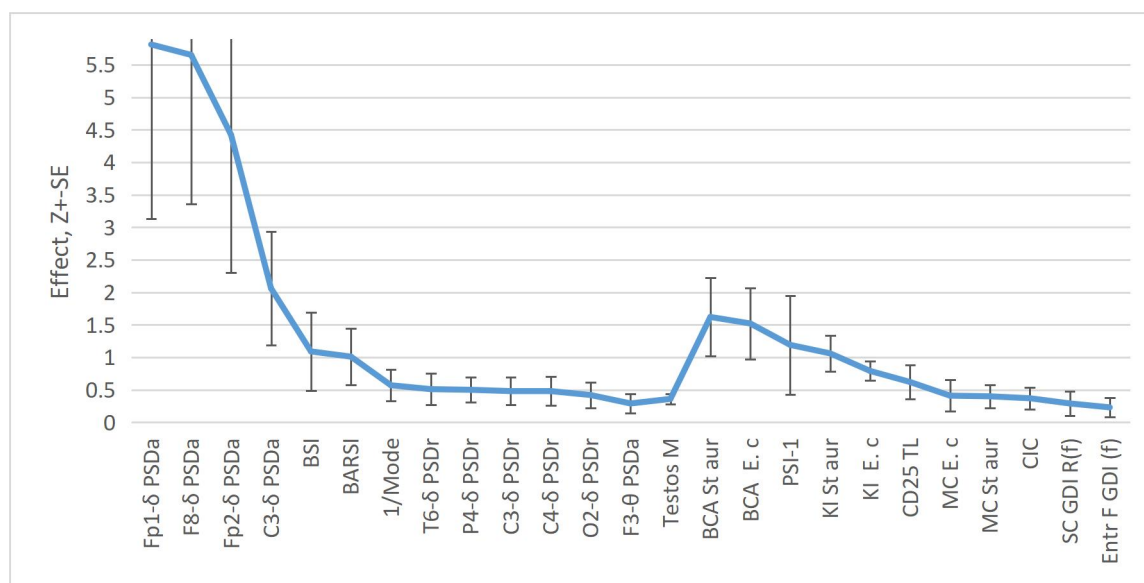

Fig. 7.16. Enhancing/upregulating effects of transcutaneous electrical stimulation

Z-scores and standard errors of the parameters displayed in the figures are reproduced in Table 7.9. In addition, parameters are grouped into clusters.

As you can see, **GDV (and acupuncture**) parameters are **organically woven into a continuous tissue of parameters of the neuro-endocrine-immune complex and metabolism**, which, in our humble opinion, is an excellent illustration of their **reality and informativeness**.

Table 7.9. Clusters of effects of transcutaneus electrical stimulation

Clusters and Variables	R	Before ES (38)	After ES (38)	Effect of ES (38)
B++/A+++ (5)				
Fp1-δ PSDa	-0,117	2,25±0,92	8,05±3,13	5,81±2,68
Fp2-δ PSDa	-0,124	1,32±0,50	5,76±2,31	4,42±2,12
F8-δ PSDa		0,56±0,29	6,21±2,40	5,65±2,29
Baevskiy's ARS Index HRV		1,32±0,35	2,33±0,46	1,01±0,43
Popovych's Strain Index-1 LCG		0,93±0,35	2,13±0,75	1,19±0,76
B+/A++ (10)				
C3-δ PSDa		0,52±0,31	2,57±0,93	2,06±0,87
T6-δ PSDr		0,55±0,25	1,05±0,29	0,51±0,24
P4-δ PSDr		0,37±0,21	0,87±0,26	0,50±0,19
C3-δ PSDr		0,33±0,18	0,82±0,24	0,48±0,21
C4-δ PSDr		0,30±0,18	0,78±0,24	0,48±0,22
O2-δ PSDr	-0,080	0,48±0,21	0,90±0,27	0,42±0,20
1/Mode HRV	-0,122	0,96±0,18	1,52±0,24	0,57±0,24
Baevskiy's Stress Index HRV		0,55±0,34	1,63±0,61	1,09±0,60
CD3$^+$CD25$^+$ T-Lymphocytes	-0,134	0,47±0,17	1,09±0,25	0,62±0,26
Microb Count vs E. coli		0,45±0,17	0,87±0,17	0,41±0,24
B--/A- (10)				
F3-θ PSDa		-0,01±0,12	0,28±0,21	0,29±0,15
Testosterone Male		-0,19±0,32	0,17±0,23	0,36±0,08
Entropy Frontal GDI (f)		0,09±0,14	0,31±0,18	0,23±0,15
Shape Coefficient GDI R(f)		-0,21±0,16	0,08±0,17	0,29±0,19
Microb Count vs St. aureus		-0,42±0,14	-0,02±0,17	0,40±0,18

CIC		-0,70±0,15	-0,33±0,18	0,37±0,17
Killing Index vs E. coli	-0,314	-2,92±0,10	-2,13±0,13	0,79±0,15
Killing Index vs Staph. aureus		-2,41±0,16	-1,34±0,20	1,06±0,28
Bactericidity vs E. coli		-2,60±0,50	-1,08±0,47	1,52±0,55
Bactericidity vs St. aureus		-2,36±0,49	-0,73±0,52	1,62±0,60
B++/A+ (8)				
PSD LF band	0,095	1,19±0,49	0,36±0,28	-0,84±0,46
AP MC (AVL) Right EC	0,105	2,63±0,56	1,64±0,22	-1,00±0,54
Asparagine ATPh	0,085	2,18±0,70	1,18±0,30	-0,99±0,64
Bilirubin direct	0,130	0,81±0,22	0,25±0,17	-0,57±0,17
HDLP Cholesterol M&F	0,093	0,67±0,16	0,38±0,14	-0,29±0,08
HDLP Cholesterol Female	0,093	0,87±0,27	0,60±0,22	-0,26±0,14
C-reactive Protein		0,79±0,17	0,57±0,17	-0,22±0,07
Interleukin-6	0,059	1,01±0,13	0,85±0,12	-0,16±0,06
B+/A0 (10)				
F8-β PSDa	0,120	0,50±0,29	-0,09±0,15	-0,59±0,31
F8-α PSDa	0,114	0,46±0,27	-0,05±0,10	-0,51±0,26
O2-θ PSDr	0,098	0,20±0,20	-0,19±0,13	-0,39±0,19
Chakra 7 Asymmetry (f)		0,17±0,12	-0,18±0,16	-0,35±0,20
Korotkov's Activation Ind GDI		0,41±0,22	0,12±0,19	-0,29±0,18
Chakra 5 Energy (f)		0,35±0,16	0,17±0,14	-0,18±0,10
Creatinine Male	0,054	0,39±0,13	-0,02±0,19	-0,37±0,16
Total Cholesterol Male	0,061	0,26±0,16	-0,09±0,18	-0,35±0,06
HDLP Cholesterol Male	0,093	0,46±0,16	0,15±0,16	-0,32±0,06
Total Cholesterol M&F	0,061	0,27±0,14	0,07±0,12	-0,21±0,07
B0/A- (18)				
C4 PSD Entropy	0,138	-0,13±0,19	-0,83±0,30	-0,70±0,27
C3 PSD Entropy		-0,12±0,21	-0,72±0,28	-0,60±0,29
F8 PSD Entropy		-0,14±0,21	-0,73±0,28	-0,59±0,28
C4-β PSDr		0,03±0,19	-0,47±0,18	-0,50±0,22
C3-β PSDr		-0,03±0,18	-0,52±0,15	-0,49±0,22
F8-θ PSDr	0,119	0,12±0,19	-0,30±0,14	-0,43±0,21
P4-β PSDr	0,109	0,05±0,18	-0,33±0,14	-0,38±0,15
P3-β PSDr	0,111	-0,27±0,16	-0,61±0,11	-0,33±0,16
O1-β PSDr		-0,12±0,17	-0,42±0,13	-0,31±0,13
Fp2-θ PSDr		-0,04±0,16	-0,34±0,11	-0,31±0,15
Total Power HRV		0,23±0,33	-0,33±0,29	-0,57±0,27
TNN HRV		0,15±0,27	-0,27±0,27	-0,42±0,22
PSD UVLF band		-0,22±0,21	-0,52±0,21	-0,30±0,20
RMSSD HRV		-0,21±0,25	-0,46±0,17	-0,25±0,16
PSD HF band	0,063	-0,33±0,26	-0,53±0,21	-0,20±0,14
SDNN HRV		-0,30±0,10	-0,48±0,09	-0,18±0,09
Symmetry GDI (f)	0,162	0,26±0,14	-0,41±0,24	-0,67±0,27
Chakra 2 Asymmetry (f)	0,188	0,29±0,12	-0,27±0,15	-0,56±0,21
Without change				
Creatinine M&F	0,054	0,63±0,17	0,44±0,14	-0,19±0,17
Creatinine Female	0,054	0,87±0,30	0,84±0,17	-0,02±0,22
Total Cholesterol Female		0,29±0,22	0,22±0,17	-0,07±0,09
Testosterone Female		1,61±0,67	1,54±0,62	-0,08±0,24

The previously selected variables were further subjected to discriminant analysis with the aim not so much to discover which of them are formally characteristic, but to visualize the integral state of each volunteer. The forward stepwise program included only 24 variables in the discriminant model (obtained structural coefficients R), including those subject to non-significant ($t<2{,}02$) effects according to the Student's criterion, while other variables were outside the model, despite significant changes (Table 7.9). On the face of it, the Wilks' and Student's statistics do not match completely.

As we can see, the reaction to electrical stimulation takes place in all participants without exception (Fig. 7.17), although the severity of the reaction has significant individual differences, which is quite natural given individual reactivity [Popovych IL et al, 2020].
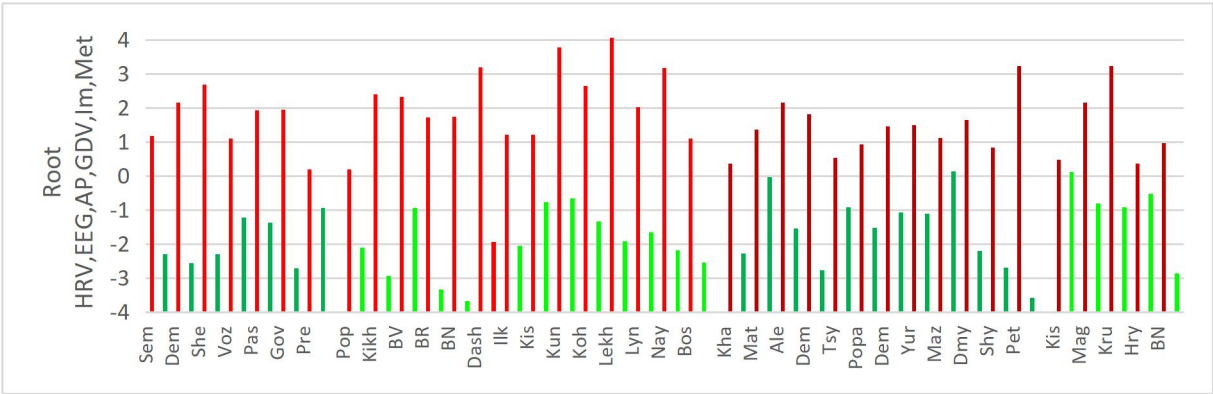

Fig. 7.17. Individual integral reactions to the course of electrical stimulation with the "VEB-1" and "VEB-2" devices of women and men

No significant differences were found either for both device models or for both sexes (Figs. 7.18 and 7.19).
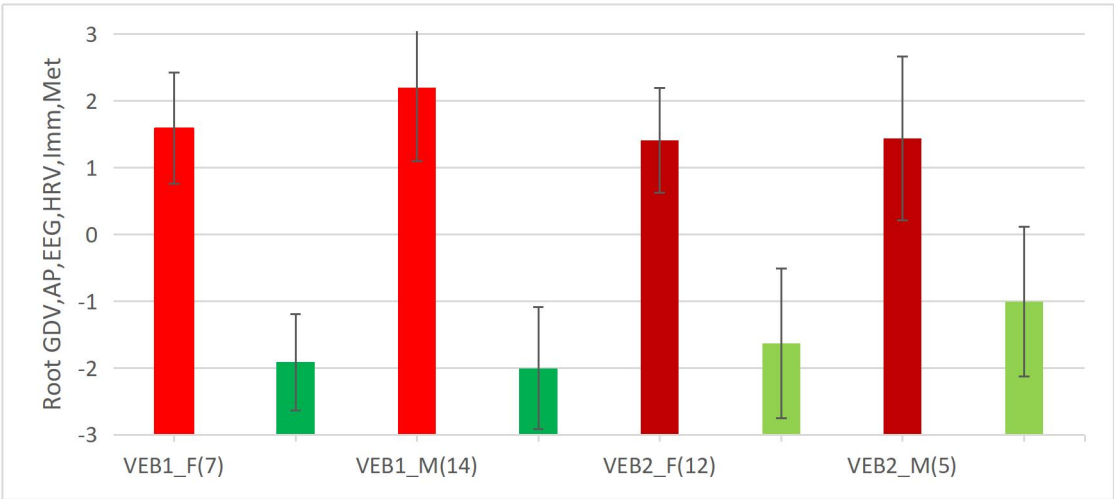
Fig. 7.18. Average values (Mean±SD) of the discriminant root before and after course of electrostimulation by "VEB-1" or "VEB-2" devices at Female and Male
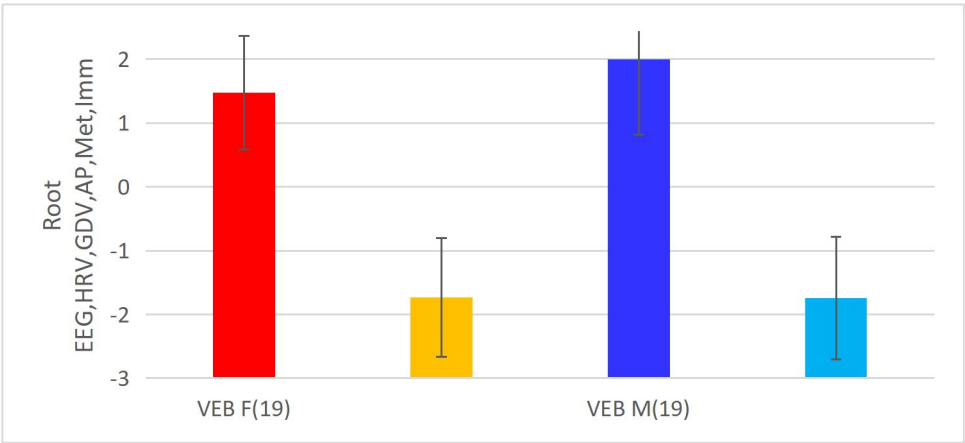

Fig. 7.19. Average values (Mean±SD) of the discriminant root before and after course of electrostimulation by VEB at Female and Male

The materials of the chapter are published in the following sources:

1. Babeluk VE. The patent of Ukraine for utility model 105875 Portable device for electrotherapy and stimulation, 2016.
2. Babelyuk VY, Dobrovolsky YyG, Popovych IL, Korsunskiy IG. Generator for electrotherapy and stimulation oh human nerve centers [in Russian]. Tekhnologiya i Konstruirovaniye v Elektronnoy Apparature. 2017; 1-2: 23-27.
3. Babelyuk V, Dobrovolsky Yu, Korsunsky I, Kuzenko V, Popovych I, Zukow W. The algorithm of the electric stimulator VEB-1 software operation. Journal of Education, Health and Sport. 2020; 10(5): 403-409.
4. Babelyuk NV, Babelyuk VYe, Dubkowa GI, Kikhtan VV, Musiyenko VY, Hubyts'kyi VY, Dobrovolsky YG, Korsunskyi IH, Kovbasnyuk MM, Korolyshyn TA, Popovych IL. Influence of the course of electrostimulation by the device "ES-01.9 WEB" on some functional systems of the organism of practically healthy men [in Ukrainian]. In: Proceedings VIII Scientific Conference "Issues of pathology in conditions of extreme factors action on the body" (Ternopil', 1-2 October 2015). Ternopil'. 2015: 5-6.
5. Babelyuk NV, Babelyuk VYe, Dubkowa GI, Korolyshyn TA, Kikhtan VV, Dobrovolsky YG, Korsuns'kyi IH, Kovbasnyuk MM. Electrical stimulation with the device "ES-01.9 WEB" activates some functional systems of the body of practically healthy men [in Ukrainian]. In: Valeology: current status, trends and persrectives of development. Abstracts. XIV Intern. scient. and practical. conf. (Kharkiv-Drohobych, 14-16 April 2016). Kharkiv. VN Karazin KhNU; 2016: 198-200.
6. Babelyuk NV, Babelyuk VYe, Dubkowa GI, Kikhtan VV, Musiyenko VY, Hubyts'kyi VY, Dobrovolsky YG, Korsuns'kyi IH, Kovbasnyuk MM, Korolyshyn TA, Popovych IL. Modulation of functional systems of practically healthy men by the course of electrostimulation [in Ukrainian]. In: IX International symposium "Actual problems of biophysical medicine" (Kyïv, 12-15 May 2016). Kyïv. OO Bohomolets' Institute of Physiology; 2016: 10-11.
7. Babelyuk VYe, Babelyuk NV, Popovych IL, Dobrovol's'kyi YG, Korsuns'kyi IH, Korolyshyn TA, Kindzer BM, Zukow W. Influence of the course of electrostimulation by the device "VEB-1" on parameters of electroencephalogram at practically healthy males. In: XVII reading named after VV Podvysotskyi. Bulletin of scientific materials conf. (May 24-25, 2018). Odesa. UkrSRI of Meicine of Transport; 2018: 11-12.
8. Kindzer BM, Babelyuk VY, Babelyuk NV, Popovych IL, Dubkova GI, Dobrovolskyi YG, Korsuns'kyi IH, Korolyshyn TA, Litosh S, Kindzer H, Zukow W. The device for electrostimulation "VEB-1" modulates parameters of electroencephalogram and gas discharge visualization. In: Science and society. Proc. of the 11th internat. confer. Hamilton, Canada. Acent Grafics Communications and Publishing; 2019: 159-171.
9. Babelyuk VY, Babelyuk NV, Popadynets' OO, Dubkova GI, Muszkieta R, Zukow W. Relationships between the entropy of gas-discharge image and the entropies of EEG, HRV, immunocytogram and leukocytogram. In: Mater of the XII All-Ukrainian Scie-Pract conf. "Actual issues of pathology under the conditions of action of extraordinary factors on the body". Galician readings II (Ternopil', October 29-30, 2020). Ternopil'; 2020: 119-120.
10. Babelyuk NV. Electrostimulation with the devices "VEB-1" and "VEB-2" causes almost identical changes in the parameters of gas-discharge visualization. Experimental and Clinical Physiology and Biochemistry. 2020; 90(2): 5-13.

11. Babelyuk VY, Tserkovniuk RG, Dubkova GI, Korolyshyn TA, Hubyts'kyi VY, Kikhtan VV, Gozhenko AI, Popovych IL. Parameters of gas discharge visualization (biophotonics) correlated with parameters of acupuncture points, EEG, HRV and hormones. In: Mater of the XIII All-Ukrainian Scie-Pract conf. "Actual issues of pathology under the conditions of action of extraordinary factors on the body". Galician readings II (Ternopil', October 26-28, 2020). Ternopil'; 2022: 79-79.

12. Babelyuk VY, Babelyuk NV, Popovych IL, Gozhenko AI, Kyrylenko IG, Korolyshyn TA, Dubkova GI, Kovbasnyuk MM, Hubyts'kyi VY, Kikhtan VV, Musiyenko VY, Dobrovolsky YG, Korsunskyi IH, Zukow W. Adaptogenic effects of transcutaneous electrical stimulation with the device "VEB" ®. In: Mater of the XIII All-Ukrainian Scie-Pract conf. "Actual issues of pathology under the conditions of action of extraordinary factors on the body". Galician readings II (Ternopil', October 26-28, 2020). Ternopil'; 2022: 78-78.

13. Babelyuk VE, Babelyuk NV, Popovych IL, Gozhenko AI, Kyrylenko IG, Korolyshyn TA, Dubkova GI, Kovbasnyuk MM, Hubyts'kyi VY, Kikhtan VV, Musiyenko VY, Dobrovolsky YG, Korsunskyi IH, Zukow W. Effects of transcutaneous electrical stimulation with the device "VEB" ® on the human body. Journal of Education, Health and Sport. 2022; 12(2): 313-335.

131

CHAPTER 8

REACTIONS OF GDV PARAMETERS TO TAKING OF NAFTUSSYA BIOACTIVE WATER AND PHYTOADAPTOGEN

Naftussya Bioactive Water was the main and practically the only object of research of the Truskavetsian department/laboratory of experimental balneology (1981-2016) of the Bohomolets' Institute of Physiology. It is symbolic that we managed to register the influence of Naftussya on GDV parameters right here, in the academic research unit, a few months before its liquidation due to lack of funding, despite the position of a solid middle peasant in the rating table of the Institute.

The object of observation (November 2015) were 20 volunteers: ten women and ten men aged 33-76 years without clinical diagnose but with dysfunction of neuro-endocrine-immune complex and metabolism, characteristic for premorbid (intermediate between health and illness) state.

We registered kirlianogram by the method of GDV by the device of "GDV Chamber" ("Biotechprogress", St-Pb., RF). In addition, the electrical conductivity of three pairs of acupuncture points (EC AP) and a number of metabolic parameters were recorded [Gozhenko AI et al, 2016].

After examination volunteers within 7 days used Naftussya Bioactive Water (250 mL three times a day), then repeated the tests listed.

Results processed using the software package "Statistica 5.5".

We found in the surveyed contingent excess energy of first, second, fourth and fifth Chakras, while the sixth Chakra energy deficit (Table 8.1). This gives grounds for assumptions about the relationship of these disorders of Chakras with detected at the same time disorders of neuro-endocrine-immune complex (see please chapters 3-5).

Table 8.1. Effects of weekly consumption of Naftussya bioactive water on virtual Chakras Energy

Variables	Baseline (20)	After drink course (20)	Change as direct differences (20)
Chakra 1	+0,17±0,07*	+0,06±0,07	-0,11±0,06
Muladhara	+0,20±0,05***	+0,16±0,05**	-0,04±0,03
Chakra 2	-0,05±0,06	-0,08±0,08	-0,03±0,08
Svadhisthana	+0,08±0,04*	+0,10±0,05*	+0,03±0,05
Chakra 3	-0,04±0,05	-0,13±0,09	-0,09±0,08
Manipura	+0,10±0,06	+0,05±0,06	-0,05±0,05
Chakra 4	+0,25±0,06***	+0,24±0,05***	-0,02±0,05
Anahata	+0,35±0,05***	+0,37±0,05***	+0,03±0,05
Chakra 5	+0,03±0,06	-0,06±0,07	-0,09±0,06
Vishudha	+0,11±0,05*	+0,11±0,07	0,00±0,05
Chakra 6	-0,15±0,06*	-0,21±0,07**	-0,06±0,06
Adjna	-0,09±0,05	-0,09±0,07	-0,01±0,05
Chakra 7	-0,08±0,05	-0,11±0,06	-0,03±0,05
Sahasrara	+0,01±0,04	+0,02±0,05	+0,01±0,04

Note. Each column in the top row shows the parameters registered without the filter, while the bottom line whith filter

An additional argument in favor of this assumption can be detected Asymmetry in first, second and third Chakras (Table 8.2).

Table 8.2. Effects of weekly consumption of Naftussya on virtual Chakras Asymmetry

Variables	Baseline (20)	After drink course (20)	Change as direct differences (20)
Chakra 1 **Muladhara**	-0,09±0,06	0,00±0,04	+0,10±0,07
	-0,02±0,04	0,00±0,04	+0,02±0,04
Chakra 2 **Svadhisthana**	+0,12±0,07	-0,01±0,07	-0,13±0,07
	0,01±0,06	-0,02±0,06	-0,03±0,06
Chakra 3 **Manipura**	+0,12±0,07	-0,04±0,07	-0,16±0,08*
	+0,03±0,05	-0,05±0,05	-0,08±0,05
Chakra 4 **Anahata**	+0,01±0,09	+0,05±0,05	+0,05±0,11
	-0,03±0,04	-0,04±0,07	-0,01±0,07
Chakra 5 **Vishudha**	+0,02±0,05	+0,03±0,05	+0,01±0,06
	+0,02±0,05	-0,02±0,09	-0,04±0,07
Chakra 6 **Adjna**	+0,04±0,05	+0,06±0,04	+0,02±0,05
	+0,04±0,05	-0,01±0,08	-0,04±0,06
Chakra 7 **Sahasrara**	+0,08±0,07	-0,05±0,06	-0,13±0,07
	0,00±0,05	+0,02±0,05	+0,01±0,06

Digital data of Table 8.1 visualized in Figures 8.1 and 8.2 show clearly the initial state of the Chakras and their response on the taking of Naftussya. The influence appears significant in normalizing the excess energy of the first Chakra (related to the Adrenal glands).
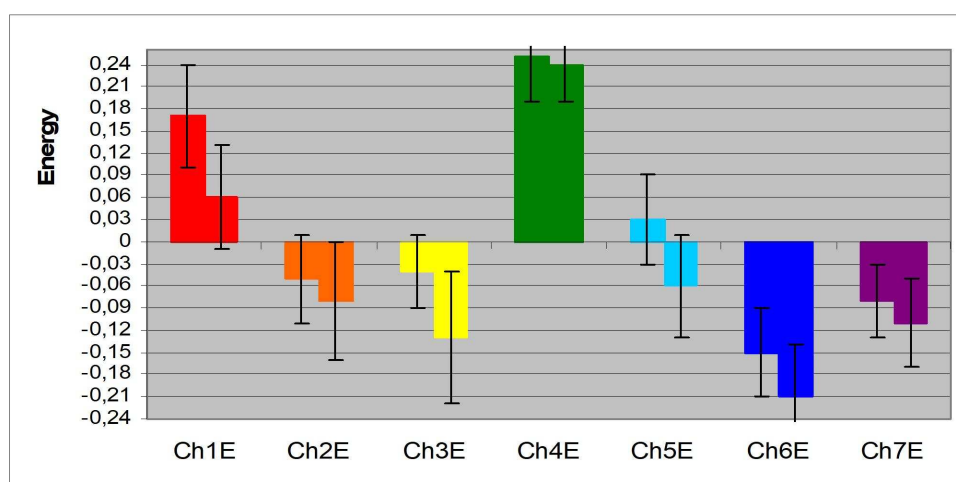
Fig. 8.1. The profiles of Energy of virtual Chakras registered without the filter before and after the course drinking of Naftussya bioactive water
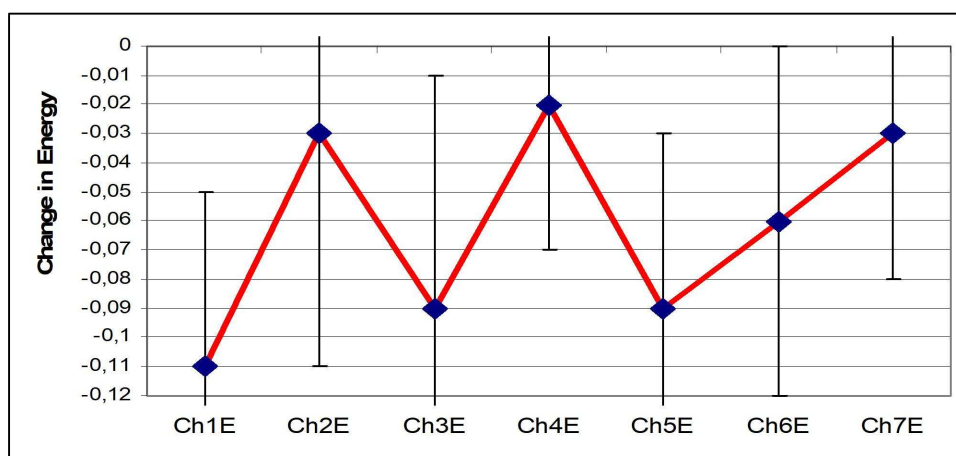

Fig. 8.2. Changes as direct differences in Energy of virtual Chakras registered without the filter caused by course drinking of Naftussya bioactive water

Other manifestations effects of NBAW are leveling left-sided asymmetry first Chakra as well as right-sided asymmetry second (related to the Gonades), third (related to the Spleen) and seventh (related to the right&upper Brain) Chakras (Figs. 8.3 and 8.4).
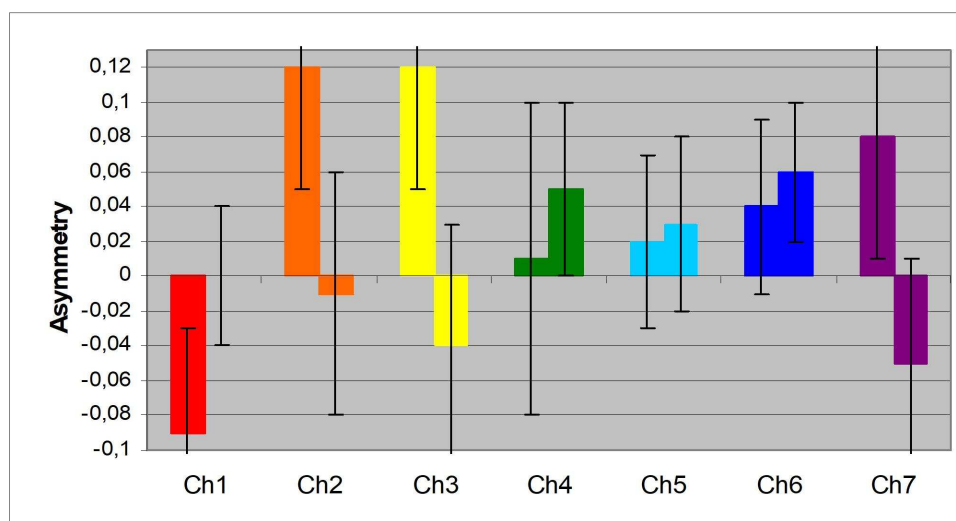

Fig. 8.3. The Asymmetry profiles of virtual Chakras registered without the filter before and after the course drinking of Naftussya bioactive water
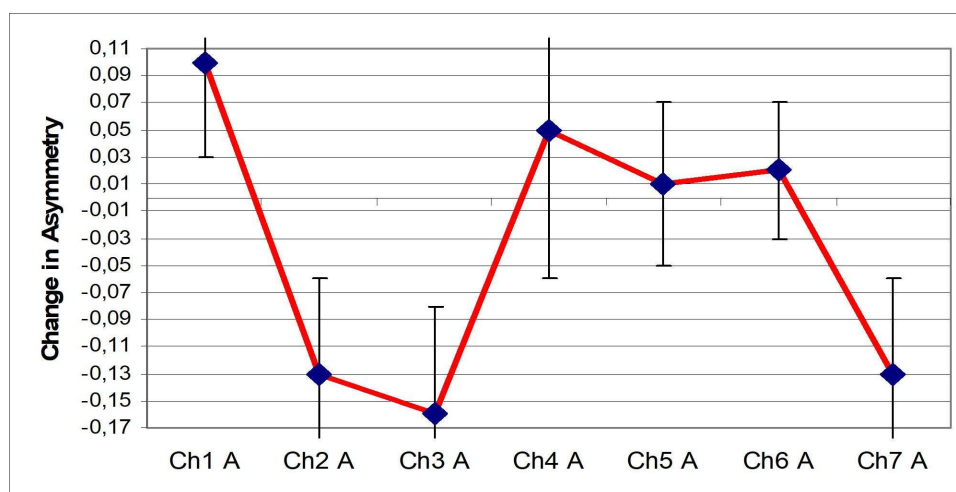
Fig. 8.4. Changes as direct differences in Asymmetry of virtual Chakras registered without the filter caused by course drinking of Naftussya bioactive water

When studying the same cohorte we detected that among hormones coefficient of canonical correlation of GDV parameters with testosterone makes 0,81, with cortisol 0,66, with calcitonin 0,61, with triiodothyronine 0,60, with MCA 0,48 (p=0,022). Thus, we confirmed that between principal neuroendocrine factors of adaptation and parameters of GDV exist significant canonical correlation suggesting informativenes GDV method.

In order to identify precisely those indicators, for which a set conditions of people before and after course drinking Naftussya vary, available information field were subjected to discriminant analysis. For inclusion in the model program selected only 12 indicators (variables), while others are out of discriminant model (Table 8.3).

There are given full **structural** coefficients, ie the coefficients correlation between the root and discriminant variables. The structural coefficient indicates how closely related variables and discriminant function, that is what share of information about root lies in this

variable. As you can see, **GDV (as well as acupuncture**) parameters display information about the state of the body along with chloride, uric acid, phosphate and cholesterol.

Table 8.3. Discriminant Function Analysis Summary
Step 12, N of vars in model: 12; Grouping: 2 grps; Wilks' Λ: 0,253; appr. $F_{(12)}$=6,6; $p<10^{-4}$

Variables currently in the model	Wilks Λ	Part Λ	F-re-move	p	Tolerance	Struct coeff	Before n=20	After n=20	Change
Chloride Plasma, mM/l	,404	,628	16,0	10^{-3}	,540	-,36	98,4 ±1,4	105,6 ±1,3	+7,2 ±1,5
Chloride Excretion, mM/24h	,301	,843	5,03	,033	,268	-,16	159 ±17	198 ±15	+39 ±22
GDV Shape Coefficient Right (f)	,311	,816	6,09	,020	,219	-,12	13,75 ±0,3	14,27 ±0,3	+0,52 ±0,31
EC AP Pg (ND) Right, units	,301	,843	5,03	,033	,644	-,10	62,3 ±1,4	64,3 ±1,2	+2,0 ±1,0
Uric Acid Urine Concentration, mM/l	,265	,958	1,18	,287	,289	,21	2,99 ±0,46	1,95 ±0,11	-1,04 ±0,43
Uric Acid Excretion, mM/24h	,321	,789	7,21	,012	,189	,20	3,54 ±0,34	2,94 ±0,24	-0,60 ±0,40
EC AP MC (AVL) LI, %	,308	,822	5,83	,023	,844	,15	+0,8 ±0,5	-1,3 ±0,9	-2,1 ±1,0
GDV Chakra 3 Asymmetry	,298	,851	4,72	,038	,754	,14	0,12 ±0,07	-0,04 ±0,07	-0,16 ±0,08
GDV Chakra 2 Asymmetry	,319	,796	6,94	,014	,485	,12	0,12 ±0,07	-0,01 ±0,07	-0,13 ±0,07
GDV Chakra 1 Energy	,277	,914	2,53	,123	,181	,12	0,17 ±0,07	0,06 ±0,07	-0,11 ±0,06
LDLP Cholesterol, mM/l	,267	,949	1,45	,239	,639	,10	3,62 ±0,22	3,27 ±0,17	-0,35 ±0,13
Phosphate Plasma, mM/l	,263	,965	,99	,328	,480	,08	1,10 ±0,05	1,05±0,04	-0,05 ±0,02
Variables currently not in the model	Wilks Λ	Part Λ	F to enter	p	Tolerance		Before n=20	After n=20	Change
GDV Entropy Left Projection	,247	,976	,643	,43	,565		3,80 ±0,04	3,73 ±0,03	-0,07 ±0,03
GDV Chakra 1 Asymmetry	,248	,978	,597	,45	,806		-0,09 ±0,06	0,00 ±0,04	+0,10 ±0,07
GDV Chakra 7 Asymmetry	,251	,990	,253	,62	,152		0,08 ±0,07	-0,05 ±0,06	-0,13 ±0,07

Phytoadaptogens were another important object of research in our laboratory [Kostyuk PG et al, 2006]. This was necessary to substantiate the concept about **Naftussya bioactive water as adaptogen** [Popovych IL, 2011]. Therefore, it was quite logical to study the responses to the use of plant adaptogens of GDV parameters.

The object of observation (February 2010) were 12 women (44±13 years) and 62 men (44±12 years) with dysfunction of neuro-endocrine-immune complex, employees of the clinical sanatoria "Kryshtalevyĭ Palats" and "Moldova" (Truskavets', Ukraine). Every of morning before work, carried out initial tests of 6 persons, then the two of them (basic group) used 5 ml of phytocomposition "Balm Truskavets" (ТУ У 15.8-24055046-005:2009, produced by PRPE "Ukrainian Balms", Mykolaïv, Ukraine), pre-diluted in 45 ml of boiled tap water. This phytocomposition is analogous to the previous "Balm Kryms'kyi" (ТУ 565/46-75-82-92), officially recognized as an adaptogenic agent [Panasyuk YM et al, 1994; Pat. 10271 Ukraine MKI A 61 K 31/00, 1996; Alyeksyeyev OI et al, 1996]. The other 4 individuals (control group) used 50 ml of the same water at room temperature.

After an hour and a half, the testing was repeated. The tests consisted of recording GDV-gram, EEG and HRV as described above.

Due to various circumstances, the main of which was the obstruction of the GDV method, the results were published only in 2021 [Fihura OA et al, 2021].

According to the algorithm, profiles of normalized parameters were created, the levels of which differ significantly before and after Balm taking, as well as several parameters which according to the following discriminant analysis were still recognizable, despite the insignificant value of Student's t criterion (Fig. 8.5).
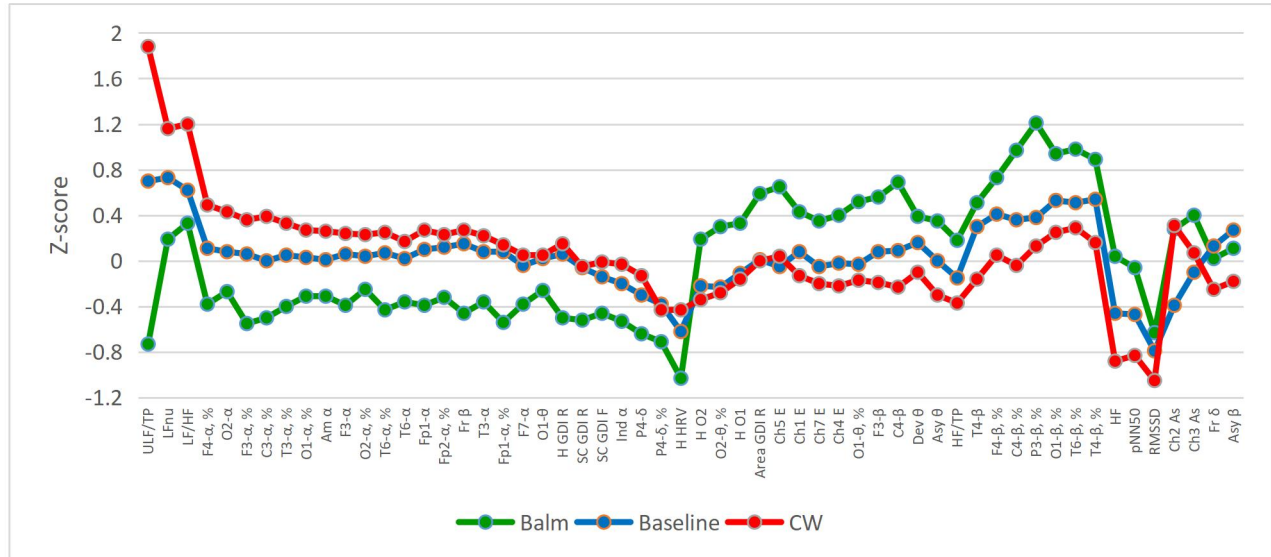

Fig. 8.5. Profiles of Z-scores of GDVs, EEGs and HRVs variables in the initial state and 1,5 hours after drinking of control water (CW) or Balm

Z-scores of the parameters displayed in the Fig. 8.5 are reproduced in Table 8.4. In addition, parameters are grouped into clusters.

Table 8.4. Factor Structure Matrix and Means of Roots and Variables

Variables, Z	Correlations Variables-Roots		After Balm (20)	Base-line (74)	After CW (54)
Root 1 (63,8%)	R1	R2	-2,96	+0,25	+0,76
ULF/TP, %	0,281	-0,200	-0,73	+0,70	+1,88
LF/HF	0,128	0,166	+0,33	+0,62	+1,20
LFnu, %			+0,19	+0,73	+1,16
F3-α PSD, %	0,250	-0,104	-0,55	+0,06	+0,36
C3-α PSD, %	0,228	-0,154	-0,50	0,00	+0,39
T6-α PSD, %	0,177	-0,048	-0,43	+0,07	+0,25
F3-α PSD, μV^2/Hz	0,155	-0,045	-0,39	+0,06	+0,24
O2-α PSD, μV^2/Hz	0,146	-0,121	-0,27	+0,08	+0,43
O2-α PSD, %	0,113	-0,065	-0,25	+0,04	+0,23
T3-α PSD, %			-0,40	+0,05	+0,33
Fp1-α PSD, μV^2/Hz			-0,39	+0,10	+0,27
F4-α PSD, %			-0,38	+0,11	+0,49
O1-α PSD, %			-0,31	+0,03	+0,27
Amplitude-α, μV			-0,31	+0,01	+0,26
Frequency-β, Hz	0,194	-0,010	-0,46	+0,15	+0,27
T3-α PSD, μV^2/Hz	0,140	-0,033	-0,36	+0,08	+0,22

Parameter					
Fp1-α PSD, %			-0,54	+0,08	+0,14
F7-α PSD, µV^2/Hz			-0,38	-0,04	+0,05
T6-α PSD, µV^2/Hz			-0,36	+0,02	+0,17
Fp2-α PSD, %			-0,32	+0,12	+0,23
Index α, %			-0,53	-0,20	-0,03
O1-θ PSD, µV^2/Hz	0,095	0,005	-0,26	+0,02	+0,05
Shape C GDI Right	0,136	0,031	-0,52	-0,06	-0,05
Shape C GDI Frontal	0,111	-0,019	-0,46	-0,14	-0,01
Entropy GDI Right			-0,50	+0,06	+0,15
P4-δ PSD, µV^2/Hz	0,162	-0,067	-0,64	-0,30	-0,13
P4-δ PSD, %	0,133	0,074	-0,71	-0,38	-0,43
Entropy HRV	0,140	-0,056	-1,03	-0,62	-0,43
C4-β PSD, µV^2/Hz	-0,262	0,122	+0,69	+0,09	-0,23
F3-β PSD, µV^2/Hz			+0,56	+0,08	-0,19
O2-θ PSD, %	-0,200	-0,015	+0,30	-0,23	-0,28
O1-θ PSD, %	-0,185	0,024	+0,52	-0,03	-0,17
Asymmetry-θ, %	-0,153	0,116	+0,35	0,00	-0,30
Deviation-θ, Hz			+0,39	+0,16	-0,10
Area GDI Right	-0,170	-0,023	+0,59	+0,01	0,00
Chakra 5 Energy	-0,166	-0,094	+0,65	-0,05	0,04
Chakra 7 Energy	-0,145	0,033	+0,35	-0,05	-0,20
Chakra 1 Energy	-0,132	0,046	+0,43	+0,08	-0,13
Chakra 4 Energy			+0,40	-0,02	-0,22
Entropy EEG O1	-0,139	-0,009	+0,33	-0,11	-0,16
Entropy EEG O2			+0,19	-0,22	-0,34
P3-β PSD, %	-0,243	0,048	+1,21	+0,38	+0,13
C4-β PSD, %	-0,215	0,120	+0,97	+0,36	-0,04
T6-β PSD, %	-0,161	0,064	+0,98	+0,51	+0,29
T4-β PSD, %	-0,157	0,135	+0,89	+0,54	+0,16
T4-β PSD, µV^2/Hz	-0,121	0,120	+0,51	+0,30	-0,16
F4-β PSD, %			+0,73	+0,41	+0,05
O1-β PSD, %			+0,94	+0,53	+0,25
HF, msec^2	-0,164	0,116	+0,04	-0,46	-0,88
RMSSD, msec	-0,136	0,152	-0,63	-0,79	-1,05
HF/TP, %			+0,18	-0,15	-0,37
pNN$_{50}$, %			-0,06	-0,47	-0,83
Root 2 (36,3%)	R1	R2	-0,45	+0,88	-1,04
Chakra 2 Asymmetry	-0,086	-0,232	+0,28	-0,39	+0,31
Chakra 3 Asymmetry			+0,40	-0,10	+0,07
Asymmetry-β, %	-0,036	0,185	+0,11	+0,27	-0,18
Frequency-δ, Hz			+0,02	+0,13	-0,25

It is clear that the neurotropic effects of the Balm are accompanied by significant changes in a number of **GDV parameters**.

First of all, it is a decrease in the initially normal values of GDI Fractality in the right and frontal projections and Entropy in the right projection in combination with a decrease in the initially normal values of **Amplitude, Index and PSD of alpha-rhythm** as well as in the initially decreased **P4-δ PSD** and **Entropy HRV** and increased **sympathetic tone** values.

Secondly, it is an increase in the initially normal GDI Area in the right projection in combination with an increase in the initially normal values of **Deviation, Asymmetry and PSD of theta-rhythm in occipital loci** and **C4&F3-β PSD** as well as in the initially increased **PSD of beta-rhythm in 6 loci** and decreased **vagal tone**.

It is important that the Entropy of HRV decreases while the Entropy of EEG in occipital loci increases. The physiological essence of Entropy is discussed in detail in a recent monograph [Gozhenko AI et al, 2021].

The most interesting thing is that along with the GDI Area the Energy of the first, fourth, fifth and seventh Chakras increases significantly. And now let's remember that **fourth** and **fifth** Chakras associated with vagus nerve, the tone of which increases; **first** Chakra is associated with adrenals, consistent with increased PSD of ULF band as a marker of circulating catecholamines and glucocorticoids; **seventh** Chakra associated with **right** (paired EEG loci!) and upper brain [Chase CR, 2018].

Contrary to expectations, in the control group there were shifts in the levels of parameters in directions opposite to those in the main group. It is unlikely that the reason for such changes in neurodynamics is the use of 50 ml of tap water. The effects of individuals' occupational activity within 1,5 hours between tests and/or the ultradian biorhythm of the autonomic nervous system and cortisol are more obvious.

Interestingly, the reversion of the left-sided asymmetry of second and third Chakras to the right-sided one were almost the same in both groups.

Having discovered the immediate neurotropic and biophysical effects of the Balm, we offered 6 women (25-63 years) and 4 men (31-60 years) to continue using it (three times a day before meals). After 11 days, repeated testing was carried out.

The results of the screening are given in the table. 8.5 and illustrated in figures 8.6 and 8.7.

Table 8.5. Effects as differences between levels (Z±SE) after and before use of Balm

| Variables	R	Baseline (10)	After Balm (10)	Difference (10)
Area GDI Left	-0,042	+0,19±0,35	+0,82±0,34	+0,63±0,28
Area GDI Frontal	-0,041	+0,34±0,03	+0,94±0,34	+0,60±0,20
Chakra 2 Energy	-0,041	+0,21±0,35	+0,71±0,18	+0,50±0,27
Entropy EEG PSD in T5	-0,065	-1,18±0,61	+0,11±0,19	+1,29±0,59
T3-β PSD		+0,66±0,55	+2,80±1,46	+2,14±1,04
F8-β PSD	-0,044	+0,22±0,31	+1,90±1,19	+1,68±0,99
P4-β PSD	-0,038	+0,20±0,29	+1,06±0,68	+0,86±0,45
T3-α PSD	-0,044	-0,32±0,20	+0,26±0,38	+0,58±0,31
T5-α PSD		-0,80±0,18	-0,37±0,20	+0,43±0,12
O2-α PSD		-0,23±0,21	-0,10±0,27	+0,13±0,07
1/Mode HRV	-0,044	+0,15±0,30	+1,00±0,55	+0,85±0,40
Heart Rate		+0,11±0,29	+1,11±0,78	+1,00±0,65
VLF/TP HRV		-0,57±0,28	-0,02±0,39	+0,55±0,30
Chakra 1 Asymmety	0,049	+1,00±0,40	+0,25±0,29	-0,75±0,34
Chakra 4 Asymmetry	0,079	+0,43±0,27	-0,27±0,09	-0,70±0,25
Chakra 7 Asymmetry		+0,20±0,40	-0,36±0,24	-0,56±0,35
Laterality α	0,042	+0,19±0,18	-0,15±0,20	-0,34±0,20
Entropy GDI Frontal (f)	0,040	+0,02±0,09	-0,14±0,10	-0,17±0,06
Entropy EEG PSD in O2	0,050	-0,16±0,35	-0,80±0,22	-0,64±0,35
O2-θ PSD	0,058	-0,28±0,27	-0,87±0,20	-0,59±0,23
RMSSD HRV		-0,18±0,40	-0,66±0,37	-0,48±0,31
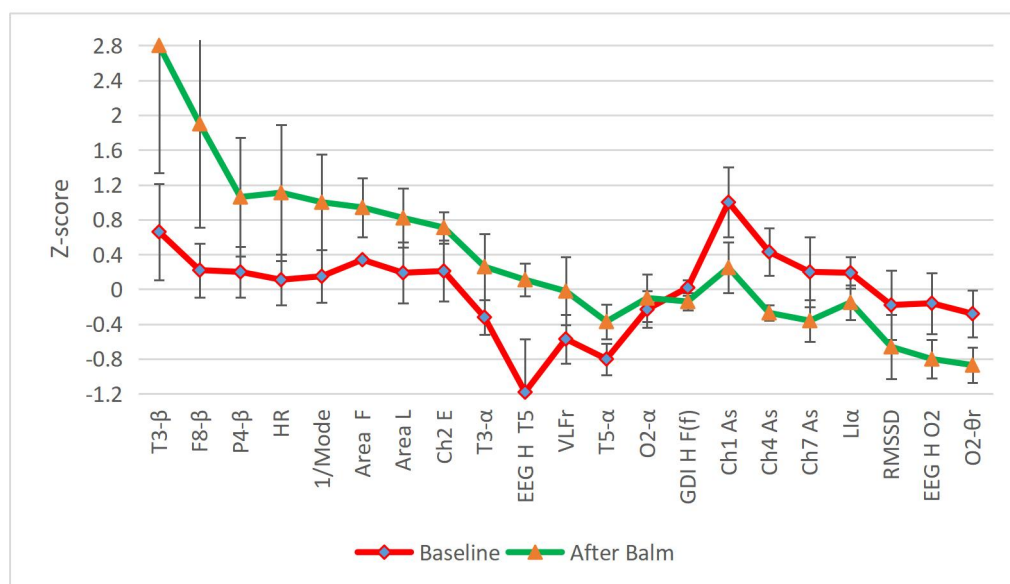
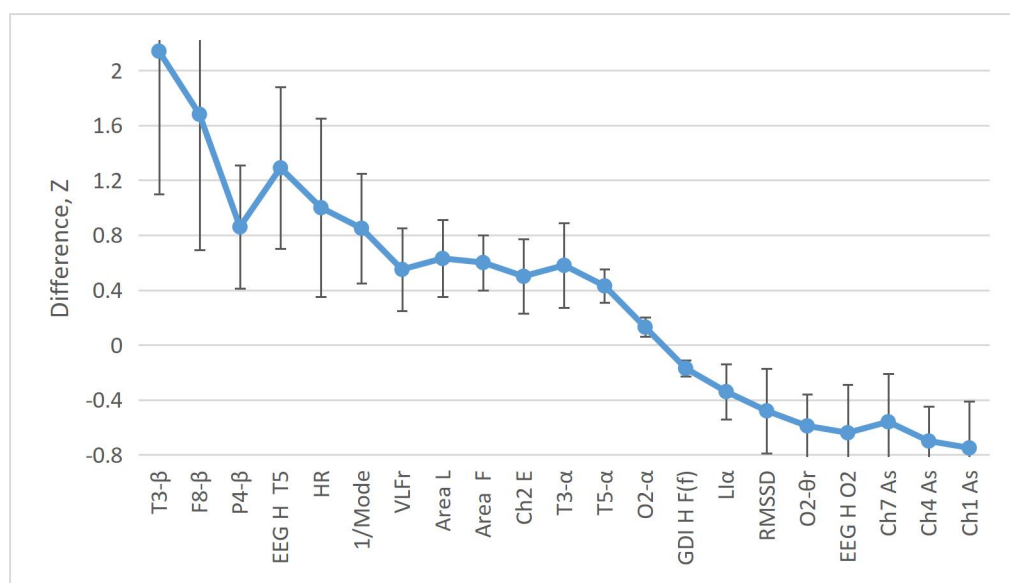**Fig. 8.6. Profiles of normalized GDV and EEG&HRV parameters (Z±SE) before and after course of Balm using**

Fig. 8.7. Effects (direct differences, Z±SE) of Balm using on the GDV and EEG&HRV parameters

As we see, the identified modulating effects of the Balm on the CNS and ANS parameters are accompanied by an expansion of the GDI Area in the frontal and left projections, which reflects an increase in the *emission of biophotons* by the skin of the fingers, mainly of the left hand. In addition, a slight but statistically significant decrease in the normal Entropy of the GDI in the frontal projection was found, reflecting "internal production of negative Entropy and stabilization of homeokinesis" [Korotkov KG, 2014].

We discovered an increase in the Energy of the **second** Chakra, related to the ovaries and **adrenals** [Puchko LG, 2004] or testes/ovaries and inferior mesenteric ganglion [Chase CR, 2018]. This is consistent with the received data on the activation of the **adrenal** glands, or rather their medullary zone as sourse of catecholamines.

Other effects of the Balm are the leveling of the pronounced right-sided Asymmetry of the **first** Chakra and the transformation of a moderate right-sided Asymmetry into a moderate left-sided one of the fourth and **seventh** Chakras.

Let's remember that the **first** Chakra is associated with adrenals and pelvic nerve plexus [Chase CR, 2018] or testicles [Puchko LG, 2004]; fourth Chakra - with celiac and cardiac plexus, vagus nerve, heart as well as thymus; **seventh** Chakra - with right&upper brain as well as pineal gland [Chase CR, 2018]. Such changes in the lateralization of the Chakras are satisfactorily consistent with the decrease in the tone of the **right vagal nerve**, which is responsible for sinus arrhythmia, as well as with the **left lateralization** of the alpha-rhythm. At the same time, this suggests the possible immunotropic effects of the Balm.

The previously identified effects of the "Balm Kryms'kyi" on the parameters of immunity and hemodynamics [Flyunt et al, 2002; Kostyuk PG et al, 2006] are consistent with the notion that **fourth** Chakra is associated with thymus, celiac and cardial plexus, heart, circulation [Chase CR, 2018]. It is appropriate to mention the research data of our laboratory on the relationship between the parameters of EEG&HRV and immunity, as well as their changes under the influence of adaptogenic factors of the resort of Truskavets' [review: Popovych IL et al, 2022].

Despite a rather small sample, the reactions of both GDV and EEG&HRV parameters to the course use of an adaptogen turned out to be very clear, and independent of neither the gender nor the age of the volunteers (Fig. 8.8).
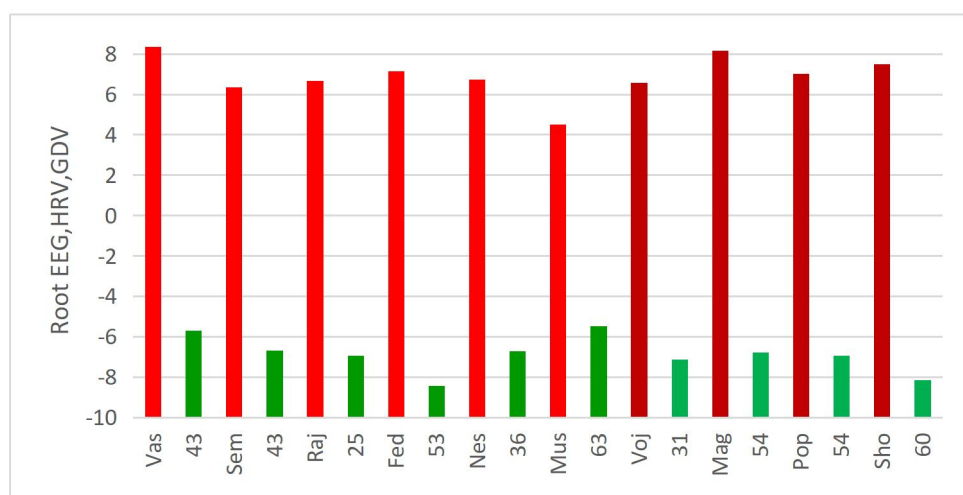
Fig. 8.8. Individual values of the discriminant root before and after course using of Phytocomposition at women and men. The code and age of the patients are indicated

Next study was conducted on a four times larger cohort and with a wider range of methods, that allow assessing the state of the neuro-endocrine-immune complex as a marker of adaptation.

The object of observation were employees of the clinical sanatorium "Moldova" and PrJSC "Truskavets' Spa": 16 women 33-71 (M±SD: 46±15) years and 24 men 24-69 (50±11) years. The volunteers were considered practically healthy (without a clinical diagnosis), but the initial testing revealed deviations from the norm in a number of parameters of the neuro-endocrine-immune complex (details follow) as a manifestation of maladaptation.

The obtained results (Table 8.6 and Figs. 8.9-8.10) confirmed the predicted immunotropic effect of the Balm as one of the manifestations of its adaptogenic properties. But more important for us was the weaving of GDV parameters into the fabric of the neuro-endocrine-immune complex.

In particular, the **reduced** levels of the Popovych's adaptation index and killing indices vs both E. coli and Staph. aureus **increase** significantly, still remaining low (cluster B--/A-).

At the same time, BCCN in relation to gram-positive microbes is completely normalized, and in relation to gram-negative microbes it even reaches the upper zone of the normal range

due to the additional slight increase of other elements of this integral parameter of phagocytosis (cluster B-/A0+).

Instead, the **increased** levels of the Popovych's strain index, plasma testosterone and triiodothyronine, LF band of HRV, Entropy of GDI in Left projection (H GDI L) as well as right-sided (positive sign of symmetry index) Asymmetry of the third Chakra **decrease** (cluster B+/A0).

Table 8.6. Clusters of effects as differences between levels (Z±SE) after and before treatment

| Clusters and Variables	Structural coefficient	Before (40)	After (40)	Effect (30)
B--/A- (3)		**-1,99±0,21**	**-1,25±0,05**	**+0,74±0,18**
Popovych's Adaptation Index-1	-0,160	-2,37±0,33	-1,28±0,36	+1,09±0,36
Killing Index vs E. coli	-0,171	-1,96±0,16	-1,32±0,21	+0,64±0,21
Killing Index vs Staph. aureus	-0,176	-1,63±0,12	-1,15±0,15	+0,48±0,20
B-/A0+ (2)		**-1,30±0,29**	**+0,28±0,48**	**+1,57±0,19**
Bactericidity vs E. coli	-0,244	-1,01±0,33	+0,75±0,39	+1,76±0,48
Bactericidity vs Staph. aureus	-0,215	-1,58±0,30	-0,20±0,35	+1,38±0,46
B0/A0+ (15)		**-0,03±0,05**	**+0,38±0,07**	**+0,41±0,04**
Asymmetry-δ	-0,147	-0,23±0,15	+0,28±0,18	+0,51±0,21
1/Mode HRV		+0,02±0,22	+0,63±0,22	+0,65±0,16
Cortisol		+0,15±0,23	+0,84±0,26	+0,69±0,34
T6-θ PSDa	-0,103	-0,12±0,15	+0,55±0,44	+0,67±0,43
T5-θ PSDa	-0,066	+0,15±0,20	+0,54±0,37	+0,39±0,28
T3-α PSDa		-0,04±0,14	+0,38±0,33	+0,41±0,27
T6-α PSDa	-0,106	-0,30±0,07	-0,04±0,16	+0,26±0,14
C3-α PSDa	-0,074	-0,12±0,13	+0,13±0,20	+0,25±0,14
T3-β PSDa	-0,111	+0,31±0,19	+1,04±0,43	+0,72±0,33
F3-β PSDa	-0,101	+0,06±0,14	+0,42±0,22	+0,36±0,19
Frequency-β	-0,091	-0,08±0,14	+0,20±0,17	+0,27±0,16
C3-β PSDa	-0,085	+0,12±0,14	+0,40±0,18	+0,27±0,15
P4-β PSDa	-0,078	+0,03±0,12	+0,35±0,26	+0,31±0,18
P3-β PSDa	-0,061	+0,15±0,13	+0,35±0,20	+0,20±0,11
Shape Coefficient GDI Right (f)		-0,61±0,13	-0,34±0,13	+0,27±0,12
B+/A++ (3)		**+0,49±0,18**	**+1,67±0,20**	**+1,17±0,13**
T6-δ PSDa	-0,114	+0,18±0,23	+1,52±0,80	+1,34±0,84
F3-δ PSDa	-0,093	+0,81±0,29	+2,07±0,93	+1,26±0,82
T3-δ PSDa		+0,49±0,26	+1,41±0,64	+0,92±0,62
B0/A0- (9)		**+0,04±0,06**	**-0,36±0,05**	**-0,40±0,03**
Laterality-α	0,167	-0,04±0,14	-0,45±0,11	-0,41±0,16
MC(AVL) EC Laterality		-0,01±0,16	-0,47±0,24	-0,46±0,28
Chakra 7 Asymmetry	0,132	+0,17±0,19	-0,38±0,17	-0,54±0,20
Fp2 PSD Entropy		-0,08±0,17	-0,61±0,26	-0,53±0,29
Fp2-θ PSDa		+0,13±0,14	-0,28±0,11	-0,41±0,22
SDNN HRV	0,104	-0,22±0,13	-0,46±0,09	-0,24±0,14
pNN$_{50}$ HRV		+0,17±0,31	-0,26±0,25	-0,42±0,18
HF HRV PSD		+0,34±0,35	-0,02±0,28	-0,36±0,24
RMSSD HRV		+0,02±0,20	-0,27±0,17	-0,29±0,16
B+/A0 (6)		**+0,72±0,15**	**+0,07±0,16**	**-0,65±0,08**
Testosterone	0,131	+0,75±0,36	-0,32±0,28	-1,07±0,34
Triiodothyronine		+0,43±0,27	-0,23±0,29	-0,66±0,22
LF HRV PSD		+0,94±0,53	+0,17±0,38	-0,77±0,46
Chakra 3 Asymmetry	0,110	+0,41±0,24	-0,15±0,21	-0,56±0,28
Entropy GDI Left	0,093	+0,53±0,18	+0,15±0,18	-0,38±0,14
Popovych's Strain Index-1		+1,35±0,36	+0,75±0,29	-0,60±0,42
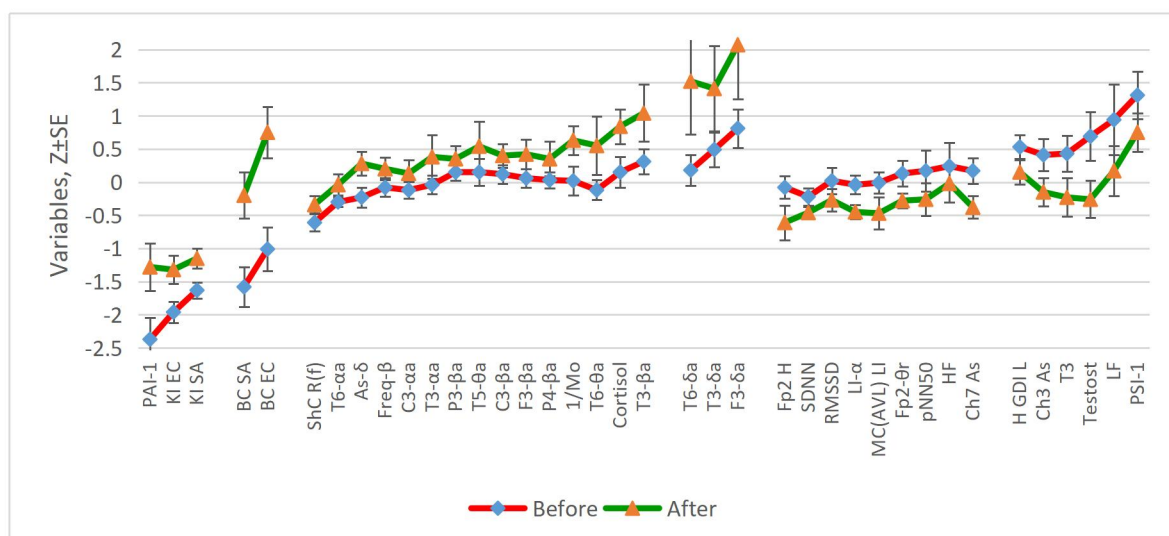
Fig. 8.9. Profiles of variables whose normalized levels (Z±SE) are changing under the influence of the Phytocomposition
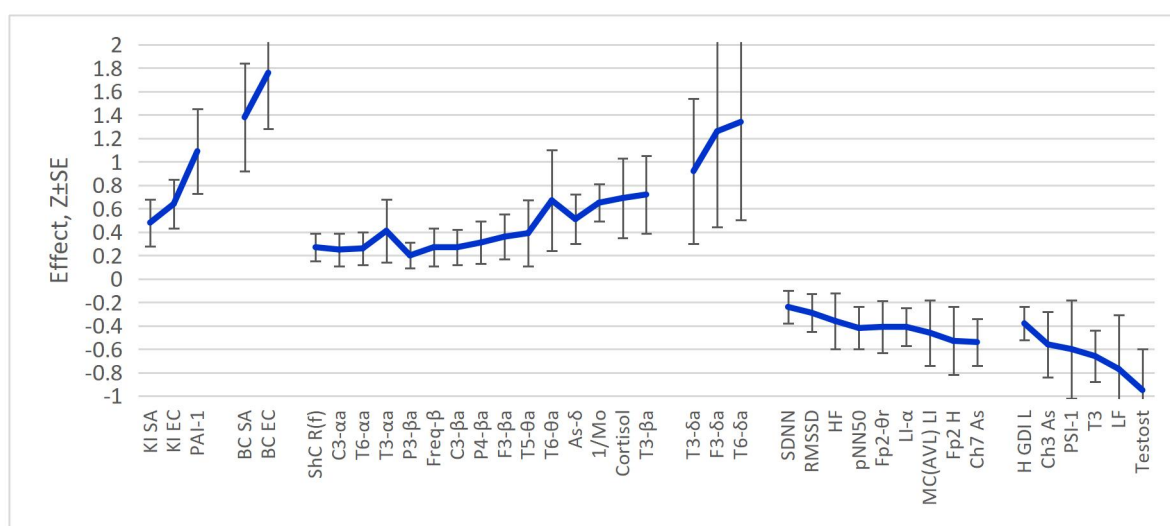
Fig. 8.10. The effects of the Phytocomposition as direct differences of normalized variables (Z±SE)

That is, there is a **normalizing** (ambivalence-equilibratory) effect as one of the attributes of adaptogens according to the good old "law of initial level".

At the same time, **normal** levels of four HRV-markers of vagal tone as well as PSD of θ-rhythm and Entropy in Fp2 locus **also decrease,** albeit slightly. This is accompanied by left lateralization (negative sign of symmetry/lateralization indices) of initially symmetrical (quasi-zero symmetry/lateralization indices) EEG α-rhythm, electrical conductivity of acupuncture points MC(AVL) and virtual seventh Chakra (cluster B0/A0-).

On the other hand, **normal** levels of cortisol and circulating catecholamines (1/Mo as marker) as well as activity of β- and α-rhythm generating neurons **also increase**, albeit slightly. This is accompanied by a rightward shift in the symmetry of δ-rhythm and an increase in Shape Coefficient of GDI in Right projection (SC GDI R) (cluster B0/A0+).

Finally, there is a further increase in the upper limit levels of activity of δ-rhythm generating neurons (cluster B+/A++).

The described changes in parameters of EEG, HRV, hormones and bioelectrophotonics are negatively/positively correlated with the changes in parameters of phagocytosis as well as

of immunity (see please chapters 3-6), so effects of the Phytocomposition are physiologically favorable and therefore adaptogenic.

Thus, unidirectional changes in the symmetry of the third and seventh Chakras, electrical conductivity of acupuncture points MC(AVL) (represent the immune system) and EEG alpha-rhythm as well as opposite changes in the delta-rhythm were found in this study. According to Ayurveda **third** Chakra associated with **celiac plexus ganglion** and **spleen**; **seventh** Chakra - with **right** (paired EEG loci) and upper brain as well as pineal gland [Chase CR, 2018]. Therefore, these parameters of bioelectrophotonics and acupuncture logically fit into the structure of the anti-inflammatory cholinergic reflex.

The materials of the chapter are reflected in the following articles:

1. Gozhenko AI, Sydoruk NO, Babelyuk VYe, Dubkowa GI, Flyunt VR, Hubyts'kyi VYo, Zukow W, Barylyak LG, Popovych IL. Modulating effects of bioactive water Naftussya from layers Truskavets' and Pomyarky on some metabolic and biophysic parameters at humans with dysfunction of neuro-endocrine-immune complex. Journal of Education, Health and Sport. 2016; 6(12): 826-842.
2. Fihura OA, Ruzhylo SV, Żukow X, Popovych IL. Immediate effects of Ukrainian phytocomposition on biophotonics (GDV), EEG and HRV parameters. Journal of Education, Health and Sport. 2021; 11(7): 349-365.
3. Fihura OA, Ruzhylo SV, Popovych IL. Ukrainian adaptogenic phytocomposition "Balm Truskavets'" modulate EEG, HRV and biophotonics (GDV) parameters. Visnyk mors'koï medytsyny. 2022; 2(95): 99-108.
4. Fihura OA, Ruzhylo SV, Korda MM, Klishch IM, Żukow X, Popovych IL. The influence of the Ukrainian phytocomposition "Balm Truskavets'" on parameters of neuro-endocrine-immune complex and biophotonics in humans with maladaptation. Journal of Education, Health and Sport. 2023; 13(1): 326-337.

CHAPTER 9

REACTIONS OF GDV PARAMETERS OF CHILDREN WITH CEREBRAL PALSY TO TREATMENT BY KOZYAVKIN METHOD

One of the important applied aspects of GDV, in our opinion, can be the use of this method to assess the state of the nervous system and hand functions of children with cerebral palsy.

The purpose of this pilot study is to analyze of relationships between caused by Kozyavkin© method changes in the neural component of muscle tome (NCMT) as well as manual functional tests, on the one hand, and parameters of GDV as well as EEG&HRV, on the other hand.

The object of observations were 14 children (6 girls and 8 boys) aged 8÷15 years with Spastic Forms of Cerebral Palsy. Diagnose, Stage, Phase as well as Gross Motor Function Classification System (GMFCS) [Russell DJ et al, 2010] and Manual Ability Classification System (MACS) [Eliasson AC et al, 2006] levels are given in the Table 9.1.

Table 9.1. Clinical characteristics of the observed children

Child	Gender	Age	Diagnose	Stage	Phase	GMFCS	MACS
Hou L	Girl	14	**G80.0 CCP: spastic tetraplegia**	movement by turning	lying to the control head	4	3
Myk	Boy	10	**G80.1 CCP: spastic diplegia**	crawling on their bellies	independent seat	4	3
Pet	Girl	10	**G80.1 CCP: spastic diplegia**	walking on the knees	getting up at the support	4	3
Hou D	Girl	14	**G80.1 CCP: spastic diplegia**	walk with aids	independent seat	3	3
Hav	Boy	10	**G80.1 CCP: spastic diplegia**	walk with aids	rising support near	3	3
Pav	Boy	9	**G80.1 CCP: spastic diplegia**	walk with aids	rising support near	3	2
Boj A	Boy	15	**G80.1 CCP: spastic diplegia**	walk with aids	self-rising	2	2
Boj D	Boy	15	**G80.1 CCP: spastic diplegia**	independent moves	self-rising	2	2
Vor	Boy	9	**G80.1 CCP: spastic diplegia**	independent moves	self-rising	2	2
Kry	Boy	8	**G80.2 CCP: spastic hemiplegia Left**	independent moves	self-rising	2	2
Lan	Girl	12	**G80.2 CCP: spastic hemiplegia Left**	independent moves	rising support near	2	2
Kul	Girl	12	**G80.1 CCP: spastic diplegia**	altenative crawling	independent seat	4	3
Kuch	Girl	13	**G80.1 CCP: spastic diplegia**	walk with aids	rising support near	3	3
Str	Boy	12	**G80.2 CCP: spastic hemiplegia Left**	independent moves	self-rising	1	1

The estimation of hand function carried out by Dynamometry, Box and Block Test and Nine Hole Peg Test.

To measure the strength of the hand we used dynamometer of "Jamar" company. In the study the patient is sitting on chair, or with good fixation on the mother's knees. The hand, which perform measurements, reduced to the torso, arms along the body, elbow bent at right angles, is on the anvil. The instructor explains and demonstrates correct assignment. Conducted 2-3 attempts to adapt and understanding of the task on each hand.

Box and Block Test is a simple, reliable and valid test of hand function. This test was developed Mathiowetz V et al [1985] to assess hand function in adults with cerebral palsy. It is widely used by specialists in physical rehabilitation and ergotherapy. The essence of the test is to determine the number of wooden cubes that patient can shift from one box to the second in a minute. For the test requires a wooden box divided into two parts by a partition height of 15 cm. One half of the box is 150 wooden blocks measuring 1 inch (2,5 cm). Patient explain and show how to rearrange blocks. At the command as soon as the patient begins to shift blocks from one box to the other half. Instructor captures a patient and stops after one minute. First, examine the dominant hand, then rearrange blocks in place and inspect second hand. Registers the number of translated blocks each hand. Time test three to five minutes.

The essence of Nine Hole Peg Test [Poole JL et al, 2005; Wang YC et al, 2011] is to determine how long the patient can turn each hand insert and then remove wooden 9 pegs in 9 holes in the wooden bar. Before the test ergotherapist shows the patient how to do it. At the command as soon as the patient begins to insert wooden plugs into the holes in the wooden bar. Instructor intersect time. At first examined the dominant hand, then the other.

For each test we calculated Laterality Index (LI) using the equation:

LI=100%•(Right - Left)/0,5•(Right + Left).

We registered also Neural, Elastic and Viscous Components of Muscle Tone by device "NeuroFlexor" (Aggero MedTech AB, Sweden). Recent studies have indicated that device is suitable for measurement changes in spasticity during CP treatment [Gäverth J et al, 2013; 2014; Kozyavkin VI et al, 2015; 2015a; Kachmar O et al, 2016].

The next morning in a sitting position we recorded during 7 min electrocardiogram in II lead by hardware-software complex "CardioLab+HRV" ("KhAI-Medica", Kharkiv, Ukraine) to assess the parameters of HRV and simultaneosly EEG for 25 sec using hardware-software complex "NeuroCom Standard" (KhAI Medica) as described above.

The Kirlianogram have been registered by the method of GDV with the use the device "GDV Chamber" ("Biotechprogress", SPb, RF).

After testing children within two weekes received a classic course rehabilitation (a detailed description is provided in the manual [Kozyavkin VI, 2003; Kozyavkin VI et al, 2007; 2012]), then repeated the tests listed.

Digital material is treated by methods factor, cross-correlation and canonical analyses with the use of package of softwares "Statistica-5.5".

In the first stage of data processing, we used a factor analysis to determine the structure of interconnections between registered variables (more precisely, their changes due to treatment) and a place among them changes in GDV variables. It was found that the variance of the information field of the changes in the registered parameters is absorbed by 15 factors (Fig. 9.11). Applying Cattel's method, the number of factors we are limited to six, the total contribution of which in the total dispersion of data is 76%, that is significantly exceeds the required critical level (2/3).
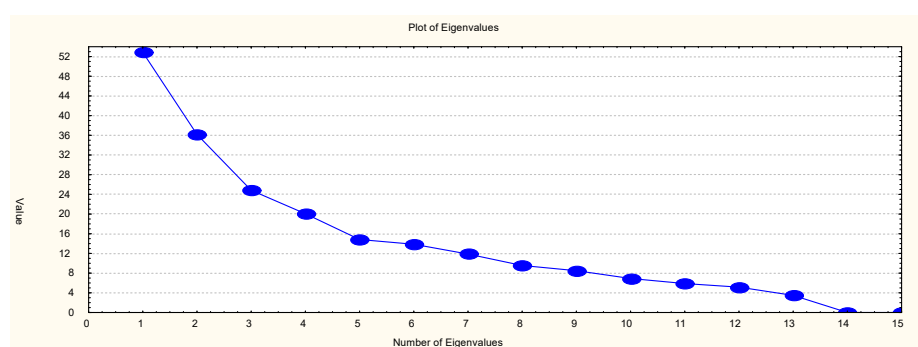

Fig. 9.1. Plot of Eigenvalues for changes in Manual tests, EEG, HRV and GDV

It was revealed (Table 9.2) that the first PC explains 24,2% of the Dispersion and includes changes in **relative** SPD of δ- α- and β-rhythms as well as in Amplitude and Laterality of δ-rhythm. When comparing factor loads from left (odd) and right (pair) loci, it can be seen that in relation to δ-rhythm in Frontalis Anterior, Occipitalis and Frontalis Medialis loci take place Left side Lateralization while in Parietalis, Frontalis Lateralis, Temporalis Anterior and Posterior as well as Centralis loci Lateralization is Right side. Regarding α-rhythm factor loads from Parietalis, Temporalis Anterior and Posterior as well as Frontalis Lateralis loci are also bigger to the right, and from Frontalis Medialis is also bigger to the left. Instead, for Occipitalis and Frontalis Anterior loci take place Right side Lateralization, while for Centralis loci Left side. Regarding β-rhythm Right side Lateralization take place in Temporalis Posterior, Parietalis, Frontalis Lateralis and Anterior as well as Centralis loci while Left side Lateralization in Temporalis Anterior, Occipitalis and Frontalis Medialis loci. It should be noted that the factor loads from δ-rhythm are negative, but positive from α- and β-rhythms.

Table 9.2. Factor Loadings (Equamax normalized). Extraction: Principal Components (Marked loadings are >0,700)

Variables	F1	F2	F3	F4	F5	F6
Fp1-δ SPDR	**-0,981**					
Fp2-δ SPDR	**-0,938**					
O1-δ SPDR	**-0,968**					
O2-δ SPDR	**-0,946**					
F3-δ SPDR	**-0,952**					
F4-δ SPDR	**-0,899**					
P4-δ SPDR	**-0,960**					
P4-δ SPDA	**-0,852**					
F7-δ SPDR	**-0,874**					
F8-δ SPDR	**-0,919**					
T3-δ SPDR	**-0,944**					
T4-δ SPDR	**-0,962**					
T5-δ SPDR	**-0,908**					
T6-δ SPDR	**-0,934**					
C3-δ SPDR	**-0,767**			-0,483		
C4-δ SPDR	**-0,908**					
Amplitude of δ	**-0,830**			0,437		
Laterality of δ	**-0,738**					
P4-α SPDR	**0,948**					
P3-α SPDR	**0,743**					
T4-α SPDR	**0,931**					
T3-α SPDR	**0,753**					
O2-α SPDR	**0,917**					
O1-α SPDR	**0,876**					
T6-α SPDR	**0,905**					
T5-α SPDR	**0,836**					
Fp2-α SPDR	**0,770**					
Fp1-α SPDR	**0,764**					
F8-α SPDR	**0,769**					
C4-α SPDR	**0,880**					
C3-α SPDR	**0,903**					
F4-α SPDR	**0,789**					
F3-α SPDR	**0,841**					
T6-β SPDR	**0,904**					
T5-β SPDR	**0,856**					
P4-β SPDR	**0,901**					
P3-β SPDR	**0,780**			0,429		
F8-β SPDR	**0,869**					
F7-β SPDR	**0,763**					
Fp2-β SPDR	**0,859**					
Fp1-β SPDR	**0,791**					
C4-β SPDR	**0,758**					
T4-β SPDR	**0,845**					
T3-β SPDR	**0,856**					

	C1	C2	C3	C4	C5	C6
O2-β SPDR	0,838					
O1-β SPDR	0,856					
F4-β SPDR	0,762					
F3-β SPDR	0,850					
Frequency of θ	0,672					
C4-θ SPDA		0,941				
C3-θ SPDA		0,784				
C3-θ SPDR		0,696				0,500
P4-θ SPDA		0,881				
P3-θ SPDA		0,741				
Fp2-θ SPDA		0,812				
Fp1-θ SPDA		0,720				
O2-θ SPDA		0,829				
O1-θ SPDA		0,894				
F4-θ SPDA		0,831				
F3-θ SPDA		0,844				
T3-θ SPDA		0,825				
T5-θ SPDA		0,819				
Amplitude of θ		0,791				
C4-α SPDA		0,909				
C3-α SPDA		0,837				
Fp2-α SPDA		0,850				
P4-α SPDA		0,846				
P3-α SPDA		0,831				
T3-α SPDA		0,873				
F4-α SPDA		0,839				
F3-α SPDA		0,862			0,418	
O1-α SPDA		0,751				
Amplitude of α		0,734				
C4-δ SPDA	-0,418	0,784				
Box&Block LI	-0,468	0,554				
VLF/TP		-0,515				-0,438
Entropy L GDI f		-0,435				
Baevskiy Stress Ind			0,953			
AMo/ΔX			0,865			
AMo			0,843			
Heart Rate			0,833			
Baevskiy ARS Ind			0,777			
MxDMn			-0,952			
SDNN			-0,934			
TINN			-0,906			
Total Power HRV			-0,819			
SP LF HRV			-0,772			
SP VLF HRV			-0,756			
Mode HRV			-0,745			
RMSSD			-0,651			0,417
Entropy F GDI f			0,710			
Shape C L GDI f			0,684			
Shape C R GDI			0,626		0,492	
Shape C F GDI f				0,869		
Area F GDI				-0,623	-0,426	
F8-β SPDA				0,855		
O1-β SPDA		0,438		0,697		
F7-δ SPDA	-0,659			0,659		
Frequency of δ	0,507			-0,679		
Viscous CMT				0,810		
Elastic CMT				0,528		
Neural CMT				-0,332		-0,299
Entropy R GDI					0,833	
Symmetry GDI					-0,702	
Area L GDI					-0,595	
O2-β SPDA					0,799	
Fp1-β SPDA					0,723	
T4-β SPDA			0,429		0,689	
Amplitude of β				0,412	0,687	
LF/TP					-0,737	
Dynamometry LI					0,421	
9-Hole Peg LI					0,244	

Deviation of θ						**-0,836**
Index of θ						**-0,743**
T3-θ SPDR		0,439				**0,628**
F7-θ SPDR				-0,462		**0,585**
F3-θ SPDR		0,445				**0,585**
HF/TP		0,593				**0,718**
(VLF+LF)/HF	-0,400					**-0,691**
LFnu HRV		-0,519			-0,413	**-0,676**
LF/HF HRV	-0,466					**-0,658**
ULF/TP						**-0,613**
Dynamometry L						**0,725**
Box&Block L					0,349	**0,720**
Box&Block R					0,351	**0,655**
9-Hole Peg R			-0,492			**-0,602**
9-Hole Peg L					-0,336	**-0,591**
Dynamometry R					0,296	**0,592**
Symmetry GDI f	-0,482					**-0,688**
Area R GDI	-0,533					**-0,617**
Entropy R GDI f						**-0,536**
Area F GDI f	-0,463					**-0,509**
Area L GDI f			0,416		0,360	**-0,505**
Area R GDI f			0,402			**-0,491**
Shape C R GDI f	0,426					**0,558**
Shape C F GDI			0,445		0,356	**0,466**
Shape C L GDI					0,312	**0,430**
Explained Variance	51,8	32,3	24,6	19,9	16,2	17,7
Proportion of Total	0,242	0,151	0,115	0,093	0,076	0,083

The second PC absorbs 15,1% of the Variance and includes changes in **absolute** (A) SPD of θ- and α-rhythms as well as their Amplitudes. If desired, it is easy to detect lateralization of loads from individual loci. Attention is drawn to the lack of loads from θ-rhythm in Frontalis Lateralis loci as well as from α-rhythm in Frontalis Lateralis and Temporalis Posterior loci. At the same time, there is a factor load, albeit insignificant, from the changes in Lateralisation of Box&Block test as well as **relative** SP VLF band HRV and **Entropy of GDI in Left projection**, which gives an idea of the relationships between the changes in these parameters.

The third PC explains 11,5% of the Dispersion, getting the maximum load exactly from the changes in Baevskiy's Stress Index as integral characteristics of sympathetic, vagal and humoral outflows on heart rate. Slightly less positively load gives AMo/ΔX ratio as marker of Sympatho/Vagal balance and Baevskiy's Activity of Regulatory Systems Index as integral characteristics of their strain as well as Amplitude of Moda and Heart Rate as markers of Sympathetic outflows while negatively load gives nine HRV markers of Parasympathetic outflows. Interestingly, the changes in 3 **parameters of the GDV** are also loaded on the same PC, which again suggests their connection with changes in parameters of the HRV.

The changes in components of muscle tone give a loads on the fourth PC only, which explains only 9,3% of the Variance. Contrary to expectations, the significant load is given by the **Viscous component**, while by the **Neural component** it is minimal. The changes in components of muscle tone associated with changes in some **parameters of GDV** and EEG.

The fifth PC explains 7,6% of the Dispersion, getting the significant loads from changes in parameters of both **GDV** and EEG&HRV, but insignificant loads from changes in Laterality of Dynamometry and 9-Hole Peg test.

Instead, the sixth PC receives significant factor loads from changes in the **functional tests of hands**. It is important to note that these changes are accompanied by concordant changes in SPD of θ-rhythm in Left Temporalis Anterior, Frontalis Lateralis and Medialis loci as well as in Vagal tone while discordant changes in markers of Sympathetic tone as well as Deviation and Index of θ-rhythm. Regarding parameters of GDV found concordant changes in **Shape Coefficients of GDI** while discordant changes in **Symmetry, Area and Entropy of GDI**.

At the second stage of factor analysis, a correlation matrix for oblique factors was obtained, which was subjected to further analysis in order to distinguish the set of orthogonal factors that divide the variability in the variables into that relating to the general dispersion (Secondary factors) and to the individual dispersions belonging to the clusters or similar variables (Primary factors) (Table 9.3).

Table 9.3. Secondary & Primary (Unique) Factor Loadings
Marked loadings are >,700

Variables	S1	S2	P1	P2	P3	P4	P5	P6
LFnu	-,668							,512
HF/TP	,610							-,568
LF/HF	-,468							,539
(VLF+LF)/HF	-,459							,576
F3-α SPDA	,524			**,720**				
Amplitude of α	,516			,598				
T4-α SPDA	,507			,582				
F4-α SPDA	,481			**,699**				
Fp1-α SPDA	,480			,563				
C4-β SPDA	,524						,510	
F3-β SPDA	,481						,569	
C4-θ SPDR	,459			,472				
T4-θ SPDR	,438		,452					
Box&Block R	,515							-,529
Box&Block L	,405							-,615
9-Holy Peg R	-,368				-,489			,510
9-Holy Peg L	-,344							,503
Entropy GDI R	,495						,715	
Symmetry GDI f	-,433							,577
Area GDI R	-,413		-,468					,510
Fp1-δ SPDA		,570	-,478			-,459		
Amplitude of δ		,561	-,710					
T6-δ SPDA		,549						
F7-δ SPDA		,526	-,544			-,556		
O2-δ SPDA		,522						
T6-θ SPDA		,530						
F8-θ SPDA		,514	-,498	,537				
F7-α SPDR	-,562	,523						
F8-α SPDR	-,511	,643						
AMo HRV		-,422			,781			

It seems that the **favorable** changes in B&B and 9-HP tests (increasing the number of transmitted blocks for a fixed time and accelerating the performance of the second test) are due to a **decrease** in the sympathetic tone and **increased** tone of the vagus as well as the Amplitude and SPD of the α-rhythm in the Left&Right Frontalis Medialis, Right Temporalis Anterior and Left Frontalis Anterior loci, β-rhythm in Right Centralis and Left Frontalis Medialis loci as well as θ-rhythm in Right Centralis and Temporalis Anterior loci. This is accompanied by an **increase** in **Entropy** and a **decrease** in the **Area of GDI in Right projection** as well as its **Symmetry**. In addition, judging by the signs of the loads on the second Secondary factor, a favorable **decrease** in sympathetic tone is accompanied by an **increase** in Amplitude and SPD of the δ-rhythm in Left Frontalis Anterior and Medialis and Right Temporalis Anterior and Occipitalis loci as well as θ-rhythm in Right Temporalis Posterior and Frontalis Lateralis loci while an **decrease** in SPD of the α-rhythm in the Left&Right Frontalis Lateralis loci.

Let's see if the results of **factor** analysis are confirmed by the results of **correlation** analysis. For a sample of 14 observations critical value of correlation coefficient module |r| at p<0,05 (t>2,14) is **0,54**, at p<0,01 (t>2,98) is **0,70**, at p<0,001 (t>4,14) is **0,84**. Nevertheless, in regressive models with step-by-step exclusion, there were separate variables with the values |r| less than critical level whereas some variables with meaningful modules were not included in the models.

Now detail the interactions between changes in manual tests and GDV parameters. But first let's go back to discuss about the argument and function. If we adopt the paradigm of Occidental (Western) medicine, then changes in photoelectron emission of the skin should be interpreted as a result of neuroendocrine effects on metabolism. Instead, from the standpoint of the paradigm of Oriental medicine, photoelectronic emission characterizes the state of Chakras as energy centers that control nervous, endocrine and other systems. We will consider GDV parameters as arguments (cause), while manual tests as a function (effect).

Already after a quick glance at the correlation matrix (Table 9.4), it seems that the favorable changes in the manual functions are accompanied by a **decrease**, first of all, in the Entropy of the GDI in Right projection recorded through the filter (f) as well as its Symmetry and Area in Frontal and Left projections, on the one hand, instead of an **increase** in Entropy in the same projection without a filter, and also in other projections (Fig. 9.2) and in Shape Coefficients of GDI, on other hand.

Table 9.4. Correlation matrix for changes in parameters of Manual Function and GDV

| Variables	B&B R	B&B L	9-HP R	9-HP L	D R	D L	NCMT L	Mean |r|
Entropy R f	**-,57**	-,34	**,58**	,46	**-,64**	**-,75**	**,58**	**0,560**
Symmetry f	-,31	-,43	,40	,28	-,24	-,41	,41	**0,354**
Symmetry	-,42	-,44	,12	,51	-,44	-,12	-,23	**0,326**
Area F	-,42	-,48	,51	,33	,00	-,18	,41	**0,333**
Area L	-,25	-,50	,37	,26	-,10	-,24	,21	**0,276**
Entropy F f	**,64**	,49	**-,60**	-,52	,50	,37	-,29	**0,487**
Shape Coef R	,52	,52	-,36	**-,61**	,52	,26	-,02	**0,401**
Entropy L f	,35	,51	-,42	-,52	,20	,37	-,42	**0,399**
Entropy R	**,62**	**,60**	-,37	-,52	,37	,12	-,08	**0,383**
Shape Coef F	,48	,50	-,35	-,51	,50	,29	,05	**0,383**
Entropy F	,38	,22	-,21	-,34	,50	,09	-,03	**0,253**

dBBR = 2,3 + 17,6*dEFf
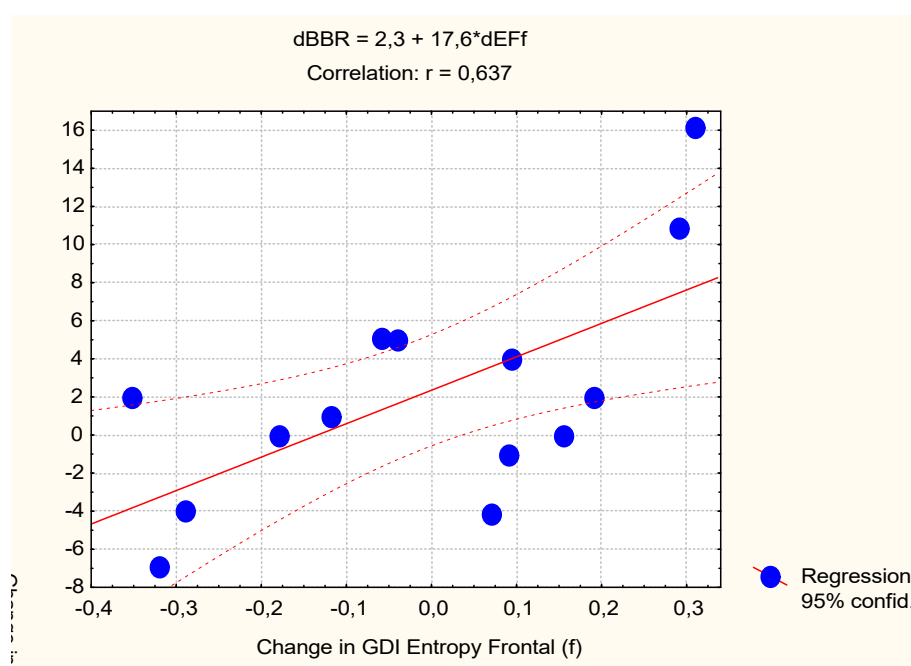
Correlation: r = 0,637

Fig. 9.2. Scatterplot of correlation between changes in Entropy of GDI in Frontal projection with filter (line X) and Box&Block test for Right hand (line Y)

We give no comments regressive models for changes in manual tests (Tables 9.5-9.10 and Figures 9.3-9.10).

Table 9.5. Regression Summary for change in Dependent Variable: Box&Block test for Right hand

R=0,840; R²=0,706; Adjusted R²=0,618; $F_{(3,1)}$=8,0; p=0,005; SE of estimate: 3,7 blocks/min

| Change in Independent Variables	r	Beta	St. Err. of Beta	B	St. Err. of B	$t_{(10)}$	p-level
			Intercpt	2,38	1,12	2,12	,060
Entropy F f	**0,64**	,347	,201	9,57	5,54	1,73	,115
Entropy R	**0,62**	,387	,198	12,03	6,15	1,96	,079
Entropy R f	**-0,57**	-,437	,176	-25,35	10,21	-2,48	,032
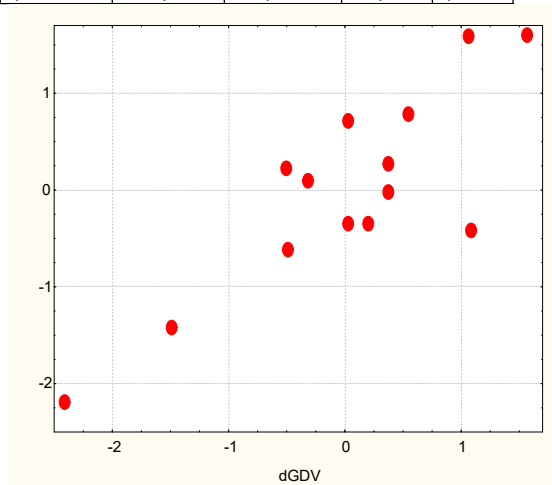
R=0,840; R²=0,706; $\chi^2_{(3)}$=12,9; p=0,005; Λ Prime=0,294

Fig. 9.3. Scatterplot of canonical correlation between changes in parameters of GDV (line X) and Box&Block test for Right hand (line Y)

Table 9.6. Regression Summary for change in Dependent Variable: Box&Block test for Left hand

R=0,680; R²=0,462; Adjusted R²=0,364; $F_{(2,1)}$=4,7; p=0,033; SE of estimate: 2,9 blocks/min

Change in Independent Variables	r	Beta	St. Err. of Beta	B	St. Err. of B	$t_{(11)}$	p-level
			Intercpt	1,81	,85	2,14	,056
Entropy L f	0,51	,485	,222	9,46	4,32	2,19	,051
Area F, pixels	-0,48	-,447	,222	-,00043	,00021	-2,02	,069
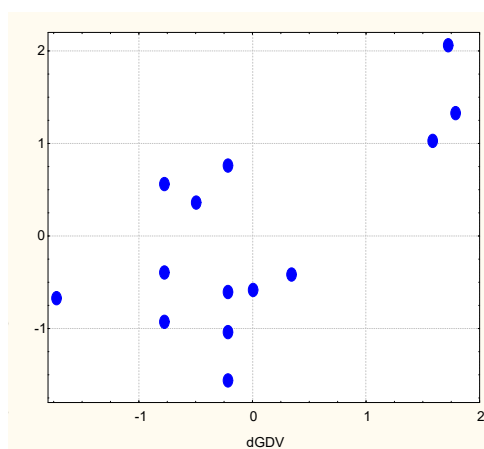
R=0,680; R²=0,462; $\chi^2_{(2)}$=6,8; p=0,033; Λ Prime=0,538

Fig. 9.4. Scatterplot of canonical correlation between changes in parameters of GDV (line X) and Box&Block test for Left hand (line Y)
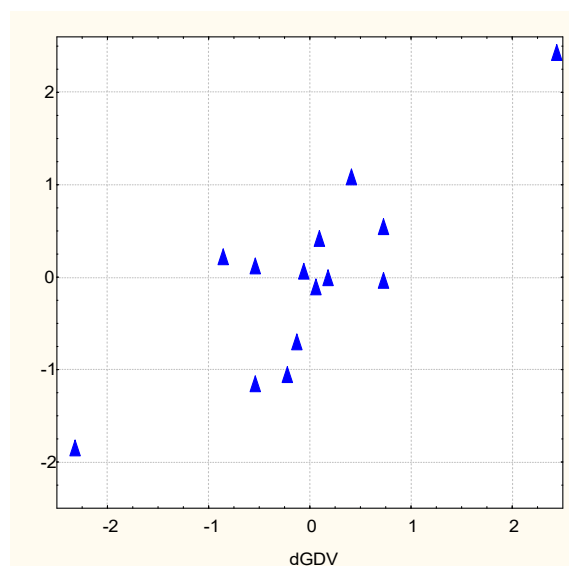

d 9-hPR = -6,9 - 120,1*dEFf

Correlation: r = -0,599

Change in GDI Entropy Frontal (f)
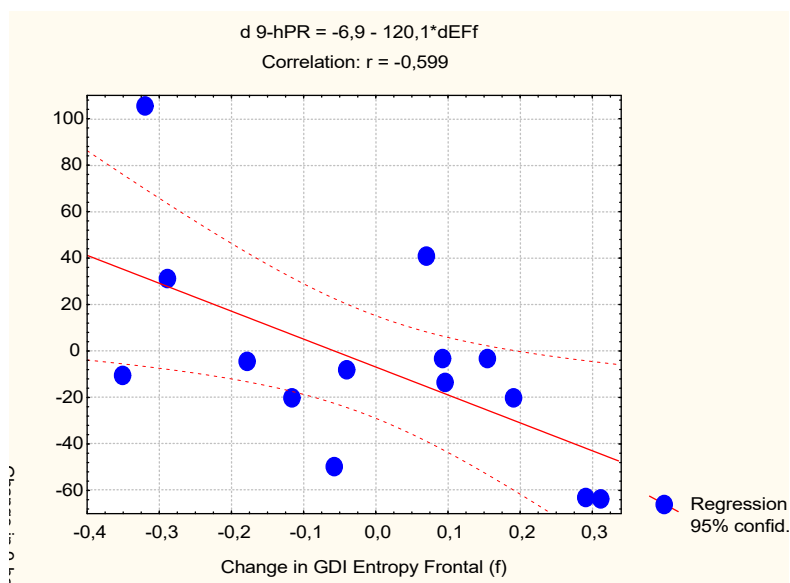
Fig. 9.5. Scatterplot of correlation between changes in Entropy of GDI in Frontal projection with filter (line X) and 9-Hole Peg test for Right hand (line Y)

Table 9.7. Regression Summary for change in Dependent Variable: 9-Hole Peg test for Right hand

R=0,824; R^2=0,679; Adjusted R^2=0,583; F$_{(3,1)}$=7,1; p=0,008; SE of estimate: 28 sec

Change in Independent Variables	r	Beta	St. Err. of Beta	B	St. Err. of B	t$_{(10)}$	p-level
			Intercpt	-11,47	8,00	-1,43	,182
Entropy F f	**-0,60**	-,456	,185	-91,4	37,1	-2,46	,033
Entropy R f	**0,58**	,399	,187	168,7	79,2	2,13	,059
Area F, pixels	0,51	,346	,185	,0039	,0021	1,87	,091

dGDV
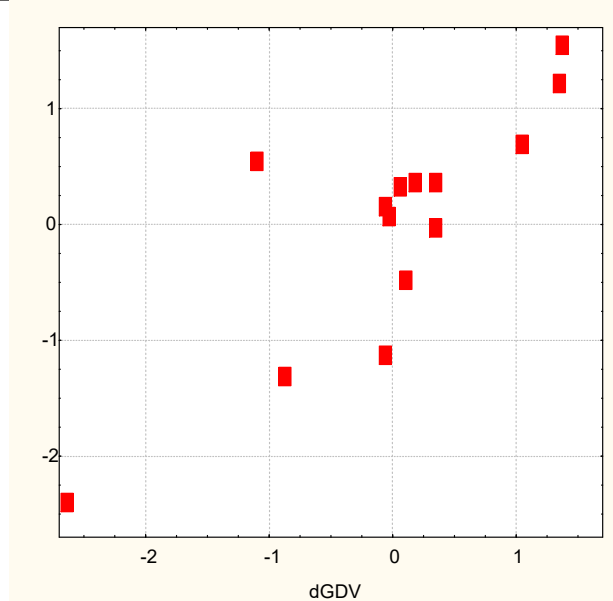
R=0,824; R^2=0,679; $\chi^2_{(3)}$=11,9; p=0,008; Λ Prime=0,321

Fig. 9.6. Scatterplot of canonical correlation between changes in parameters of GDV (line X) and 9-Hole Peg test for Right hand (line Y)

Table 9.8. Regression Summary for change in Dependent Variable: 9-Hole Peg test for Left hand

R=0,637; R^2=0,405; Adjusted R^2=0,297; F$_{(2,1)}$=3,7; p=0,057; SE of estimate: 44 sec

Change in Independent Variables	r	Beta	St. Err. of Beta	B	St. Err. of B	t$_{(11)}$	p-level
			Intercpt	-5,5	13,5	-0,40	,694
Entropy L f	-0,52	-,406	,244	-113,3	68,2	-1,66	,125
Symmetry, %	0,51	,383	,244	7,8	5,0	1,57	,145
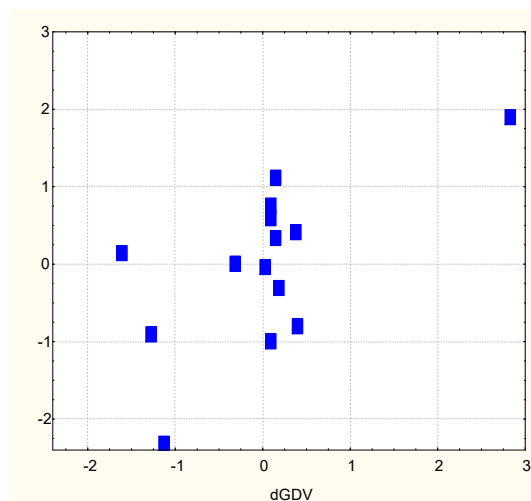
R=0,637; R^2=0,405; χ^2$_{(2)}$=5,7; p=0,057; Λ Prime=0,598

Fig. 9.7. Scatterplot of canonical correlation between changes in parameters of GDV (line X) and 9-Hole Peg test for Left hand (line Y)

Table 9.9. Regression Summary for change in Dependent Variable: Dynamometry for Right hand

R=0,848; R^2=0,719; Adjusted R^2=0,668; F$_{(2,1)}$=14,1; p=0,0009; SE of estimate: 3,3 kG

Change in Independent Variables	r	Beta	St. Err. of Beta	B	St. Err. of B	t$_{(11)}$	p-level
			Intercpt	4,38	,94	4,68	,001
Entropy R f	**-0,64**	-,668	,160	-37,1	8,9	-4,17	,002
Shape Coef R	0,52	,552	,160	1,34	,39	3,45	,005
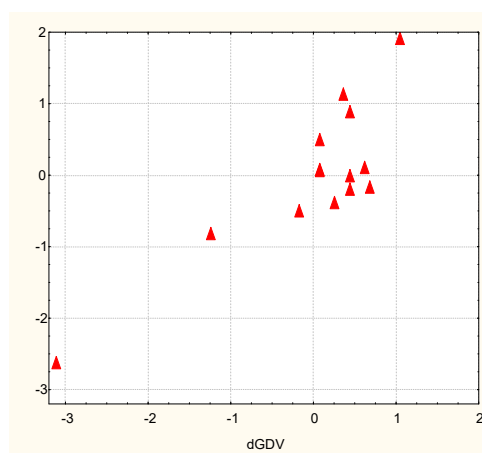
R=0,848; R^2=0,719; χ^2$_{(2)}$=14,0; p<10^{-3}; Λ Prime=0,281

Fig. 9.8. Scatterplot of canonical correlation between changes in parameters of GDV (line X) and Dynamometry for Right hand (line Y)
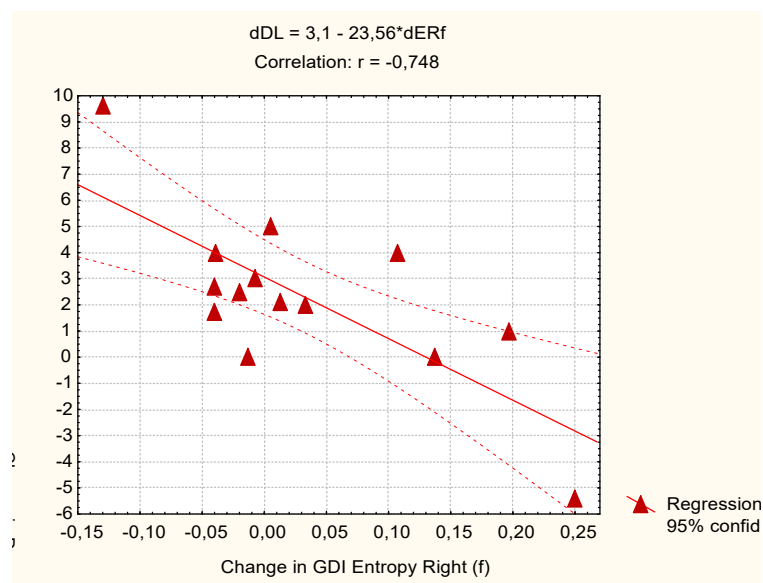
Fig. 9.9. Scatterplot of correlation between changes in Entropy of GDI in Right projection with filter (line X) and Dynamometry for Left hand (line Y)

Table 9.10. Regression Summary for change in Dependent Variable: Dynamometry for Left hand

R=0,842; R^2=0,709; Adjusted R^2=0,622; $F_{(3,1)}$=8,1; p=0,005; SE of estimate: 2,0 kG

Change in Independent Variables	r	Beta	St. Err. of Beta	B	St. Err. of B	$t_{(10)}$	p-level
			Intercpt	3,35	,60	5,60	,0002
Entropy R f	**-0,75**	-,651	,181	-20,5	5,7	-3,60	,0048
Symmetry f, %	*-0,41*	-,232	,181	-,28	,22	-1,28	,2288
Entropy L f	*0,37*	,342	,172	5,89	2,96	1,99	,0743

R=0,842; R^2=0,709; $\chi^2_{(3)}$=13,0; p=0,005; Λ Prime=0,291

Fig. 9.10. Scatterplot of canonical correlation between changes in parameters of GDV (line X) and Dynamometry for Left hand (line Y)

According to the outcome of the canonical analysis, the maximum **negative** (here, absolutely unnecessarily, the mathematical sign reflects just the **adverse** effect) factor load on

the root of the changes in GDV gives Entropy of GDI in Right projection registered **with the filter.** Instead, Entropy, registered in the same projection **without a filter**, as well as in the Frontal and Left projections **with the filter,** give **positive (favorable)** factor loads. (Table 9.11). Taken together, changes in GDV parameters determine changes in hand function parameters by 95% (Fig. 9.11).

Table 9.11. Factor Structure for changes in parameters of GDV (left set) and Manual Function (right set)

Left set	R
Entropy R f	**-,768**
Entropy F f	**,446**
Shape Coef R	**,368**
Entropy L f	**,260**
Entropy R	**,107**
Area F	**-,008**
Right set	**R**
D R	,898
D L	,866
9-HP L	-,657
9-HP R	-,494
B&B R	,523
B&B L	,352
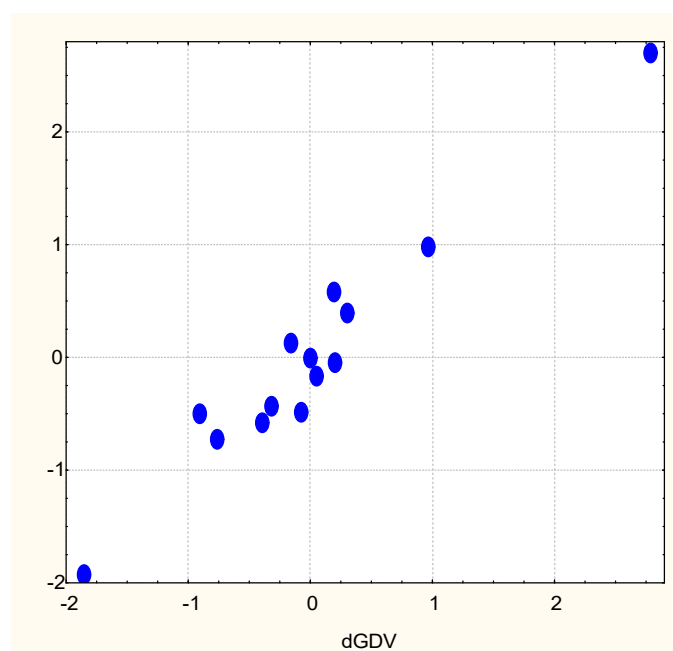
R=0,974; R^2=0,949; $\chi^2_{(36)}$=53; p=0,035; Λ Prime=0,0003

Fig. 9.11. Scatterplot of canonical correlation between changes in parameters of GDV (line X) and Functional tests for both hands (line Y)

Our data are not entirely consistent with the statement Korotkov KG [2001; 2007; 2014] that GDI, taken off **without** filter, characterizes the **current** (functional) vegetative status and psychophysiological condition of organism while registered **with** a filter characterizes vegetative regulation at the level of **stable** (organic) physiological processes.

The same applies also to the role of changes in Entropy in changes in Neural Component of Muscle Tone (Table 9.12 and Fig. 9.11). Now our data on an example of changes in

Symmetry of GDI confirm the position on the normality of asymmetry and abnormality of symmetry.

Table 9.12. Regression Summary for change in Dependent Variable: Neural Component of Muscle Tone for Left hand

R=0,746; R²=0,556; Adjusted R²=0,423; $F_{(3,1)}$=4,2; p=0,037; SE of estimate: 5,9 Newtons

Change in Independent Variables	r	Beta	St. Err. of Beta	B	St. Err. of B	$t_{(10)}$	p-level
			Intercpt	-5,93	1,75	-3,39	,007
Entropy R f	**0,58**	,458	,223	34,2	16,6	2,05	,067
Symmetry f, %	*0,41*	,294	,223	,83	,63	1,32	,218
Entropy L f	*-0,42*	-,407	,212	-16,6	8,6	-1,92	,084
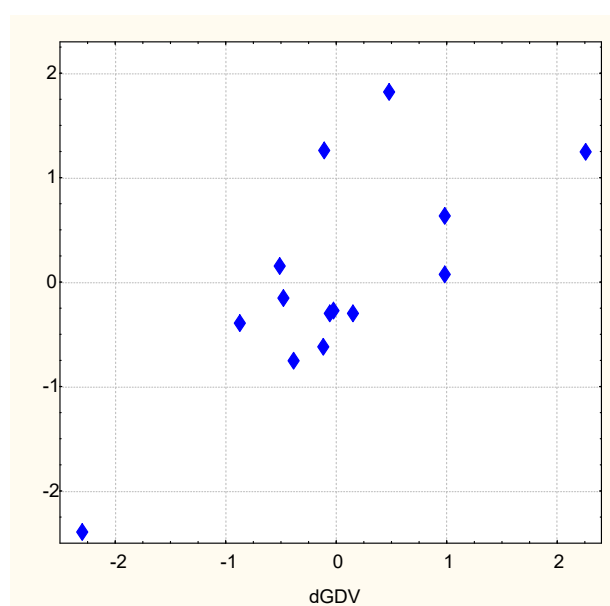
R=0,746; R²=0,556; $\chi^2_{(3)}$=8,5; p=0,036; Λ Prime=0,444

Fig. 9.12. Scatterplot of canonical correlation between changes in parameters of GDV (line X) and Neural Component of Muscle Tone of Left hand (line Y)

Now we present new evidence of the interrelationships between changes in GDV parameters, on the one hand, and HRV and EEG parameters, on the other hand.

Regarding HRV, the following is revealed (Table 9.13 and 9.14, Fig. 9.13).

Table 9.13. Correlations between changes in GDV and HRV parameters

Variables	Entropy F f	Shape Coef R	Entropy L f	Entropy R f	Symmetry	Area F
VLF	**-,70**	*-,39*	*-,33*	*,39*	*-,13*	*,29*
ULF	-,45	**-,65**	*-,30*	*,19*	*,50*	*-,12*
LF	**-,59**	*-,35*	*-,25*	*,24*	*-,07*	**,54**
LF/(LF+HF)	*-,23*	*-,28*	*,09*	*,52*	*,42*	*,45*
HF/TP	*,46*	*,40*	*,04*	**-,54**	*-,34*	*-,25*
HF	*,15*	*,15*	*,02*	*-,29*	*-,41*	*,19*

Table 9.14. Factor Structure for changes in GDV (left set) and HRV (right set)

Left set	R
Entropy F f	**,939**
Shape Coef R	**,692**
Entropy L f	**,642**

Entropy R f	**-,407**
Symmetry	**-,364**
Area F	**-,035**
Right set	**R**
VLF	**-,650**
ULF	**-,543**
LF	**-,461**
LF/(LF+HF)	**-,248**
HF/TP	**,491**
HF	**,264**
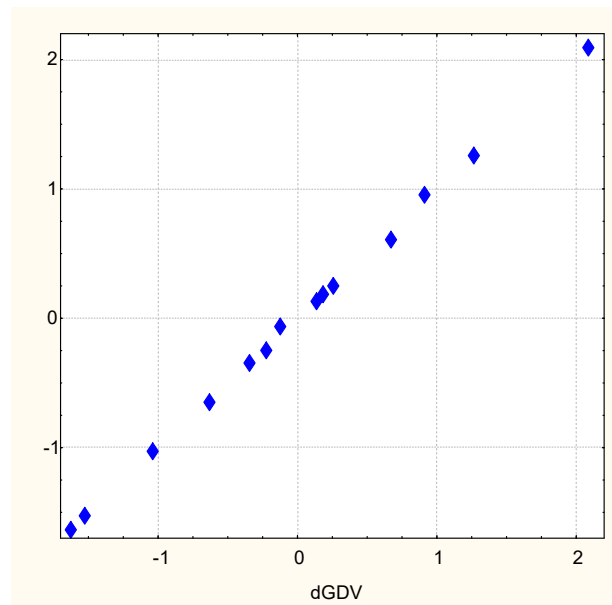
$R = 0,9996$; $R^2 = 0,999$; $\chi^2_{(36)} = 75$; $p = 10^{-4}$; Λ Prime $< 10^{-5}$

Fig. 9.13. Scatterplot of canonical correlation between changes in parameters of GDV (line X) and HRV (line Y)

As you can see, there is a very strong dependence between changes in vagal and sympathetic tones as well as circulating cathecholamines level, on the one hand, and in GDV parameters, on the other hand.

With regard to EEG, the canonical correlation coefficient is also close to 1, but the factor structure for GDV includes only three variables from the six previous ones (Table 9.15 and 9.16, Fig. 9.14).

Table 9.15. Correlations between changes in GDV and EEG parameters

Variables	Area F	Entropy F f	Entropy R f
T4-β SPDA	**-,55**	*,47*	*,08*
Asymmetry θ	-,45	*,45*	*,03*
F4 Entropy	,46	*-,26*	*-,06*
F8-α SPDA	-,43	*,23*	*-,23*
Fp1 Entropy	,44	*,11*	*,10*
Index θ	*,20*	*-,30*	**,54**
T3-β SPDR	*,14*	*-,39*	,46
Laterality α	*-,16*	*-,01*	**-,60**
T6 Entropy	*,15*	*,14*	**,61**

Table 9.16. Factor Structure for changes in GDV (left set) and EEG (right set) parameters

Left set	R
Area F	**,930**
Entropy R f	**,183**
Entropy F f	**-,494**
Right set	**R**
T4-β SPDA	**-,672**
Asymmetry θ	**-,574**
F8-α SPDA	**-,446**
Laterality α	**-,078**
F4 Entropy	**,508**
Fp1 Entropy	**,337**
Index θ	**,235**
T3-β SPDR	**,228**
T6 Entropy	**,016**
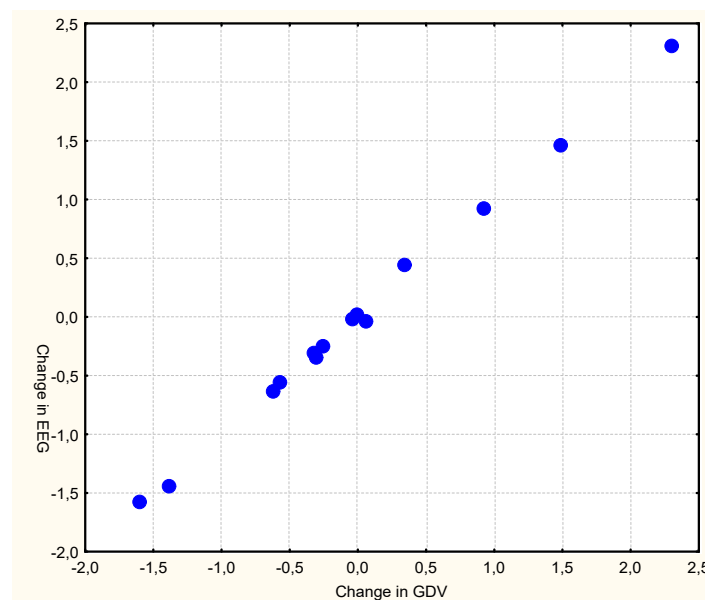
R=0,9989; R^2=0,998; $\chi^2_{(27)}$=68; p=10^{-4}; Λ Prime<10^{-4}

Fig. 9.14. Scatterplot of canonical correlation between changes in parameters of GDV (line X) and EEG (line Y)

The preliminary analysis revealed the ambiguity of the responses of hand function parameters to the course of treatment. Ago was carried out Cluster analysis of changes in hand function. Use of Cluster analysis makes possible the simultaneous consideration of all the signs. Considering the totality of characteristics of persons undertaken in their relationship and conditionality of some of these (derivatives) other (main determinants) allows as to make a natural classification that reflects the nature of things, their essence. It is believed that knowledge of the essence of the object is to identify those of its quality properties that actually define the object, distinguish it from other. Clustering cohort of persons is realized by iterative k-means method. In this method, the object belongs to the class Euclidean distance to which is minimal. The main principle of the structural approach to the allocation of uniform groups consists in the fact that objects of same class are close but different classes are distant.

In other words, a cluster (the image) is an accumulation of points in n-dimensional geometric space in which average distance between points is less than the average distance from the data points to the rest points [Aldenderfer MS&Blashfield, 1985; Mandel ID, 1986].

Clusters appeared clearly delineated, as evidenced by the ratio between Distances from Respective Cluster Center (Table 9.17) and Euclidean Distances between Clusters (40,5).

Table 9.17. Cluster Analysis Summary.
Members of Cluster N1 and Distances from Respective Cluster Center

	Kuc	Kul	Str
Distance	10,3	6,91	16,8

Members of Cluster N2 and Distances from Respective Cluster Center

	Hav	Pav	Vor	Lan	HL	Kry	Pet	Myk	HD	BA	BD
Distance	17,8	44,8	9,23	2,32	4,30	5,49	9,64	6,37	7,21	9,27	8,62

It is stated (Table 9.18) that members of the major cluster due to the course of rehabilitation increases the speed of manipulation of objects with both hands, as well as their strength (D). This is combined with a decrease in the neural component of the muscle tone (NCMT) of the left hand in the absence of changes in the viscous and elastic components.

Table 9.18. Cluster Analysis Summary. Changes in Hand Function and Analysis of Variance

Changes in Variables	Cluster No. 1 (3)	Cluster No. 2 (11)	Betwe-en SS	Within SS	η^2	R	F	p
BB Left, blocks/min	-4,9±0,2	+2,9±0,6	140,6	38,6	0,784	0,886	43,7	$<10^{-4}$
NHP Right, sec	+63±23	-23±7	16214	8839	0,647	0,804	22,0	$<10^{-3}$
NHP Left, sec	+66±7	-21±13	18027	18753	0,490	0,700	11,5	,005
BB Right, blocks/min	-5,0±1,0	+4,1±1,6	195,9	277,1	0,414	0,644	8,5	,013
D Left, kG	-0,4±2,5	+3,0±0,8	27,76	111,65	0,199	0,446	3,0	,110
Viscous CMT, Newtons	-0,36±0,06	+0,12±0,14	0,546	2,24	0,196	0,443	2,9	,113
Neural CMT, Newtons	+1,7±5,8	-5,2±2,0	115,4	663,5	0,148	0,385	2,1	,174
Elastic CMT, Newtons	+1,4±0,4	+1,2±0,9	,115	90,25	0,001	0,040	0,02	,904
D Right, kG	+3,1±3,8	+3,5±1,8	0,39	432,2	0,001	0,030	0,01	,918

Notes.

$\eta^2 = Sb^2/(Sb^2 + Sw^2)$; $R = \eta$; $F = [Sb^2(n-k)]/[Sw^2(k-1)]$, where
Sb^2 is Between Variance; Sw^2 is Within Variance; n is number of persons (14);
k is number of groups-clusters (2).

Thus, in 11 children, functional changes are clearly favorable. Instead, in three children, the D and NCMT indices have changed uncertainly, and speed tests, unfortunately, have deteriorated, that is, it should be noted that adverse changes in the hands functions. Interestingly, this was accompanied by a negligible but statistically significant decrease in viscous and elastic components of the muscle tone.

In the second stage carried out Analysis of Variance and ranking variables for coefficient η^2. It was found that the largest contribution to the distribution of clusters gives the BB test of the left hand and the NHP test of the right hand, while the contributions of the elastic CMT and the right-hand dynamometry are worthless.

In the third stage carried out Discriminant analysis (method forward stepwise). This analysis is applied in order to identify exactly those indicators of the functions of hands, in which the clusters essentially differ from each other. Contrary to the expectation inspired by the results of the dispersion analysis, the program included a discriminant model of the

change of D of the right hand, whereas the analogue index of the left hand was out of the model (Table 9.19). This indicates that the discriminant (distinctive) sign is not the average value, but the variance of this variable, as well as its Laterality.

Table 9.19. Discriminant Function Analysis Summary. Changes in Hand Function

Step 6, N of vars in model: 6; Grouping: 2 grps; Wilks' Λ: 0,0131; approx. $F_{(7,6)}=65$; $p<10^{-5}$

Variables currently in the model	Unfavorable changes (3)	Favorable changes (11)	Wilks' Λ	Parti-al Λ	F-re-move	p-level	Tole-rancy
BB Left, blocks/min	-4,9±0,2	+2,9±0,6	,094	,139	37,1	,001	,094
NHP Right, sec	+63±23	-23±7	,013	,979	,1	,733	,019
NHP Left, sec	+66±7	-21±13	,020	,664	3,0	,132	,008
BB Right, blocks/min	-5,0±1,0	+4,1±1,6	,036	,366	10,4	,018	,036
D Right, kG	+3,1±3,8	+3,5±1,8	,089	,148	34,6	,001	,022
D Laterality, %	+19±15	0±5	,027	,492	6,2	,047	,064
NHP Laterality, %	+1±27	0±15	,015	,854	1,0	,350	,013
Variables currently not in the model			Wilks' Λ	Parti-al Λ	F to enter	p-level	Tole-rancy
D Left, kG	-0,4±2,5	+3,0±0,8	,012	,885	,652	,456	,004
Neural CMT, N	+1,7±5,8	-5,2±2,0	,013	,967	,170	,697	,485
Viscous CMT, N	-0,36±0,06	+0,12±0,14	,012	,941	,312	,600	,792
Elastic CMT, N	+1,39±0,40	+1,17±0,90	,013	1,000	,002	,968	,586
BB Laterality, %	-0,4±3,2	+4,5±6,7	,013	1,000	,001	,971	,026

Next, the 6-dimensional space of discriminant variables transforms into one-dimensional space of a canonical discriminant function (canonical root), which is a linear combination of discriminant variables. The discriminating (differentiating) ability of the root characterizes the canonical correlation coefficient (r*) as a measure of connection, the degree of dependence between groups and a discriminant function.

Table 9.20 presents raw (actual) and standardized (normalized) coefficients for discriminant variables. The raw coefficient gives information on the absolute contribution of this variable to the value of the discriminative function, whereas standardized coefficients represent the relative contribution of a variable independent of the unit of measurement. They make it possible to identify those variables that make the largest contribution to the discriminatory function value.

Table 9.20. Summary of Stepwise Analysis and Coefficients for Canonical Variables (Changes in Hand Function)

Variables currently in the model	Parameters of Wilk's Statistics					Coefficients for Canonical Variables		
	F to enter	p-level	Λ	F-va-lue	p-level	Standar-dized	Struc-tural	Raw
BB Left, blocks/min	43,7	10^{-4}	,215	44	10^{-4}	-3,046	-,220	-1,698
BB Right, blocks/min	2,4	,163	,027	43	10^{-4}	4,255	-,097	,886
D Right, kG	14,4	,003	,093	53	10^{-5}	6,241	-,003	1,040
NHP Right, sec	4,7	,056	,064	49	10^{-5}	1,041	,156	,038
NHP Left, sec	2,1	,178	,051	41	10^{-5}	6,544	,113	,166
D Laterality, %	6,2	,047	,013	65	10^{-4}	-2,837	,050	-,150
NHP Laterality, %	3,5	,099	,036	43	10^{-4}	3,330	,001	,068
	r*=0,993; Wilks' Λ=0,013; $\chi^2_{(7)}=37$;p<10^{-5}						**Constant**	-2,102

The same is the full structural coefficients, that is, the coefficients of correlation between the discriminant root and variables.

As you can see, the root inversely reflects the information on changes in BB tests and D of Right hand. Instead, with a another constellation of functional parameters is discrimint root tied in a directly manner.

The sum of products of raw coefficients on the value of discriminant variables together with the constant gives the value of discriminant function (root) for each child and allow their visualization (Fig. 9.15).
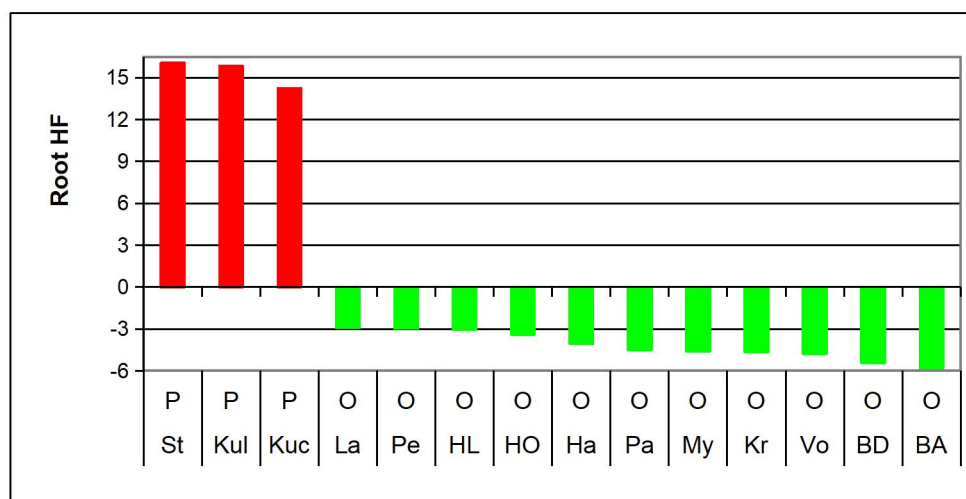

Fig. 9.15. Individual values of canonical Root of unfavorable (P) and favorable (O) changes in Hand Function

Even at first glance it is possible to state a drastically difference between the changes in Hand Function in members of two clusters. Positive individual columns show decrease of these variables, which correlate with the canonical discriminant root inversely, and increase of directly correlated variables. The visual impression is documented by calculating the square of Mahalanobis distance between the values of discriminant roots: $D^2_M=447$ (F=53; $p<10^{-4}$).

Now let's consider the changes of exactly what EEGs HRVs and GDVs parameters reflect opposite changes in the parameters of the hands functions. Among EEGs parameters revealed (Table 9.21) that unfavorable changes are accompanied by a decrease in the asymmetry of the θ- and δ-rhythms, the SPD of β-rhythm in loci F8 and Fp1, instead, it increases in loci O1 and T3, leading to left-sided lateralization of the β-rhythm. At the same time, the SPD of the α-rhythm in locus O1 and the θ-rhythm in locus F4 rises as well as its Deviation (variability). These changes in the EEG are accompanied by a reduction in vagal and an increase in sympathetic tones. Instead, favorable changes in the parameters of the hand function are accompanied by opposite changes in the listed EEGs, HRVs and GDVs parameters or their absence.

Table 9.21. Discriminant Function Analysis Summary. Changes in EEGs and HRVs parameters

Step 10, N of vars in model: 10; Grouping: 2 gr; Wilks' Λ: 0,0327; approx. $F_{(10)}$=8,9; p=0,049

Variables currently In the model	Unfavorable changes (3)	Favorable changes (11)	Wilks' Λ	Parti-al Λ	F-re-move	p-level	Tole-rancy
Θ-rhythm Asymmetry, %	-27±12	+8±4	,033	,988	,0	,859	,511
Δ-rhythm Asymmetry, %	-33±13	+9±7	,123	,265	8,3	,063	,151
B-rhythm Laterality, %	-54±3	-8±10	,037	,872	,4	,555	,173
F8-β SPD, µV²/Hz	-32±22	+41±27	,076	,430	4,0	,140	,239
HF HRV, %	-3,4±2,8	+6,6±4,3	,053	,622	1,8	,270	,077
Θ-rhythm Deviation, Hz	+1,00±0,29	-0,05±0,30	,040	,818	,7	,474	,184
LFnu HRV, %	+5,2±3,9	-11,2±4,9	,061	,534	2,6	,204	,093
O1-β SPD, µV²/Hz	+178±81	-5±58	,050	,657	1,6	,300	,181

O1-α SPD, μV²/Hz	+116±20	-20±50	,071	,462	3,5	,158	,080
F4-θ SPD, %	+4,3±1,7	-2,1±2,9	,093	,350	5,6	,099	,147
Variables currently not In the model			Wilks' Λ	Parti-al Λ	F to enter	p-level	Tole-rancy
Fp1-β SPD, μV²/Hz	-77±17	+19±31	,024	,746	,68	,496	,272
T3-β SPD, %	+9,0±5,6	-6,7±6,0	,031	,946	,11	,768	,356
C3-α SPD, %	+1,0±1,7	-7,7±3,3	,028	,845	,37	,606	,186

Repeating the procedure described above, we obtain an illustration of the neurophysiological support of individual changes in the functions of the hands (Fig. 9.16).
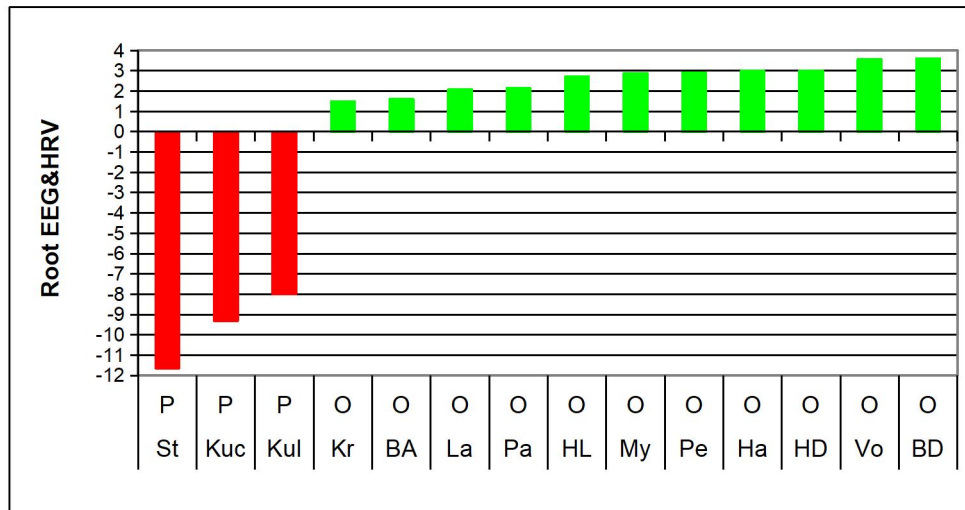
Fig. 9.16. Individual values of canonical Root of unfavorable (P) and favorable (O) changes in EEGs and HRVs parameters

162

After expanding the database for discriminant analysis at the expense of GDVs parameters, the model turned on only Entropy of the Gas Discharge Image in Left projection with filter, the value of which significantly decreased with adverse changes in the functions of the hands, remaining unchanged with favorable changes. Worthy of attention is also not included in the model changes, namely an increase in the Area of the GD Image in the frontal projection without filter, coupled with a decrease in its Entropy in the Frontal projections with filter in members of first cluster (Table 9.21).

Table 9.21. Discriminant Function Analysis Summary. Changes in EEGs, HRVs and GDVs parameters
Step 9, N of vars in model: 9; Grouping: 2 grps; Wilks' Λ: 0,0166; approx. $F_{(9,4)}$=26; p=0,003

Variables currently in the model	Unfavorable changes (3)	Favorable changes (11)	Wilks' Λ	Parti-al Λ	F-re-move	p-level	Tole-rancy
Θ-rhythm Asymmetry, %	-27±12	+8±4	,017	,985	0,1	,814	,562
Δ-rhythm Asymmetry, %	-33±13	+9±7	,080	,207	15,3	,017	,169
B-rhythm Laterality, %	-54±3	-8±10	,026	,638	2,3	,207	,354
Entropy GDI Left (f)	-0,27±0,04	+0,03±0,04	,078	,212	14,9	,018	,164
F8-β SPD, μV²/Hz	-32±22	+41±27	,023	,719	1,6	,279	,481
HF HRV, %	-3,4±2,8	+6,6±4,3	,023	,714	1,6	,275	,113
Θ-rhythm Deviation, Hz	+1,00±0,29	-0,05±0,30	,031	,539	3,4	,138	,391
LFnu HRV, %	+5,2±3,9	-11,2±4,9	,081	,206	15,4	,017	,028
F4-θ SPD, %	+4,3±1,7	-2,1±2,9	,023	,714	1,6	,275	,113
Variables currently not in the model			Wilks' Λ	Parti-al Λ	F to enter	p-level	Tole-rancy
Entropy GDI Frontal (f)	-0,18±0,13	+0,06±0,05	,016	,980	,06	,822	,131
Area GDI Frontal, kPx	+3,94±2,12	-0,94±0,99	,014	,858	,50	,532	,082

Despite the seemingly slight structural changes in the discriminatory model the power of discrimination, estimated by the criterion Wilks' Lambda, increases from 0,0327 (approx. $F_{(10,3)}=8,89$; p=0,049) to 0,0166 (approx. $F_{(9,4)}=26$; p=0,003) as well as D^2_M between clusters increases from 176 (F=7,33; p=0,064) to 352 (F=22; p=0,005). The increase in the power of discrimination is noted in Fig. 9.17.
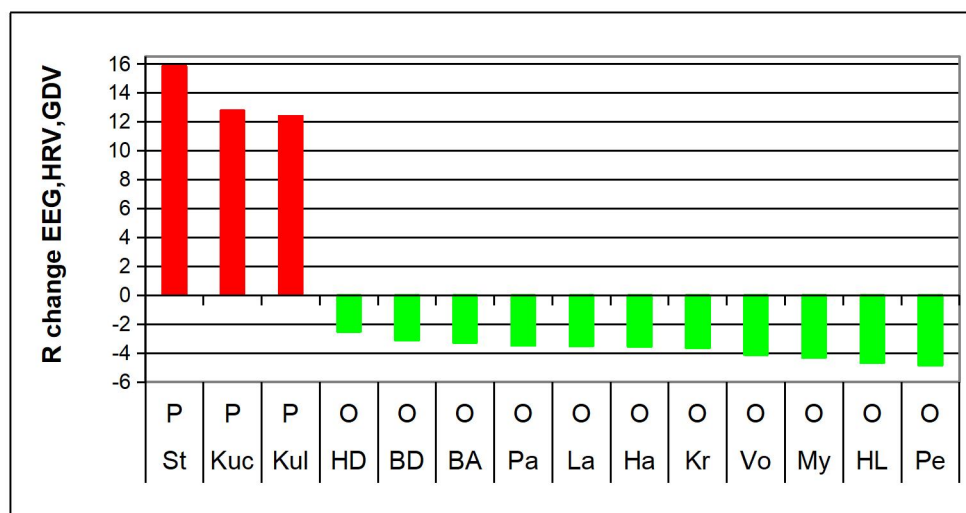
Fig. 9.17. Individual values of canonical Root of unfavorable (P) and favorable (O) changes in EEGs, HRVs and GDVs parameters

Therefore, this pilot study also demonstrates that at least one GDV parameter is organically combined with EEG and HRV parameters, which reflect the response of children with cerebral palsy to treatment according to the Kozyavkin© method.

Proceeding from this, at the next stage, parameters were identified, the totality of which the initial state of children and their state after the various consequences of rehabilitation are significantly different from each other. The program selected 18 parameters, namely 3 **hand function** parameters, 10 **EEGs**, 2 **HRVs** and 3 **GDVs**. The hierarchy of parameters for their differentiation ability, estimated by criterion Λ, is given in Table. 9.22.

Table 9.22. Summary of Stepwise Analysis. The scale of ranks for variables

Variables currently in the model	F to enter	p-level	Λ	F-value	p-level
LF HRV, sec^2	5,9	,008	,681	5,9	,008
LFnu HRV, %	5,6	,010	,464	5,6	10^{-3}
δ-rhythm Deviation. Hz	3,1	,066	,366	5,0	10^{-3}
β-rhythm Amplitude, µV	3,5	,047	,277	5,0	10^{-3}
F8-β SPD, µV^2/Hz	2,1	,148	,231	4,5	10^{-3}
Entropy Right GDV	2,4	,119	,186	4,4	10^{-3}
θ-rhythm Deviation, Hz	2,0	,168	,155	4,2	10^{-3}
O1-θ SPD, µV^2/Hz	1,9	,184	,128	4,0	10^{-3}
O2-θ SPD, %	2,3	,129	,101	4,1	10^{-3}
β-rhythm Laterality, %	2,2	,143	,079	4,1	10^{-3}
Area Frontal GDI, 10^3 pixels	3,0	,082	,057	4,4	10^{-3}
F4-β SPD, µV^2/Hz	3,6	,056	,037	4,9	10^{-4}
F3-β SPD, %	1,8	,204	,029	4,8	10^{-4}
Fp1-β SPD, µV^2/Hz	3,1	,084	,019	5,3	10^{-4}
Entropy Frontal (f) GDI	1,7	,221	,015	5,3	10^{-4}
Dynamometry Right, kG	6,8	,014	,006	7,3	10^{-4}
9 Hole Peg Left, sec	2,3	,157	,004	7,7	10^{-4}
Dynamometry Laterality, %	1,6	,253	,003	7,8	10^{-4}

Next, the 18-dimensional space of discriminant variables transforms into 2-dimensional space of a canonical discriminant roots. The first root contains 81% discriminant capacity, while the second root 19% only.

Table 9.23 presents coefficients for discriminant variables.

Table 9.23. Standardized, Structural and Raw Coefficients and Constants for Canonical Variables

Variables currently in the model	Standardized		Structural		Raw	
	Root 1	Root 2	Root 1	Root 2	Root 1	Root 2
β-rhythm Laterality, %	-3,628	,062	**-,069**	-,052	-,1449	,0025
F4-β SPD, µV²/Hz	-2,238	,094	**-,060**	-,049	-,0304	,0013
β-rhythm Amplitude, µV	4,151	1,839	**-,039**	,015	,8056	,3569
O1-θ SPD, µV²/Hz	-5,090	-,533	**-,028**	-,013	-,0294	-,0031
Dynamometry Right, kG	3,595	,154	**,041**	,012	,4837	,0207
O2-θ SPD, %	5,150	,261	**,025**	-,018	,8834	,0447
LF HRV, sec²	-2,123	,053	-,002	**,236**	-,0029	,0001
Area Frontal GDI, 10³ pixels	4,189	1,177	,005	**,126**	1,7	0,5
Dynamometry Laterality, %	-1,414	1,757	,019	**,125**	-,0658	,0817
δ-rhythm Deviation. Hz	-1,239	1,205	,007	**,123**	-3,5178	3,4198
θ-rhythm Deviation, Hz	3,605	1,665	,019	**,120**	5,2427	2,4220
F3-β SPD, %	-4,591	-1,112	-,017	**,113**	-,2940	-,0712
LFnu HRV, %	-3,060	-,444	-,047	**,091**	-,2132	-,0309
9 Hole Peg Left, sec	-,702	-1,333	-,003	**,045**	-,0100	-,0190
Entropy Right GDI	-,686	-1,398	,044	**-,135**	-5,0259	-10,243
Fp1-β SPD, µV²/Hz	-1,491	,004	-,007	**-,108**	-,0245	,0001
F8-β SPD, µV²/Hz	3,634	-,091	,031	**-,099**	,0514	-,0013
Entropy Frontal (f) GDI	-5,125	-3,298	,002	**-,084**	-27,67	-17,80
Eigenvalues	**35,13**	**8,42**	**Constants**		75,95	89,90
		Discriminant Properties, %			81	19
	r*₁=0,986; Wilk's Λ=0,003; χ²(36)=96; p<10⁻⁶					
	r*₂=0,945; Wilk's Λ=0,106; χ²(17)=37; p=0,003					

As you can see, the first root **inversely** reflects the information on 4 **EEGs parameters** while **directly** on O1-θ SPD and Dynamometry of Right hand. The second root represents directly 2 **HRVs**, 3 **EEGs**, 2 **functional hand** parameters as well as one parameter of **GDV**, while inversely reflects others 2 **GDVs** and 2 **EEGs** parameters.

The sum of products of raw coefficients on the value of discriminant variables together with the constant gives the values of roots for each child and allow their visualization (Figs. 9.18-9.22) as well as clusters of children (Fig. 9.23).
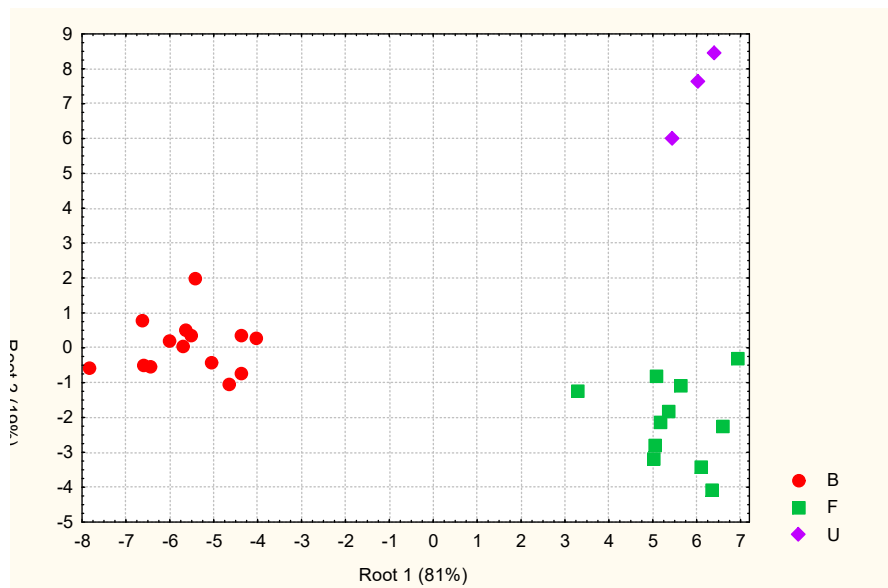
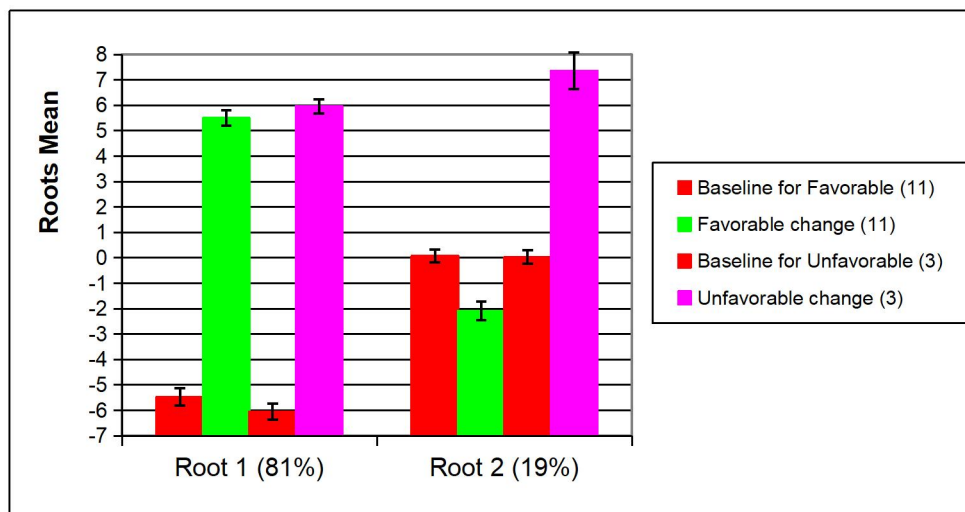**Fig. 9.18. Individual sizes of canonical discriminatory roots of children before rehabilitation (Baseline) and with its favorable (F) and unfavorable U) consequences**

Even at first glance it is possible to state a drastically difference between clusters. The visual impression is documented by calculating the square of Mahalanobis distance (D^2_M). Between initial cluster and cluster with favorable consequences $D^2_M=143$ (F=14,4; p<10^{-3}), with unfavorable changes: 209 (F=6,4; p=0,006), while between two post-rehabilitated clusters: 100 (F=3,0; p=0,06).
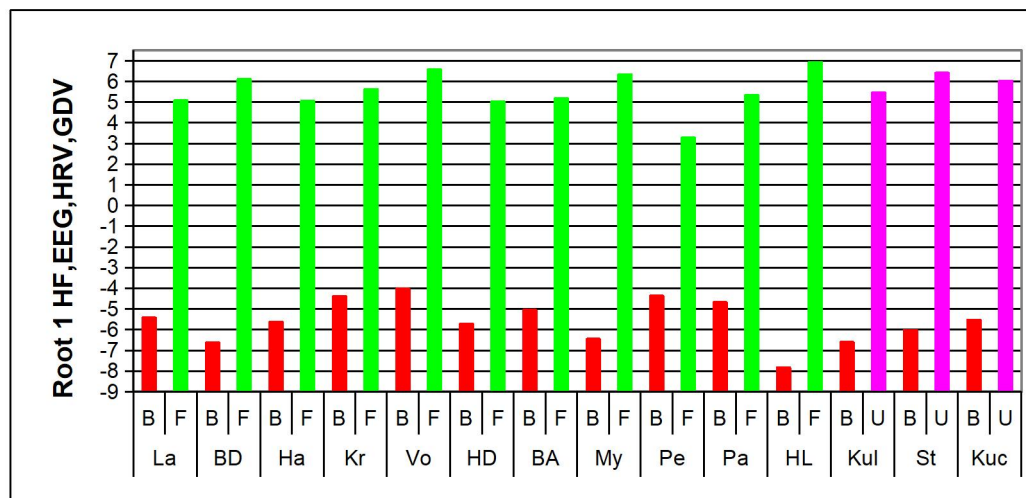
Fig. 9.19. Individual sizes of first root of children before rehabilitation and with its favorable (F) and unfavorable (U) consequences
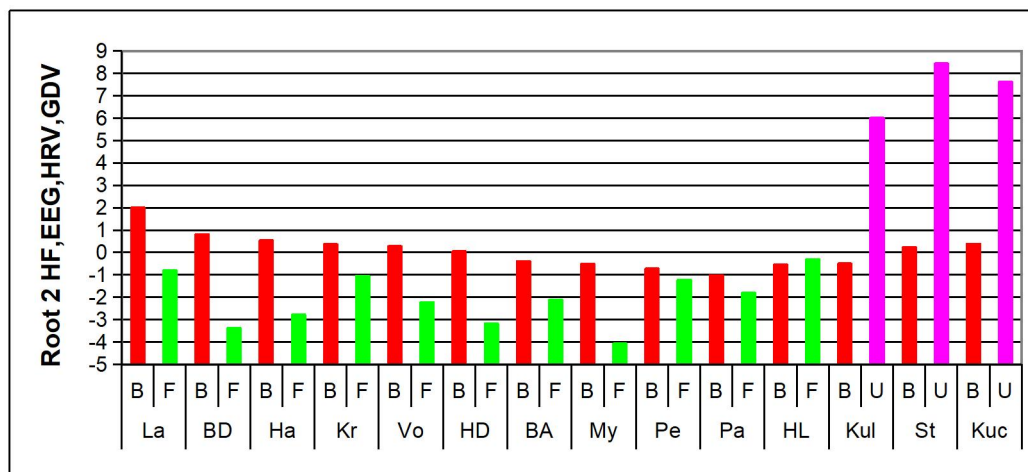
Fig. 9.20. Individual sizes of second root of children before rehabilitation and with its favorable (F) and unfavorable (U) consequences
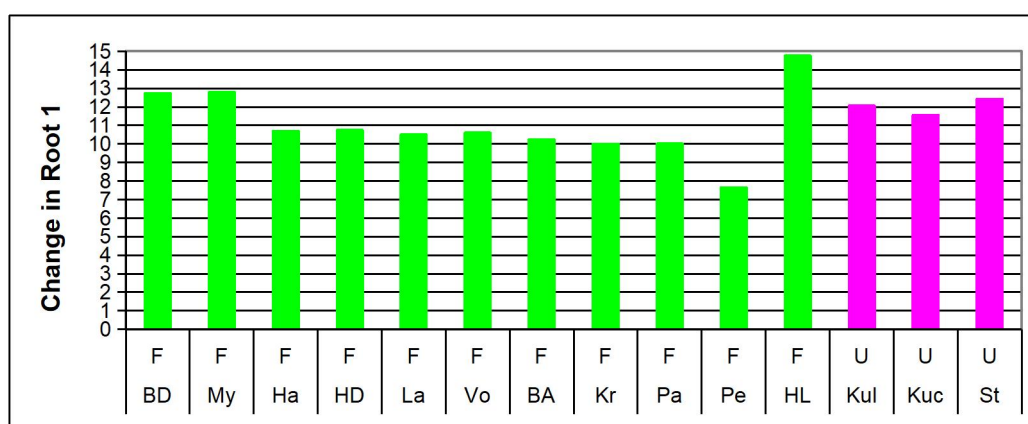
Fig. 9.21. Individual changes in first root of children with favorable (F) and unfavorable (U) consequences of rehabilitation
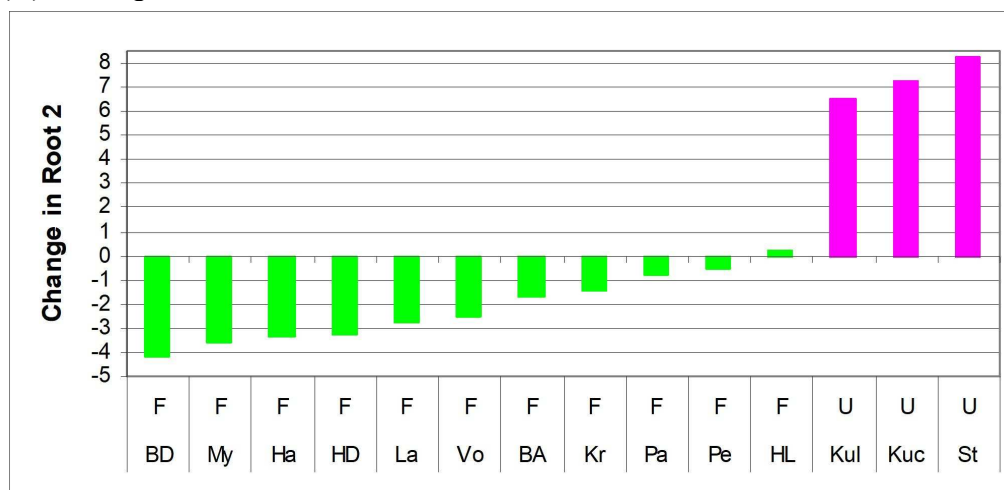
Fig. 9.22. Individual changes in second root of children with favorable (F) and unfavorable (U) consequences of rehabilitation

Fig. 9.23. Means of canonical discriminatory roots of children before rehabilitation (Baseline) and with its favorable (F) and unfavorable (U) consequences

Localization of representative children's points along the axis of the first root (Figs. 9.18 and 9.19) reflects, firstly, significant changes under the influence of rehabilitation in six parameters associated with the roots (Table. 9.23), in particular, alignment of the right lateralization of β-rhythm, reduction of its amplitude and SPD in locus F4 as well as SPD of θ-rhythm in locus O1 while increase it in locus O2 as well as increase strength of the right hand and right-site lateralization of dynamometry. At the same time, intercluster differences for these parameters are insignificant, which is documented as the average values of centroid clusters (Fig. 9.23) and their displacements (+11,0±0,6 and +12,0±0,2 with favorable and unfavorable changes of functions of hands, respectively, please see Fig. 9.21).

The clear separation of clusters occurs along the axis of the second root, herewith the centroids of the post-rehabilitation clusters shift relative to the initial in opposite directions (Figs 9.18, 9.20 and 9.22). In particular, unfavorable changes in the functions of the hands are accompanied by an: 1) extension of the GDV Area in the frontal projection, coupled with a decrease in its Entropy in the same place and in the right projection; 2) increase in volatility of δ- and θ-rhythms as well as in SPD of β-rhythm in locus F3 while decrease its in loci F8 and Fp1; 3) increase in power of LF band of HRV as marker of sympathetic tone. On the other hand, favorable functional changes are accompanied by opposite changes in GDVs, EEGs and HRVs parameters or no changes in relation to the initial levels.

Now let's move on to the realization of the main goal of the study, namely the retrospective prediction of the effect of rehabilitation of motor function of the hands. The same method of discriminant analysis is applied.

The set of eight predictors, which includes representatives of all research methods (Table 9.24), was the most reliable in forecasting. The most informative, judging by the Λ and Structural coefficient, was the Entropy of the GDI (filmed with the filter) in the **left** projection (Table 9.24 and 9.25). It, as well as the frequency of theta-rhythm, were significantly higher in children with an unfavorable effect of rehabilitation. Instead, the SPD beta- and alpha-rhythms in the two **left** loci of these children, as well as the power of the ULF band of the HRV, were significantly lower (Table 9.26).

Table 9.24. Summary of Stepwise Analysis for optimal set of parameters. The scale of ranks for variables

Variables currently in the model	F to enter	p-level	Λ	F-value	p-level
Entropy Left (f) GDI	17,9	,001	,401	17,9	,0012

θ-rhythm Frequency, Hz	4,1	,067	,292	13,3	,0012
B&B Right, blocks/min	8,4	,016	,159	17,6	,0003
F7-α SPD, μV^2/Hz	2,4	,159	,126	15,6	,0004
O1-β SPD, μV^2/Hz	5,5	,047	,075	19,9	,0003
ULF HRV, %	1,7	,236	,060	18,2	,0006
ULF HRV, msec^2	2,7	,154	,042	19,7	,0010
F7-β SPD, μV^2/Hz	4,4	,090	,022	27,5	,0010

Table 9.25. Standardized, Structural and Raw Coefficients and Constant for optimal set of parameters

Variables currently in the model	Standar-dized	Structu-ral	Raw
Entropy Left (f) GDI	2,871	,184	27,93
θ-rhythm Frequency, Hz	4,210	,056	3,505
B&B Right, blocks/min	1,868	,052	,326
F7-β SPD, μV^2/Hz	-2,003	-,072	-,025
ULF HRV, %	-6,490	-,064	-1,873
F7-α SPD, μV^2/Hz	-2,593	-,061	-,043
O1-β SPD, μV^2/Hz	5,350	-,060	,059
ULF HRV, msec^2	4,937	-,053	,057
Eigenvalue	44,06	**Constant**	-136,1
r*=0,989; Wilk's Λ=0,0222; χ$^2_{(8)}$=30,5; p=0,0002			
Squared Mahalanobis Distance=262; F=22,7; p=0,0016			

Table 9.26. Discriminant Function Analysis Summary for optimal set of parameters

Step 8, N of vars in model: 8; Grouping: 2 grps; Wilks' Λ: ,0222; approx. $F_{(8,5)}$=27,5; p=10^{-3}

Variables currently in the model	Unfavorable changes (3)	Favorable changes (11)	Wilks' Λ	Parti-al Λ	F-re-move	p-level	Tole-rancy
Entropy Left (f) GDI	4,10±0,06	3,82±0,03	,367	,061	78	<10^{-3}	,117
θ-rhythm Frequency, Hz	7,33±0,17	6,30±0,42	,212	,105	43	,001	,052
B&B Right, blocks/min	18,8±2,0	14,3±1,8	,071	,313	11	,021	,201
F7-α SPD, μV^2/Hz	52±22	109±20	,076	,291	12	,017	,108
O1-β SPD, μV^2/Hz	88±17	172±31	,117	,189	21	,006	,029
ULF HRV, %	0,3±0,2	3,7±1,1	,069	,321	11	,023	,016
ULF HRV, msec^2	8±3	76±29	,057	,391	8	,038	,026
F7-β SPD, μV^2/Hz	51±14	138±27	,042	,532	4	,090	,119

The maximum difference between clusters by the combination of these predictors is illustrated in Figure 9.24.
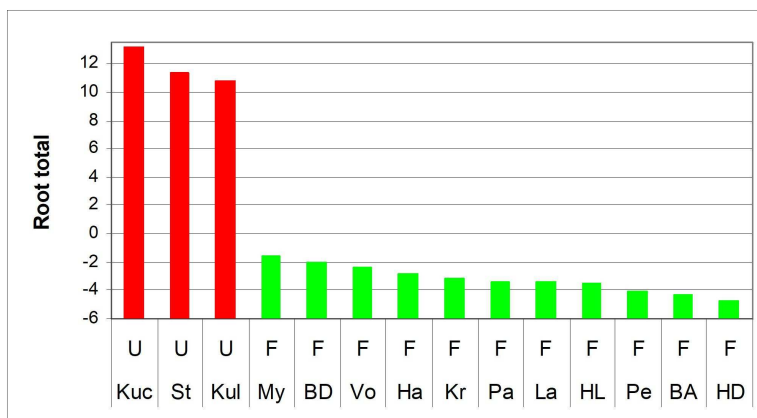
Fig. 9.24. Individual values of optimal set of predictors of unfavorable and favorable effects of rehabilitation

The forecast is realized by the coefficients and constants for Classification Functions given in Table 9.27. These functions are special linear combinations that maximize

differences between groups and minimize dispersion within groups. The coefficients of the classifying functions are not standardized therefore they are not interpreted. An object belongs to a group with the maximum value of a function calculated by summing the products of the values of the variables by the coefficients of the classifying functions plus the constant. In this case, we can retrospectively recognize members of all groups unmistakably.

Table 9.27. Coefficients and Constants for Classification Functions for optimal set of parameters

Variables currently in the model	Unfavorable changes (3)	Favorable changes (11)
Entropy Left (f) GDI	4242	3824
θ-rhythm Frequency, Hz	515,9	463,4
B&B Right, blocks/min	49,41	44,53
F7-α SPD, $μV^2/Hz$	-6,20	-5,56
O1-β SPD, $μV^2/Hz$	8,53	7,65
ULF HRV, %	-265,0	-236,9
ULF HRV, $msec^2$	8,15	7,30
F7-β SPD, $μV^2/Hz$	-3,48	-3,10
Constants	-11168	-9064

Thus, despite the small contingent of the observed children with spastic form of cerebral palsy, we have proved that the differently directed changes in the parameters of manual tests caused by two-week rehabilitation course by Kozyavkin© method are due to differently directed changes in parameters of EEG, HRV as well as GDV. The character of the changes in the parameters of the motor function of the hands is conditioned both by their initial level and by the set of parameters of EEG, HRV and GDV and is subject to reliable prediction. Increasing the effectiveness of rehabilitation, perhaps, is possible through additional electrostimulation of the vagus nerve and/or certain scalp loci. GDV is a completely suitable non-invasive method for assessing the effectiveness of rehabilitation.

Publications in which the materials of the chapter are reflected:

1. Kozyavkin VI, Kozyavkina OV, Kozyavkina NV, Voloshyn TB, Gordiyevych MS, Popovych IL. Relationships between changes in neural component of muscle tone and parameters of EEG, HRV, gas disharge visualization at children with spastic form of cerebral palsy during intensive neurophysiological rehabilitation. In: Pathophysiology and Pharmacy: ways of integration. Abstracts VII National Congress of Pathophysiologists Ukraine with international participation (5-7 October 2016). Kharkiv. NPhU; 13-13.

2. Kozyavkin VI, Kozyavkina OV, Kozyavkina NV, Voloshyn TB, Gordiyevych MS, Popovych IL. Changes in neural component of muscle tone at children with spastic form of cerebral palsy caused by intensive neurophysiological rehabilitation, their relationship with changes in parameters of EEG, HRV, GDV and possibility of forecasting. In: XVI International Conference "The current status and approaches to development of physical and rehabilitation medicine in Ukraine according to international standards" (15-16 December 2016, Kiev). Kyïv, 2016: 74-75.

3. Kozyavkin VI, Kozyavkina NV, Kozyavkina OV, Voloshyn TB, Hordiyevych MS, Popovych IL. Relationships between changes in neural component of muscle tone and parameters of EEG, HRV, GDV at children with spastic form of cerebral palsy. In: Mater of the X Sci-Pract conf "Actual issues of pathology under the conditions of action of extraordinary factors on the body" (Ternopil', October 5-6, 2017). Ternopil'; 2017: 56-57.

4. Babelyuk VY, Dubkova HI, Korolyshyn TA, Mysula IR, Popovych DV, Popovych IL, Zukow W. Relationships between caused by Kozyavkin© method changes in parameters of manual function and electroencephalogram, heart rate variability as well as gas

discharge visualization in children with spastic form of cerebral palsy. Journal of Education, Health and Sport. 2018; 8(4): 159-194.

5. Popovych IL, Babelyuk VY, Dubkova HI, Korolyshyn TA, Zukow W. Relationships between changes in parameters of manual function and electroencephalogram, heart rate variability as well as gas discharge visualization in children with spastic form of cerebral palsy caused by Kozyavkin© method. Experimental and Clinical Physiology and Biochemistry. 2018; 1(81): 39-50.

6. Kozyavkina OV, Kozyavkina NV, Voloshyn TB, Hordiyevych MS, Lysovych VI, Babelyuk VY, Dubkova HI, Korolyshyn TA, Mysula IR, Popovych DV, Zukow W, Popovych IL. Caused by Kozyavkin© method changes in hand function parameters in children with spastic form of cerebral palsy and their EEGs, HRVs and GDVs accompaniments. Journal of Education, Health and Sport. 2018; 8(10): 11-30.

7. Kozyavkina OV, Kozyavkina NV, Hordiyevych MS, Voloshyn TB, Lysovych RV, Popovych IL. Caused by Kozyavkin© method changes in hand function parameters in children with spastic form of cerebral palsy and their forecasting. In: Rehabilitation Medicine and Health-Resort Institutions Development. Proceedings of the 19th International Applied Research Conference (Kyïv, 11-12 December 2019). Edited by O. Gozhenko, W. Zukow. Toruń, Kyïv. 2019: 81-82.

8. Kozyavkina OV, Kozyavkina NV, Hordiyevych MS, Voloshyn TB, Lysovych VI, Babelyuk VY, Dubkova HI, Korolyshyn TA, Popovych DV, Mysula IR, Zukow W, Popovych IL. Forecasting caused by Kozyavkin© method changes in hand function parameters in children with spastic form of cerebral palsy at their baseline levels as well as EEGs, HRVs and GDVs. Achivments of Clinical and Experimental Medicine. 2018; 4: 17-35.

170

CONCLUSION

Comparing the results obtained by us during the years 2010-2022 with the data of the available literature, we take the courage to affirm our priority to create a reliable academic foundation for the GDV/EPI (Kirlianography) method. For the first time, we discovered significant connections between the parameters of GDV/EPI, on the one hand, and the parameters of the neuro-endocrine-immune complex, on the other hand, which, sorry for the tautology, connected the Eastern and Western paradigms of medicine into a single entity. By including the GDV/EPI method in the battery of conventional methods, we demonstrated that the GDV/EPI parameters are literally woven into the fabric of the factor structure, which reflects the integral state of the organism and its changes under the influence of factors of various nature. Indeed, there is nothing more practical than a good theory!

In conclusion, we would like to announce the release of the next monograph, which will reflect the results of our research on the influence of Prayer, a Reiki session, Kyokushin karate kats and Space Weather on the parameters of GDV/EPI and the neuro-endocrine-immune complex of human volunteers, as well as on the glow of distilled water. In addition, data on the effect on GDV/EPI, EEG and HRV parameters of Holy water and distilled water exposed to various factors will be presented.

ACCORDANCE TO ETHICS STANDARDS

Tests in patients are carried out in accordance with positions of Helsinki Declaration 1975, revised and complemented in 2002, and directive of National Committee on ethics of scientific researches. During realization of tests from all participants or parents of children the informed consent is got and used all measures for providing of anonymity of participants.

REFERENCES

Adams DS, Tseng AS, Levin M. Light-activation of the Archaerhodopsin H^+-pump reverses age-dependent loss of vertebrate regeneration: sparking system-level controls in vivo. Biol Open. 2013; 2(3): 306–313.

Aharonov Y, Bohm D. Significance of electromagnetic potentials in the quantum theory. Phys Rev. 1959; 115(3): 485–491.

Akmayev PG. Modern understanding of the interactions of regulatory systems: the nervous, endocrine and immune [in Russian]. Uspekhi fiziologicheskikh nauk. 1996; 27(1): 3-20.

Akselrod S, Gordon D, Ubel FA, Shannon DC, Barger AC, Cohen RJ. Power spectrum analysis rate fluctuation: a quantitative probe of beat-to-beat cardiovascular control. Science (NY). 1981; 213(4504): 220-222.

Albrecht-Buehler G. Rudimentary form of cellular "vision". Proc Natl Acad Sci USA. 1992; 89(17): 8288–8292.

Aldenderfer MS, Blashfield RK. Cluster analysis (Second printing, 1985) [trans. from English in Russian]. In: Factor, Discriminant and Cluster Analysis. Moskva. Finansy i Statistika; 1989: 139-214.

Alyeksyeyev OI, Popovych IL, Panassyuk YM, Barylyak LG, Sarancha SM, Shumakov MF. Adaptogens and radiation [in Ukrainian]. Kyïv. Naukova dumka; 1996: 126.

Aspect A, Grangier P, Roger G. Experimental realization of Einstein-Podolsky-Rosen-Bohm Gedankenexperiment: A new violation of Bell's inequalities. Phys Rev Lett. 1982; 49(2): 91–94.

Babeluk VE. The patent of Ukraine for utility model 105875 Portable device for electrotherapy and stimulation, 2016.

Babelyuk NV, Babelyuk VYe, Dubkowa GI, Kikhtan VV, Musiyenko VY, Hubyts'kyi VY, Dobrovolsky YG, Korsunskyi IH, Kovbasnyuk MM, Korolyshyn TA, Popovych IL. Influence of the course of electrostimulation by the device "ES-01.9 WEB" on some functional systems of the organism of practically healthy men [in Ukrainian]. In: Proceedings VIII Scientific Conference "Issues of pathology in conditions of extreme factors action on the body" (Ternopil', 1-2 October 2015). Ternopil'. 2015: 5-6.

Babelyuk NV, Babelyuk VYe, Dubkowa GI, Kikhtan VV, Musiyenko VY, Hubyts'kyi VY, Dobrovolsky YG, Korsuns'kyi IH, Kovbasnyuk MM, Korolyshyn TA, Popovych IL. Modulation of functional systems of practically healthy men by the course of electrostimulation [in Ukrainian]. In: IX International symposium "Actual problems of biophysical medicine" (Kyïv, 12-15 May 2016). Kyïv. OO Bohomolets' Institute of Physiology; 2016: 10-11.

Babelyuk NV, Babelyuk VYe, Dubkowa GI, Korolyshyn TA, Kikhtan VV, Dobrovolsky YG, Korsuns'kyi IH, Kovbasnyuk MM. Electrical stimulation with the device "ES-01.9 WEB" activates some functional systems of the body of practically healthy men [in Ukrainian]. In: Valeology: current status, trends and persrectives of development. Abstracts. XIV Intern. scient. and practical. conf. (Kharkiv-Drohobych, 14-16 April 2016). Kharkiv. VN Karazin KhNU; 2016: 198-200.

Babelyuk NV. Electrostimulation with the devices "VEB-1" and "VEB-2" causes almost identical changes in the parameters of gas-discharge visualization. Experimental and Clinical Physiology and Biochemistry. 2020; 90(2): 5-13.

Babelyuk V, Dobrovolsky Yu, Korsunsky I, Kuzenko V, Popovych I, Zukow W. The algorithm of the electric stimulator VEB-1 software operation. Journal of Education, Health and Sport. 2020; 10(5): 403-409.

Babelyuk VE, Babelyuk NV, Popovych IL, Gozhenko AI, Kyrylenko IG, Korolyshyn TA, Dubkova GI, Kovbasnyuk MM, Hubyts'kyi VY, Kikhtan VV, Musiyenko VY, Dobrovolsky YG, Korsunskyi IH, Zukow W. Effects of transcutaneous electrical stimulation with the

172

device "VEB" ® on the human body. Journal of Education, Health and Sport. 2022; 12(2): 313-335.

Babelyuk VE, Gozhenko AI, Dubkova GI, Babelyuk NV, Zukow W, Kovbasnyuk MM, Popovych IL. Causal relationships between the parameters of gas discharge visualization and principal neuroendocrine factors of adaptation. Journal of Physical Education and Sport. 2017; 17(2): 624-637.

Babelyuk VY, Babelyuk NV, Popadynets' OO, Dubkova GI, Muszkieta R, Zukow W. Relationships between the entropy of gas-discharge image and the entropies of EEG, HRV, immunocytogram and leukocytogram. In: Mater of the XII All-Ukrainian Sci-Pract conf "Actual issues of pathology under the conditions of action of extraordinary factors on the body". Galician readings II (Ternopil', October 29-30, 2020). Ternopil'; 2020: 119-120.

Babelyuk VY, Babelyuk NV, Popovych IL, Gozhenko AI, Kyrylenko IG, Korolyshyn TA, Dubkova GI, Kovbasnyuk MM, Hubyts'kyi VY, Kikhtan VV, Musiyenko VY, Dobrovolsky YG, Korsunskyi IH, Zukow W. Adaptogenic effects of transcutaneous electrical stimulation with the device "VEB" ®. In: Mater of the XIII All-Ukrainian Scie-Pract conf. "Actual issues of pathology under the conditions of action of extraordinary factors on the body". Galician readings II (Ternopil', October 26-28, 2020). Ternopil'; 2022: 78-78.

Babelyuk VY, Dobrovolsky YyG, Popovych IL, Korsunskiy IG. Generator for electrotherapy and stimulation oh human nerve centers [in Russian]. Tekhnologiya i Konstruirovaniye v Elektronnoy Apparature. 2017; 1-2: 23-27.

Babelyuk VY, Dubkova HI, Korolyshyn TA, Mysula IR, Popovych DV, Popovych IL, Zukow W. Relationships between caused by Kozyavkin© method changes in parameters of manual function and electroencephalogram, heart rate variability as well as gas discharge visualization in children with spastic form of cerebral palsy. Journal of Education, Health and Sport. 2018; 8(4): 159-194.

Babelyuk VY, Gozhenko AI, Dubkova GI, Babelyuk NV, Zukow W, Kindzer BM, Kovbasnyuk MM, Popovych IL. Causal relationships between the parameters of gas discharge visualization and phagocytosis. Journal of Education, Health and Sport. 2021; 11(6): 268-276.

Babelyuk VY, Tserkovniuk RG, Babelyuk NV, Żukow X, Ruzhylo SV, Dubkova GI, Korolyshyn TA, Hubyts'kyi VY, Kikhtan VV, Gozhenko AI, Popovych IL. The parameters of gas discharge visualization (biophotonics) correlated with parameters of acupuncture points, EEG, HRV and hormones. Journal of Education, Health and Sport. 2021; 11(12): 359-373.

Babelyuk VY, Tserkovniuk RG, Dubkova GI, Korolyshyn TA, Hubyts'kyi VY, Kikhtan VV, Gozhenko AI, Popovych IL. Parameters of gas discharge visualization (biophotonics) correlated with parameters of acupuncture points, EEG, HRV and hormones. In: Mater of the XIII All-Ukrainian Scie-Pract conf. "Actual issues of pathology under the conditions of action of extraordinary factors on the body". Galician readings II (Ternopil', October 26-28, 2020). Ternopil'; 2022: 79-79.

Babelyuk VY, Tserkovniuk RG, Dubkova GI, Kruhliy YS, Korolyshyn TA, Babelyuk NV, Zukow W, Ruzhylo SV, Fihura OA, Gozhenko AI, Popovych IL. Relationships between the neuro-endocrine parameters and virtual chakras energy and asymmetry. Journal of Education, Health and Sport. 2022; 12(1): 235-249.

Babelyuk VY, Tserkovnyuk RG, Ruzhylo SV, Dubkova GI, Babelyuk NV, Zukow W, Popovych IL. Causal relationships between the parameters of gas discharge visualization and leukocytogram. Journal of Education, Health and Sport. 2021; 11(7): 258-269.

Babelyuk VYe, Babelyuk NV, Popovych IL, Dobrovol's'kyi YG, Korsuns'kyi IH, Korolyshyn TA, Kindzer BM, Zukow W. Influence of the course of electrostimulation by the device "VEB-1" on parameters of electroencephalogram at practically healthy males. In: XVII

reading named after VV Podvysotskyi. Bulletin of scientific materials conf. (May 24-25, 2018). Odesa. UkrSRI of Meicine of Transport; 2018: 11-12.

Babelyuk VYe, Dubkova GI, Kikhtan VV, Korolyshyn TA, Popovych IL. The relationship between the parameters of gas discharge visualization and neuro-endocrine regulation [in Ukrainian]. In: Valeology: current status, trends and prospects development. Abstracts XIV International scientific and practical conference (Kharkiv-Drohobych, 14-16 April 2016). Kharkiv. VN Karazin KhNU; 2016: 360-361.

Babelyuk VYe, Dubkova GI, Kikhtan VV, Korolyshyn TA, Zukow W, Popovych IL. The parameters of gas discharge visualization and principal neuroendocrine factors of adaptation closely correlated. In: IX International symposium "Actual problems of biophysical medicine" (Kyïv, 12-15 May 2016). Kyïv. OO Bohomolets' Institute of Physiology; 2016: 9-10.

Babelyuk VYe, Dubkova GI, Korolyshyn TA, Zukow W, Popovych IL. The correlationships between parameters of gas discharge visualization and principal neuroendocrine factors of adaptation. In: Pathophysiology and Pharmacy: ways of integration. Abstracts VII National Congress of Pathophysiologists Ukraine with international participation (5-7 October 2016). Kharkiv. NPhU; 2016: 8-8.

Babelyuk VYe, Dubkova GI, Popovych IL. Correlation parameters of electrophotonics (kirlianogram) with neuroendocrine parameters [in Ukrainian]. In: Materials of V scientific-practical conference "Issues of pathology in conditions of extreme factors action on the body" (Ternopil', 1-2 November 2012): Achievements of Clinical and Experimental Medicine. 2012; 2(17): 158-158.

Babelyuk VYe, Dubkova GI, Popovych IL. Gas discharge visualization parameters correlate with some psycho-physiological and endocrine parameters of healthy men [in Ukrainian]. In: "Actual problems of biophysical medicine". Materials of VII International symposium (Kyïv, 14-17 May 2014). Kyïv. OO Bohomolets' Institute of Physiology; 2014: 11-13.

Babelyuk VYe, Gozhenko AI, Dubkova GI, Zukow W, Hubyts'kyi VY, Ruzhylo SV, Fedyayeva SI, Kovalchuk HY, Popovych IL. Causal relationships between the parameters of gas discharge visualization and immunity. Pedagogy and Psychology of Sport. 2021; 7(1): 115-134.

Babelyuk VYe, Popadynets' OO, Dubkova GI, Zukow W, Muszkieta R, Gozhenko OA, Popovych IL. Entropy of gas-discharge image correlates with the entropies of EEG, immunocytogram and leukocytogram but not HRV. Pedagogy and Psychology of Sport. 2020; 6(2): 30-39.

Babelyuk VYe, Popovych IL. Some biophysical and hematological correlates testosteronemia levels in healthy men [in Ukrainian]. Zdorovye muzhchiny. Health males. 2013; 2(45): 180-181.

Babelyuk VYe. The parameters of gaz discharge visualization (kirlianogram) appropriately associated with some psychophysiological and endocrine parameters of healthy men. Medical Hydrology and Rehabilitation. 2013; 11(1): 21-30.

Baevskiy RM, Ivanov GG. Heart Rate Variability: theoretical aspects and possibilities of clinical application [in Russian]. Ultrazvukovaya i funktsionalnaya diagnostika. 2001; 3: 106-127.

Balle M, Bornas X, Tortella-Feliu M, Llabrés J, Morillas-Romero A, Aguayo-Siquier B, Gelabert JM. Resting parietal EEG asymmetry and cardiac vagal tone predict attentional control. Biol Psychol. 2013; 93(2): 257–261.

Bankovskii NG, Korotkov KG, Petrov NN. Physical processes of image formation during gas-discharge visualization (the Kirlian effect) (Review) [in Russian]. Radiotekhnik Elektronik. 1986; 31: 625–643.

Barylyak LG, Kruhliy YuZ, Zukow W, Yanchiy OR, Popovych IL. Indicators, distinctive for women with different ovarian status and different responses streslimiting effect of bioactive water Naftussya spa Truskavets'. Journal of Education, Health and Sport. 2015; 5(3): 247-258.

Becker RO. Stimulation of partial limb regeneration in rats. Nature. 1972; 235(5333): 109–111.

Becker RO. The bioelectric factors in amphibian-limb regeneration. J Bone Joint Surg Am. 1961; 43-A: 643–656.

Bell JS. On the Einstein Podolsky Rosen paradox. Physics (College Park Md). 1964; 1(3): 195–200.

Bellis M. Wilhelm Reich and the orgone accumulator. About Money. http://inventors.about.com/od/qrstartinventors/a/orgone.htm

Beloussov LV, Opitz JM, Gilbert SF. Life of Alexander G. Gurwitsch and his relevant contribution to the theory of morphogenetic fields. Int J Dev Biol. 1997; 41(6): 771-777; comment 778–779.

Berntson GG, Bigger JT jr, Eckberg DL, Grossman P, Kaufman PG, Malik M, Nagaraja HN, Porges SW, Saul JP, Stone PH, Van der Molen MW. Heart Rate Variability: Origines, methods, and interpretive caveats. Psychophysiology. 1997; 34: 623-648.

Bhat RK, Mavathur R, Srinivasan T. Diabetes mellitus type 2 and yoga: Electrophotonic imaging perspective. Int J Yoga. 2017; 10(3): 152-159.

Binhi VN, Rubin AB. Magnetobiology: the kT paradox and possible solutions. Electromagn Biol Med. 2007; 26(1): 45–62.

Bischof M, Del Giudice E. Communication and the emergence of collective behavior in living organisms: a quantum approach. Mol Biol Int. 2013; 2013:987549.

Bischof M. Vitalistic and mechanistic concepts in the history of bioelectromagnetics. In: Beloussov L, Popp F, eds. Biophotonic: non-equilibrium and coherent systems in biophysics, biology, and biotechnology. Proceedings of International Alexander Gurwitch Conference, Sept 28-Oct 2, 1994, Moscow: Bioinform Services; 1995: 3–14.

Bista S, Jasti N, Bhargav H, Sinha S, Gupta S, Ramarao P, Chaturvedi SK, Gangadhar BN. Applications of Gas Discharge Visualization Imaging in Health and Disease: A Systematic Review. Altern Ther Health Med. 2022; AT6764. Epub ahead of print. PMID: 35648690.

Bista S, Jasti N, Bhargav H. How to Interpret Integral Area Variable of Gas Discharge Visualization. Response to the Letter to Editor. Int J Yoga-Philos Psychol Parapsychol. 2019; 7(1): 24-25.

Blumenfeld R. Willhelm Reich and character analysis. In: Blumenfeld R, ed. Tools and techniques for character interpretation: a handbook of psychology for actors, writers, and directors. Pompton Plains, NJ: Limelight Editions; 2006: 135–137.

Bohm D. Wholeness and the Implicate Order. London: Routledge and Kegan Paul; 1980.

Bordyugov G, Westermark P, Korenčič A, Bernard S, Herzel H. Mathematical modeling in chronobiology. Handb Exp Pharmacol. 2013; (217): 335-357.

Boyers DG, Tiller WA. Corona Discharge Photography. J Applied Physics. 1973; 44(7): 3102-3112.

Bundzen PV, Korotkov KG, Belobaba O, et al. Correlation between the parameters of induced opto-electron emission (Kirlian effect) and the processes of corticovisceral regulation. In: Proceedings of VII International Scientific Congress on Bioelectrography, St. Petersburg, Russia, 2003: 89–91.

Bykov AT, Chernousova LD, Brodnikova NN. Bioelectrography in complex evaluation of adaptation under laser therapy in sanatorium conditions. In: Proceedings of X International Scientific Congress on Bioelectrography, St. Petersburg, Russia, 2006: 170–171.

Carney RM, Freedland KE, Stein PK, Miller GE, Steinmeyer B, Rich MW, Duntley SP. Heart rate variability and markers of inflammation and coagulation in depressed patients with coronary heart disease. J Psychosom Res. 2007; 62(4): 463-467.

Cassidy CM. What does it mean to practice an energy medicine? J Altern Complement Med. 2004; 10(1): 79–81.

Chang EH, Chavan SS, Pavlov VA. Cholinergic Control of Inflammation, Metabolic Dysfunction, and Cognitive Impairment in Obesity-Associated Disorders: Mechanisms and Novel Therapeutic Opportunities. Front Neurosci. 2019; 13: 263.

Chase CR. The Geometry of Emotions: Using Chakra Acupuncture and 5-Phase Theory to Describe Personality Archetypes for Clinical Use. Med Acupunct. 2018; 30(4): 167-178.

Chavan SS, Pavlov VA, Tracey KJ. Mechanism and therapeutic relevance of neuro-imune communication. Immunity. 2017; 46(6): 927-942.

Chavan SS, Tracey KJ. Essencial neuroscience in immunology. J Immunol. 2017; 198: 3389-3397.

Chrousos GP. Stressors, stress and neuroendocrine integration of the adaptive response. The 1997 Hans Selye memorial lecture. In: Stress of life: from molecules to man / Ed by P Csermely. Ann NYAS. 1998; 851: 311-335.

Chrousos GP. The stress response and immune function: Clinical implications: Novera H. Spector Lecture. In: Neuroimmunomodulation. Perspectives at the new millennium / Ed by A Conti et al. Ann NYAS. 2000; 917:38-67.

Ciesielska IL. Images of corona discharges as a source of information about the influence of textiles on humans. Autex Res J. 2009; 9(3): 36-41.

Cioca GH, Giacomoni P, Rein G. A correlation between GDV and heart rate variability measures: a new measure of well being. In: K.G. Korotkov (Ed.). Measuring Energy Fields: Current Research. Backbone Publishing Co. Fair Lawn, USA; 2004: 59-64.

Cosic I, Pirogova E, Vojisavljevic V, Fang Q. Electro-magnetic properties of biomolecules. FME Transanct. 2006; 34(2): 71–80.

Creath K, Schwartz GE. Measuring effects of music, noise, and healing energy using a seed germination bioassay. J Altern Complement Med. 2004; 10(1): 113–122.

Csaba G. The Immunoendocrine Thymus as a Pacemaker of Lifespan. Acta Microbiol Immunol Hung. 2016; 63(2): 139-158.

Deadman P. The five shu-points. J Chinese Med. 1993; 42: 31–38.

Del Valle-Mondragón L, Becerra-Luna B, Cartas-Rosado R, et al. Correlation between Angiotensin Serum Levels and Very-Low-Frequency Spectral Power of Heart Rate Variability during Hemodialysis. Life (Basel). 2022; 12(7): 1020.

Deo G, Itagi RK, Srinivasan TM, Kuldeep K. Effect of anapanasati meditation technique through electrophotonic imaging parameters: A pilot study. Int J Yoga. 2015; 8(2): 117-121.

Deo G, Kumar IR, Srinivasan TM, Kushwah KK. Changes in electrophotonic imaging parameters associated with long term meditators and naive meditators in older adults practicing meditation. Eur J Integr Med. 2015; 7(6): 663-668.

Deo G, Kumar IR, Srinivasan TM, Kushwah KK. Cumulative effect of short-term and long-term meditation practice in men and women on psychophysiological parameters of electrophotonic imaging: A cross-sectional study. J Complement Integr Med. 2016; 13(1): 73-82.

Dobson P, O'Keeffe E. Investigation into the GDV technique and personality. In: Proceedings of the International Scientific Conference: Measuring energy fields. Kamnik-Tunjice, Slovenia, 2007: 111–113.

Dodla R, Wilson CJ. Interaction function of oscillating coupled neurons. Phys Rev E Stat Nonlin Soft Matter Phys. 2013; 88(4): 042704.

Douglas SD, Quie PG. Investigation of Phagocytes in Disease. Churchil; 1981: 110.

Dunlap JH. Use of the GDV in Intercessory Prayer Research: Findings and Considerations. In: Measuring Energy Fields: Current Research. Fair Lawn, USA: Backbone Publishing Co.; 2004: 223-233.

Earle L. Electrophotography. San Francisco: And/Or Press; 1975.

Einstein A, Podalsky B, Rosen N. Can quantum-mechanical description of physical reality be considered complete? Phys Rev. 1935; 47: 777–780.

Eliasson AC, Krumlinde SL, Rösblad B, Beckund E, Arner M, Öhrvall AM, Rosenbaum P. The Manual Ability Classification System (MACS) for children with cerebral palsy: scale development and evidence of validity and rehabilitee. Dev Med Child Neur. 2006; 48: 549-554.

Fajda OI, Hrinchenko BV, Snihur OV, Barylyak LG, Zukow W. What Kerdoe's Vegetative Index really reflects? Journal of Education, Health and Sport. 2015; 5(12): 279-288.

Ferrell JE, Tsai TY-C, Yang Q. Modeling the cell cycle: why do certain circuits oscillate? Cell. 2011; 144(6): 874–885.

Fihura OA, Ruzhylo SV, Korda MM, Klishch IM, Żukow X, Popovych IL. The influence of the Ukrainian phytocomposition "Balm Truskavets'" on parameters of neuro-endocrine-immune complex and biophotonics in humans with maladaptation. Journal of Education, Health and Sport. 2023; 13(1): 326-337.

Fihura OA, Ruzhylo SV, Popovych IL. Ukrainian adaptogenic phytocomposition "Balm Truskavets'" modulate EEG, HRV and biophotonics (GDV) parameters. Visnyk mors'koï medytsyny. 2022; 2(95): 99-108.

Fihura OA, Ruzhylo SV, Żukow X, Popovych IL. Immediate effects of Ukrainian phytocomposition on biophotonics (GDV), EEG and HRV parameters. Journal of Education, Health and Sport. 2021; 11(7): 349-365.

Flyunt IS, Chebanenko OI, Hrinchenko BV, Barylyak LG, Popovych IL. Balneophytoradiodefensology. Influence of therapeutic factors of Truskavets' spa on the state of adaptation and protection systems of the victims of the Chernobyl disaster [in Ukrainian]. Kyiv. Computerpress; 2002: 112.

Friedman RS, Burg MM, Miles P, Lee F, Lampert R. Effects of Reiki on autonomic activity early after acute coronary syndrome. J Am Coll Cardiol. 2010; 56(12): 995–996.

Funk RH, Monsees T, Ozkucur N. Electromagnetic effects - from cell biology to medicine. Prog Histochem Cytochem. 2009; 43(4): 177–264.]

Funk RH, Monsees TK. Effects of electromagnetic fields on cells: physiological and therapeutical approaches and molecular mechanisms of interaction. A review. Cells Tissues Organs. 2006; 182(2): 59–78.

Galantsev VP, Kovalenko SG, Moltchanov AA, Prutskov VI. Lipid peroxidation, low-level chemiluminescence and regulation of secretion in the mammary gland. Experientia. 1993; 49(10): 870–875.

Gardner M. Fads and fallacies in the name of science. New York: Dover; 1957.

Garkavi LKh, Kvakina YB, Kuz'menko TS. Antistress Reactions and Activation Therapy [in Russian]. Moskva. Imedis; 1998: 654.

Garkavi LKh, Kvakina YeB, Ukolova MA. Adaptive Reactions and Resistance of the Organism [in Russian]. Rostov n/D. Rostov University Publishing House, 3rd ed add; 1990: 224.

Garkavi LKh, Romassyuk SI, Barantsev FG, Kuz'menko TS, Otkidach SA, Tatkov OV, Barantseva LP. Activation therapy in the complex of the sanatorium-resort stage of rehabilitation of patients with diseases of internal organs [in Russian]. Sochi; 2000: 94.

Gäverth J, Eliasson ACh, Kullander K, Jörgen B, Lindberg PG, Forssberg H. Sensitivity of the NeuroFlexor method to measure change in spasticity after treatment with botulinum toxin A in wrist and finger muscles. J Rehabil Med. 2014; 46(7): 629-634.

Gäverth J, Sandgren M, Lindberg PG, Forssberg H, Eliasson ACh. Test-retest and inter-rater reliability of a method to measure wrist and finger spasticity. J Rehabil Med. 2013; 45(7): 630-636.

Gibson SS. Effect of Listening to Music and Focused Meditation on the Human Energy Field as Measured by the GDV and the Profile of Mood States. In: Measuring Energy Fields: Current Research. Fair Lawn, USA: Backbone Publishing; 2004: 209-222.

Glass L. Synchronization and rhythmic processes in physiology. Nature. 2001; 410(6825): 277–284.

Gozhenko AI, Sydoruk NO, Babelyuk VYe, Dubkowa GI, Flyunt VR, Hubyts'kyi VYo, Zukow W, Barylyak LG, Popovych IL. Modulating effects of bioactive water Naftussya from layers Truskavets' and Pomyarky on some metabolic and biophysic parameters at humans with dysfunction of neuro-endocrine-immune complex. Journal of Education, Health and Sport. 2016; 6(12): 826-842.

Gozhenko AI, Korda MM, Popadynets' OO, Popovych IL. Entropy, Harmony, Synchronization and Their Neuro-Endocrine-Immune Correlates [in Ukrainian]. Odesa. Feniks; 2021: 232.

Gronowicz G, Bengston W, Yount G. Challenges for Preclinical Investigations of Human Biofield Modalities. Glob Adv Health Med. 2015; 4(Suppl): 52-57.

Hahnemann S. Organon of medicine. 6th ed. Germany: WF Wakeman; 1833.

Halberg F, Cornélissen G, Otsuka K, et al. The International BIOCOS Study Group. Cross-spectrally coherent ˜10.5- and 21-year biological and physical cycles, magnetic storms and myocardial infarctions. Neuro Endocrinol Lett. 2000; 21(3): 233–258.

Hameroff S, Nip A, Porter M, Tuszynski J. Conduction pathways in micro-tubules, biological quantum computation, and consciousness. Biosystems. 2002; 64(1-3): 149–168.

Hameroff S, Penrose R. Consciousness in the universe: A review of the "Orch OR" theory. Phys Life Rev. 2014; 11(1): 39–78.

Hameroff SR. Quantum coherence in microtubules: A neural basis for emergent consciousness? J Conscious Stud. 1994; 1(1): 91–118.

Hammerschlag R, Marx BLB, Aickin M, Marx A. Nontouch biofield therapy: a systematic review of human randomized controlled trials reporting use of only nonphysical contact treatment. J Altern Complement Med. 2014; 20(12): 881–892.

Hankey A. The influence of psychic phenomena: a new light on health. J Altern Complement Med. 2007; 13(8): 787–788.

Hasson D, Theorell T, Liljeholm-Johansson Y, Canlon B. Psychosocial and physiological correlates of self-reported hearing problems in male and female musicians in symphony orchestras. Int J Psychophysiol. 2009; 74(2): 93-100.

Haun J, Patel N, Schwartz G, Ritenbaugh C. Evaluating the use of gas discharge visualization to measure massage therapy outcomes. J Complement Integr Med. 2015; 12(3): 231-239.

Havelka D, Cifra M, Kucera O, Pokorný J, Vrba J. High-frequency electric field and radiation characteristics of cellular microtubule network. J Theor Biol. 2011; 286(1): 31–40.

Heart Rate Variability. Standards of Measurement, Physiological Interpretation, and Clinical Use. Task Force of ESC and NASPE. Circulation. 1996; 93(5): 1043-1065.

Hintz KJ, Yount GL, Kadar I, Schwartz G, Hammerschlag R, Lin S. Bioenergy definitions and research guidelines. Altern Ther Heal Med. 2003; 9(3 Suppl): A13–A30.

Ho MW, Knight DP. The acupuncture system and the liquid crystalline collagen fibers of the connective tissues. Am J Chin Med. 1998; 26(3-4): 251–263.

Ho MW, Popp FA, Warnke U, eds. Bioelectrodynamics and Biocommunication. London: World Scientific; 1994.

Ho MW. Illuminating water and life. Entropy. 2014; 16(9): 4874–4891.

Hubyts'kyi VY, Humenna OP, Barylyak LG, Bolyukh VV, Popovych IL, Maluchkova RV. Electro-skin resistance of points of acupuncture correlates with some parameters of neuroendocrine-immune complex [in Ukrainian]. Medical Hydrology and Rehabilitation. 2013; 11(2): 4-11.

Iseger TA, van Bueren NER, Kenemans JL, Gevirtz R, Arns M. A frontal-vagal network theory for Major Depressive Disorder: Implications for optimizing neuromodulation techniques. Brain Stimul. 2020; 13(1): 1-9.

Ives JA, van Wijk EP, Bat N, et al. Ultraweak photon emission as a non-invasive health assessment: a systematic review. PLoS One. 2014; 9(2): e87401.

Jain S, Hammerschlag R, Mills P, Cohen L, Krieger R, Vieten C, Lutgendorf S. Clinical Studies of Biofield Therapies: Summary, Methodological Challenges, and Recommendations. Glob Adv Health Med. 2015; 4(Suppl): 58-66.

Jain S, Mills PJP. Biofield therapies: helpful or full of hype? A best evidence synthesis. Int J Behav Med. 2010; 17(1): 1–16.

Jain S, Pavlik D, Distefan J, et al. Complementary medicine for fatigue and cortisol variability in breast cancer survivors. Cancer. 2012; 118(3): 777–787.

Jakovleva E, Korotkov K, editors. Electrophotonic applications in medicine: GDV bioelectrography research. e-book 2013.

Jerman I, Krasovec R, Leskovar RT. Deep significance of the field concept in contemporary biomedical sciences. Electromagn Biol Med. 2009; 28(1): 61–70.

Kachmar O, Voloshyn T, Hordiyevych M. Changes in Muscle Spasticity in Patients With Cerebral Palsy After Spinal Manipulation: Case Series. J Chiropr Med. 2016; 15: 299-304.

Kerdö I. Ein aus Daten der Blutzirkulation kalkulierter Index zur Beurteilung der vegetativen Tonuslage. Acta Neurovegetativa (Wien). 1966; 29(2): 250-268.

Kim JO, Mueller ChW. Factor analysis: statistical methods and practical issues (eleventh printing, 1986). In: Factor, discriminant and cluster analysis [transl. from English to Russian]. Moskva: Finansy i statistika; 1989: 5-77.

Kindzer BM, Babelyuk VY, Babelyuk NV, Popovych IL, Dubkova GI, Dobrovolskyi YG, Korsuns'kyi IH, Korolyshyn TA, Litosh S, Kindzer H, Zukow W. The device for electrostimulation "VEB-1" modulates parameters of electroencephalogram and gas discharge visualization. In: Science and society. Proc. of the 11th internat. confer. Hamilton, Canada. Acent Grafics Communications and Publishing; 2019: 159-171.

Kirlian SD, Kirlian VKh. Photographing and visual observation by means of high frequency currents. Sci Appl Photogr. 1961; 6(6): 397-403.

Klecka WR. Discriminant Analysis [trans. from English in Russian] (Seventh Printing, 1986). In: Factor, Discriminant and Cluster Analysis. Moskwa: Finansy i Statistika. 1989: 78-138.

Kohane MJ, Tiller WA. Biological processes, quantum mechanics and electromagnetic fields: the possibility of device-encapsulated human intention in medical therapies. Med Hypotheses. 2001; 56(6): 598–607.

Konikiewicz LW. Introduction to electrography: A handbook for prospective researchers of the Kirlian effect in biomedicine. Harrisburg, PA: Leonard's Associates; 1979.

Korneva EA, Shkhinek EK, Frolov BA. Neuroendocrine mechanisms of regulation of immune system functions. In: Immunophysiology / Ed Korneva EA. SPb. Nauka; 1993: 5-15.

Korneva EA. Pathways of neuro-immune communication: past and present time, clinical application [in Russian]. Meditsinskaya Immunologiya. 2020; 22(3): 405-418.

Korobka IE, Yakovleva TG, Belonosov SS, Korotkov KG, Zarubina TV. Gender Differences in the Activity of the Autonomic Nervous Systems of Healthy and Hypertensive Patients in Russia. J Appl Biotechnol Bioeng. 2017; 3(6): 84-87.

Korotkov K, Shelkov O, Shevtsov A, Mohov D, Paoletti S, Mirosnichenko D, et al. Stress reduction with osteopathy assessed with GDV electrophotonic imaging: Effects of osteopathy treatment. J Altern Complement Med. 2012; 18(3): 251-257.

Korotkov K, Williams B, Wisneski LA. Assessing biophysical energy transfer mechanisms in living systems: The basis of life processes. J Altern Complement Med. 2004; 10(1): 49-57.

Korotkov K. Review of EPI papers on medicine and psychophysiology published in 2008-2018. Int J Complement Alt Med. 2018; 11(5): 311-315.

Korotkov KG, Matravers P, Orlov DV, Williams BO. Application of electrophoton capture (EPC) analysis based on gas discharge visualization (GDV) technique in medicine: a systematic review. J Altern Complement Med. 2010; 16(1): 13-25.

Korotkov KG, Williams BO, Bugno TJ, Parsons PH, et al., editors. Human energy field: study with GDV bioelectrography. Fair Lawn, NJ: Backbone Publishing; 2002.

Korotkov KG. Basics GDV Bioelectrography [in Russian]. SPb. SPbGITMO(TU); 2001: 360.

Korotkov KG. Energy Fields Electrophotonic Analysis in Humans and Nature. Second updated edition. Translated from Russian by the author. Edoted by Berney Williams and Lutz Rabe. 2014: 233.

Korotkov KG. Principles of Analysis in GDV Bioelectrography [in Russian]. SPb. Renome; 2007: 286.

Korotkov KG. Principles of the human body functioning and their applications in integrative medicine (review). J Appl Biotechnol Bioeng. 2018; 5(6): 346–348.

Korotkova AK. Gas discharge visualization bioelectrography method in studies of master-sportsmens psychophysiology. Abstract of a PhD thesis in psychology [in Russian]. St Petersburg, Russia, 2006.

Kostyuk PG, Popovych IL, Ivassivka SV (editors). Chornobyl', Adaptive and Defensive Systems, Rehabilitation [in Ukrainian]. Kyiv. Computerpress; 2006: 348.

Kotelnikov SA, Nozdrachov AD, Odinak MM, Shustov EB, Kovalenko IY, Davidenko VYu. Heart rate variability: ideas about mechanisms [in Russian]. Fiziologiya cheloveka. 2002; 28(1): 130-143.

Kozyavkin VI, Babadahly MO, Lun HP, Kachmar OO, Hordiyevych SM, Lysovych VI, Voloshyn BD. Intensive Neurophysiological Rehabilitation System – the Kozyavkin method. A manual for Rehabilitation Spetialists. L'viv. "Papuga" Publishing Hous; 2012: 240.

Kozyavkin VI, Kachmar OO, Voloshyn TB, Hordiyevych MS. Muscular tone components and methods of quantitative measurement of spasticity [in Ukrainian]. J of Neuroscience of BM Mankovskyi. 2015; 3(1): 72-76.

Kozyavkin VI, Kozyavkina NV, Kozyavkina OV, Gordiyevych MS, Lysovych VI, Voloshyn TB, Popovych IL, Zukow W. Effect of spine biomechanical correction Kozyavkin's method (INRS) on components of muscle tone in children with spastic form of Cerebral Palsy and its possible prediction. Journal of Education, Health and Sport. 2015; 5(1): 11-30.

Kozyavkin VI, Kozyavkina NV, Kozyavkina OV, Voloshyn TB, Hordiyevych MS, Popovych IL. Relationships between changes in neural component of muscle tone and parameters of EEG, HRV, GDV at children with spastic form of cerebral palsy. In: Mater of the X Sci-Pract conf "Actual issues of pathology under the conditions of action of extraordinary factors on the body" (Ternopil', October 5-6, 2017). Ternopil'; 2017: 56-57.

Kozyavkin VI, Kozyavkina OV, Kozyavkina NV, Gordiyevych MS, Lysovych VI, Voloshyn TV, Zukow W, Popovych IL. Estimation of effectivenes of spine biomechanical correction Kozyavkin method (INRS) in children with spastic form of cerebral palsy. Journal of Education, Health and Sport. 2015; 5(2): 208-217.

Kozyavkin VI, Kozyavkina OV, Kozyavkina NV, Voloshyn TB, Gordiyevych MS, Popovych IL. Relationships between changes in neural component of muscle tone and parameters of EEG, HRV, gas disharge visualization at children with spastic form of cerebral palsy during

intensive neurophysiological rehabilitation. In: Pathophysiology and Pharmacy: ways of integration. Abstracts VII National Congress of Pathophysiologists Ukraine with international participation (5-7 October 2016). Kharkiv. NPhU; 13-13.

Kozyavkin VI, Kozyavkina OV, Kozyavkina NV, Voloshyn TB, Gordiyevych MS, Popovych IL. Changes in neural component of muscle tone at children with spastic form of cerebral palsy caused by intensive neurophysiological rehabilitation, their relationship with changes in parameters of EEG, HRV, GDV and possibility of forecasting. In: XVI International Conference "The current status and approaches to development of physical and rehabilitation medicine in Ukraine according to international standards" (15-16 December 2016, Kiev). Kyïv, 2016: 74-75.

Kozyavkin VI, Sak NM, Kachmar OO, Babadahly MO. Basics of Rehabilitation of Motor Disfunctions by Kozyavkin method [in Ukrainian]. L'viv. Ukrainian technologies; 2007: 192.

Kozyavkin VI. The system of intensive neurophysiological rehabilitation [in Ukrainian]. Medical Hydrology and Rehabilitation. 2003; 1(2): 63-67.

Kozyavkina OV, Kozyavkina NV, Gozhenko OA, Gozhenko AI, Barylyak LG, Popovych IL. Bioactive Water Naftussya and Neuroendocrine-Immune Complex [in Ukrainian]. Kyïv. UNESCO-SOCIO; 2015: 349.

Kozyavkina OV, Kozyavkina NV, Hordiyevych MS, Voloshyn TB, Lysovych RV, Popovych IL. Caused by Kozyavkin© method changes in hand function parameters in children with spastic form of cerebral palsy and their forecasting. In: Rehabilitation Medicine and Health-Resort Institutions Development. Proceedings of the 19th International Applied Research Conference (Kyïv, 11-12 December 2019). Edited by O. Gozhenko, W. Zukow. Toruń, Kyïv. 2019: 81-82.

Kozyavkina OV, Kozyavkina NV, Hordiyevych MS, Voloshyn TB, Lysovych VI, Babelyuk VY, Dubkova HI, Korolyshyn TA, Popovych DV, Mysula IR, Zukow W, Popovych IL. Forecasting caused by Kozyavkin© method changes in hand function parameters in children with spastic form of cerebral palsy at their baseline levels as well as EEGs, HRVs and GDVs. Achivements of Clinical and Experimental Medicine. 2018; 4: 17-35.

Kozyavkina OV, Kozyavkina NV, Voloshyn TB, Hordiyevych MS, Lysovych VI, Babelyuk VY, Dubkova HI, Korolyshyn TA, Mysula IR, Popovych DV, Zukow W, Popovych IL. Caused by Kozyavkin© method changes in hand function parameters in children with spastic form of cerebral palsy and their EEGs, HRVs and GDVs accompaniments. Journal of Education, Health and Sport. 2018; 8(10): 11-30.

Krashenuk AI, Danilov AD, Korotkov KG. Investigation of system optimization of vegetative nervous system work under hirudotherapy impact as a result of comparative analysis of GDV signal and cardiorhythm nonlinear analysis. In: Proceedings of X International Scientific Congress on Bioelectrography, St. Petersburg, Russia, 2006: 31–35.

Kruhliy YuZ. Features of the influence of bioactive water Naftussya on the level of chronic stress in women with different ovarian status [in Ukrainian]. Medical hydrology and rehabilitation. 2010; 8(4): 62-68.

Kruhliy YuZ. Neuroendocrine support of polyvariant effects of Naftussya bioactive water on the level of chronic stress in women with different ovarian status [in Ukrainian]. Medical hydrology and rehabilitation. 2012; 10(2): 92-96.

Kul'chyns'kyi AB, Gozhenko AI, Zukow W, Popovych IL. Neuro-immune relationships at patients with chronic pyelonephritis and cholecystitis. Communication 3. Correlations between parameters EEG, HRV and Immunogram. Journal of Education, Health and Sport. 2017; 7(3): 53-71.

Kul'chyns'kyi AB, Kovbasnyuk MM, Korolyshyn TA, Kyjenko VM, Zukow W, Popovych IL. Neuro-immune relationships at patients with chronic pyelonephrite and cholecystite.

Communication 2. Correlations between parameters EEG, HRV and Phagocytosis. Journal of Education, Health and Sport. 2016; 6(10): 377-401.

Kul'chyns'kyi AB, Kyjenko VM, Zukow W, Popovych IL. Causal neuro-immune relationships at patients with chronic pyelonephritis and cholecystitis. Correlations between parameters EEG, HRV and white blood cell count. Open Medicine. 2017; 12(1): 201-213.

Kul'chyns'kyi AB, Zukow W, Korolyshyn TA, Popovych IL. Interrelations between changes in parameters of HRV, EEG and humoral immunity at patients with chronic pyelonephritis and cholecystitis. Journal of Education, Health and Sport. 2017; 7(9): 439-459.

Kumar K, Mondal B, Nagendra H, Ilavarasu J, Srinivasan T. Classification of electrophotonic images of yogic practice of mudra through neural networks. Int J Yoga. 2018; 11(2): 152-156.

Kushwah KK, Nagendra HR, Srinivasan TM. Effect of integrated yoga program on energy outcomes as a measure of preventive health care in healthy people. Cent Eur J Sport Sci Med. 2015; 12(4): 61-71.

Kushwah KK, Srinivasan T, Nagendra H, Ilavarasu JV. Development of normative data of electrophotonic imaging technique for healthy population in India: A normative study. Int J Yoga [Internet]. 2016; 9(1): 49-56.

Kushwah KK, Srinivasan TM, Nagendra HR, Ilavarasu JV. Effect of yoga-based techniques on stress and health indices using electrophotonic imaging technique in managers. J Ayurveda Integr Med. 2016; 7(2): 119-123.

Kuzin AM, Surkenova GM. Secondary biogenic irradiation of plant structures after gamma-irradiation at low dose. In: Beloussov LV, Editor. Biophotonics. Moscow: Bioinform Services; 1995: 257–265.

Lambrou P, Pratt G, Chevalier G. Physiological and psychological effects of a mind/body therapy on claustrophobia. Subtle Ener Ener Med. 2003; 14(3): 767–774.

Lampert R, Bremner JD, Su S, Miller A, Lee F, Cheema F, Goldberg J, Vaccarino V. Decreased heart rate variability is associated with higher levels of inflammation in middle-aged men. Am Heart J. 2008; 156(4): 759.e1-7.

Langevin HM. Connective tissue: a body-wide signaling network? Med Hypotheses. 2006; 66(6): 1074–1077.

Lapovets' LYe, Lutsyk BD. Handbook of Laboratory Immunology [in Ukrainian]. L'viv. 2004: 173.

Lara-Aparicio M, Barriga-Montoya C, Padilla-Longoria P, Fuentes-Pardo B. Modeling some properties of circadian rhythms. Math Biosci Eng. 2014; 11(2): 317–330.

Levin M. Endogenous bioelectrical networks store non-genetic patterning information during development and regeneration. J Physiol. 2014; 592(Pt 11): 2295–2305.

Levin M. The wisdom of the body: future techniques and approaches to morphogenetic fields in regenerative medicine, developmental biology and cancer. Regen Med. 2011; 6(6): 667–673.

Lindberg PG, Gäverth J, Islam M, Fagergren A, Borg J, Forssberg H. Validation of a new biomechanical model to measure muscle tone in spastic muscles. Neurorehabil Neural Repair. 2011; 25(7): 617-625.

Lovygina ON. The method of gas discharge visualization within the system of assessment of vegetative functions in sportsmen's organisms. In: Proceedings of IX International Scientific Congress on Bioelectrography, St. Petersburg, Russia, 2005: 21–22.

Lutgendorf SK, Mullen-Houser E, Russell D, et al. Preservation of immune function in cervical cancer patients during chemoradiation using a novel integrative approach. Brain Behav Immun. 2010; 24(8): 1231–1240.

Maizes V, Rakel D, Niemiec C. Integrative medicine and patient-centered care. Explore (NY). 2009; 5(5): 277–89.

Markus RP, Fernandes PA, Kinker GS, da Silveira Cruz-Machado S, Marçola M. Immune-pineal axis - acute inflammatory responses coordinate melatonin synthesis by pinealocytes and phagocytes. Br J Pharmacol. 2018; 175(16): 3239-3250.

Markus RP, Ferreira ZS, Fernandes PA, Cecon E. The immune-pineal axis: a shuttle between endocrine and paracrine melatonin sources. Neuroimmunomodulation. 2007; 14(3-4): 126-133.

Marques-Deak A, Cizza G, Sternberg E. Brain-immune interactions and disease susceptibility. Mol Psychiatry. 2005; 10(3): 239-250.

Mathiowetz V, Federman S, Wiemer D. Box and Block Test of Manual Dexterity: Norms for 6-19 Year Olds. Canad J Occup Ther. 1985; 52(5): 241-245.

McCraty R, Atkinson M, Tomasino D, Bradley RT. The coherent heart, heart–brain interactions, psychophysiological coherence, and the emergence of system-wide order. Integr Rev. 2009; 5(2): 10–115.]

McCraty R, Deyhle A, Childre D. The global coherence initiative: creating a coherent planetary standing wave. Global Adv Health Med. 2012; 1(1): 64–77.

McCraty R. The energetic heart: Bioelectromagnetic communication within and between people. In: Rosch PJ, Markov MS, eds. Bioelectromagnetic Medicine. New York: Marcel Dekker; 2005: 511–530.

Mintser OP, Potiazhenko MM, Nevoit GV. Evaluation of the human bioelectromagnetic field in medicine: the development of methodology and prospects are at the present scientific stage. Wiadomości Lekarskie. 2019; 5(II): 1117-1121.

Miskovic V, Schmidt LA. Frontal brain electrical asymmetry and cardiac vagal tone predict biased attention to social threat. Int J Psychophysiol. 2010; 75(3): 332-338.

Movaffaghi Z, Farsi M. Biofield therapies: biophysical basis and biological regulations? Complement Ther Clin Pr. 2009; 15(1): 35–37.

Muehsam D, Chevalier G, Barsotti T, Gurfein BT. An Overview of Biofield Devices. Glob Adv Health Med. 2015; 4(Suppl): 42-51.

Muehsam D, Ventura C. Life rhythm as a symphony of oscillatory patterns: electromagnetic energy and sound vibration modulates gene expression for biological signaling and healing. Glob Adv Heal Med. 2014; 3(2): 40–56.

Muehsam DJ, Pilla AA. A Lorentz model for weak magnetic field bioeffects: part II - secondary transduction mechanisms and measures of reactivity. Bioelectromagnetics. 2009; 30(6): 476–488.

Muehsam DJ, Pilla AA. The sensitivity of cells and tissues to exogenous fields: effects of target system initial state. Bioelectrochem Bioenerg. 1999; 48(1): 35–42.

Nance DM, Sanders VM. Autonomic innervation and regulation of immune system (1987-2007). Brain Behav Immun. 2007; 21(6): 736-745.

Nelson R, Bancel P. Effects of mass consciousness: changes in random data during global events. Explore (NY). 2011; 7(6): 373–383.

Neuroimmunomodulation. Perspectives at the new millennium / Ed by A Conti, GJM Maestroni, SM McCann, EM Sternberg, JM Lipton and CC Smith. Ann NYAS. Vol 917. NY; 2000: 987.

Nevoit GV, Potiazhenko MM, Mintser OP, Babintseva LYu. Electro-photonic emission analysis and hardware-software recording of heart rate variability during an objective structured clinical examination. Svit Medytsyny ta Biologiyi. 2020; 4(74): 107-111.

Noguchi A, Shikano Y, Toyoda K, Urabe S. Aharonov-Bohm effect in the tunnelling of a quantum rotor in a linear Paul trap. Nat Commun. 2014; 5: 3868.

Northrup GW. Osteopathic medicine: an american reformation. Chicago: American Osteopathic Association; 1966.

O'Keeffe E. The GDV technique as an aide to stress assessment and its potential application in recruitment and selection of individuals suited to positions associated with high level of stress. In: Proceedings of X International Scientific Congress on Bioelectrography, St. Petersburg, Russia, 2006: 202–204.

Panossian AG, Efferth T, Shikov AN, Pozharitskaya ON, Kuchta K, Mukherjee PK, Banerjee S, Heinrich M, Wu W, Guo DA, Wagner H. Evolution of the adaptogenic concept from traditional use to medical systems: Pharmacology of stress- and aging-related diseases. Med Res Rev. 2021; 41(1): 630-703.

Pat. 10271 Ukraine MKI A 61 K 31/00. Adaptogenic agent [in Ukrainian]. Panasyuk YM, Levkut LG, Popovych IL, Shumakov MF, Sychova AO, Alekseyev OI, Bakova MM. 1996. Bull № 4.

Patten T, Hutchison M. Interview with Lt. Col. Thomas E. Bearden (ret). Megabrain Report. February 4, 1991. http://www.cheniere.org/misc/interview1991.htm.

Pavlov VA, Chavan SS, Tracey KJ. Molecular and functional neuroscience in immunity. Annu Rev Immunol. 2018; 36: 783-812.

Pavlov VA, Tracey KJ. The vagus nerve and the inflammatory reflex-linking immunity and metabolism. Nat Rev Endocrinol. 2012; 8(12): 743-754.

Petsyukh SV, Petsyukh MS, Kovbasnyuk MM, Barylyak LG, Zukow W. Relationships between Popovych's Adaptation Index and parameters of ongoiging HRV and EEG in patients with chronic pyelonephrite and cholecystite in remission. Journal of Education, Health and Sport. 2016; 6(2): 99-110.

Pilla AA. Mechanisms and therapeutic applications of time varying and static magnetic fields. In: Biological and Medical Aspects of Electromagnetic Fields. Barnes FS, Greenebaum B, Editors. Boca Raton, FL: CRC Press; 2007: 351–411.

Pizzi R, Fantasia A, Gelain F, Rossetti D, Vescovi A. Non-local correlations between separated neuronal networks. Proc SPIE. 2004; 5436: 107–117.

Plankar M, Brežan S, Jerman I. The principle of coherence in multi-level brain information processing. Prog Biophys Mol Biol. 2013; 111(1): 8–29.

Polushin US, KorotkovKG, Korotkina SA, et al. Perspectives of the application of gas discharge visualization for the estimation of organism condition at critical states. In: Proceedings of IX International Scientific Congress on Bioelectrography. St. Petersburg, Russia: 2004: 115–116.

Poole JL, Burtner PA, Torres TA, McMullen CK, Markham A, Marcum ML, Anderson JB, Qualls C. Measuring Dexterity in Children using the Nine Hole Peg Test. J Hand Ther. 2005; 18(3): 348-351.

Popovych IL, Babelyuk VY, Dubkova HI, Korolyshyn TA, Zukow W. Relationships between changes in parameters of manual function and electroencephalogram, heart rate variability as well as gas discharge visualization in children with spastic form of cerebral palsy caused by Kozyavkin$^©$ method. Experimental and Clinical Physiology and Biochemistry. 2018; 1(81): 39-50.

Popovych IL, Babelyuk VYe, Dubkova GI. Parameters of bioelectrography (kirlianography) is closely correlated with parameters of heart rate variability and blood pressure [in Ukrainian]. In: IX VV Podvysotskyi reading: Bulletin Materials Scientic Conference (Odesa, 27-28 May 2010). Odesa. OSMU; 2010: 143-144.

Popovych IL, Babelyuk VYe, Dubkova GI. Relations between the parameters bioelectrography (kirlianography) and heart rate variability and blood pressure [in Ukrainian]. Medical Hydrology and Rehabilitation. 2010; 8(1): 4-16.

Popovych IL, Flyunt IS, Alyeksyeyev OI, Barylyak LG, Bilas VR. Sanogenetic Bases of Rehabilitation on Spa Truskavets' Urological Patients from Chornobylian Contingent [in Ukrainian]. Kyiv. Computerpress; 2003: 192.

Popovych IL, Flyunt IS, Nishcheta IV et al. General adaptive reactions and resistance of the organism of liquidators of the Chornobyl' accident [in Ukrainian]. Kyiv. Computerpress; 2000: 117.

Popovych IL, Gozhenko AI, Korda MM, Klishch IM, Popovych DV, Zukow W (editors). Mineral Waters, Metabolism, Neuro-Endocrine-Immune Complex. Odesa. Feniks; 2022: 252.

Popovych IL, Gozhenko AI, Zukow W, Polovynko IS. Variety of Immune Responses to Chronic Stress and their Neuro-Endocrine Accompaniment. Scholars' Press. Riga; 2020: 172.

Popovych IL, Kozyavkina OV, Kozyavkina NV, Korolyshyn TA, Lukovych YuS, Barylyak LG. Correlation between Indices of the Heart Rate Variability and Parameters of Ongoing EEG in Patients Suffering from Chronic Renal Pathology. Neurophysiology. 2014; 46(2): 139-148.

Popovych IL, Kul'chyns'kyi AB, Gozhenko AI, Zukow W, Kovbasnyuk MM, Korolyshyn TA. Interrelations between changes in parameters of HRV, EEG and phagocytosis at patients with chronic pyelonephritis and cholecystitis. Journal of Education, Health and Sport. 2018; 8(2): 135-156.

Popovych IL, Kul'chyns'kyi AB, Korolyshyn TA, Zukow W. Interrelations between changes in parameters of HRV, EEG and cellular immunity at patients with chronic pyelonephritis and cholecystitis. Journal of Education, Health and Sport. 2017; 7(10): 11-23.

Popovych IL, Lukovych YuS, Korolyshyn TA, Barylyak LG, Kovalska LB, Zukow W. Relationship between the parameters heart rate variability and background EEG activity in healthy men. Journal of Health Sciences. 2013; 3(4): 217-240.

Popovych IL. Similarity effects of two types of adaptogens (transcutaneous electrical stimulation with the device "VEB" ® and using of bioactive Naftussya water) on the human body. Journal of Education, Health and Sport. 2022; 12(4): 213-258.

Popovych IL. Stresslimiting Adaptogene Mechanism of Biological and Curative Activity of Water Naftussya [in Ukrainian]. Kyïv. Computerpress; 2011: 300.

Popovych IL. The concept of neuro-endocrine-immune complex (review) [in Russian]. Medical Hydrology and Rehabilitation. 2009; 7(3): 9-18.

Popp FA, Becker G, Konig H, Peschka W, eds. Elektromagnetic Bioinformation. Munich: Urban und Schwarzenberg; 1979.

Popp FA, Chang JJ. The physical background and the informational character of biophoton emission, In: Chang JJ, Fisch J, Popp FA; Editors. Biophotons. Dordrecht, The Netherlands: Kluwer; 1998: 238–250.

Popp FA, Nagl W, Li KH, Scholz W, Weingärtner O, Wolf R. Biophoton emission. New evidence for coherence and DNA as source. Cell Biophys. 1984; 6(1): 33–52.

Popp FA. Electromagnetic Bio-Information. Baltimore, MD: Urban und Schwarzenberg; 1989. Practical psychodiagnostics. Techniques and tests [in Russian]. Samara. Bakhrakh; 1998: 59-64.

Puchko LG. Multidimensional Medicine. Systen of Self-diagnosis and Self-healing of Human [in Russian]. 10th ed. rev. and ext. Moskva. ANS: 2004: 432.

Radin D, Nelson R. Meta-analysis of mind-matter interaction experiments: 1959-2000, I.a.E.M. In: Healing , ed. London: Harcourt Health Sciences; 2003: 39–48.

Radin D, Schlitz M, Baur C. Distant Healing Intention Therapies: An Overview of the Scientific Evidence. Glob Adv Health Med. 2015; 4(Suppl): 67-71.

Radin D, Stone J, Levine E, et al. Compassionate intention as a therapeutic intervention by partners of cancer patients: effects of distant intention on the patients' autonomic nervous system. Explore (NY). 2008; 4(4): 235–243.

Radin D, Yount G. Effects of healing intention on cultured cells and truly random events. J Altern Complement Med. 2004; 10(1): 103–112.

Radin DI. Event-related electroencephalographic correlations between isolated human subjects. J Altern Complement Med. 2004; 10(2): 315–323.

Rao IT, Nagendra RH. The effect of active and silent music interventions on patients with type 2 diabetes measured with electron photonic imaging technique. Int J Humanit Soc Sci. 2014; 3(5): 7-14.

Rao TI, Kushwah KK, Srinivasan TM. Effect of Indian devotional music on students and performers measured with electron photonic imaging. Online Int Interdiscip Res J. 2014; 4(4): 284-291.

Rein G. Bioinformation within the biofield: beyond bioelectromagnetics. J Altern Complement Med. 2004; 10(1): 59–68.

Rezzani R, Franco C, Hardeland R, Rodella LF. Thymus-Pineal Gland Axis: Revisiting Its Role in Human Life and Ageing. Int J Mol Sci. 2020; 21(22): 8806.

Richards TL, Kozak L, Johnson LC, Standish LJ. Replicable functional magnetic resonance imaging evidence of correlated brain signals between physically and sensory isolated subjects. J Altern Complement Med. 2005; 11(6): 955–963.

Roberts NR, Shealy CN, Tiller WA. Are There Electrical Devices that can Measure the body's Energy State Change to an Acupuncture Treatment? Part II. The Gas Discharge Visualization (GDV) Device. In: Measuring Energy Fields: Current Research. Fair Lawn, USA: Backbone Publishing; 2004: 31-38.

Roe CA, Sonnex C, Roxburgh EC. Two meta-analyses of noncontact healing studies. Explore (NY). 2015; 11(1): 11–23.

Romodanov AP (editor). Postradiation Encephalopathy. Experimental Researches and Clinical Observations [in Ukrainian and Russian]. Kyïv. USRI of Neurosurgery; 1993: 224.

Rubik B, Brooks AJ. Digital high-voltage electrophotographic measures of the fingertips of subjects pre- and post-Qigong. Evidence-Based Integr Med. 2005; 2(4): 245-252.

Rubik B, Muehsam D, Hammerschlag R, Jain S. Biofield Science and Healing: History, Terminology, and Concepts. Glob Adv Health Med. 2015; 4(Suppl): 8-14.

Rubik B, Pavek R, Greene E, Laurence D, Ward R, Al E. Manual healing methods. In: Rubik B, et al, eds. Alternative medicine: expanding medical horizons: a report to the National Institutes of Health on alternative medical systems and practices in the United States (NIH Publication). Washington, DC: US Government Printing Office; 1995: 113–157.

Rubik B, Walleczek J, Liboff A, Hazelwood C, Becker R. Bioelectromagnetics Applications in Medicine. In: Rubik B, Al E. (11-member editorial review board), eds. Alternative Medicine: Expanding Medical Horizons: A Report to the National Institutes of Health on Alternative Medical Systems and Practices in the United States. Washington, DC: US Government Printing Office; 1995: 45–65.

Rubik B. Energy medicine and the unifying concept of information. Altern Ther Health Med. 1995; 1(1): 34–39.

Rubik B. Information, energy, and the unpredictable whole. Adv J Mind-Body Heal. 1997; 13(2): 67–70.

Rubik B. The biofield hypothesis: its biophysical basis and role in medicine. J Altern Complement Med. 2002; 8(6): 703–717.

Russell DJ, Avery LM, Walter SD, Hanna SE, Bartlett DJ, Rosenbaum PL, Palisano RJ, Gorter JW. Development and validation of item sets to improve efficiency of administration of the 66-item Gross Motor Function Measure in children with cerebral palsy. Dev Med Child Neur. 2010; 52(2): 48-54.

Sahoo S, Pradhan B. The immediate effect on psycho-physiological changes after practice set of asana. Int J Yoga-Philos Psychol Parapsychol. 2015; 1(2): 82-86.

Scalar Waves Healing Center. History and health benefits of scalar wave healing. www.wavesofhealing.net/aboutscalarwaves.html.

Schiegl H. Healing magnetism. Freiburg, Germany: Herman Verlag KG; 1983.

Schlitz M, Hopf HW, Eskenazi L, Vieten C, Radin D. Distant healing of surgical wounds: an exploratory study. Explore (NY). 2012; 8(4): 223–230.

Senzon SA. Chiropractic and energy medicine: a shared history. J Chiropr Humanit. 2008: 27–54.

Shaffer F, Ginsberg JP. An Overview of Heart Rate Variability Metrics and Norms. Front Public Health. 2017; 5: 258.

Shankar NR, Palukuru S, Deo G, Manjunath N, Nagendra H. Comparative study of diet effect (fresh coconut and groundnut) on healthy adults using electrophotonic imaging parameters. Indian J Basic Appl Med Res. 2016; 6(1): 147-153.

Shannon CE. A mathematical theory of information. Bell Syst Tech J. 1948; 27: 379-423.

Sheldrake R. A New Science of life: the hypothesis of formative causation. London: Blond and Briggs; 1981.

Shen X, Bei L, Hu TH, Aryal B. The possible role played by biophotons in the long-range interaction between neutrophil leukocytes. In: Beloussov LV, Voeikov VL, VanWijk R, Editors. Biophotonics and coherent systems in biology. Moscow: Moscow University Press; 2000: 336–346.

Shupak N. Therapeutic uses of pulsed magnetic-field exposure: A review. Radio Sci Bull. 2003; 307: 9–32.

Sorokin OV, Druzhinin VS, Efimenko VG, Golubkov ME, Popov KV, Kuimov AD, Korotkov KG, Kulikov VY. The nature of the relationship between photoelectron emission and autonomic regulation of cardiac rhythm in patients with ischemic heart disease. Medicine and Education in Siberia. 2009; 4: 23-27.

Spielberger CD. Manual for the State-Trait Anxiety Inventory (Form Y) Consulting Psychologists Press; Palo Alto (CA): 1983.

Standish LJ, Johnson LC, Kozak L, Richards T. Evidence of correlated functional magnetic resonance imaging signals between distant human brains. Altern Ther Health Med. 2003; 9(1): 128, 122–125.

Standish LJ, Kozak L, Johnson LC, Richards T. Electroencephalographic evidence of correlated event-related signals between the brains of spatially and sensory isolated human subjects. J Altern Complement Med. 2004; 10(2): 307–314.

Stapp HP. Mind, Matter and Quantum Mechanics. Berlin, Heidelberg: Springer Verlag; 2009.

Steinhoff U, Schnabel A, Burghoff M, et al. Spatial distribution of cardiac magnetic vector fields acquired from 3120 SQUID positions. Neurol Clin Neurophysiol. 2004; 2004: 59.

Sternberg EM. Neural regulation of innate immunity: a coordinated nonspecific response to pathogens. Nat Rev Immunol. 2006; 6(4): 318-328.

Stoupel E. The effect of geomagnetic activity on cardiovascular parameters. Biomed Pharmacother. 2002; 56(Suppl 2): 247s–256s.

Sushrutha S, Hegde M, Nagendra HR, Srinivasan TM. Comparative study of influence of Yajna and Yoga sana on stress level as measured by electron photonic imaging (EPI) technique. Int J Sci Res. 2014; 3(8):1402-1406.

Sushrutha S, Madappa K, Nagendra HR. Effect of Bhaishajya Maha Yajna on human energy field and environment. Int J Innov Res Sci Eng. 2014; 1-8.

Swanson C. Life force, the scientific basis: breakthrough physics of energy medicine, healing, chi and euantum consciousness. Tucson, AZ: Poseidia Press; 2011.

Syldona M, Rein G. The use of DC electrodermal potential measurements and healer's felt sense to assess the energetic nature of qi. J Altern Complement Med. 1999; 5(4): 329–347.

Taylor JA, Carr DL, Myers CW, Eckberg DL. Mechanisms underlying very-low-frequency RR-interval oscillations in humans. Circulation. 1998; 98(6): 547-555.

Thaheld FH. An interdisciplinary approach to certain fundamental issues in the fields of physics and biology: towards a unified theory. Biosystems. 2005; 80(1): 41–56.

Thayer JF, Lane RD. Claude Bernard and the heart-brain connection: further elaboration of a model of neurovisceral integration. Neurosci Biobehav Rev. 2009; 33: 81-88.

Thayer JF, Sternberg EM. Neural aspects of immunomodulation: Focus on the vagus nerve. Brain Behav Immun. 2010; 24(8): 1223-1228.

Thayer JF, Sternberg EM. Neural concomitants of immunity - focus on the vagus nerve. Neuroimage. 2009; 47(3) :908-910.

Theorell T, Liljeholm-Johansson Y, Björk H, Ericson M. Saliva testosterone and heart rate variability in the professional symphony orchestra after "public faintings" of an orchestra member. Psychoneuroendocrinology. 2007; 32(6): 660-668.

Tiller WA, Kohane MJ, Dibble WE. Can an aspect of consciousness be imprinted into an electronic device? Integr Physiol Behav Sci. 2000; 35(2): 142–162; discussion 163.

Tolkunov D, Rubin D, Mujica-Parodi LR. Power spectrum scale invariance quantifies limbic dysregulation in trait anxious adults using fMRI: adapting methods optimized for characterizing autonomic dysregulation to neural dynamic timeseries. Neuroimage. 2010; 50(1): 72-82.

Tracey KJ. Physiology and immunology of the cholinergic antiinflammatory pathway. J Clin Invest. 2007; 117(2): 289-296.

Tracey KJ. Reflex control of immunity. Nat Rev Immunol. 2009; 9(6): 418-428.

Tracey KJ. The inflammatory reflex. Nature. 2002; 420: 853-859.

Tracey KJ. Understanding immunity requires more than immunology. Nature Immunology. 2010; 11(7): 561-564.

Tsuchita K, Motoyama H. Study of body's energy changes in non-touch energy healing 1. Pranic healing protocol applied for a breast cancer subject. Subtle Ener Ener Med. 2009; 20(2): 15–30.

Uchakin PN, Uchakina ON, Tobin BV, Yershov FI. Neuroendocrine Immunomodulation [in Russian]. Vestnik Ross. AMN. 2007; 9: 26-32.

Van Wijk R. Bio-photons and bio-communication. J Sci Explor. 2001; 15(2): 183–197.

Wackermann J, Seiter C, Keibel H, Walach H. Correlations between brain electrical activities of two spatially separated human subjects. Neurosci Lett. 2003; 336(1): 60–64.

Walker SI, Davies PC. The algorithmic origins of life. J R Soc Interface. 2012; 10(79): 20120869.

Wang YC, Magasi SR, Bohannon RW, Reuben DB, McCreath HE, Bubela DJ, Gershon RC, Rymer WZ. Assessing Dexterity Function: A Comparison of Two Alternatives for the NIH Toolbox. J Hand Ther. 2011; 24(4): 313-321.

Warber SL, Cornelio D, Straughn J, Kile G. Biofield energy healing from the inside. J Altern Complement Med. 2004; 10(6): 1107–1113.

Winkelmann T, Thayer JF, Pohlak ST, Nees F, Grimm O, Flor H. Structural brain correlates of heart rate variability in healthy young adult population. Brain Structure and Function. 2017; 222(2): 1061-1068.

Wisneski LA, Anderson L. The Scientific Basis of Integrative Medicine, Second Edition. CRC Press; 2009: 205–229.

Yakovleva E, Korotkov K. Electrophotonic Analysis in Medicine: GDV Bioelectrography Research. Amazon.com Publishing. Saint Petersburg, Russia; 2012: 143.

Yoo BB, Sarkis KM. The Enteric Network: Interactions between the Immune and Nervous Systems of the Gut. Immunity. 2017; 46(6): 910-926.

Yoo HJ, Thayer JF, Greenig S, Lee TH, Ponzio A, Min J, Sakaki M, Nga L, Mater M, Koenig J. Brain structural concomitants of resting state heart rate variability in the young and old:

evidence from two independent samples. Brain Structure and Function. 2018; 223(2): 727-737.

Yurth DG. Torsion field mechanics: verification of non-local field effects in human biology. June 23, 2000. http://www.clayandiron.com/news.jhtml?method=view&news.id=1509.

Zhadin MN. Review of Russian literature on biological action of DC and low-frequency AC magnetic fields. Bioelectromagnetics. 2001; 22(1): 27–45.

Zhao Y, Zhan Q. Electric fields generated by synchronized oscillations of microtubules, centrosomes and chromosomes regulate the dynamics of mitosis and meiosis. Theor Biol Med Model. 2012; 9: 26.

Zhao Y, Zhan Q. Electric oscillation and coupling of chromatin regulate chromosome packaging and transcription in eukaryotic cells. Theor Biol Med Model. 2012; 9: 27.

189

Bohomolets' Institute of Physiology
National Academy of Sciences, Kyïv, Ukraine
Ukrainian Scientific Research Institute of Medicine of Transport
Ministry of Health of Ukraine, Odesa
Kozyavkin International Rehabilitation Clinic, Truskavets', Ukraine
Yuriy Fed'kovych National University
Ministry of Science and Education, Chernivtsi, Ukraine

Editors

Valeriy Y. Babelyuk
Igor L. Popovych

GAS DISCHARGE VISUALIZATION
(ELECTROPHOTONIC IMAGING, KIRLIANOGRAPHY).
THEORETICAL AND APPLIED ASPECTS

ODESA
FENIKS
2023

Authors

Valeriy Y. Babelyuk, MD, PhD; Clinical sanatorium "Moldova", Truskavets'; UkrSR Institute of Medicine of Transport valeriybabelyk64@gmail.com

Igor L. Popovych, MD, PhD, senior res. fel.; Bohomolets' Institute of Physiology; Kozyavkin International Rehabilitation Clinic; UkrSR Institute of Medicine of Transport i.l.popovych@gmail.com

Anatoliy I. Gozhenko, MD, DS, Prof.; UkrSR Institute of Medicine of Transport prof.gozhenko@gmail.com

Galyna I. Dubkova, MD, PhD; Clinical sanatorium "Moldova", Truskavets' dubkovahalyna@gmail.com

Olga V. Kozyavkina, MD, PhD; Kozyavkin International Rehabilitation Clinic clinic@kozyavkin.com

Tetyana A. Korolyshyn, MD; UkrSR Institute of Medicine of Transport; Bohomolets' Institute of Physiology Korolushun777@gmail.com

Nazariy V. Babelyuk, MD; Clinical sanatorium "Moldova", Truskavets'

Marta M. Kovbasnyuk, PhD, senior res. fel.; Bohomolets' Institute of Physiology mmkovbasnyuk@gmail.com

Oksana A. Fihura, MD; UkrSR Institute of Medicine of Transport; Ivan Franko State Pedagogical University, Drohobych, Ukraine oksanafigura08@gmail.com

Yuriy G. Dobrovolskyi, DS, Prof. ass.; Yuriy Fed'kovych National University y.dobrovolsky@chnu.edu.ua

Walery Zukow, MD, DS, Prof. ass.; Nicolaus Copernicus University, Torun, Poland w.zukow@wp.pl

Roman I. Yanchij, DS, Prof.; Bohomolets' Institute of Physiology janchij2014@gmail.com

**We dedicate the monograph to the 115th anniversary of the birth
of the Luminary of Neurophysiology
Academician Philip Nikolayevich Serkov (1908-2011)
with gratitude for the support of the Truskavetsian Scientific School**

The monograph highlights the results of priority clinical-physiological studies of the relationships between gas discharge visualization (electrophotonic imaging, kirlianography) parameters, on the one hand, and electroencephalograms, heart rate variability, immunograms, phagocytosis, the content of the main adaptation hormones (cortisol, aldosterone, testosterone, triiodothyronine, calcitonin) in the blood as well as acupuncture points - on the other hand. It is shown that the GDV/EPI method reliably reflects the state of the body's neuro-endocrine-immune complex as well as others parameters and has the right to take its place in the arsenal of physiological/biophysical methods.

For biophysicists, physiologists, psychophysiologists, endocrinologists, immunologists, medical rehabilitation specialists.